Tenocyte-Like Cells of the Intermuscular Fascia are Causal Cells of Heterotopic Ossification in a Mouse Model of Fibrodysplasia Ossificans Progressiva

Amanda H. DelVichio
University of Connecticut, 2024

Heterotopic ossification (HO) is the formation of bone in skeletal muscle and associated soft tissues, which can result from a gene mutation or occur without a genetic link. The most severe form of genetic HO is observed in the disease fibrodysplasia ossificans progressiva (FOP), where patients are inundated with HO that slowly locks joints in place, eventually forming a second skeleton and significantly decreasing their quality of life. Fibro/adipogenic progenitors (FAPs) were identified as a causal cell of HO in a mouse model of FOP. **This project aims to identify and characterize additional causal cells of HO.** We have identified two causal cells of HO that are distinct from FAPs: Schwann cells and Tenocyte-Like cells (TLCs), which contribute to HO formation in a mouse model of FOP. Schwann cells exhibited a cell-autonomous osteogenic capability, and TLCs directly contributed to HO formation through an accelerated endochondral ossification pathway. Notably, most HO formed by TLCs resorbed within 21 days post-injury, indicating a unique, unstable bone response. Transcriptional analysis via bulk RNA-sequencing showed that while TLCs share similarities with FAPs, they expressed a distinct set of genes, including those typically associated with tenocytes and hindlimb fibroblasts. TLCs are a previously uncharacterized connective tissue cell type defined by their specific HO response, localization to the intermuscular fascial regions of the posterior hindlimb, and unique gene expression profile.

Identifying Additional Causal Cells of Heterotopic Ossification in a Mouse Model of Fibrodysplasia Ossificans Progressiva

Amanda H. DelVichio

B.S., University of Dubuque, 2017

A Dissertation
Submitted in Partial Fulfillment of the
Requirements for the Degree of
Doctor of Philosophy
At the
University of Connecticut

2024

Copyright by

Amanda H. DelVichio

2024

APPROVAL PAGE

Doctor of Philosophy Dissertation

Identifying Additional Causal Cells of Heterotopic Ossification in a Mouse Model of Fibrodysplasia Ossificans Progressiva

Presented by

Amanda H. DelVichio, B.S.

Major Advisor_____
David Goldhamer, Ph.D.

Associate Advisor_____
Charles Giardina, Ph.D.

Associate Advisor_____
Michael O'Neill, Ph.D.

Associate Advisor_____
Akiko Nishiyama, Ph.D.

Associate Advisor_____
Kenneth Campellone, Ph.D.

University of Connecticut

2024

Acknowledgements:

The success I've experienced during my Ph.D. journey has not been solely my own. As the saying goes, 'it takes a village,' originally intended for raising a child, I believe it also applies to obtaining a Ph.D. I would not be where I am today without the support and encouragement of my community.

First and foremost, I would like to express my deepest gratitude to my incredible Ph.D. mentor, Dr. David Goldhamer, for his unwavering support and guidance throughout my graduate career. David believed in me when I did not believe in myself. Most importantly, I am thankful for the humor that David instilled in the lab. There was never a day that the lab wasn't filled with laughter

I am also immensely grateful to the members of my Ph.D. committee, Drs. Charles Giardina, Akiko Nishiyama, Michael J. O'Neill, and Ken Campellone. The advice and support they provided have been instrumental to my success.

Additionally, I extend gratitude to the other Hammerheads, both past and present, whose discussions, camaraderie, and collaboration have enriched my academic experience. Whether it was a moment of comic relief or healthy competition, there was never a dull moment. I cherish the time we had together. To Katherine and Ingrid, who will be continuing my work, I wish you all the best!

To the peers who became family, Kate DeNegre and Ryan Drennan, I am forever grateful for the coffee runs and lunch venting sessions. Graduate school often feels like navigating a blizzard without a jacket, but your friendship has helped me weather the storm.

I owe a debt of gratitude to my wonderful teachers and mentors throughout my life. Thank you for fostering my love of learning and curiosity. I would not be the scientist and person I am today without each and every one of you.

To my family, specifically my parents, Robin and Jeffy, who have provided me unconditional love my entire life. I would not be who I am without them. Their invaluable advice and support throughout this process have been paramount to my success. To my brother, Cameron, thank you for setting an example for me to aspire to.

Lastly, I want to express my deepest appreciation to my husband, Jayson. I genuinely would not have made it through this process without you. Thank you for being my guiding light.

Table of Contents

List of Figures and Tables

Intentionally left blank

Chapter 1: Introduction

1.1 Introduction

All cells in the human body stem from two totipotent haploid cells: the sperm and the egg. During sexual reproduction, these cells fuse into a zygote, which can differentiate into every cell type of the developing fetus. This highly regulated process must work seamlessly to form a fully functional organism, but cellular differentiation does not stop after embryonic development. Different progenitor and stem cells in the adult organism undergo differentiation. When skeletal muscle is injured, muscle-specific stem cells, called satellite cells, are activated. These cells proliferate, differentiate, and fuse to remake the damaged skeletal muscle fibers (Yin et al., 2013). Just as cells appropriately differentiate into their target cell types, cells can inappropriately differentiate and become cell types they are not meant to be, wreaking havoc on the organism. This thesis will characterize cells within the skeletal muscle environment that can inappropriately differentiate into exogenous bone.

1.1.1 Heterotopic ossification

The word heterotopic stems from the Greek root words “heteros” and “topos,” which translates to other places, while ossification translates to “turn to bone”; therefore, heterotopic ossification (HO) at its most literal form means “other places turning to bone” (Meyers et al., 2019). HO is the formation of bone in skeletal muscle and its associated soft tissues. It can be a product of a gene mutation or independent of genetic influence (Bossche, 2005). In both HO modalities, acquired and genetic, the exogenous bone growth is formed through the endochondral ossification pathway (Meyers et al., 2019),

the same process employed for long bone formation in the embryo (McCarthy et al., 2005; Breeland et al., 2023). The exogenous bone growth causes a great deal of pain and can often result in the ankylosing of joints, leading to reduced range of motion, poor quality of life, and even premature death (Xu et al., 2022).

1.1.2 The two routes of bone formation: endochondral ossification and intramembranous ossification

Bone is mineralized connective tissue critical to an organism's overall function. Despite its appearance, bone is a dynamic tissue constantly being reorganized (Florencio-Silva et al., 2015). The cell types housed within fully mature bone are osteocytes, which regulate the mineral deposition and bone matrix; osteoblasts are bone-forming cells; and osteoclasts are bone-resorbing cells (Florencio-Silva et al., 2015). Maintaining the balance of osteoblasts and osteoclasts is essential to bone's overall function and formation (Florencio-Silva et al., 2015). Bone formation can occur through endochondral or intramembranous ossification (Gaela et al., 2021). The following section will provide a review of both bone-forming processes.

Interestingly, much of our understanding of endochondral ossification stems from studying the mechanisms of wing development in chicken embryos and limb development in mice (Hu et al., 2017). Long bones, defined as bones that are longer than they are wide, are formed through the endochondral ossification pathway **(**Breeland et al., 2023**)**. The formation of bone through the endochondral ossification pathway is not exclusive to

embryonic development; long bone fractures are healed through this process (Mackie et al., 2008).

Endochondral ossification begins with a mesenchymal progenitor cell. These progenitors will initiate the cartilage condensation process by upregulating SRY-box transcription factor 9 (*Sox9*), a transcription factor and master regulator of cartilage (Bagheri-Fam, 2006; Song et al., 2020). When *Sox9* was ablated from the developing embryo, osteocompetent cells failed to initiate the cartilage condensation process; therefore, in the absence of *Sox9*, downstream chondrogenesis and osteogenesis were halted (Akiyama et al., 2002), indicating that *Sox9* is required for the early stages of cartilage formation.

The next phase of endochondral ossification is the differentiation of the cartilage condensates to cartilage. Unsurprisingly, *Sox9* is also required for cartilage differentiation (Akiyama et al., 2022). SRY-box transcription factor 5 (*Sox5*) and SRY-box transcription factor 6 (*Sox6),* which are cofactors of *Sox9* (*Sox9, Sox5,* and *Sox6* are referred to as the Sox trio), drive the expression of early cartilaginous extracellular matrix (ECM) components, such as Collagen 2 (*Col2*) and Aggrecan (*Acan*) (Akiyama et al., 2002). At the center of the cartilage ECM, chondrocytes will undergo hypertrophy, which is accompanied by a decrease in *Sox9* expression and an increase in master regulators of osteogenesis, such as Runt-related transcription factor 2 (*Runx2)* (Galea et al., 2020). The SOX9 protein must be degraded for the chondrocyte-to-osteocyte transition (Zhou et al., 2006). Once cartilage is differentiated, the chondrocytes then proliferate, creating hypertrophic cartilage. The hypertrophic cartilage will remodel the ECM and stimulate the vascularization (Ortega et al., 2007). The hypertrophic cartilage is replaced by immature

bone, which will ultimately mature into fully mineralized bone, marked by the expression of Dentin matrix protein (*Dmp1*) and Osteocalcin (*Bglap*) (Gaela et al., 2020).

Flat bones of the skull, cranial vault, and some bones of the body's trunk, such as the clavicle, form through intramembranous ossification (Huang et al., 1997). Interestingly, intramembranous ossification is frequently observed throughout the amphibian and fish taxonomies (Hirasawa et al., 2015). The intramembranous ossification pathway begins with osteocompetent progenitor cells that mature into immature osteocytes (Gaela et al., 2020). These osteocytes then further differentiate into mineralized bone without involving an intermediary cartilaginous step (Gaela et al., 2020). *Runx2* is necessary to initiate this process, as the removal of *Runx2* resulted in defective intramembranous ossification (Takarada et al., 2016). The osteocompetent progenitor cell will upregulate osteoblast differentiation markers such as Osterix (*Sp7*), Collagen 1 (*Col1*), and *Bglap,* thus marking differentiation into an immature osteoblast. The maturation process will begin, and the matrix will be remodeled simultaneously as immature osteoblasts differentiate into mature osteoblasts. Mature osteoblasts are identified by the expression of late osteoblast genes, such as Dentin matrix protein (*Dmp1*) and Sclerostin (*Sost*) (Gaela et al., 2020). Interestingly, cartilage markers are expressed in chick and mouse embryos during the initial differentiation process of the osteocompetent cells down the intramembranous ossification pathway (Nah et al., 2000; Abzhanov et al., 2007; Gaela et al., 2020).

Both pathways of bone formation, endochondral ossification and intramembranous ossification, ultimately have the same goal of forming fully calcified, mature bone. Regardless of how bone forms, both differentiation pathways require similar inducers of

bone. For example, *Runx2* is an early osteoblastic differentiation marker and a transcription factor required in the bone-forming process regardless of the route of bone growth. Both bone-forming pathways are critical to an organism's overall skeletal development and function.

1.1.3 Traumatic HO

HO can be considered a tissue repair process that goes awry and results in exogenous bone growth, formed through the endochondral ossification pathway, that otherwise would not be present (Xu et al., 2018; Peterson et al., 2015; Dey et al., 2017). Traumatic HO forms due to bodily injury where there is no genetic link to explain the bone formation. This form of HO can occur due to brain or spinal cord injuries, hip arthroplasties, burns, combat-related injuries, or blast injuries (Chen et al., 2009; Dey et al., 2017; Ranganathan et al., 2015). About 64.6% of veterans who had combat-related blast injuries from Operation Iraqi Freedom developed traumatic HO (Potter et al., 2017). HO can occur either at or away from the site of the trauma. For instance, traumatic HO commonly develops around joints, even if the joints were not directly affected by the initial trauma (Ranganathan et al., 2015). A burn/tenotomy mouse model can recapitulate the traumatic HO phenotype observed in the human patient population (Peterson et al., 2015). This mouse model of traumatic HO involves a partial thickness contact burn of the dorsal skin and the division of the Achilles tendon at the midpoint (Peterson et al., 2015). HO formed due to the burn/tenotomy model is generally associated with the Achilles tendon, which correlates to the patient population as the Achilles tendon is a common site of traumatic HO (Peterson et al., 2015; Ranganathan et al., 2015). Another mouse model

of non-genetic HO induces HO by injecting supraphysiological levels of bone morphogenetic proteins (BMPs) into the skeletal muscle. BMPs, which possess osteoinductive characteristics (Urist et al., 1971), will signal to the surrounding osteocompetent cells and push them down the endochondral ossification pathway, thus resulting in HO (Li et al., 2020; Wosczyna et al., 2012; Katagiri et al., 2016). The burn/tenotomy and the BMP inducible mouse model of acquired HO have paved the way for identifying potential causal cells and the mechanisms of HO formation. Using a BMP2 inducible model of HO mesenchymal Tie2+ progenitors, later identified as FAPs (Fibro/adipogenic progenitors), were discovered as a causal cell of HO (Wosczyna et al., 2012). Using the burn/tenotomy mouse model of traumatic HO, Agarwal et al. found that cells of the Scleraxis (Scx) lineage are also causal cells of traumatic HO (Agarwal et al., 2017). FAPs and *Scx-expressing* cells are present at both the cartilage and bone stages of the endochondral ossification pathway, suggesting that both cell types can contribute to the entire bone-forming process. (Agarwal et al., 2017; Wosczyna et al., 2012). In addition, a recent study identified a tendon stem cell (TDSC) as an additional causal cell of acquired HO of the Achilles tendon in the burn/tenotomy model (Harvey et al., 2019; Yea et al., 2023). When traumatic HO is forming, all 3 cell types (TDSC, FAPs, and *Scx-expressing* cells), and potentially other unidentified causal cells, are contributing to the HO formation. The downstream goal of identifying osteocompetent cells in traumatic HO is the development of cellular-specific therapies that aim to prevent the debilitating HO from forming.

1.1.4 Neurogenic HO

Neurogenic HO is a subset of traumatic HO where exogenous bone develops due to traumatic injury to the brain or spinal cord. The HO that occurs is generally associated with the muscles of the hip, knee, elbow, or shoulder (Cipriano et al., 2009). Neurogenic HO is one of the most common types of traumatic HO. As many as 1 in 5 patients who have experienced a traumatic brain injury will be affected by neurogenic HO (Sullivan et al., 2013). As in most cases of exogenous bone growth, the HO can cause increased pain, impaired movement, and a reduced quality of life (Cipriano et al., 2009). The only cure for neurogenic HO is the removal of the newly formed, fully mineralized bone; however, approximately 6% of patients will have a reoccurrence of bone growth post-resection (Wong et al., 2020**)**; therefore, even resecting the HO is not a guaranteed solution. In general, the mechanism of neurogenic HO has yet to be fully understood. It is unclear how injury of the central nervous system (CNS) can result in bone growth at specific locations removed from the CNS. Levesque et al. developed the first mouse model of neurogenic HO utilizing a polytraumatic mechanism (Levesque et al., 2015). Combining a spinal cord injury and providing a spot of localized muscular inflammation (via crush or myotoxin injury) resulted in the formation of HO mimicking neurogenic HO seen in the human population (Levesque et al., 2015). Using this mouse model, it was found that neurogenic HO was dependent upon an inflammatory environment, specifically phagocytotic macrophages, as removing macrophages reduced exogenous bone growth (Genet et al., 2015). Brady et al. proposed a generic overview of the possible mechanism of Neurogenic HO, in which a polytraumatic injury occurs, affecting the CNS and the

peripheral body (Brady et al., 2018). The injury response releases a pool of osteogenic and inflammatory factors that signal osteocompetent cells to proliferate and differentiate down the endochondral ossification pathway (Wong et al., 2020). Potential therapies for neurogenic HO are non-steroidal anti-inflammatory drugs (NSAIDs), radiation therapy, and surgical resection of the HO (Brady et al., 2018). These therapies treat the symptoms of neurogenic HO and potentially remove the exogenous bone; however, identifying a causal cell of neurogenic HO may allow for further development of cell-based therapies. One potential causal cell type is FAPs, as lineage labeled FAPs were found to be present within neurogenic HO lesions (Tseng et al., 2022). Cells of the nerves are predicted to send signals down to the sites where FAP-derived HO is established (Tseng et al., 2022). Causal cells of traumatic HO could also contribute to neurogenic HO; however, not all traumatic HO causal cells have been tested in the mouse model of neurogenic HO. Taken together, FAPs and the inflammatory environment are key factors in the development of neurogenic HO. However, further experimentation is required to establish the neurogenic HO mechanism fully.

1.1.5 Genetic HO

HO can also form due to a genetic mutation, which discriminates this form of HO from traumatic or neurogenic HO. Genetic HO generally affects fewer people but to a more extensive degree. Diseases such as Fibrodysplasia Ossificans Progressiva (FOP) or Progressive Osseous Heteroplasia (POH) are two examples of genetic HO (Kaplan et al., 2000; Kaplan et al., 1994). Both diseases result in bone occurring in the soft tissues, significantly affecting the patient's quality of life. The modality of bone growth, locations

or predictability of HO, and disease progression differ between POH and FOP (Shore, 2012). This highlights the heterogeneity between bone-forming diseases and the critical need to determine the causal cells of the HO with the hope of developing a cellular-specific therapy. The following thesis will focus on the bone-forming disease FOP and the causal cells of HO.

1.1.6 Fibrodysplasia ossificans progressiva (FOP)

FOP is a rare autosomal dominant genetic disorder that affects about 1 in 1 million people (Kaplan et al., 2008). The first signs of FOP may be evident at birth, with potential malformations in the great toe, digits, or cervical spine (Shore et al., 2012). If present, these malformations do not hinder patients from developing normally. HO formation will occur before the first decade of life (Conner et al., 1982). Flare-ups generally precede the presence of HO and are characterized by large, painful lumps of swelling and inflammation (Pignolo et al., 2015). While flare-ups are common before HO formation, they are not required; there is radiological evidence of patients undergoing bone remodeling, leading to HO in the absence of a flare (Botman et al., 2019).

Approximately 97% of patients with FOP share the same point mutation in the Type 1 Bone Morphogenetic Protein (BMP) receptor, ACVR1 (ALK2) (Shore et al., 2006). This point mutation causes a single amino acid change in the coding sequence of ACVR1 (Shore et al., 2006; Fukuda et al., 2009). Shore et al. mapped the FOP mutation to chromosome 2q23-24 and identified that an arginine is replaced by a histidine at codon position 206 (617G -> A; R206H) (Shore et al., 2006). This mutation occurs in the highly conserved glycine-serine (GS) activation domain at the junction of the protein kinase

domain of ACVR1, referred to as R206H-ACVR1 (Shore et al., 2006). The GS domain of the ACVR1 receptor is a conserved segment of the protein and is the site of phosphorylation, which initiates the process of downstream signaling (Huse et al., 2001).

1.1.7 Wild-type BMP signaling through the ACVR1 receptor

ACVR1 is a type1 serine/threonine kinase BMP receptor, a member of the Transforming Growth Factor β (TGFβ) superfamily of proteins (Schmierer et al., 2007). The TGFβ superfamily was initially found in a hunt for autocrine factors that promote the transformation of oncogenic cells (Roberts et al., 1981). This superfamily of proteins is a conserved family of proteins involved in many cellular processes, including but not limited to cell proliferation, differentiation, morphogenesis, tissue homeostasis, and regeneration (Massague, 2012). TGFβ receptors signal through heterotetrameric complexes containing 2 type 1 and 2 type 2 receptors. Ligands, such as activins, nodals, TGFBs, BMPs, and growth differentiation factors, bind TGFβ superfamily receptors. Specifically, ligand binding to the type 2 receptors promotes the formation of the heterotetrameric complex (Wrana, 2013). The type 2 receptors then phosphorylate the GS domain of the type 1 receptors, which initiates intracellular signaling (Wrana, 2013; Agnew et al., 2021). In a wild-type cell, BMP4 signals through ACVR1 as follows: BMP4 will bind any of the type 2 counterpart receptors of ACVR1, which are BMPR2, ACVR2A, ACVR2B, and initiate the formation of the heterotetrameric complex (Valer et al., 2019). The type 2 receptors will phosphorylate ACVR1 and its other type 1 counterpart. The phosphorylation of the type 1 receptor will signal the conical smads response, which activates Smads 1/5/8 intracellularly (Valer et al., 2019). Smads 1/5/8 then binds Smad

4, a cofactor that allows for the translocation of the complex into the nucleus, resulting in the transcription of osteogenic genes and, thus, an osteogenic response (Valer et al., 2019). Additionally, not every ligand that binds this heterotetrameric signaling complex will elicit a signaling response. Activin A binding to a heterotetrameric complex containing ACVR1 results in a non-signaling complex (Hatsell et al., 2015).

1.1.8 Abnormal signaling of an R206H cell

Historically, it was believed that the formation of HO through osteocompetent cells expressing the R206H-ACVR1 receptor occurred as a result of the R206H-ACVR1 hypersensitivity to BMP ligands (Culbert et al., 2014). However, the exogenous bone growth results from a neofunction of the R206H-ACVR1 receptor (Hatsell et al., 2015; Hino et al., 2015). As mentioned above, when an activin A ligand binds a wild-type ACVR1, a non-signaling complex forms; however, when cells express the R206H-ACVR1 receptor, activin A binding will result in Smads 1/5/8 signaling and, therefore, an osteogenic response (Hatsell et al., 2015; Hino et al., 2015). The discovery that activin A induces an osteogenic response was a pivotal moment in the FOP field, which led to one of the first successful therapeutics to prevent HO formation in a mouse model of FOP (Hatsell et al., 2015). This therapeutic, an activin A monoclonal antibody, sequesters the activin A ligand from the injury environment and can prevent HO formation in a mouse model of FOP (Hatsell et al., 2015; Lees-Shepard et al., 2018b; Upadhyay et al., 2017).

1.1.9 Injury-induced and spontaneous HO

Injury-induced HO is exogenous bone growth that appears as a response to a soft tissue injury. In a mouse model of FOP, injury-induced HO develops through the endochondral ossification pathway and follows a generally predictable pattern, location, and timeline to mature bone (Lees-Shepard et al., 2018b; Dey et al., 2016). Osteocompetent cells will differentiate into cartilage around 6 days post-injury, and the first evidence of fully mineralized bone will appear between 10 to 14 days post-injury (Lees-Shepard et al., 2018b). Injury-induced HO is commonly induced via myotoxin or pinch injury and can be associated with the endogenous skeleton, fascial planes, or intramuscularly, depending on the injury. Cardiotoxin is a myotoxin produced in snake venom and is commonly used as a tool for intramuscular injury (Harvey et al., 2008). In the skeletal muscle environment, myotoxic injuries like cardiotoxin specifically target the muscle cells by causing depolarization of cell membranes and an influx of calcium to myofibers within the muscle (Harvey et al., 2008; Hardy et al.,2016). In contrast to a myotoxin injury, a pinch injury is a physical injury to the skeletal muscle. It will damage all cells present in the hindlimb environment as the entire limb is crushed. Both injury modalities are used extensively in the field and throughout this body of work to study injury-induced HO formation in a mouse model of FOP.

Spontaneous HO results in bone formation without a known trigger. In mouse models of FOP, spontaneous HO is generally associated with joints (Lees-Shepard et al., 2018a; Lees-Shepard et al., 2018b; Dey et al., 2016). Like injury-induced HO, spontaneous HO in mouse models of FOP also follows the endochondral ossification

pathway (Lees-Shepard et al., 2018b; Dey et al., 2016). In human FOP patients, both modalities of bone formation are likely observed simultaneously.

1.2 Cells Comprising the Skeletal Muscle Environment

Cells of multiple lineages that arise from many germ layers are found within skeletal muscle tissue. Connective tissues are derived from the lateral plate mesoderm (Prummel et al., 2020), satellite cells are derived from the somites (Tani et al., 2020), and peripheral nerve cells are derived from the neural crest lineage (Solovieva et al., 2021). All cell types must synchronously come together to form fully functional tissue. Figure 1.1 provides a schematic representation of the cell types comprising the skeletal muscle environment. The following sections will identify some key players in the skeletal muscle environment that support the tissue system's development and response to injury. This thesis will display evidence of the supportive cell types highlighted in the following section and their contribution to HO in a mouse model of FOP.

Figure 1.1: Schematic overview of the known cell types comprising the skeletal muscle environment.

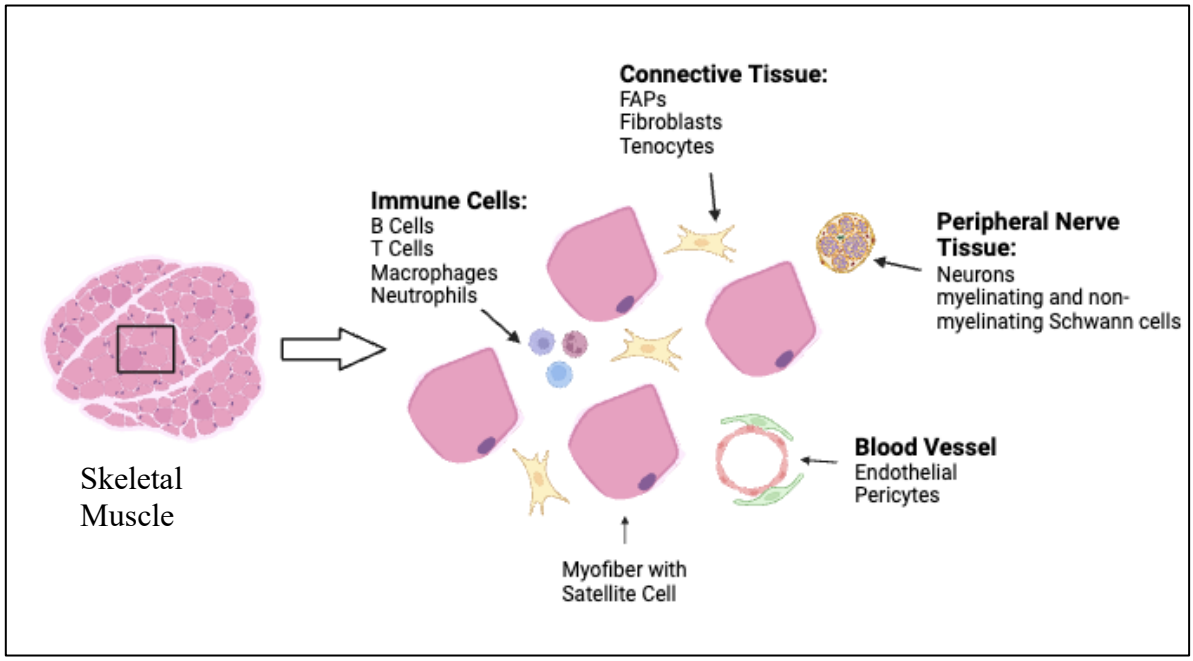

1.2.1 Fibro\adipogenic progenitors (FAPs), identification, characterization, and response to injury

FAPs are progenitor cells found within the muscle interstitium that were initially identified due to their ability to differentiate into multiple lineages (Joe et al., 2010; Uzemi et al., 2011). As suggested by their name, FAPs display a bipotent ability to differentiate into fibrotic and adipogenic lineages and cannot differentiate into a myogenic lineage (Joe et al., 2010; Uzemi et al., 2010; Uzemi et al., 2011; Lemos et al., 2015). FAPs are also anatomically defined within the skeletal muscle environment by their localization to the interstitial space of muscle tissue (Joe et al., 2010; Uzemi et al., 2010; Uzemi et al., 2014). More recently, the understanding of FAP localization within the skeletal muscle

environment has expanded. Now it is accepted that FAPs or FAP-like populations are found in all layers of skeletal muscle connective tissue (the epimysium, perimysium, and endomysium) but appear to be more abundant in the epimysium and perimysium layers (Contreras et al., 2021**).**

FAPs were initially isolated using flow cytometry and identified by the absence of endothelial markers (PECAM-1 or CD31), hematopoietic markers (PTPRC or CD45), and muscle lineage markers (as A-7integrin-negative (ITGA7) and Paired box 7 (PAX7), while expressing Stem Cell Antigen 1 (SCA1), a marker associated with progenitor cells (Joe et al., 2010). FAPs have since been found to express THY1 (CD90), CD34, and Platelet-Derived Growth Factor Receptor a (PDGFRα), the single best marker for FAPs (Uzemi et al., 2011; Uzemi et al., 2010; Lees-Shepard et al., 2018b; Woscznya et al., 2012; Biswas and Goldhamer., 2016; Contreras et al., 2021). The Goldhamer lab utilizes the dual expression of PDGFRα and SCA1 to isolate FAPs from the hindlimb environment (Lees-Shepard et al., 2018b; Burdick et al., 2024; Biswas and Goldhamer, 2016; Woscznya et al., 2012). Other cell types express PDGFRα and SCA1 individually, but the dual expression of these surface proteins serves as a specific marker combination for FAPs (unpublished data).

FAPs are a heterogeneous population of cells that contain multiple subpopulations (Contreras et al., 2021; McKellar et al., 2021; Oprescu et al., 2020; Malecova et al., 2018; unpublished data). The identification of FAP subpopulations was investigated further with the advancement of single-cell and bulk RNA-sequencing and single-cell mass cytometry. All subpopulations of FAPs express the conical FAP gene expression profile (*Pdgfra, Sca1*) and are located in the fascial planes and muscle interstitial spaces; however,

subpopulations of FAPs exhibit differences in gene expression when compared to each other (Osprescu et al., 2020; Malecova et al., 2018; McKellar et al., 2021) Some but not all FAP subpopulations express *Tie2* or *Tek (Malecova et al., 2018; unpublished data),* which is expressed by mesenchymal progenitors, hematopoietic, and endothelial cells (Kisanuki et al., 2001). Oprescu et al. showed that FAPs in uninjured muscle can display two lineage trajectories: a lineage of Dipeptidyl peptidase 4 (*Dpp4+)* FAPs and C_X_C Motif Chemokine Ligand 14 (*Cxcl14+)* (Oprescu et al., 2020). The *Dpp4*+ subpopulations were found to have a greater adipogenic capacity than the *Cxcl14*+ subpopulation. Large-scale integration of many publicly available datasets of injured and uninjured muscle reveals 3 distinct FAP clusters: remodeling, stem, and adipogenic FAPs (McKellar et al., 2021). The heterogeneity of FAPs has just begun to be investigated.

Naturally, FAPs play a supportive role in the skeletal muscle environment, where they provide signaling cues to muscle-resident stem cells and reorganize the ECM of the hindlimb environment (Contreras et al., 2021). They are critical to the tissue homeostasis of skeletal muscle, as the removal of FAPs results in impaired muscle regeneration and muscle atrophy (Wosczyna et al., 2019). In wild-type uninjured muscle, FAPs make up a small percentage of cells in the total environment, roughly 3- to 5- percent (Lees-Shepard et al., 2018b; Burdick et al., 2024; Lemos et al., 2015)**.** Immediately upon injury, FAPs will decrease in number as the immune system infiltrates and removes damaged cells (Oprescu et al., 2020; Lemos et al., 2015). After the inflammatory response, FAPs will then proliferate, reaching their peak numbers 3- to 5- days post-injury (Joe et al., 2010; Lees-Shepard et al., 2018b; Lemos et al., 2015). At this point, the FAPs support the

proliferation and differentiation of the neighboring muscle stem cells to proliferate and fuse into new muscle fibers (Oprescu et al., 2018; Joe et al., 2010; Lemos et al., 2015). After this peak proliferative stage, FAPs will return to their baseline numbers (Joe et al., 2010). More information outlining FAPs response to injury is outlined in Chapter 3. See the following sections for FAPs involvement with FOP pathogenesis (Section 1.3.1 Causal cells of HO).

1.2.2 Tenocyte development, identification, and response to Injury

Tendons are specialized connective tissue that joins muscle and bone (Elliot, 1965). Muscle contraction will generate forces that transmit to the bones through the tendons; therefore, tendons are essential to everyday mobility and stability (Gaut et al., 2015). Tendons can be classified into different groups based on their location and biomechanical function: force-transmitting tendons, intermuscular tendons, and anchor tendons (He et al., 2022). As their name implies, force-transmitting tendons generally transfer the force between muscle and bones (Murchison et al., 2007). Intermuscular tendons are characterized by their function of connecting two muscle segments and located at the muscle junctions (He et al., 2022). Anchoring tendons are primarily found near the organism's extremities and anchor the muscle to bone entheses, such as insertion sites, osteotendinous junctions, or osteoligamentous junctions (He et al., 2022). Regardless of their characterization, all tendons are hypocellular and have a specific spatial organization (Franchi et al., 2007). Tendons are composed of tenocytes, which are specialized fibroblasts that synthesize the collagen to make Collagen 1 fibrils (Benjamin et al., 2000). Collagen fibrils of mature tendons are then organized into

collagen fascicles. Multiple collagen fascicles are organized into mature tendons with tenocytes scattered around. The hierarchical organization of collagen fibrils provides the tendons with the strong and sturdy ECM structure required for cellular function (Franchi et al., 2007). Additional information about tendon organization is explained in Chapter 4.

The first marker of tendons, Scleraxis *(Scx),* was discovered in the early 2000s and was identified as a basic helix-loop-helix transcription factor (Schweitzer et al., 2001). Originally, *Scx* was thought to be specific to the connective tissue that attaches muscle to bone in chick and mice (Schweitzer et al., 2001); however, *Scx* expression is found in cardiac fibroblasts and intramuscular connective tissue of the tibialis anterior muscle (Bagchi et al., 2016; Levay et al., 2009; Giordani et al., 2019; Sugimoto et al., 2013). Furthermore, the research presented in this thesis demonstrates the presence of *Scx*-expressing cells within the intermuscular fascial connective tissue regions of the hindlimb (Figure 3.5 and Figure 4.1). Regardless of its specificity, *Scx* plays a critical role in tendon proliferation and matrix production, as a *Scx* null mouse displayed significant tendon defects. The loss of *Scx* expression resulted in the loss of tendon segments, disorganized and small tendons, and a reduced, less organized matrix. (Murchison et al., 2007). It was shown that an increase in *Scx* expression is sufficient for *Col1* expression, as ectopic *Scx* expression increases the expression of *Col1* (Tanzil et al., 2022). In mice, *Scx* expression was first observed in mesenchymal progenitor cells of the limb buds, peaking by embryonic day (E)9.5-10, which coincides with the developmental timepoint of mesenchymal progenitors differentiating into *Scx* expressing tendon progenitor cells (Schweitzer et al., 2001). Tendon progenitor cells are a heterogeneous population, as some, but not all, express *Sox9,* resulting in either

a *Scx+/Sox9+* or *Scx+/Sox9-* population. Double positive, *Scx+/Sox9+,* progenitor cells mature into the articular cartilage of the joint, while the single positive population, *Scx+/Sox9-,* will mature into tenocytes that eventually make up tendons found elsewhere in the body (Sugimoto et al., 2013; Soeda et al., 2010). Interestingly, while *Scx* expression is widely expressed by tendon progenitor cells in utero, 4-month-old adult tendon *Scx* expression is mainly restricted to the epitenon and the paratenon (Mendias et al., 2011; Sakabe et al., 2018). Though *Scx* is the most common marker for tendon development, adult and embryonic tendons are also identified by the expression of Tenomodulin (*Tnmd*), a key marker of tendon differentiation (Qi et al., 2012). Other tenocyte markers are Mohawk (*Mkx*), *Col1*, Tenascin-C *(TNC)*, *and Collagen XIII* (*Col13*) (Jo et al., 2019). *Co1* and *Col13* are not specific to tendons, but they are highly upregulated in tenocytes compared to other connective tissue cells, such as FAPs (Jo et al., 2019).

The tendon injury response can be separated into 3 distinct stages (Hope et al., 2007). The first stage is called the inflammatory stage, which typically lasts approximately 3 to 7 days and involves the recruitment of different immune cell populations that phagocytose the damaged tissues and cells (Muller et al., 2015). In addition to the immune cell infiltration, tenocytes and tendon progenitor cells are recruited to the injury site and begin proliferating, thus marking the proliferative stage, the second stage of tendon healing. This phase of healing generally lasts between 7 to 21 days, depending on the severity of the injury (Chartier et al., 2021). The tenocytes and tendon progenitor cells secrete components of the tendon matrix and thus initiate the rebuilding of the tendons (Chartier et al., 2021; Muller et al., 2015). The final stage of tendon healing is the

remodeling stage. In this stage, *Col1* is synthesized, and the ECM becomes more organized, like that of a mature tendon (Hope et al., 2007). Unlike the other stages of tendon healing, which are relatively short, this stage can last anywhere from 1 month to a year, depending on the severity of the injury and other external factors of the host. After the remodeling stage, the newly formed tendon is considered mature; however, it will never regain full functionality compared to the original uninjured tendon (Leadbetter, 1992). Future sections will discuss the tendon lineage involvement in FOP pathogenesis (Section 1.3.1 Causal Cells of HO and Chapter 2).

1.2.3 Schwann cell development, identification, and response to injury

The Schwann cell was first observed by Theodor Schwann in the mid-18th century and was described as a myelin sheath-surrounded cell (Owecki, 2021). Schwann cell knowledge has evolved tremendously from the first description. Schwann cells are a supportive glial cell type in the peripheral nervous system (PNS) that plays an essential role in developing, maintaining, and regenerating peripheral nerves (Horner, 2022**)**. Schwann cells can be categorized as either myelinating or non-myelinating, also called Remark Schwann cells. The myelinating Schwann cells provide the myelin sheath, which allows for efficient propagation of action potential across axons of the PNS (Glenn et al., 2013). Myelinating Schwann cells generally enwrap larger axons in a 1:1 Schwann cell-to-axon ratio (Feltri et al., 2015; Balakrishnan et al., 2020). Remark Schwann cells support nerves of the PNS by ensheathing multiple small-caliber axons into Remark bundles (Griffen et al., 2008; Salzer, 2012). Remark Schwann cells and myelinating Schwann cells are essential to the functional health and signaling of the PNS. Myelinating and remark

Schwann cells are characterized by location within the peripheral nerves and their gene expression. Both share Schwann cell markers, such as SRY-box transcription factor 10 (*Sox10*) or S100 calcium-binding protein B (*S100b).* However, subpopulation-specific markers differentiate between the myelinating and non-myelinating Schwann cells, such as Myelin basic protein (*Mbp*) or Myelin protein zero (*Mpz*) and Neural cell adhesion molecule (*Ncam*) *or* L1 Cell adhesion molecule (*L1cam*), respectively (Gerber et al., 2021).

Schwann cells are descendants of the neural crest lineage, a germ layer in the embryo known to give rise to the tissues of the cranium and the entire nervous system of the body (Achilleos et al., 2012). Schwann cell development begins with a neural crest cell differentiating into a Schwann Cell Precursor (SCP), first seen at (E)12-13 in mouse development. SCPs are a multipotent cell type capable of differentiating into Melanocytes, endoneurial fibroblasts, dental mesenchymal stem cells, chondrocytes, osteoblasts, enteric neurons, parasympathetic neurons, and immature Schwann cells (Solovieva et al., 2022; Jessen et al., 2015; Morrison et al., 1999). For the Schwann cell lineage specifically, the SCP will differentiate into an immature Schwann Cell, further differentiating into myelinating and non-myelinating Schwann cells (Jessen et al., 2015).

In response to an injury stimulus, Schwann cells display the unique ability to dedifferentiate post-injury (Fawcett et al., 1990; Chen et al., 2007)**.** Injury to the peripheral nerve via crush or transection of the peripheral nerve will lead to inflammation at the injury site, causing the damaged axons to degenerate. Losing contact with the axon will trigger Schwann cells (myelinating and non-myelinating) to enter a dedifferentiation state. The dedifferentiated cell halts myelin-associated gene expression and expresses a gene

expression profile closer to an Immature Schwann cell (Kim et al., 2014; Jessen et al., 2008**)**. At the same time as Schwann cell dedifferentiation, inflammatory immune cells, such as macrophages and tissue-resident fibroblasts, flood the injured region (Chen et al., 2019; Gaudet et al., 2011; Kim et al., 2014). The invading immune cells and the dedifferentiated Schwann cells remove neuronal debris (Parrinello et al., 2010). Once the newly formed axon grows, the Schwann cells, fibroblasts, and immune populations secret pro-regenerative factors to support growth. This continues until the dedifferentiated Schwann cells differentiate into myelinating and non-myelinating Schwann cells and repopulate the newly formed nerve bundle (Kim et al., 2014).

Interestingly, the original identity of a Schwann cell is not representative of the cell's capacity after injury. Myelinating Schwann cells can redifferentiate into non-myelinating Schwann cells after injury and vice versa (Jessen et al., 2019). Schwann cells are unique cells that play a vital role in the overall PNS health and functionality. See below for potential Schwann cell involvement in FOP pathogenesis (Section 1.3.1 Causal Cells of HO and Chapter 3).

1.3 Background Information and Preliminary Data

The following section will further explain the potential causal cells of HO and how different lineages could be involved in FOP pathogenesis. Future sections will also focus on background information from the FOP field, mouse genome manipulation techniques used throughout this thesis, and the preliminary thought process that led to the experiments described in the following chapters.

1.3.1 Causal cells of HO

One of the first parameters investigated in FOP research was the cell type(s) within the skeletal muscle environment responsible for the devastating and debilitating HO formation. Instrumental to the identification of the discovery of the causal cell of FOP was the development of a conditional, knockin, Cre-dependent mouse model of FOP (*Acvr1*^{tnR206H}) that fully recapitulates the human disease (Lees-Shepard et al., 2018b). Cell-specific Cre-drivers can target the recombination of the *Acvr1*^{tnR206H} allele (*Acvr1*^{R206H}) to different cellular lineages, resulting in cell-specific expression of *Acvr1*^{R206H}. Using this mouse model, FAPs were found to be a causal cell of HO (Lees-Shepard et al., 2018b). Many cell types expressing the mutant ACVR1 receptor have been tested for osteogenic potential. Satellite cells, pericytes, smooth muscle, endothelial, and hematopoietic cells do not contain osteocompetent abilities when tested using a mouse model of the FOP (See Table 3.1)(Dey et al., 2016; Lees-Shepard et al., 2018b). Further experimentation is required to test the potential of these cells for playing supportive roles in the formation of HO, such as creating an environment conducive to osteogenesis. *Prx1, Mx1, Tie2*, *P0, Scx,* and *Pdgfra* lineages were found to display an osteogenic response and, therefore, contain a causal cell of HO (Dey et al., 2016; Lees-Shepard et al., 2018; Chakkalakal et al., 2016; Zhao et al., 2023). Unsurprisingly, the lineages listed have the potential to differentiate into *Pdgfra*-expressing cells, presumably FAPs (See table 3.1). In conclusion, FAPs are a causal cell of HO in a mouse model of FOP. All the cellular lineages tested for HO formation in a mouse model of FOP are not specific to FAPs; they target a multitude of cell types. Cell types other than FAPs may be contributing to the HO formation that is observed. Determining all the causal cells of HO

is critical as identification of the bone-forming cells could allow for cellular-specific therapies of FOP.

1.3.2 Cre-lox recombination: a genetic tool in mouse genome manipulation

Mouse models of FOP are an essential tool to further the understanding of the disease progression, causal cells, and mechanisms of HO formation. The current FOP mouse models utilize genome modification tools that allow for the cell lineage-specific expression of the mutant ACVR1 receptor. The most common tool used in the field is the Cre-loxP system, as it allows for control over the location and timing of gene expression (Kim et al., 2018). The Cre-loxP system relies on the Cre-recombinase enzyme, an endonuclease belonging to the integrase family of site-specific recombinases (Nagy, 2000**)**. Cre-recombinase is a 34kD protein first identified from a bacteriophage P1 and has since been critical for mouse genomic manipulation (Hamilton et al., 1984). Cre-recombinase recognizes the locus of x-over, P1 (*lox*P) sites, which are 34-base pair palindromic sequences consisting of two 13-base pair inverted sequences and an 8-base pair core sequence (Sauer et al., 1988). Upon recognition of the *loxP* site, Cre-recombinase will modify the DNA found between these sites (Kim et al., 2018). The orientation of loxP sites will dictate how the DNA is altered. The *loxP* sites can be oriented so that the DNA between them is inverted, excised, or translocated (Nagy, 2000). The work described in this thesis utilizes Cre-recombinase to target the expression of the mutant ACVR1 receptor to specific cellular lineages.

1.3.3 Preliminary project data and research focus

The central hypothesis of this thesis is that additional causal cells contribute to the HO in a mouse model of FOP. As mentioned previously, using the Goldhamer Lab's Cre-dependent mouse model of FOP (*Acvr1*^{tnR206H}), FAPs were identified as a causal cell of HO (Lees-Shepard et al., 2018b). FAPs lack a single cell type-specific marker; therefore, targeting the expression of the R206H mutation to FAPs results in many cell types expressing the mutation. The cell types that are not FAPs are the cell types of question throughout this thesis. The experiments and conclusions laid out in this document will demonstrate that,

1. Two additional cell types, Schwann cells and Tenocyte-Like Cells (TLC), contribute to HO in a mouse model of FOP.
2. The TLCs are a potential novel intermuscular fascial connective tissue cell.

The University of Connecticut's Institutional Animal Care and Use Committee reviewed and approved all animal procedures under protocol A23007.

Chapter 2: Determining the Identity and Osteogenic Capabilities of PDGFRα-Negative Cells

2.1 Abstract

Heterotopic Ossification (HO) can be conceptualized as aberrant muscle regeneration that results in exogenous bone growth. The most dramatic form of HO is observed in the disease Fibrodysplasia Ossificans Progressiva (FOP). The Goldhamer lab developed a Cre-dependent mouse model of FOP (*Acvr1*^{tnR206H}) that allows for cell-specific expression of the FOP mutation. Using the *Acvr1*^{tnR206H} mouse model, fibro/adipogenic progenitors (FAPs) have previously been identified as a causal cell in injury-induced and spontaneous HO (Section 1.2.1) (Lees-Shepard et al., 2018b). Recombination of the *Acvr1*^{tnR206H} allele (*Acvr1*^{R206H}) is targeted to FAPs using either Pdgfra-Cre or Tie2-Cre drivers; however, the Pdgfra-Cre model elicits a more robust HO response than the Tie2-Cre model. Flow cytometry analysis revealed that in addition to FAPs, Pdgfra-Cre recombined a population of cells that historically expressed *Pdgfra* but lacked current PDGFRα expression (referred to as PDGFRα-negative cells or PNCs). As PDGFRα is the single best marker for FAPs, the lack of current PDGFRα expression discriminates PNCs from FAPs. Single-cell RNA-sequencing (scRNA-seq) and histological analysis revealed the cell identities and anatomical locations of the four cell types comprising the PNC population: Schwann cells, pericytes/smooth muscle, satellite cells, and tenocytes. When the *Acvr1*^{R206H}-expressing PNC population was transplanted into an immunocompromised host, an osteogenic response was observed, suggesting that the PNC population harbors an additional causal cell of HO.

2.2 Introduction

97% of FOP cases result from a single amino acid change (arginine to histidine at position 206; R206H) in the glycine-serine domain of ACVR1 (Shore et al., 2006; Kaplan et al., 2009). The Goldhamer lab developed a conditional, Cre-dependent, knockin mouse model of FOP, referred to as *Acvr1*^{tnR206H}, that fully recapitulates the human disease (Lees-Shepard et al., 2018b). Briefly, expression of the mutant *Acvr1* allele (*Acvr1*^{R206H}) is dependent upon Cre-recombinase mediated recombination. The Cre-dependent characteristic of the *Acvr1*^{tnR206H} allele enables cell-specific and temporal control of *Acvr1*^{R206H} expression. A floxed tdTomato reporter-stop cassette was inserted into intron 4 of the *Acvr1* allele, upstream of the R206H mutation, located in exon 5. Expression of the tdTomato reporter-stop cassette is driven by a constitutively active CAG promoter (Figure 2.1A). The tdTomato reporter-stop cassette will label all cells with the tdTomato fluorescent reporter and halt transcription upstream of the R206H mutation (resulting in a presumptive null allele). Cre-recombinase will recognize the loxP sites and excise the tdTomato reporter-stop cassette, which results in the permanent loss of the tdTomato reporter and transcription of the R206H mutation (Lees-Shepard et al., 2018b).

Using the accurate, *Acvr1*^{tnR206H} mouse model of FOP, FAPs were found to be a causal cell of HO (see Section 1.3.1) (Lees-Shepard et al., 2018b). FAPs are heterogeneous connective tissue progenitors, defined by their location within the skeletal muscle interstitial space and connective tissue layers, dual expression of Stem cell antigen 1 (*Sca1*) and Platelet-derived growth factor receptor a (*Pdgfra*), and their ability to differentiate into adipogenic and fibrotic lineages (Joe et al., 2010; Uzemi et al., 2010; Uzemi et al., 2011; Lemos et al., 2015; Lees-Shepard et al., 2018b). *Acvr1*^{tnR206H} recombination can be targeted to FAPs using two Cre-drivers: Pdgfra-Cre and Tie2-Cre (Lees-Shepard and Goldhamer, 2018c; Lees-Shepard et al., 2018b). Unfortunately, the expression of the Pdgfra-Cre and Tie2-Cre is not solely specific to FAPs (Roesch et al., 2008; Kisanuki et al., 2001). Pdgfra-Cre is a constitutive

Cre-driver, where the expression of the Cre-recombinase is controlled by the *Pdgfra* promoter (Roesch et al., 2008). The Cre-recombinase enzyme will permanently excise the tdTomato reporter-stop cassette in cells that have expressed *Pdgfra* at any point in their lifetime. *Pdgfra* is widely expressed throughout mesoderm and neural crest development (Orr-Urtreger et al., 1992; Schatteman et al., 1992; Smith et al., 2010; Roesch et al., 2008); therefore, the *Acvr1*^{tnR206H} allele has the potential to be recombined (*Acvr1*^{R206H}) in many cell types. The Tie2-Cre is also a constitutive Cre-driver and is active in cells that express *Tie2* at any point in their development (Kisanuki et al., 2001). The known cell types targeted by the Tie2-Cre are a subset of the total FAP population, endothelial, and hematopoietic cells (Kisanuki et al., 2001).

When recombination of the *Acvr1*^{tnR206H} allele is targeted to the *Pdgfra* or *Tie2* lineage, different HO responses are observed (Lees-Shepard et al., 2018b). *Acvr1*$^{tnR206H/+}$;Tie2-Cre mice are referred to as the injury-induced HO mouse model and displayed reproducible HO in response to muscle injury. The HO observed in this model follows a predictable pattern. Bone first appears between 10 to 14 days post-injury and peaks between 14 and 21 days post-injury (Lees-Shepard et al., 2018b). FAPs were found to be the only cell type of the *Tie2* lineage directly contributing to the formation of HO (Lees-Shepard et al., 2018b; Dey et al., 2016). In stark contrast to the injury-induced HO model, spontaneous HO is observed in *Acvr1*$^{tnR206H/+}$;Pdgfra-Cre mice (referred to as the spontaneous HO model). Spontaneous HO is exogenous bone growth that occurs without a known trigger. By 4-weeks-of-age, 100% of *Acvr1*$^{tnR206H/+}$;Pdgfra-Cre mice had evidence of at least one site of spontaneous HO (Lees-Shepard et al., 2018a). *Acvr1*$^{tnR206H/+}$;Pdgfra-Cre mice must be utilized by 6-weeks-of-age due to the formation of HO at the jaw, which results in ankylosing of the jaw (Lees-Shepard et al., 2018a). The spontaneous HO model also forms injury-induced HO (Lees-Shepard et al., 2018b). The injury-induced HO response of *Acvr1*$^{tnR206H/+}$;Pdgfra-Cre mice is more dramatic and robust in terms of volume and progression of HO, with an earlier appearance

of exogenous bone observed at 8 days post-injury (unpublished observations- Figure 3.5).

This chapter will highlight the discovery of a heterogeneous population of cells, PDGFRa-negative cells (PNCs), found solely in the spontaneous HO model. PNCs are distinct from FAPs based on the lack of PDGFRa expression and anatomical location throughout the hindlimb. *Acvr1*^{R206H}-expressing PNCs (R206H-PNCs) can differentiate into HO when transplanted into an immunocompromised host. scRNA-seq revealed that Schwann cells, pericytes/smooth muscle, tenocytes, and satellite cells comprise the PNC population. These results provide evidence for an additional causal cell of HO housed within the PNC population. The additional causal cell(s) of HO may potentially contribute to the greater HO response observed in the spontaneous HO model.

2.3 Materials and Methods

2.3.1 Genetic mouse models and mouse crosses

The accurate, Cre-dependent, knockin mouse model of FOP (*Acvr1*$^{tnR206H/+}$) is described previously (Section 2.1) (Lees-Shepard et al., 2018b). The Tie2-Cre driver was a generous gift from Dr. Tom Sato (UT Southwestern) (Kisanuki et al., 2001)**.** The Pdgfra-Cre was purchased from Jackson Laboratories (stock #013148) (Roesch et al., 2008). The *Pdgfra*^{CreER} driver was a kind gift from Dr. Brigid Hogan (Duke University) (Eisner et al., 2020). Two Cre-dependent fluorescent reporters under the control of the endogenous *Rosa26* machinery, *R26*^{NG} (Yamamoto et al., 2009) and *R26*^{mCherry} (stock #023139) (Peron et al., 2015), were used to permanently label cells where Cre-recombinase was active. The *Pdgfra*$^{H2B-GFP}$ reporter was purchased from Jackson Laboratories (stock #007669) (Hamilton et al., 2003). Mice were genotyped by PCR and, when applicable, by the presence or absence of fluorescence reporters (see Appendix IB). Immunocompromised mice (SCIDs) were used in osteogenic transplantation assays and purchased from Charles River (stock #474-SHO).

Experimental mice used in injury assays, flow cytometry, and transplantations were generated by crossing *Acvr1*$^{tnR206H/+}$ females with *R26*$^{NG/+}$ males. The resulting *Acvr1*$^{tnR206H/+}$;*R26*$^{NG/+}$ females were then mated with either with Tie2-Cre, Pdgfra-Cre, or *Pdgfra*^{CreER} males to produce *Acvr1*$^{tnR206H/+}$;*R26*$^{NG/+}$;Tie2-Cre, *Acvr1*$^{tnR206H/+}$;*R26*$^{NG/+}$;Pdgfra-Cre, or *Acvr1*$^{tnR206H/+}$;*R26*$^{NG/+}$;*Pdgfra*$^{CreER/+}$ mice. Mice used in the scRNA-seq, cell culture assays, and the histological analysis were generated by mating *Pdgfra*$^{H2B-GFP/+}$ females with *R26*$^{mCherry/+}$ males. The resulting *Pdgfra*$^{H2B-GFP/+}$;*R26*$^{mCherry/+}$ females were mated with Pdgfra-Cre males to produce *Pdgfra*$^{H2B-GFP/+}$;*R26*$^{mCherry/+}$;Pdgfra-Cre experimental mice. Offspring of all matings were viable and thrifty. Male and female mice were used equally, and all procedures were approved by the University of Connecticut Animal Care Committee in accordance with IACUC. Mice were held and maintained in a climate-controlled vivarium at the University of Connecticut.

2.3.2 Tamoxifen dosing

Tamoxifen (Sigma Aldrich, #T5648; St. Louis, MO, USA) was prepared as a 50 mg/mL stock in corn oil (Sigma Aldrich, #C8267) and administered via intraperitoneal injection (IP) at a 5 mg dose to induce recombination of the Acvr*1*^{tnR206H} allele in 4 week-old *Acvr1*$^{tnR206H/+}$;*R26*$^{NG/+}$;*Pdgfra*$^{CreER/+}$ mice. Recombination of the Acvr*1*^{tnR206H} allele in *Acvr1*$^{tnR206H/+}$;*R26*$^{NG/+}$;*Pdgfra*$^{CreER/+}$pups from 2 days post birth to 7 days post birth (P2 to P7) was accomplished via tamoxifen delivery through their mother's milk. Mothers were dosed with 5 mg of tamoxifen via IP injection for 5 days, starting 2 days after birth and continuing for 5 consecutive days. Weans occurred 28 days after birth to allow pups to thrive.

2.3.3 Pinch injury of distal hindlimbs

Mice were anesthetized via isoflurane and placed on their ventral side. Both heads of the gastrocnemius (GA) muscle were pinched at 4000g of force using a Randall Selitto Paw Pressure Test Apparatus (IITC Life Science; Woodland Hills, CA) (Burdick et al., 2024). µCT images were acquired at 7, 10, 14, and 21 days post-injury using an IVIS Spectrum-CT under medium resolution (75 µm voxel size; estimated radiation dose of 132 mGy; 210 scan time). 3D Slicer V5.2 software (www.slicer.org) was used to segment and quantify HO volume (mm^3).

2.3.4 Skeletal muscle dissociation and FACS preparation

Mice were sacrificed via cervical dislocation and hindlimb muscles were dissected and placed in a 35 mm dish that contained approximately 100 µL of digestion media, Dulbecco's Modified Eagle Medium (DMEM; Thermo Fisher; Waltham, MA, USA), 600–700 U/mL Collagenase Type II (Worthington Biochemical; Lakewood, NJ, USA), and 0.5 U/mL Dispase (Thermo Fisher; Waltham, MA, USA). Muscle was minced with scissors for 8– to 10- minutes and then placed at 37°C for 1 hour, with gentle agitation every 10 minutes. Digestion was then quenched with quench media (DMEM containing 10% HyClone characterized fetal bovine serum (FBS; GEHealthcare, Lot #A00168; Chicago, IL, USA)) and filtered through 70 mm mesh cell strainers (Corning Life Sciences; Tewksbury, MA, USA). Single-cell suspensions are then spun at 500g for 5 minutes at 4°C. Pellets were washed in 1X Dulbecco's phosphate-buffered saline (DPBS; Gibco; Grand Island, NY, USA), spun down, and resuspended in blocking buffer (1X DPBS supplemented with 10% FBS). Antibodies were added in optimal concentrations (see Appendix IB) and incubated for 1 hour on ice in low light conditions. Samples were spun

down, washed with 1X DPBS, resuspended in FACS Buffer (DPBS supplemented with 2% FBS), and filtered through FACS tubes with a 35 µm cell strainer (Corning Life Sciences; Tewksbury, MA). Samples were brought to the University of Connecticut Flow Cytometry Facility where target populations were analyzed using a BD LSRFortessa X-20 Cell Analyzer equipped with 5 lasers (355nm, 405nm, 488nm, 561nm, and 640nm) or collected using a BD FACSAria II Cell Sorter equipped with 5 lasers (355nm, 405nm, 488nm, 561nm, and 640nm).

2.3.5 Cell culturing conditions

Samples were seeded at a 2500 – 3000 cells/cm^2 seeding density and were placed in growth media composed of 20% FBS (R&D Systems, Lot #C19032; Minneapolis, MN, USA) in DMEM supplemented with 50 U/mL penicillin and 50 µg/mL streptomycin (Pen/Strep; Gibco, Grand Island, NY, USA) and 2.5 ng/mL recombinant Human Fibroblastic Growth Factor (bFGF; Gibco, Grand Island, NY, USA) on rat tail collagen I (Invitrogen; Carlsbad, CA, USA) coated plates and incubated at 37°C with 5% CO2. Cells were trypsinized and split when 70%-80% confluency was reached.

2.3.6 Transplantations of PNC and FAPs

PNCs or FAPs were cultured until sufficient cell numbers were reached. Cells were detached, counted, and resuspended in 1X DPBS in a 1 x 10^6 cell per 50 µL concentration. Each population, respectively, PNCs or FAPs, were transplanted into a pre-injured GA muscle of a SCID host. Crush injury to the SCID host GA muscle was performed using serrated forceps to avoid breaking or tearing of the skin and occurred

directly before transplanting the PNC or FAP populations. HO was determined and quantified as explained in Section 2.3.3.

2.3.7 Histological analysis of PNC transplantations

Limbs were collected and fixed in 4% paraformaldehyde (PFA) in 1X DPBS and placed at 4°C for 3 days with constant agitation. Samples were washed with DPBS, and a decalcification step was performed to remove the calcium ions of the endogenous skeleton and newly formed HO. Decalcification was obtained by incubating samples in decal solution (12.5% ethylenediaminetetraacetic acid (EDTA) with 1% sodium hydroxide in 1X DPBS) for a month, and the solution was replaced every other day. Once decalcification was completed, samples were washed with 1X PBS and placed in a cytoprotectant solution containing 30% sucrose in 1X PBS overnight. Protected samples were flash frozen in Tissue-Tek O.C.T. compound (O.C.T.; Thermo Fisher; Waltham, MA, USA) using a dry-ice and ethanol slurry. Samples were stored at -80°C until sectioning. Samples were then sectioned using a Leica cryostat (CM3050S) at 10 µm thickness, and slides were stored at -20°C. Sections were counterstained with 10 µg/mL DAPI (Sigma-Aldrich, St Louis, MO, USA) and coverslipped using FluoroGel mounting medium (Electron Microscopy Sciences; Hatfield, PA, USA). Sections were analyzed using a Leica Thunder imaging platform at UCONN's Advanced Light Microscopy COR2E.

2.3.8 Hematoxylin and eosin (H&E) staining

Sections were incubated at room temperature for 20 minutes and rehydrated in nanopure water, washing away the O.C.T. Sections were placed in Mayer’s

hematoxylin (Sigma-Aldrich; St. Louis, MO, USA) for 8 minutes. After hematoxylin staining, sections were placed in a 2% ammonium bluing solution and dehydrated using increasingly concentrated ethanol solutions. Samples were placed in eosin Y (Sigma-Aldrich; St. Louis, MO, USA) for 5 seconds. Excess eosin Y was washed away with 95% ethanol washes. Sections were fully dehydrated using 100% ethanol and xylene. Slides were mounted using Permount, mounting medium (Thermo Fisher; Waltham, MA, USA), and imaged using the Leica Thunder imaging platform the following day**.**

2.3.9 In vitro fixation and staining

Cells were isolated via FACS, plated on rat tail collagen 1 coated dishes, and grown in growth media to approximately 70-80% confluency with media changes every other day. Cells were washed in 1X DPBS, fixed with 4% PFA for 10 minutes at room temperature, and washed in 1X DPBS. Cells were counterstained with 10 µg/mL DAPI and imaged using a Nikon Eclipse E600 microscope with a Retiga e7 camera.

2.3.10 Single-cell RNA-sequencing cell isolation and library prep

Pdgfra$^{H2B\text{-}GFP/+}$*;R26*$^{mCherry/+}$*;*Pdgfra-Cre mice were sacrificed at 4-weeks-of-age. A muscle biopsy from the GA was collected and digested as previously described in Section 2.3.5 with minor modifications based on Chromium 10X Genomics recommendations. Changes were as follows: samples were incubated in digest media at 37°C for 30 minutes, with gentle vortexing or agitation every 5 minutes (as opposed to a 1-hour incubation previously). Cells were collected using a BD FACSAria II Cell Sorter with 5 lasers (355nm, 405nm, 488nm, 561nm, and 640nm). Collected samples were centrifuged

at 500g for 5 min at 4°C and resuspended in 1X DPBS at a 1000 cells/µL concentration. Samples were brought to the UCONN Center for Genome Innovation (UCONN CGI; Storrs, CT, USA). cDNA libraries were made using the 10x Genomics Chromium Single Cell 3' Library Kit Version 3.1. Cells were loaded on the 10x Chromium Genomics fluidics platform. Libraries were sequenced with roughly 400 million, 75 base pair reads per sample using the Novaseq 600 Illumina platform (Illumina; San Diego, CA, USA).

2.3.11 Single-cell RNA-sequencing analysis and processing

Basecall files were uploaded from baseSpace to the University of Connecticut Xanadu server. A custom genome was built using the Cell Ranger pipeline, where the mm10 genome was modified to include the *Pdgfra*$^{H2B\text{-}GFP}$ and *R26*^{mCherry} DNA sequences. The Cell Ranger pipeline was used to generate FastQ files, demultiplex the sample, map reads to a custom genome containing fluorescent reporters, count the transcripts with unique molecular identifiers (UMIs), and filter out droplets that did not contain cells (Zheng et al., 2017). The Cell Ranger pipeline produced the final count matrices of the sequenced samples. The count matrices were further analyzed using the Seurat V4 pipeline (Hao et al., 2021). Briefly, the count matrices were filtered by removing damaged cells, cells containing less than 500 genes, or cells containing greater than 10% mitochondrial content. The data was then log-normalized, and cell cycle genes were removed from the sample. The top 5000 differentially expressed features were used to identify and run Principal Component Analysis (PCA), Jackstraw plots, elbow plots, and various unsupervised clustering algorithms to determine the number of principal components for downstream analysis. 20 PCs were chosen, and the top 50 differentially expressed genes were used for cluster identification.

2.3.12 Statical analysis

Statistical analysis was performed using GraphPad Prism (GraphPad; La Jolla, CA, USA). All numerical values are presented as mean values ± standard error of the mean. Differences were considered significant at $p \leq 0.05$.

2.4 Results

2.4.1 Comparative analysis of HO formation in injury-induced and spontaneous HO models

The spontaneous HO model develops HO of the jaw by 6-weeks-of-age, ultimately leading to ankylosing of the jaw and premature death (Lees-Shepard et al., 2018b). In contrast, the injury-induced HO model has historically been used at 8- to 12-weeks-of-age (Lees-Shepard et al., 2018b). We were curious whether the spontaneous HO and injury-induced HO model still display distinct injury-induced HO responses at the same developmental age. To avoid HO of the jaw and allow for a direct age-matched comparison between models, we pinch-injured the GA muscle of Acvr*1*$^{tnR206H/+}$;Pdgfra-Cre and *Acvr1*$^{tnR206H/+}$;Tie2-Cre mice at 3-weeks-of-age. HO was quantified at 14 days post-injury. *Acvr1*$^{tnR206H/+}$;Pdgfra-Cre mice displayed a more robust HO response than *Acvr1*$^{tnR206H/+}$;Tie2-Cre mice (Figure 2.1B and Figure 2.1C). On average *Acvr1*$^{tnR206H/+}$;Pdgfra-Cre mice formed over 50 mm^3 more injury-induced HO compared to *Acvr1*$^{tnR206H/+}$;Tie2-Cre mice (Figure 2.1F).

To account for the formation of spontaneous HO in *Acvr1*$^{tnR206H/+}$;Pdgfra-Cre mice before the pinch injury, potentially inflating the quantification of injury-induced HO, a cohort of control mice, including both *Acvr1*$^{tnR206H/+}$;Pdgfra-Cre and *Acvr1*$^{tnR206H/+}$;Tie2-Cre mice that received no injury were included in the study. No spontaneous HO was observed in *Acvr1*$^{tnR206H/+}$;Tie2-Cre mice (Figure 2.1D). *Acvr1*$^{tnR206H/+}$;Pdgfra-Cre mice exhibited spontaneous HO, associated with the joints and fused with the endogenous skeleton (Figure 2.1E). In summary, *Acvr1*$^{tnR206H/+}$;Pdgfra-Cre mice exhibit a more robust

HO response than *Acvr1*$^{tnR206H/+}$;Tie2-Cre mice when pinch-injured at the same developmental age.

Figure 2.1

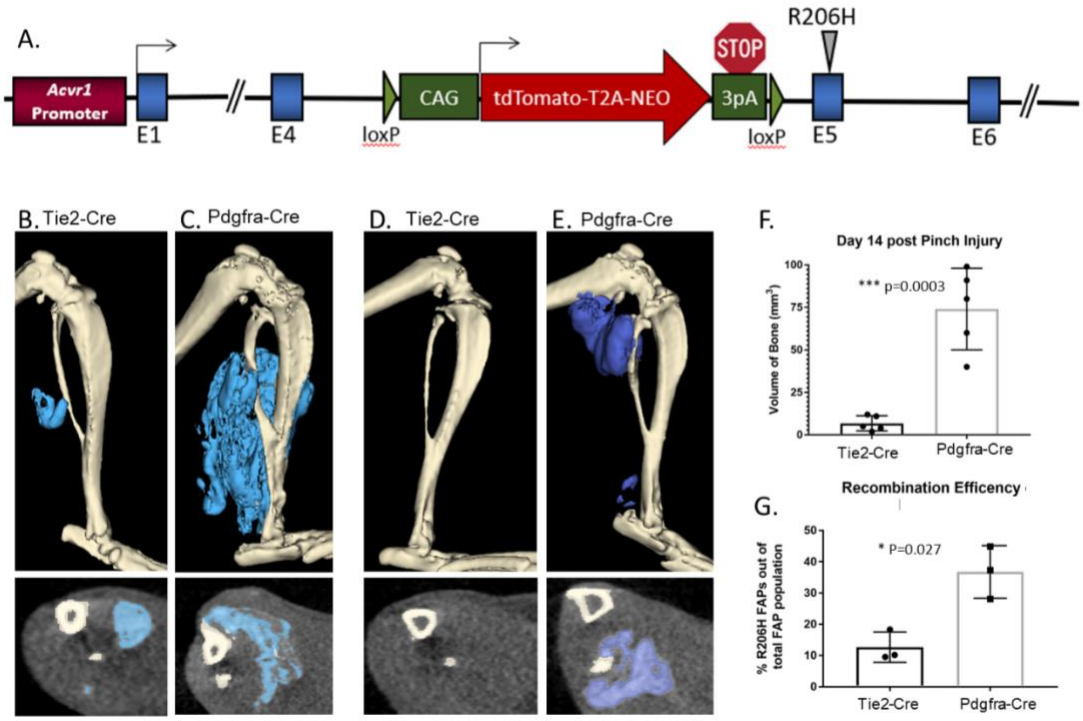

Figure 2.1: HO responses of the injury-induced HO and spontaneous HO models

A. Conditional, knockin, Cre-dependent *Acvr1*^{tnR206H} allele construct. **B-C.** Representative mCT images of *Acvr1*$^{tnR206H/+}$;Tie2-Cre (**B**, N=5) and *Acvr1*$^{tnR206H/+}$;Pdgfra-Cre (**C**, N=5) mice 14 days after pinch-injury to the GA. Cross-sections of lesional tissue are shown below distal hindlimb images. The exogenous HO is pseudo-colored blue. The endogenous skeleton is pseudo-colored white. **D-E.** Representative mCT images of spontaneous HO observed at 6-weeks-of-age from uninjured *Acvr1*$^{tnR206H/+}$;Tie2-Cre (**D**, N=4) or *Acvr1*$^{tnR206H/+}$;Pdgfra-Cre mice (**E**, N=4). Cross-sections of lesional tissue are shown below the distal hindlimb images. The exogenous HO is pseudo-colored in dark blue. The endogenous skeleton is pseudo-colored white. **F.** Quantification of HO volume (mm^3) formed in *Acvr1*$^{tnR206H/+}$;Tie2-Cre or *Acvr1*$^{tnR206H/+}$;Pdgfra-Cre mice 14 days post-pinch-injury. **G**. Recombination efficiency of the Tie2-Cre (N=3) or Pdgfra-Cre (N=3) of FAPs determined by flow cytometry. FAPs were determined by PDGFRa and SCA1 expression. Recombined FAPs were determined via lack of tdTomato fluorescence and dual expression of PDGFRa and SCA1. An unpaired t-test determined statistical significance. * $p < 0.05$; ** $p < 0.01$; *** $p < 0.002$.

2.4.2 The spontaneous HO model has a higher recombination efficiency

The first factor tested to explain the difference in injury-induced HO responses between the spontaneous and injury-induced HO models was the recombination efficiency of the Pdgfra-Cre and Tie2-Cre. The efficiency of a Cre-driver to recombine the *Acvr1*^{tnR206H} allele could directly impact the amount of bone that can potentially form. Historically, the Pdgfra-Cre driver displayed a higher recombination efficiency than the Tie2-Cre driver, 30%-40% versus 10%-15%, respectively; however, different ages of mice were tested. To test the recombination efficiency of both the Pdgfra-Cre and Tie2-Cre at recombining the *Acvr1*^{tnR206H} allele at a consistent developmental age flow cytometry was performed on 4-week-old *Acvr1*$^{tnR206H/+}$;Pdgfra-Cre and *Acvr1*$^{tnR206H/+}$;Tie2-Cre mice. We tested the recombination status of the *Acvr1*^{tnR206H} allele in FAPs, which were defined as CD31-;CD45-;PDGFRa+;SCA1+ cells (Lees-Shepard et al., 2018b; Woscznya et al., 2012; Biswas and Goldhamer., 2016).

The tdTomato fluorescent reporter within the *Acvr1*^{tnR206H} construct allows for the identification of unrecombined (*Acvr1*^{tnR206H}-expressing) and recombined (*Acvr1*^{R206H}-expressing) cells. The recombination status of the *Acvr1*^{tnR206H} allele in FAPs was determined by assessing what percentage of tdTomato-negative cells were present within the total FAP population. The recombination efficiency of the Pdgfra-Cre and Tie2-Cre was found to be 37% and 13%, respectively (Figure 2.1G). The greater recombination efficiency of the spontaneous HO model could partly explain the robust HO response.

2.4.3 The PNC population is present within the spontaneous HO model

Neither Pdgfra-Cre nor Tie2-Cre will specifically recombine the *Acvr1*^{tnR206H} allele to FAPs. We hypothesized that recombined cells, distinct from FAPs, may contribute to the heightened HO response observed in *Acvr1*$^{tnR206H/+}$;Pdgfra-Cre mice. To label cells where the *Acvr1*^{tnR206H} allele was recombined, we employed a Cre-dependent fluorescent reporter, *R26*^{NGn} (Yamamoto et al., 2009). The *R26*^{NG} allele permanently labels cells with

GFP fluorescence if Tie2-Cre or Pdgfra-Cre was active at any point in the cells' developmental lifetime. Flow cytometry was performed on 4-week-old *Acvr1*$^{tnR206H/+}$;*R26*$^{NG/+}$;Pdgfra-Cre and *Acvr1*$^{tnR206H/+}$;*R26*$^{NG/+}$;Tie2-Cre mice. The flow scheme used is outlined in Figure 2.2A. Endothelial (CD31+) and hematopoietic (CD45+) cells were removed as their lack of osteogenic ability has previously been observed (Woscznya et al., 2012). Recombined cells were identified through the absence of tdTomato fluorescence coupled with the presence of the GFP fluorescence. FAPs, CD31-;CD45-;PDGFRa+ cells, were present within the recombined population in *Acvr1*$^{tnR206H/+}$;*R26*$^{NG/+}$;Pdgfra-Cre and *Acvr1*$^{tnR206H/+}$;*R26*$^{NG/+}$;Tie2-Cre mice (Figure 2.2B and Figure 2.2C – yellow box). Within the recombined population of cells from *Acvr1*$^{tnR206H/+}$;*R26*$^{NG/+}$;Pdgfra-Cre mice, a subset of cells that lack PDGFRa expression was observed (compare Figure 2.2B to Figures 2.2C- green box). We called this population of cells PDGFRa-Negative Cells (PNCs) (Figure 2.2C- green box). The PNCs must have expressed *Pdgfr*a at some stage of their development lifetime to be recombined by the Pdgfra-Cre; however, the PNCs have since downregulated PDGFRa expression, differentiating PNCs from FAPs.

Figure 2.2

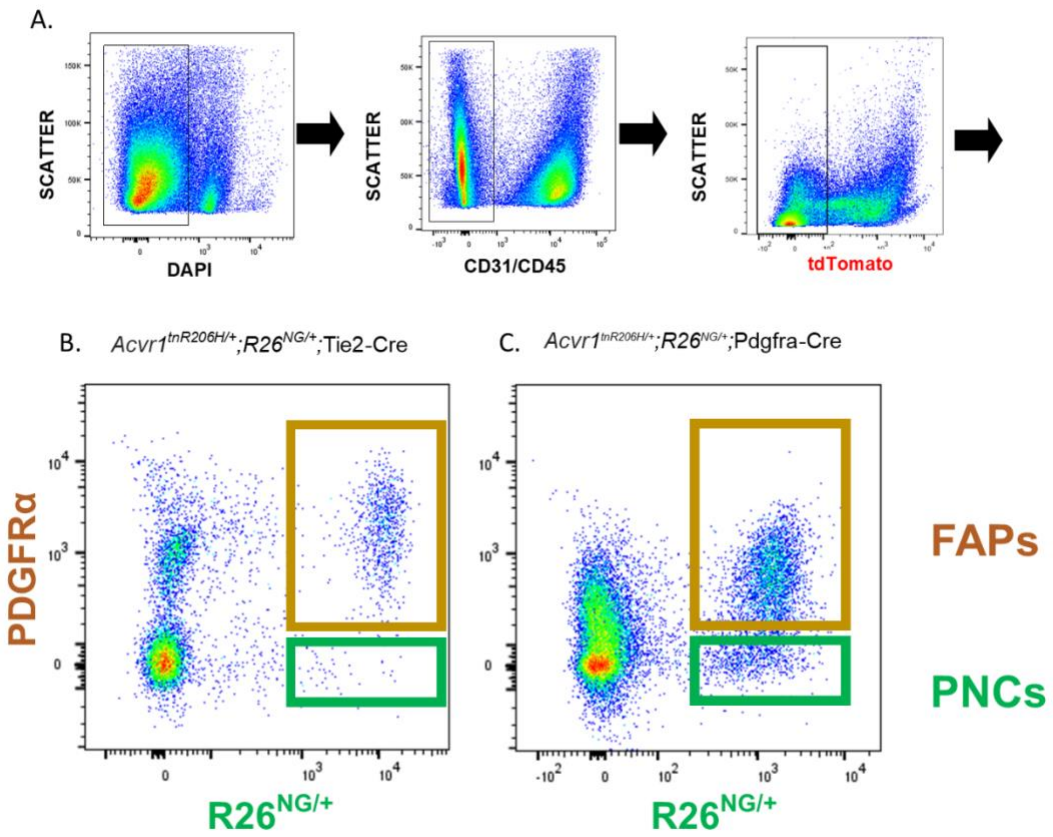

Figure 2.2: Identification of the PNC population via flow cytometry

A. Flow cytometry gating strategy used to eliminate dead, CD31+, CD45+ , and unrecombined cells within 4-week-old *Acvr1*$^{tnR206H/+}$;*R26*$^{NG/+}$;Tie2-Cre (N=3) or *Acvr1*$^{tnR206H/+}$;*R26*$^{NG/+}$;Pdgfra-Cre (N=3) mice. **B-C.** The absence or presence of the PNC population (green boxes) or FAPs (yellow boxes) within the recombined cell population of *Acvr1*$^{tnR206H/+}$;*R26*$^{NG/+}$;Tie2-Cre (**B.** N=3) or *Acvr1*$^{tnR206H/+}$;*R26*$^{NG/+}$;Pdgfra-Cre (**C.** N=3) mice.

2.4.4 The PNC population does not contain FAPs

We wanted to explore whether the PNC population, which was identified by the lack of PDGFRα expression, are FAPs that have downregulated PDGFRα. In order to recombine the *Acvr1*^{tnR206H} allele in solely PDGFRα-expressing cells, we utilized a temporally inducible Cre-driver, *Pdgfra*^{CreER} (Eisner et al., 2020). Only in the presence of tamoxifen can the Cre^{ER} enter the nucleus and subsequently recombine the *Acvr1*^{tnR206H} allele. Only cells actively expressing *Pdgfra* during tamoxifen administration will be recombined. *Acvr1*$^{tnR206H/+}$;*R26*$^{NG/+}$;*Pdgfra*$^{CreER/+}$ mice were administrated tamoxifen at 4-weeks-of-age. If the PNC population arises from FAPs downregulating PDGFRα expression, we would expect to observe a population of cells that are recombined (tdTomato-;GFP+) and devoid of current PDGFRα expression. Flow cytometry revealed that FAPs but not tdTomato-;GFP+;PDGFRα- cells are present within the recombined population (Figure 2.3A). Therefore, the PNC population is not comprised of FAPs that have downregulated PDGFRα expression (Figure 2.3A- green box).

Acvr1$^{tnR206H/+}$;*R26*$^{NG/+}$;*Pdgfra*$^{CreER/+}$ mice dosed at 4-weeks-of-age were pinch injured, and HO was observed 14 days post-injury (Figure 2.3B). It is assumed that FAPs are the cells contributing to the HO response. Notably, the volume of bone growth observed in *Acvr1*$^{tnR206H/+}$;*R26*$^{NG/+}$;*Pdgfra*$^{CreER/+}$ mice dosed at 4-weeks-of-age resembled that of *Acvr1*$^{tnR206H/+}$;*R26*$^{NG/+}$;Tie2-Cre mice rather than *Acvr1*$^{tnR206H/+}$;*R26*$^{NG/+}$;Pdgfra-Cre mice (compare Figure 2.1B to Figure 2.3B). However, a direct comparison of the three models was not performed.

In an attempt to capture when the PNC population would begin to emerge, the recombination of the *Acvr1*^{tnR206H} allele through *Pdgfra*^{CreER} activity was induced at an earlier developmental time point. *Acvr1*$^{tnR206H/+}$;*R26*$^{NG/+}$;*Pdgfra*$^{CreER/+}$ pups, referred to as P2-dosed mice, were exposed to tamoxifen through their mother's milk from 2 days postnatally to 7 days postnatally. Tamoxifen-dosed pups were thrifty and developed as expected. P2-dosed *Acvr1*$^{tnR206H/+}$;*R26*$^{NG/+}$;*Pdgfra*$^{CreER/+}$ mice were pinch injured at 4-weeks-of-age and bone was observed 14 days later (Figure 2.3D). The HO formed was lineage labeled, supporting that the HO was derived from R206H-expressing cells (Figure

2.3C). Like mice that were dosed at 4-weeks-of-age, the volume of HO formed in P2-dosed *Acvr1*$^{tnR206H/+}$;*R26*$^{NG/+}$;*Pdgfra*$^{CreER/+}$ mice was more similar to the HO response of *Acvr1*$^{tnR206H/+}$;*R26*$^{NG/+}$;Tie2-Cre mice (compare the volume of HO in Figure 2.3D to Figure 2.1B). Flow cytometry did not detect the PNC population in 4-week-old P2-dosed mice (Figure 2.3E – green box), suggesting that the PNC population downregulates PDGFRa expression earlier than 2 days after birth.

P2-dosed *Acvr1*$^{tnR206H/+}$;*R26*$^{NG/+}$;*Pdgfra*$^{CreER/+}$ mice rarely showed spontaneous HO (2/9 scored), while no spontaneous HO was observed in mice dosed at 4-weeks-of-age. Spontaneous HO observed in P2-dosed *Acvr1*$^{tnR206H/+}$;*R26*$^{NG/+}$;*Pdgfra*$^{CreER/+}$ mice was an outgrowth of tuberosities of the forelimbs (Figure 2.3F – white arrow), while the spontaneous HO observed in *Acvr1*$^{tnR206H/+}$;*R26*$^{NG/+}$;Pdgfra-Cre mice displayed a greater volume of HO and were located more so in the joints of the forelimbs and hindlimbs, back, and jaw.

FAPs are recombined in *Acvr1*$^{tnR206H/+}$;*R26*$^{NG/+}$;*Pdgfra*$^{CreER/+}$ mice when Cre activity is induced at 4 weeks and 2-7 days postnatally. The PNC population downregulates PDGFRα expression earlier than 2 days postnatally. The HO response of *Acvr1*$^{tnR206H/+}$;*R26*$^{NG/+}$;*Pdgfra*$^{CreER/+}$ mice was like that of an *Acvr1*$^{tnR206H/+}$;*R26*$^{NG/+}$;Tie2-Cre animal. Given the lack of the PNC population and the volume of HO formed in 4-week and P2-dosed mice, we hypothesize that the PNC population could be contributing to the greater HO response observed in the *Acvr1*$^{tnR206H/+}$;Pdgfra-Cre model.

Figure 2.3

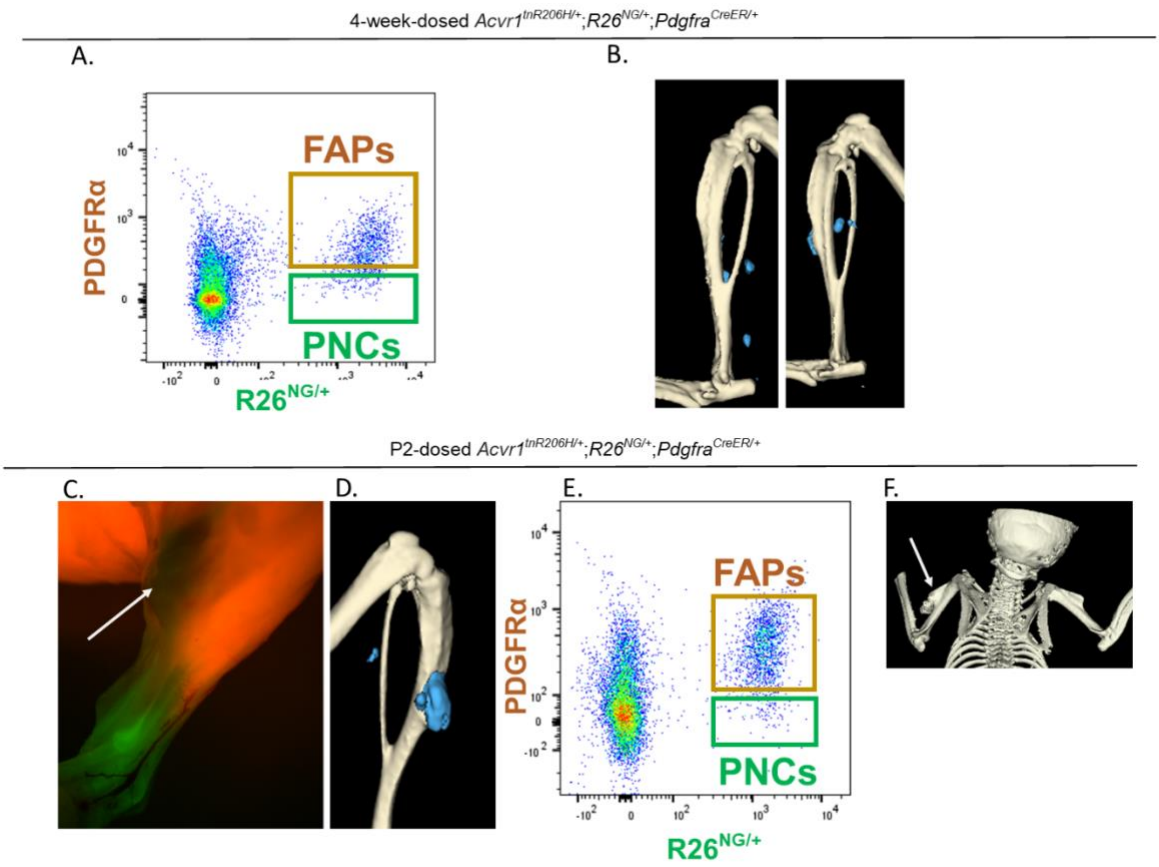

Figure 2.3: *Acvr1*$^{tnR206H/+}$;*R26*$^{NG/+}$;*Pdgfra*$^{CreER/+}$ mice do not contain the PNC population.

A. Recombined cells of *Acvr1*$^{tnR206H/+}$;*R26*$^{NG/+}$;*Pdgfra*$^{CreER/+}$ mice, dosed with tamoxifen at 4-weeks-of-age, contain FAPs (yellow box) and not the PNC population (green box) **B**. Representative images of HO formation of 4-week dosed *Acvr1*$^{tnR206H/+}$;*R26*$^{NG/+}$;*Pdgfra*$^{CreER/+}$ mice 14 days post-pinch injury to the GA (N=7). **C.** Fluorescent whole-mount images showing injury-induced HO of P2-dosed *Acvr1*$^{tnR206H/+}$; *R26*$^{NG/+}$;*Pdgfra*^{CreER}/+ mice. The white arrow indicates HO that is pseudo-colored blue in D. **D.** Representative mCT image of HO 14 days post-pinch injury of P2-dosed *Acvr1*$^{tnR206H/+}$; *R26*$^{NG/+}$;*Pdgfra*$^{CreER/+}$ mice (N=12). **E.** Recombined cells of P2-P7 dosed *Acvr1*$^{tnR206H/+}$;*R26*$^{NG/+}$;*Pdgfra*$^{CreER/+}$ mice contain FAPs (yellow box) and not the PNC population (green box) **F.** Representative mCT image of P2 dosed *Acvr1*$^{tnR206H/+}$;*R26*$^{NG/+}$;*Pdgfra*$^{CreER/+}$ mice that formed spontaneous HO (white arrow).

2.4.5 The PNC population displays a cell-autonomous osteogenic response

We were interested in whether the PNC population contained any osteocompetent cells. *Acvr1*^{tnR206H}-expressing PNC (R206H-PNC) was tested for cell-autonomous osteogenic capabilities through a transplantation assay. *Acvr1*^{tnR206H}-expressing FAPs (R206H-FAPs) were used as a positive control. R206H-PNCs and R206H-FAPs were FACS isolated from 4-week-old *Acvr1*$^{tnR206H/+}$;*R26*$^{NG/+}$;Pdgfra-Cre mice as previously described (Figure 2.2A and Figure 2.4A) and cultured for 14 days. The R206H-PNC and R206H-FAP populations were cultured, and 1 x 10^6 cells of each population were transplanted into separate GA muscles of the same SCID host (Figure 2.4A). HO was quantified 14 days post-transplantation (Figure 2.4B, Figure 2.4C, and Figure 2.4F). R206H-PNC derived HO was lineage labeled (Figure 2.4D and Figure 2.4E), which confirmed that the PNC population houses an osteocompetent cell type.

Figure 2.4

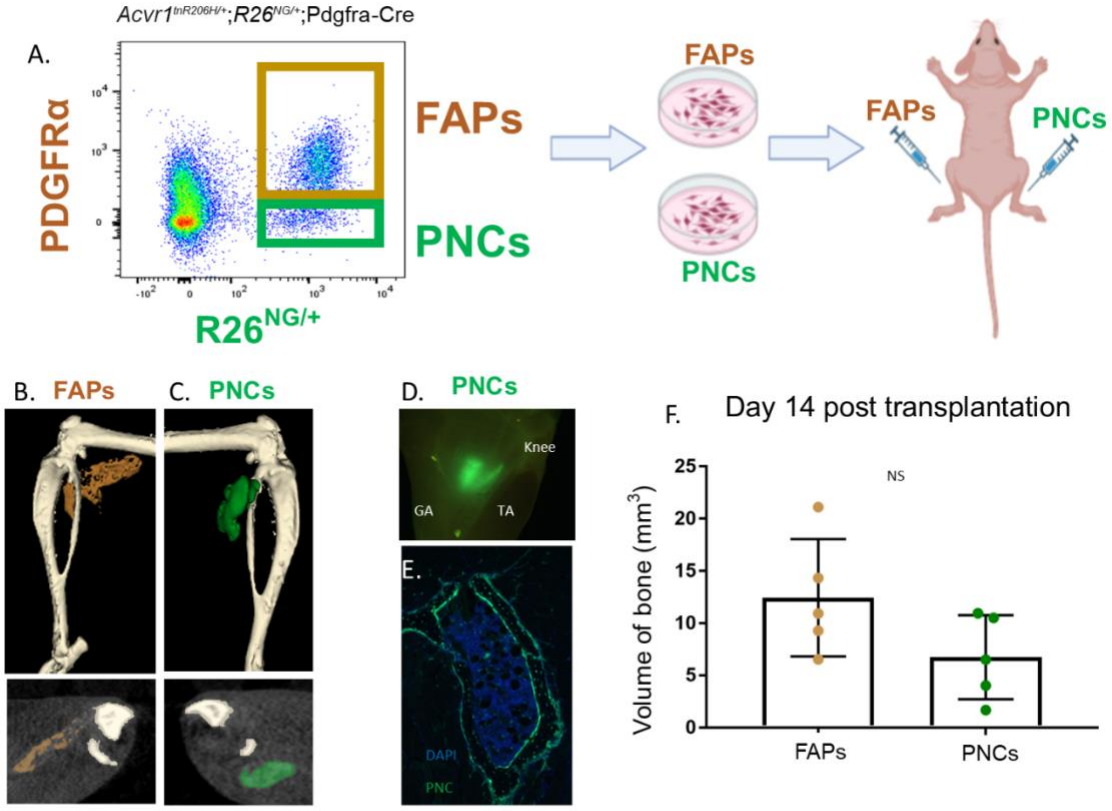

Figure 2.4: The PNC population displays a cell-autonomous osteogenic response

A. Experimental overview of the transplantation assay. PNC (green box) and FAP (yellow box) populations were isolated via FACS from *Acvr1*$^{tnR206H/+}$;*R26*$^{NG/+}$;Pdgfra-Cre mice and placed in culture. After two weeks of culturing, 1x10^{6} cells of each population were transplanted into separate GA muscles of a SCID host (N=5 of each population). **B-C.** Representative mCT images of bone growth at 14 days post-transplantation. Cross-sections of HO lesions are below mCT scans. R206H-FAP-derived HO is pseudo-colored yellow (**B**). R206H-PNC-derived HO is pseudo-colored green (**C**). **D.** Fluorescent whole-mount representative images confirming HO the presence of R206H-PNC-derived HO**E.** Cross-section of bone lesion displaying R206H-PNC-derived HO. **F.** Quantification of bone volume (mm^{3}) of R206H-FAP and R206H-PNC-derived HO 14 days post-transplantation. Statistical significances were determined by an unpaired t-test. NS = not significant

2.4.6 The characterization of PDGFRa expression within the PNC and FAP population

FAPs downregulate PDGFRa prior to differentiation along the endochondral ossification pathway (unpublished data). We were interested in whether the PNC population continues downregulating PDGFRa prior to osteogenesis. R206H-PNC and R206H-FAP populations were collected from *Acvr1*$^{tnR206H/+}$;*R26*$^{NG/+}$;Pdgfra-Cre mice (Figure 2.5A) and cultured for 14 days. 1x10^{6} R206H-PNCs and R206H-FAPs were transplanted into separate GAs of a SCID host, as previously described (Figure 2.4A). Five days after transplantation, the SCID host GAs were collected, and PDGFRa expression of the transplanted R206H-PNCs and R206H-FAPs was assessed via flow cytometry (Figure 2.5A). Transplanted R206H-PNCs and R206H-FAPs were identified by GFP fluorescence. The majority of the transplanted R206H-FAPs downregulated PDGFRa expression, and a subset of R206H-FAPs (approximately 25% of FAPs) continued to express PDGFRa 5 days post-transplantation (Figure 2.5A). The differentiation of FAPs along the endochondral ossification pathway is not a synchronized process. Thus, FAPs within the same transplanted population may be initiating the endochondral ossification pathway at varying times, potentially explaining the heterogeneity of PDGFRa expression within the transplanted R206H-FAP population. Surprisingly, a subset of transplanted R206H-PNCs upregulated PDGFRa (approximately 20% of transplanted PNCs) (Figure 2.5A). The heterogeneity of the PNC population is unknown, but we hypothesize many cell types to be present, which potentially could explain the variation in PDGFRα expression post-transplantation.

For the following experiments, the *Acvr1*$^{tnR206H/+}$;*R26*$^{NG/+}$;Pdgfra-Cre mouse model was replaced with a dual fluorescent reporter system, *Pdgfra*$^{H2B\text{-}GFP/+}$;*R26*$^{mCherry/+}$;Pdgfra-Cre. This system will fluorescently label cells that currently and historically express *Pdgfr*a through GFP (Figure 2.5B) and mCherry fluorescence (Figure 2.5C), respectively. *Pdgfra*$^{H2B\text{-}GFP}$ is a fluorescent reporter created by knocking in an H2B-eGFP fusion gene into the native *Pdgfra* locus (Hamilton et al., 2003). Thus, cells expressing *Pdgfra* are labeled by GFP fluorescence (Figure 2.5B).

The *R26*^{mCherry} reporter is a Cre-dependent reporter, where a *loxP*-flanked STOP sequence followed by an H2B-mCherry fusion protein was inserted into the *Rosa26* locus (Figure 2.5C) (Peron et al., 2015). Cre-recombinase will recognize the floxed stop cassette and permanently excise the DNA between them. The Pdgfra-Cre driver, in which Cre-recombinase is under the control of the Pdgfra promoter, enables cells that have expressed *Pdgfra* at any point during their lifetime to express the recombined *R26*^{mCherry} allele (Figure 2.5C). The PNC population will be labeled by *R26*^{mCherry} fluorescence, and FAPs will be labeled by *Pdgfra*$^{H2B\text{-}GFP}$ and *R26*^{mCherry} fluorescence. There is no documentation that the expression of the R206H mutation influences the presence or absence of *Pdgfra* expression; therefore, there should be no difference in the composition of cell types comprising the PNC population between *Acvr1*$^{tnR206H/+}$;*R26*$^{NG/+}$;Pdgfra-Cre and *Pdgfra*$^{H2B\text{-}GFP/+}$;*R26*$^{mCherry/+}$;Pdgfra-Cre mice.

The transplantation of PNCs requires a culturing step prior to transplanting the PNC population. To determine the stability of *Pdgfra* expression in culture, PNCs were FACS isolated from 4-week-old *Pdgfra*$^{H2B\text{-}GFP/+}$;*R26*$^{mCherry/+}$;Pdgfra-Cre mice and cultured. Many morphologies were observed when cells were cultured, which suggested that the PNCs are a heterogeneous population (Figure 2.5D). The upregulation of *Pdgfra* expression within the PNC population was determined by *Pdgfra*$^{H2B\text{-}GFP}$ fluorescence. The PNC population downregulated *Pdgfra* until 21 days in culture (Figure 2.5E).

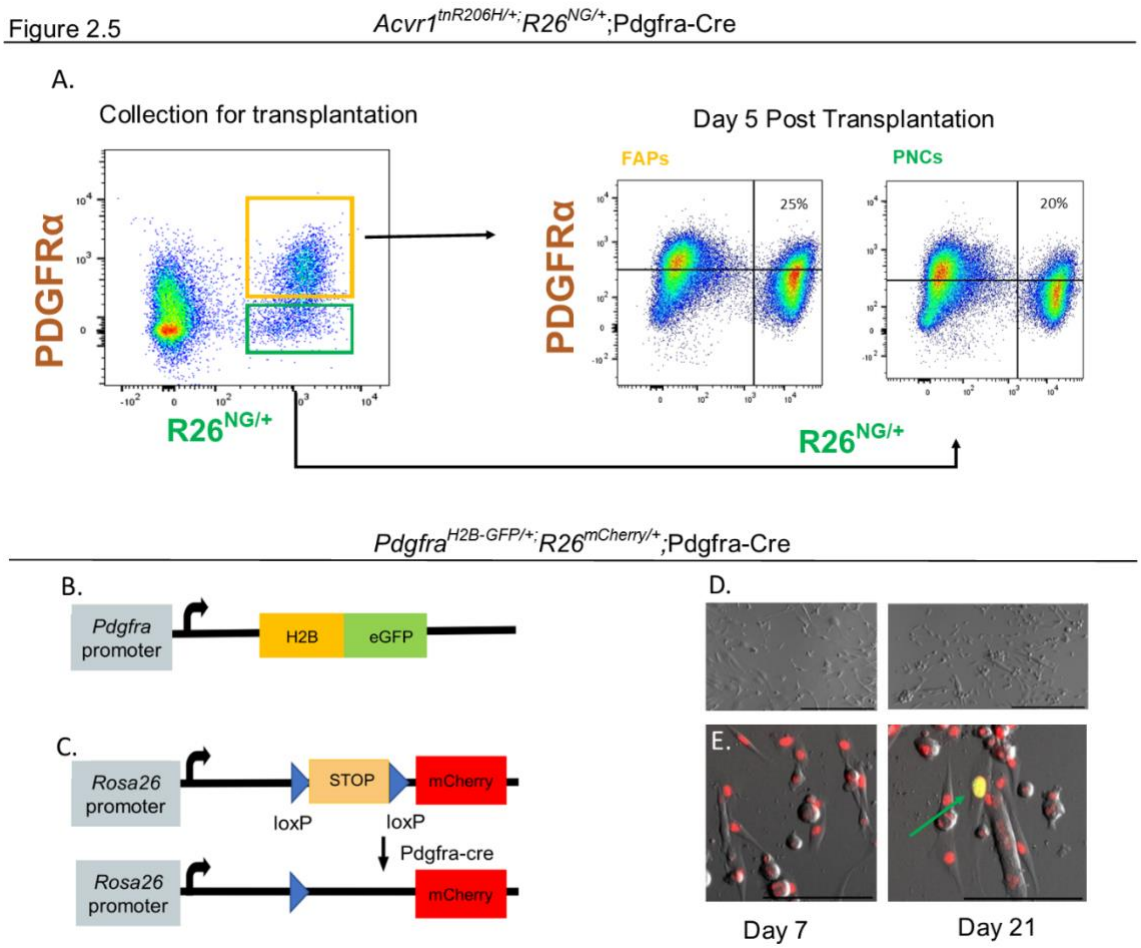

Figure 2.5: Transplantation and culturing of the PNC population influences the expression of PDGFRa

A. R206H-FAPs and R206H-PNCs were collected and transplanted as previously described. Current PDGFRa expression was determined in the transplanted PNC and FAP populations via flow cytometry 5 days post-transplantation (N=2 for both PNCs and FAPs). **B-C.** Dual fluorescent reporter constructs of *Pdgfra*$^{H2B\text{-}GFP/+}$;*R26*$^{mCherry/+}$;Pdgfra-Cre mice will label current and historical *Pdgfra* expression. Current *Pdgfra* expression is assessed via the *Pdgfra*$^{H2B\text{-}GFP}$ allele. An H2B-eGFP fusion protein was knocked into the *Pdgfra* locus (**B**). Historical *Pdgfra* expression is determined via the permanent recombination of the *R26*^{mCherry} allele by the Pdgfra-Cre. Cells will express mCherry after removing a floxed stop cassette via the Pdgfra-Cre (C). **D.** Representative images of morphologies of the PNC population after 1 week of culturing. **E.** *Pdgfra* expression of the PNC population 7 and 21 days post-culturing (N=3). The PNC expresses *Pdgfra* after 21 days in culture (green arrow).

2.4.7 scRNA-seq determines the cell types comprising the PNC population

To confirm what cell types comprise the PNC population, scRNA-seq was performed on a muscle biopsy of *Pdgfra*$^{H2B\text{-}GFP/+}$;*R26*$^{mCherry/+}$;Pdgfra-Cre mice. All cells of the *Pdgfra* lineage, which includes FAPs and PNCs, were FACS isolated and brought to the UCONN Center for Genome Innovation, where Chromium 10x Genomics scRNA-seq library prep was performed (Figure 2.6A). cDNA libraries were sequenced using the Novaseq 600 platform with roughly 400 million, 75 base pair reads. Samples were processed using the Cell Ranger and Seurat pipelines (Hao et al., 2021; Zheng et al., 2017). After quality control of the cells, normalization, and cell cycle regression, 1904 cells were analyzed and clustered into 11 clusters (Figure 2.6B). All 11 clusters historically expressed *Pdgfra,* based on mCherry transcripts, and 7 of the 11 clusters were actively expressing *Pdgfra,* based on GFP and *Pdgfra* transcripts (Figure 2.6C). The GFP and *Pdgfra* expression highly overlapped, further supporting *Pdgfra*$^{H2B\text{-}GFP}$ as an accurate readout of *Pdgfra* expression.

Out of the 7 *Pdgfra* expressing cell clusters, 5 fall into the *Pdgfra*+ and *Ly6a (Sca1)*+ FAP gene expression profile (Figure 2.6D) (Woscznya et al., 2012; Lees-Shepard et al., 2018b). Of the 5 *Pdgfra+;Sca1+* clusters, 3 express transcripts of the *Tek (Tie2)* gene (Figure 2.6D). We hypothesize that these 3 clusters are the osteocompetent cells directly contributing to HO in *Acvr1*$^{tnR206H/+}$;Tie2-Cre mice. There were 2 clusters that expressed *Pdgfra* but displayed a more neuronal fibroblastic-like signature (Figure 2.6D). The epineural clusters contain cells of the epineurium, which express secreted frizzled-related protein 2 (*Sfrp2*) transcripts (Figure 2.6D) (Gerber et al., 2021). Interestingly, the epineural clusters expressed transcripts of *Tie2* and, therefore, have the potential to be recombined by the Tie2-Cre driver(Figure 2.6D) and could potentially be contributing to the HO observed in *Acvr1*$^{tnR206H/+}$;*R26*$^{NG/+}$;Tie2-Cre mice. The remaining *Pdgfra* neural fibroblastic cluster displayed a perineurial and endoneurial signature (Figure 2.6D) (Gerber et al., 2021; Wolbert et al., 2020). Interestingly, the perineurial cluster, defined by Integrin subunit beta 4 (*Itgb4)* and Solute carrier family 2-member (*Slc2a1)* transcripts, lacked *Pdgfra* transcripts, while the endoneurial cluster,

characterized by the lack of SRY-box transcription factor 10 (*Sox10*) and presence of Nerve growth factor receptor (*Ngfr*) transcripts, expressed *Pdgfra* (Figure 2.6D) (Carr et al., 2019; Gerber et al., 2021; Wolbert et al., 2020)

The remaining 4 cell clusters comprise the PNC population (Figure 2.6B and Figure 2.6C). The PNC population is comprised of clusters that aligned with the gene expression profiles of tenocytes (Scleraxis (*Scx*), Mohawk (*Mkx*), Tenomodulin (*Tnmd*)), pericytes/smooth muscle (Chondroitin sulfate proteoglycan 4 (*Cspg4*), Nestin (*Nes*), and Platelet-derived growth factor receptor b (***Pdgfrβ***)), satellite cells (Paired box 7 (*Pax7*), Myogenic factor 5 (*Myf5*), and Vascular cell adhesion molecule 1 (*Vcam1*)), and Schwann cells (Proteolipid (*Plp1*), Myelin basic protein (*Mbp*), L1 cell adhesion molecule (*L1cam*), *and* Neural cell adhesion molecule 1 (*Ncam1*)) (Figure 2.6D) (Gerber et al., 2021; Micheli et al., 2020; McKellar et al., 2021). The Schwann cell cluster was comprised of both myelinating and non-myelinating Schwann cells (Figure 2.6D) (Gerber et al., 2021). When the tenocyte subcluster was integrated with additional scRNA-seq data generated in the lab, the tenocytes of the PNC population clustered closer to FAPs than tenocytes from bona fide tendons of the hindlimb; therefore, the tenocytes of the PNC population may be transcriptionally distinct from tenocytes comprising bona fide tendons (see Chapters 3 and 4 for further evaluation).

Figure 2.6

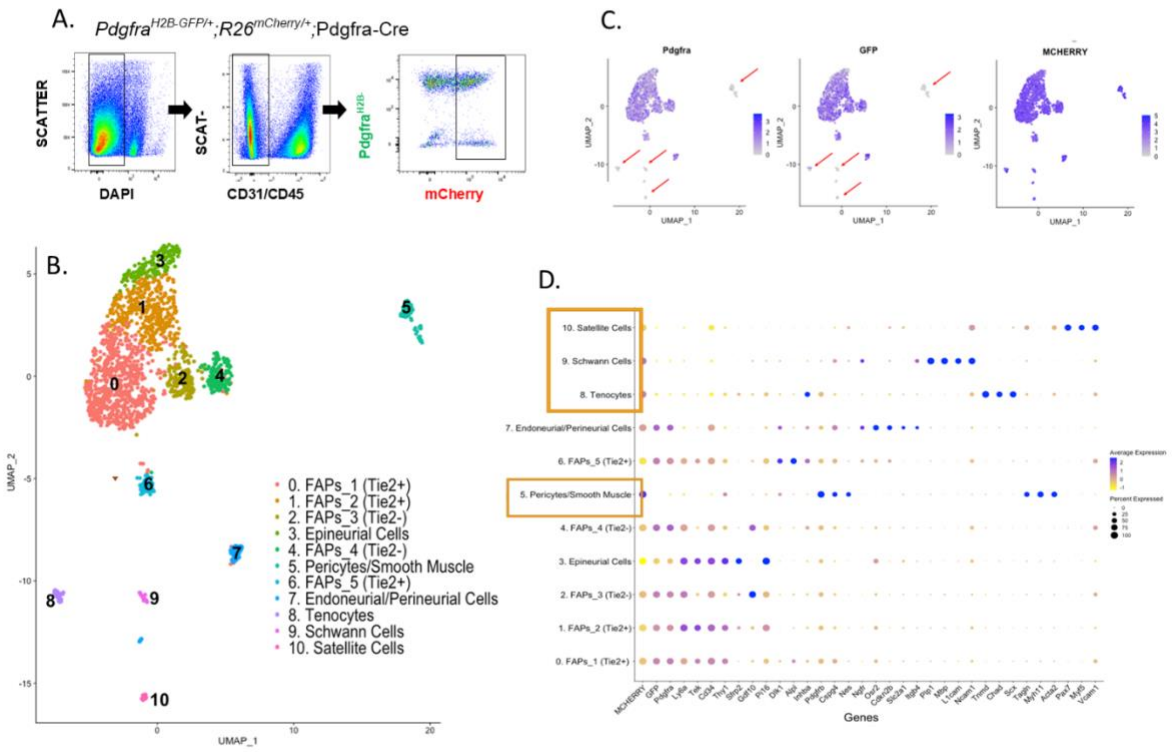

Figure 2.6: scRNA-seq determined the cell types comprising the PNC population

A. Gating strategy used to FACS isolate all cells of the *Pdgfra* lineage from *Pdgfra*$^{H2B\text{-}GFP/+}$;*R26*$^{mCherry/+}$;Pdgfra-Cre mice. **B.** Uniform Manifold Approximation and Projection (UMAP) showing the population structure of the recombined cell types. 11 cell clusters were identified in total. **C.** Feature plots determining what cell types currently and historically express *Pdgfra.* Current *Pdgfra* expression was determined through the presence of *Pdgfra* and *GFP* transcripts. Historical *Pdgfra* expression was determined through the presence of mCherry transcripts. 7 clusters currently express *Pdgfra,* and 4 historically express *Pdgfra* **D**. Dot plot displaying cell type identity and cluster-specific gene expression profiles. Yellow boxes are clusters that fall within the PNC population. The PNC population is comprised of Schwann cells, pericytes/smooth muscle, satellite cells, and tenocytes.

2.4.8 Determining the anatomical location of FAPs and PNCs

We investigated the spatial distribution of FAPs and PNCs throughout the hindlimb. Figure 2.7 is intended to be a reference image of hindlimb architecture and muscle organization. We first wanted to establish the FAP distribution throughout the hindlimb. FAP identity was determined based on the presence of *Pdgfra* expression. The *Pdgfra*$^{H2B\text{-}GFP}$ reporter was used as a reliable readout of *Pdgfra* expression. We selected four distinct anatomical locations throughout the hindlimb to track the distribution of FAPs (Figure 2.8). These locations were identified based on the structure of the musculature and the position of the tibia and fibula. Consistently among the locations chosen, *Pdgfra*-expressing cells were restricted to the known anatomical locations of FAPs, the epimysium, perimysium, and endomysium (Figure 2.8A – D) (Contreras et al., 2021; Joe et al., 2010; Uzemi et al., 2010). There was an increase in *Pdgfra*-expressing cells in the more distal anatomical locations (compare Figure 2.8E to Figure 2.8F). The distal regions of the lower hindlimb are a common site for HO to occur in our mouse model of FOP, which could be explained by the increase in *Pdgfra*-expressing cells (unpublished data).

Next, we investigated the spatial organization of PNCs compared to FAPs and cells of the *Tie2* lineage. Our analysis focused on the midpoint of the hindlimb, a well-known site for injury-induced HO. We identified anatomical landmarks and skeletal muscle structures through H&E staining of whole limb cross-sections (Figure 2.7 and Figure 2.9A).

PNCs were identified in *Pdgfra*$^{H2B\text{-}GFP/+}$*;R26*$^{mCherry/+}$;Pdgfra-Cre mice based on historical *Pdgfra* expression and lack of current *Pdgfra* expression (mCherry+ cells). *Pdgfra*$^{H2B\text{-}GFP/+}$*;R26*$^{mCherry/+}$;Tie2-Cre mice were used to identify FAPs. All FAP subpopulations were detected via *Pdgfra* expression (GFP cells). Tie2+ FAP subpopulations were detected via *Pdgfra* expression and historical or current *Tie2* expression (GFP+;mCherry+ cells). Cells of the *Tie2* lineage that were not FAPs were labeled via historical or current *Tie2* expression only (mCherry+ cells). PNCs

were found intramuscularly, consistent with the satellite cell PNC cell type (Figure 2.9B). Satellite cells typically reside in the interstitial spaces of skeletal muscle fibers, specifically between the basal lamina and the sarcolemma (plasma membrane) of the muscle fiber (Yin et al., 2013). FAPs were also located intramuscularly (Figure 2.9B). An expected result as FAPs reside in the interstitial spaces between skeletal muscles (Contreras et al., 2021; Joe et al., 2010; Uzemi et al., 2010).

PNCs were observed near peripheral nerve bundles, consistent with the Schwann cell lineage, as myelinating and non-myelinating Schwann cells are found in peripheral nerve bundles (Figure 2.9C – white circles) (Jessen et al., 2015). *Pdgfra*-expressing cells of the *Tie2* lineage were detected around peripheral nerves (Figure 2.9C). scRNA-seq revealed the presence of *Tie2* and *Pdgfra* transcripts in the epineurial cluster (Figure 2.6D). We hypothesize that the *Pdgfra*-expressing cells of the *Tie2* lineage are cells of the epineural cluster rather than FAPs.

Furthermore, PNCs were associated with blood vessels, suggesting a pericyte/smooth muscle identity, as pericytes and smooth muscle cells are associated with the vasculature (Figure 2.9D) (Yamazaki and Mukouyama, 2018). In comparison, cells of the *Tie2* lineage mice were found within the vasculature lumen, which is consistent with the location of endothelial cells (Figure 2.9D) (Kisanuki et al., 2001).

The intermuscular fascial regions are surrounded by cells that express *Pdgfra,* presumably FAPs (Figure 2.9E). When compared to *Pdgfra*$^{H2B\text{-}GFP/+}$*;R26*$^{mCherry/+}$;Tie2-Cre mice, cells of the *Tie2* lineage that are currently expressing *Pdgfra* (Tie2+ FAPs) were found to be localized to the periphery of the intermuscular fascial regions (Figure 2.9E). A PNC population was located intrafascially within the intermuscular fascia of the posterior compartment of the hindlimb (Figure 2.9E). The intermuscular fascial regions could be comprised of PNC tenocytes. *Scx* expression was found in tendons and developing connective tissue regions of the hindlimb (Sugimoto et al., 2013; Pryce et al., 2007). Interestingly, the intermuscular fascial areas of the hindlimb are a common site of HO occurrence in injury-induced and spontaneous HO

models. Further exploration of the PNC cell type within the intermuscular fascial region is characterized in Chapters 3 and 4.

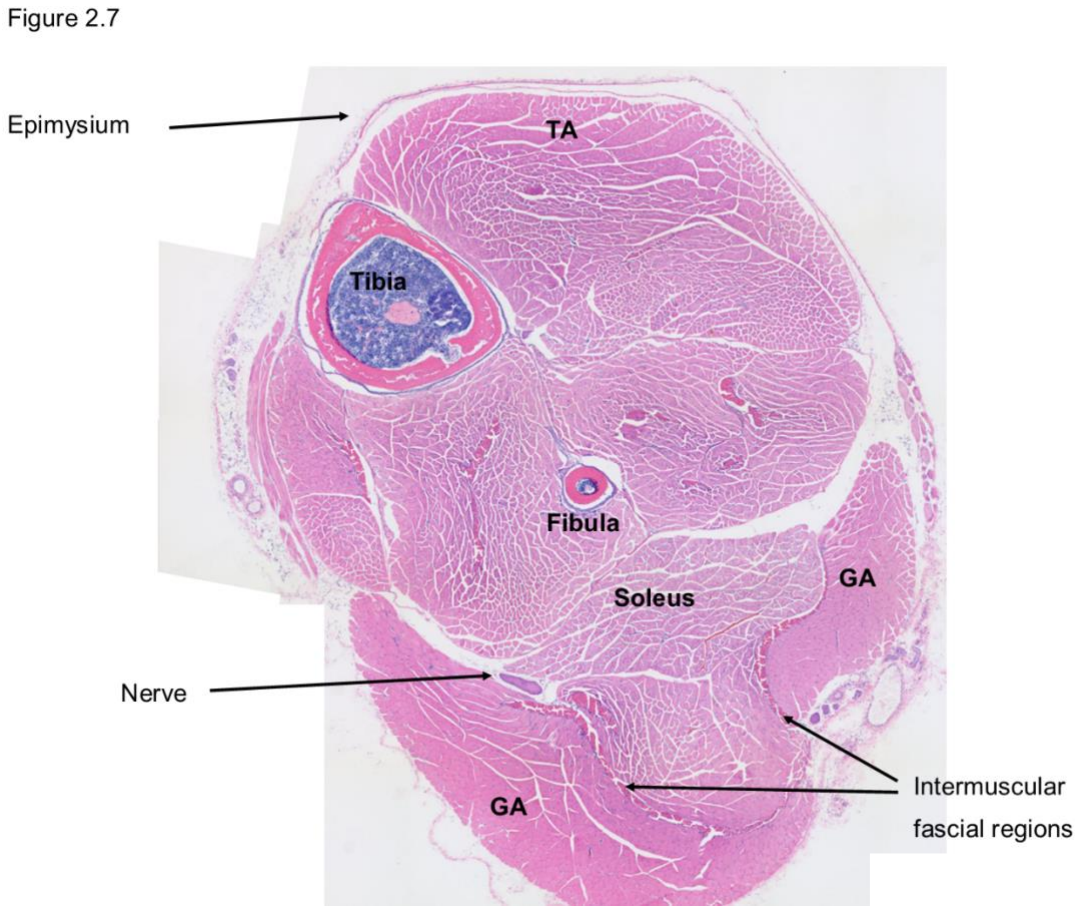

Figure 2.7: H&E stained cross-section of distal hindlimb

Representative H&E stained cross-section of the distal hindlimb. GA – gastrocnemius, TA- tibialis anterior.

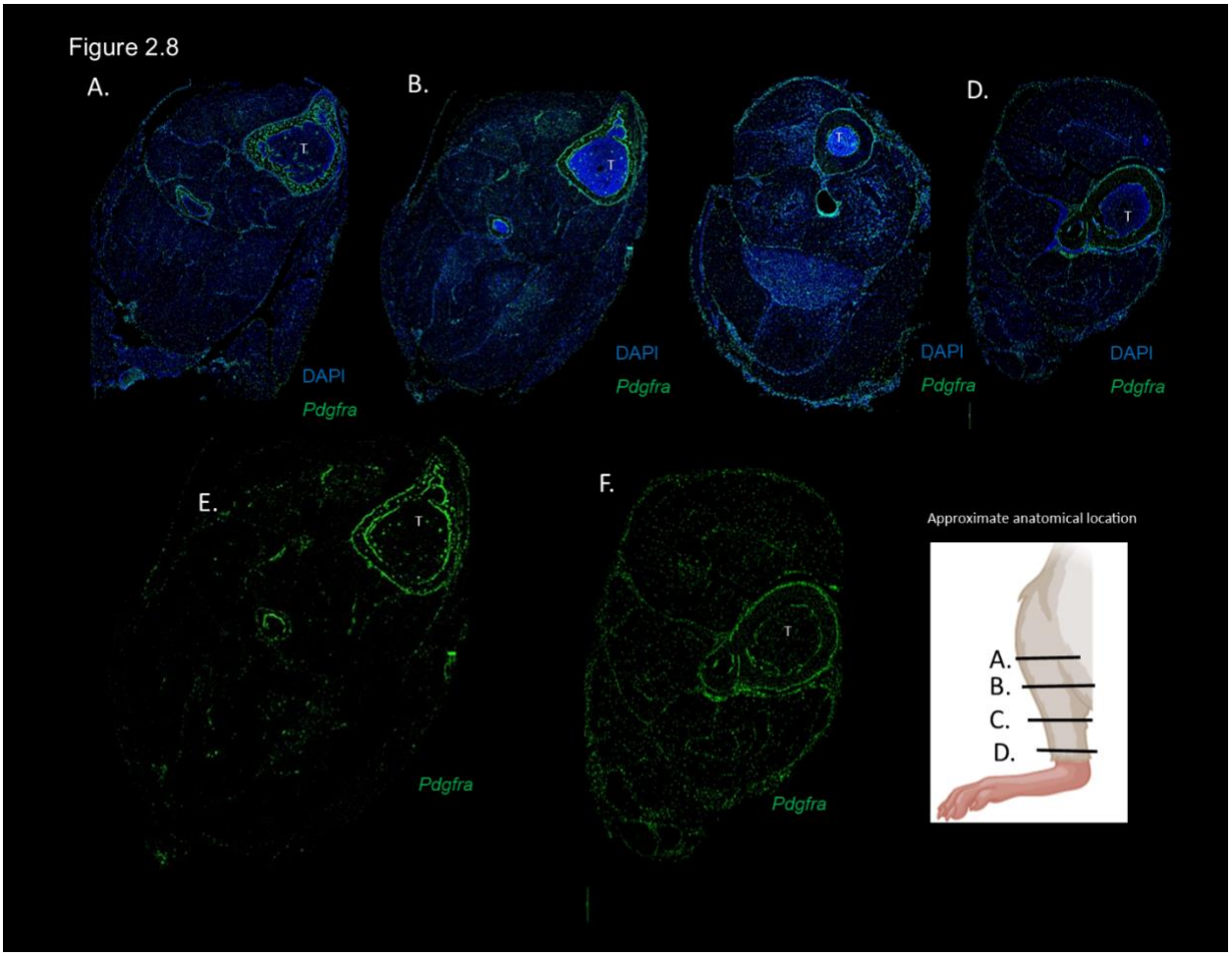

Figure 2.8: FAPs distribution throughout the distal hindlimb

Schematic representing the anatomical locations chosen for analysis in the bottom right corner. **A-D.** A histological analysis displaying the location of *Pdgfra*-expressing cells throughout the hindlimb. Nuclei were counterstained with DAPI. **A.** The most proximal anatomical location chosen for analysis. **B.** Midpoint of the distal hindlimb. **C.** Distal to the mid-belly of the lower hindlimb. **D.** Merging of the tibia and fibula. The most distal hindlimb region chosen for analysis. **E-F.** Comparison of *Pdgfra* expression at anatomical locations A (**E**) and D (**F**). (N=3). T- tibia

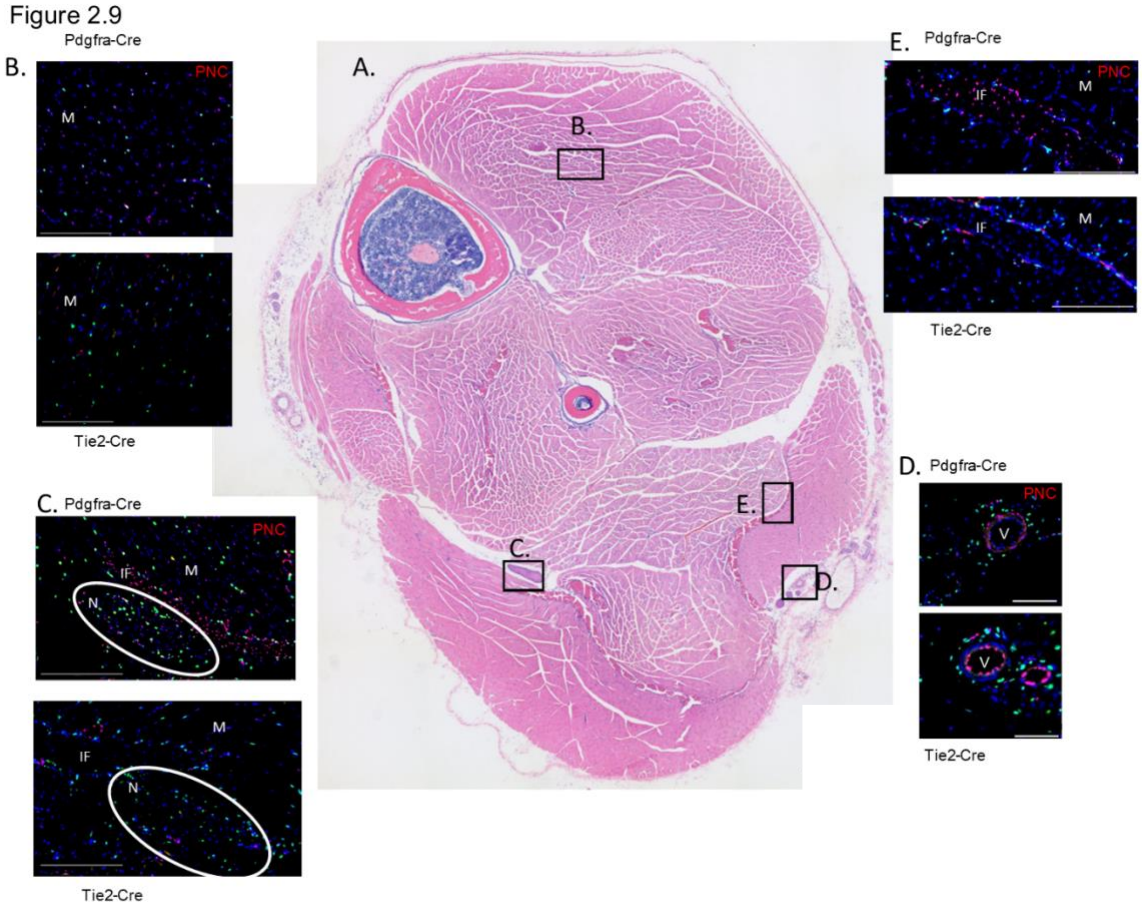

Figure 2.9: PNC and FAP distribution throughout the midpoint of distal hindlimb

A. H&E stained hindlimb cross-section used to identify anatomical structures. Black boxes are specific regions where PNC populations are found. **B-E.** The Cre-driver driving recombination of the *R26*^{mCherry} allele resulting in mCherry expression is labeled above or below the representative image. *Pdgfra*$^{H2B\text{-}GFP/+}$*;R26*$^{mCherry/+}$;Pdgfra-Cre or *Pdgfra*$^{H2B\text{-}GFP/+}$*;R26*$^{mCherry/+}$;Tie2-Cre mice were used to compare the location of PNCs and cells of the *Tie2* lineage, including FAPs. **B.** Intermuscular regions of the tibialis anterior muscle comparing PNC cells (top, presumed satellite cell cluster, mCherry+ cells) to Tie- and Tie2+ FAPs (GFP+ or mCherry+;GFP+, respectively) **C.** Neuronal structures (white circle) comparing PNC cells (top, presumed Schwann cell cluster, mCherry+) to historically or currently *Tie2* and currently *Pdgfra* expressing cells (presumed neural fibroblastic populations, bottom, mCherry+GFP+). **D.** Vasculature of the hindlimb comparing PNC cells (top, presumed pericytes/smooth muscle cluster, mCherry+) to historically or currently *Tie2* expressing cells (presumed endothelial cells, bottom, mCherry+). **E.** Intermuscular fascial regions of hindlimb comparing PNC cells (top, presumed tenocyte cluster, mCherry+) to Tie- and Tie2+ FAPs (bottom, GFP+ or mCherry+;GFP+, respectively). (N=3) M- muscle, IF- intermuscular fascial region, N- nerve, V- vasculature

2.5.1 Discussion

The primary research question of this chapter was to address why the spontaneous HO model forms a more robust HO response than the injury-induced model. FAPs were previously identified as a casual cell of HO in a conditional, Cre-dependent, knockin mouse model of FOP (Lees-Shepard et al., 2018b). Recombining the Acvr*1*^{tnR206H} allele in FAPs via the Pdgfra-Cre or the Tie2-Cre, resulted in many cell types transcribing the R206H mutation. The present chapter uncovers an osteogenic (Figure 2.4) and heterogeneous population of cells (PNCs) (Figure 2.6) that are distinct from FAPs (Figure 2.2) and are only present in the spontaneous HO model (Figure 2.2). PNCs could play a role in the robust HO response observed in the spontaneous HO model post-injury (Figure 2.1).

Two parameters that were immediately addressed between the injury-induced and spontaneous HO models are the recombination efficiencies of the Cre-drivers and the presence of osteocompetent cell types. The efficiency of a Cre-driver recombining the Acvr*1*^{tnR206H} allele plays a significant role in the volume of HO observed. A lower recombination efficiency may limit the osteogenic response, as fewer osteocompetent cells are recombined overall. The Pdgfra-Cre was found to have a higher recombination efficiency than the Tie2-Cre, 37% to 13%, respectively, which could be playing a role in the greater HO response as more osteocompetent cell types are transcribing the R206H mutation. In addition to the recombination efficiency, the presence of an osteocompetent cell type is necessary for HO formation. When the *Acvr1*^{tnR206H} allele was explicitly recombined to the muscle lineage via *MyoD*^{iCre} (Kanisicak et al., 2009), which displayed a 99% recombination efficiency in muscle stem cells, no HO was observed (Lees-Shepard and Goldhamer, 2018; Lees-Shepard et al., 2018b). Therefore, the presence of an *Acvr1*^{R206H}-expressing osteocompetent cell type and a sufficient recombination efficiency are two components that are required for HO formation in the Cre-dependent mouse model of FOP.

Acvr1$^{tnR206H/+}$;*R26*$^{NG/+}$;Pdgfra-Cre mice formed a robust injury-induced HO response, and the *Acvr1*^{tnR206H} allele is recombined in all FAP subpopulations; therefore,

the heightened HO response could be attributed to the expression of *Acvr1*^{R206H} in all FAP subpopulations. FAPs are presumed to be the only causal cells of HO in *Acvr1*$^{tnR206H/+}$;*Pdgfra*^{CreER} mice when tamoxifen was administered at P2-P7 and 4-weeks-of age (Figure 2.3). Interestingly, the volume of HO observed was a similar HO response as Acvr*1*$^{tnR206H/+}$;Tie2-Cre mice. A low recombination efficiency of the *Pdgfra*^{CreER} does not seem to explain the minimal HO response, as the recombination efficiency was higher than the Tie2-Cre, approximately 25% to 13%, respectively. This suggests that the PNC involvement is a driving factor for a more robust HO response in *Acvr1*$^{tnR206H/+}$;*R26*$^{NG/+}$;Pdgfra-Cre mice.

The transplantation of *Acvr1*^{R206H}-expressing cells is a technique that was developed to test cells' autonomous ability to differentiate towards the osteogenic lineage. This technique transplants a large quantity of cells into a preinjured GA muscle of a SCID host. The transplantation model may not be directly comparable to in vivo targeting of the *Acvr1*^{R206H} allele to a specific cell lineage; however, it is an accepted proxy for determining cells' osteogenic capabilities. Wild-type FAPs and FAPs transplanted along with an HO-blocking antibody did not result in HO formation (Lees-Shepard et al., 2018b). Additionally, a titration of the amount of transplanted R206H-FAPs resulted in a lower HO volume, which corresponds to the transplanted FAP concentration (unpublished data). A necessary control experiment is transplanting *Acvr1*^{R206H}-expressing non-osteocompetent cells, such as cells of the muscle lineage, into a SCID host. This experiment will help conclude whether the HO response genuinely reflects the inherent osteogenic properties of the cells.

scRNA-seq revealed two neuronal fibroblastic populations that express *Pdgfra,* epineurial, and endoneurial fibroblasts (Figure 2.6D). All recombined PDGFRa-expressing cells from *Acvr1*$^{tnR206H/+}$;*R26*$^{NG/+}$;Pdgfra-Cre mice were transplanted into a SCID host, and bone was observed 7- to 10- days post-transplantation (Figure 2.4). The neuronal fibroblasts are included in the transplanted population and potentially contributed to the HO observed. In a nerve injury and digit tip regeneration model, endoneurial fibroblasts were found to have a mesenchymal-like phenotype post-injury

and display osteogenic potential (Carr et al., 2019). Epineurial cells were found to upregulate osteogenic markers after nerve injury; however, the contribution to osteogenesis was minimal (Carr et al., 2019). Experiments specifically testing the osteogenic capability of the *Acvr1*^{R206H}-expressing epineurial and endoneurial populations could reveal the potential contribution of neuronal fibroblast populations to HO formation.

ScRNA-seq revealed the cellular identity of all recombined cell types within *Pdgfra*$^{H2B\text{-}GFP/+}$*;R26*$^{mCherry/+}$;Pdgfra-Cre mice. In total, 11 cell clusters were identified, which fall into 7 cell types (FAPs, neuronal fibroblasts, Schwann cells, satellite cells, tenocytes, pericytes, and smooth muscle). The mouse model used to identify the cell types comprising the PNC population was not a mouse model of FOP; however, we are confident that the cell type identities remain constant between FOP and non-FOP mouse models. Previously obtained scRNA-seq data within the Goldhamer lab revealed no difference between the identity of cell types present between wild-type and the FOP mouse model in uninjured skeletal muscle (unpublished data). The histological analysis of the *Pdgfra* lineage revealed a cell type within the PNC population localized to the intermuscular fascial regions of the posterior compartment (Figure 2.9). Cells of the *Scx* lineage, which could potentially include the tenocytes comprising the PNC population, have been documented to be present in the developing connective tissue structures of the hindlimb (Pryce et al., 2007); therefore, the tenocytes of the PNC population could be localized to the intermuscular fascial regions. The intermuscular fascial areas are a common reproducible location of HO formation. Further investigation correlating the location of tenocyte PNC cells to the intermuscular fascial regions and HO formation is explained in Chapter 3. In conclusion, this chapter reveals a population of cells that contains an additional causal cell of HO in a mouse model of FOP.

Chapter 3: Determining the Osteogenic Cell Type(s) within the PDGFRα-Negative Population

3.1.1 Abstract:

FAPs are a causal cell of genetic and traumatic HO (Lees-Shepard et al., 2018b; Woscznya et al., 2012; Li et al., 2020). We have identified a heterogeneous population of cells that are distinct from FAPs, called PDGFRα-negative cells (PNCs), that contribute to HO formation in a transplantation model (Section 2.4.5). This chapter characterizes the cell type(s) within the PNC population responsible for the osteogenic response. Single-cell RNA-sequencing (scRNA-seq) established the identities of the cell types comprising the PNC population as Schwann cells, tenocytes, satellite cells, and pericytes/smooth muscle (Section 2.4.7). Among these, Schwann cells and tenocytes exhibit osteogenic potential, representing two additional causal cells of HO. Injury-induced HO derived from tenocytes of the PNC population exhibited an earlier onset of bone and differences in HO stability and growth modality when compared to HO derived from other known causal cells of HO. Additionally, the tenocytes localized to the intermuscular fascial regions of the posterior hindlimb, an anatomical location where bona fide tendons are not found. Given the novel bone response and anatomical location, we suggested that the tenocytes of the PNC population are distinct from tenocytes comprising bona fide tendons of the hindlimb and will be referred to as Tendon-Like Cells (TLCs) throughout the remainder of this document.

3.2 Introduction:

Injury to skeletal muscle can result from physical or chemical trauma. Upon experiencing such injury, the body initiates a complex cascade of events to repair the damaged tissue and restore functionality to the affected area. The injury response triggers a near-immediate inflammatory response, where the immune system infiltrates the injured environment and clears away the damaged tissue. At the same time as the immune system activation, satellite cells are activated and begin proliferating, differentiating, and fusing to form regenerated muscle fibers (Pizza and Buckley et al., 2023). Additionally, FAPs are activated by the skeletal muscle injury. FAPs reach peak proliferation approximately 3 to 5 days post-injury, where they provide necessary signaling cues to the surrounding satellite cells to differentiate and fuse into nascent myofibers (Joe et al., 2010; Lemos et al., 2015; Oprescu et al., 2020). After proliferating, FAPs are cleared from the environment and return to their baseline cell numbers (Joe et al., 2010; Lemos et al., 2015). The skeletal muscle environment is restored to full functionality between 14 to 21 days post-injury.

The formation of HO can be thought of as aberrant muscle regeneration. In a mouse model of FOP, injury-induced HO is also initiated by a physical or chemical injury (Lees-Shepard et al., 2018b; Burdick et al., 2024). The initial stages of the injury repair process are similar between wild-type and mutate FOP environments. However, FAPs do not return to their baseline numbers post-proliferation in a mouse model of FOP. They continue to proliferate and ultimately undergo differentiation along the endochondral ossification pathway. Initially, FAPs differentiate into cartilage, identified by the expression of SRY-box transcription factor 9 (SOX9), 5 to 6 days post-injury. Subsequently, 10 to 14

days post-injury, the cartilage intermediate is replaced by osteoprogenitors, identified by Osterix (OSX) expression. The osteoprogenitors then mature into fully mineralized bone. The peak of HO formation occurs between 14 to 21 days post-injury (Lees-Shepard et al., 2018b; Burdick et al., 2024).

Lees-Shepard et al. utilized lineage-tracing and a Cre-dependent mouse model of FOP (*Acvr1*^{tnR206H}, Section 2.2) to show that FAPs are a causal cell of HO (Lees-Shepard et al., 2018b); however, obtaining cell-type-specific recombination of the *Acvr1*^{tnR206H} allele presents challenges, as many cell types lack specific cellular markers. For example, cells targeted for recombination by a Glast-Cre^{ERT} Cre-driver, which labels various cellular lineages including astrocytes, satellite cells of the dorsal root ganglion, macrophage lineage, lymphocytes, adipogenic cells, and PDGFRα+ cells within the muscle interstitium (presumably FAPs), were found to contribute to a BMP-inducible model of traumatic HO (Kan et al., 2013). The array of cell types targeted using the Glast-Cre^{ERT} complicates the analysis because recombination of the Glutamate aspartate transporter 1 (*Glast)* lineage includes FAPs as one of the targeted cell types, which contribute to an HO response, potentially masking an osteogenic response of non-FAP cells.

Scleraxis *(Scx)* and Mx dynamin like *(Mx1)* lineages were found to contribute to an HO response in a Cre-dependent mouse model of FOP (*Acvr1*$^{[R206H]FIEx/+}$)(Dey et al., 2016). Interestingly, the *Scx* lineage only contributed to spontaneous HO, first observed at 4-weeks-of-age, while the *Mx1* lineage contributed to injury-induced HO (Dey et al., 2016). Dey et al. concluded that the PDGFRα-expressing cells within the *Scx* and *Mx1* lineages were responsible for the observed HO (Dey et al., 2016). However*, Scx* and *Mx1*

lineages target a broad spectrum of cell types, and the potential contribution of other recombined cell types within these lineages was not explicitly evaluated for their osteogenic capabilities.

The PNC population is a heterogeneous population comprised of Schwann cells, tenocytes, pericytes/smooth muscle, and satellite cells that display osteogenic potential in a transplantation model of HO (Section 2.4.5 and Section 2.4.7). The data presented in this chapter will demonstrate that Schwann cells and tenocytes are two PNC cell types that display an osteogenic response, thus identifying them as two additional causal cells of HO. Interestingly, tenocytes of the PNC population exhibit distinct characteristics from FAPs and tenocytes comprising hindlimb tendons. Henceforth, we will refer to PNC-tenocytes as Tendon-Like Cells (TLCs) due to the shared expression of *Scx* between TLCs and tenocytes of bona fide tendons. HO derived from *Acvr1*^{R206H}-expressing TLCs (R206H-TLCs) displays variations in the mode, timeline, onset, and stability of HO when compared to HO derived from *Acvr1*^{R206H}-expressing FAPs (R206H-FAPs). TLCs localize to the intermuscular fascial regions of the hindlimbs, a common site of HO occurrence in a mouse model of FOP. Overall, this chapter characterizes Schwann cells and TLCs as two additional causal cells of HO and suggests that TLCs are distinct from FAPs and other cells of the *Scx* lineage.

3.3 Materials and Methods

3.3.1 Genetic mouse models and mouse crosses

Pdgfra$^{H2B\text{-}GFP/+}$;*R26*$^{mCherry/+}$;Pdgfra-Cre or *Pdgfra*$^{H2B\text{-}GFP/+}$;*R26*$^{mCherry/+}$;Tie2-Cre mice, used in histological analyses, were generated as previously described (see Section 2.3.1 for more information). The Wnt1-Cre driver (strain 022501) was purchased from Jackson Laboratories (Lewis et al., 2013). *Scx*^{CreERT2} (Howell et al., 2017) and *Scx*^{GFP} (Pyrce et al., 2007) mice were kindly provided by Dr. Ronen Schweitzer (Shriners Hospital for Children; Portland, OR). *Scx*^{GFP} mice express GFP under the control of the endogenous *Scx* locus. The GFP open reading frame was inserted into exon 1, beginning at the initiator ATG of the *Scx* gene and replacing most of the first exon (Pryce et al., 2007). Mice were genotyped by PCR and, when applicable, by the presence or absence of fluorescence reporters (see Appendix IA). Immunocompromised mice, SCID Hairless Outbred mice (SCID) (Charles River: strain code 474), were used as recipients for osteogenic transplantations. Mice were used at 6- to 8-weeks-of-age and were held and maintained in a climate-controlled vivarium at the University of Connecticut in accordance with the UConn IACUC.

Experimental mice used in flow cytometry and osteogenic transplantation assays were generated by crossing *Acvr1*$^{tnR206H/+}$ females with *Pdgfra*$^{H2B\text{-}GFP/+}$ males. The resulting *Acvr1*$^{tnR206H/+}$;*Pdgfra*$^{H2B\text{-}GFP/+}$ females were then mated with Pdgfra-Cre males to produce *Acvr1*$^{tnR206H/+}$;*Pdgfra*$^{H2B\text{-}GFP/+}$;Pdgfra-Cre mice. For injury studies, *Acvr1*$^{tnR206H/+}$ females were crossed with *Scx*$^{CreERT2/+}$ males to produce *Acvr1*$^{tnR206H/+}$;S*cx*$^{CreERT2/+}$

experimental mice. Histological studies utilizing R*26*$^{mCherry+}$;*Scx*$^{GFP/+}$;Pdgfra-Cre mice were generated by crossing *R26*$^{mCherry/+}$ females with *Scx*$^{GFP/+}$ males to produce *R26*$^{mCherry/+}$;*Scx*$^{GFP/+}$ female breeders. *R26*$^{mCherry/+}$;*Scx*$^{GFP/+}$ females were crossed with Pdgfra-Cre male mice to generate *R26*$^{mCherry/+}$;*Scx*$^{GFP/+}$;Pdgfra-Cre mice. For osteogenic BMP6 studies, *R26*$^{mCherry/+}$ females were mated with *Scx*$^{CreERT2/+}$ males to produce *R26*$^{mCherry/+}$;*Scx*$^{CreERT2/+}$ experimental mice. Males and females were used in experiments at equal frequencies.

3.3.2 Tamoxifen dosing

Tamoxifen (Sigma Aldrich, #T5648; St. Louis, MO, USA) was prepared as a 20 mg/mL stock in corn oil (Sigma Aldrich, #C8267) and administered via intraperitoneal injection at 150 mg/kg concentration for three consecutive days. Tamoxifen was pre-warmed to 37°C prior to administering and held at 4°C for short term and -20°C for long-term storage. Mice administered with tamoxifen were held for a 5- to 7-day washout period before use. Mice that received tamoxifen behaved normally compared to their wild-type counterparts.

3.3.3 Skeletal muscle injury and HO quantification

Hindlimb muscles of *Acvr1*$^{tnR206H/+}$;Tie2-Cre, *Acvr1*$^{tnR206H/+}$;Pdgfra-Cre, or *Acvr1*$^{tnR206H/+}$;*Scx*$^{CreERT2/+}$ mice were injured by cardiotoxin injection. *Acvr1*$^{tnR206H/+}$;Pdgfra-Cre and *Acvr1*$^{tnR206H/+}$;*Scx*$^{CreERT2/+}$ Mice were at 4- to 6 weeks-of-age, while *Acvr1*$^{tnR206H/+}$;Tie2-Cre mice were used at 8- to 12 weeks-of-age. 100 µL of 10 µM cardiotoxin (Latoxan, #L8102-1MG; Portes-lès-Valence, France) in sterile 1X DPBS

(Gibco; Grand Island, NY, USA) was injected into the tibialis anterior (TA) or gastrocnemius (GA) muscle. Mice subjected to treatment with the anti-ACVR1 antibody, JAB0505, treatment were given a single intraperitoneal dose of JAB0505 (10 mg/kg) on the day of injury (Lees-Shepard et al., 2022).

R26$^{mCherry/+}$*;Scx*$^{CreERT2/+}$ mice subjected to BMP treatment were injected with a 100 µL of a suspension consisting of 2.5µg of rhBMP6 (Keros Therapeutics; Lexington MA, USA) suspended in sterile 1X DPBS and 1% alum adjuvant solution (Invivogen; Alhydrogel adjuvant 2%; San Diego, CA, USA) into the GA muscle. BMP adsorption to the adjuvant carrier was completed by gentle shaking at room temperature for 15 minutes before use. Mice were collected at 10 days post-injection.

µCT images were acquired at 4, 7, 10, 14, 21, and 28 days post-injury, depending on the experimental design, using an IVIS Spectrum-CT under medium resolution (75 µm voxel size; estimated radiation dose of 132 mGy; 210 scan time). 3D Slicer V5.2 software (www.slicer.org) was used to segment and quantify HO volume (mm^3).

3.3.4 Skeletal muscle dissociation, flow cytometry, and cell culturing

Mice were sacrificed via cervical dislocation, and hindlimb muscles were dissected and placed in a 35 mm dish containing approximately 100 µL of digestion media. Digestion media is comprised of Dulbecco's Modified Eagle Medium (DMEM; Thermo Fisher; Waltham, MA, USA), 600–700 U/mL Collagenase Type II (Worthington Biochemical; Lakewood, NJ, USA), and 0.5 U/mL Dispase (Thermo Fisher, Waltham, MA, USA). Muscle was minced with scissors for 8- to 10- minutes and then placed at 37°C for 1 hour, with gentle titrations every 10 minutes. Digestion was then quenched with quench

media (DMEM containing 10% HyClone characterized fetal bovine serum (FBS; GEHealthcare, Lot #A00168; Chicago, IL, USA) and filtered through 70 μM mesh cell strainers (Corning Life Sciences; Tewksbury, MA, USA). Single-cell suspensions were spun down at 500g for 5 minutes at 4°C. Pellets were washed in 1X DPBS, spun down, and resuspended in blocking buffer (1X DPBS supplemented with 10% FBS). Antibodies were added in optimal concentrations (see Appendix IA) and incubated for 1 hour on ice in low light conditions. Samples were spun down, washed with DPBS, resuspended in FACS Buffer (DPBS supplemented with 2% FBS), and filtered through FACS tubes with a 35 μm cell strainer (Corning Life Sciences; Corning, NY. USA). Samples were brought to the University of Connecticut Flow Cytometry Facility where target populations were analyzed using a BD LSRFortessa X-20 Cell Analyzer equipped with 5 lasers (355nm, 405nm, 488nm, 561nm, and 640nm) or collected using a BD FACSAria II Cell Sorter equipped with 5 lasers (355nm, 405nm, 488nm, 561nm, and 640nm).

The collected samples were seeded at a density of 2500 cells/cm^2 and placed in growth media comprising 20% FBS in DMEM supplemented with 50 U/mL penicillin and 50 μg/mL streptomycin (Pen/Strep; Gibco, Grand Island, NY, USA), and 2.5 ng/mL recombinant Human Fibroblastic Growth Factor (bFGF; Gibco; Grand Island, NY, USA). The plates were coated with rat tail collagen I (Invitrogen; Waltham, MA, USA) before seeding and then incubated at 37°C with 5% CO2. Cells were trypsinized to split when 70% confluency was reached and used within 3 weeks of culturing.

3.3.5 Transplantation assays

Cultured cells were trypsinized, counted, and resuspended in 1X DPBS. Cells were transplanted into the TA or GA muscle of SCID hosts at a concentration of 2.7 x 10^5 cells per 50 µL or 1 x 10^6 cells per 50 µL, respectively. HO was determined and quantified as explained in Section 3.3.3.

3.3.6 Sectioning and immunofluorescence staining

Limbs were collected at the desired time point, fixed in 4% paraformaldehyde, and rocked at 4°C for 3 days. Samples were washed with 1x DPBS, and a decalcification step was performed to remove the calcium ions within the mineralized endogenous skeleton or newly formed HO. Decalcification was obtained by incubating samples in decal solution, 12.5% ethylenediaminetetraacetic acid (EDTA) with 1% Sodium Hydroxide in 1X DPBS, for 1 month. The decal solution was replaced every other day. Once decalcification was completed, samples were washed with 1X PBS and placed in a cryoprotectant solution, 30% sucrose in 1X PBS, overnight. Protected samples were flash frozen in Tissue-Tek O.C.T. compound (OCT; Thermo Fisher, Waltham, MA, USA) using a dry-ice and 70% ethanol slurry and stored at -80°C until sectioning. Samples were then sectioned using a Leica cryostat (CM3050S) at a 10 µm thickness, and slides were stored at -20°C until used. 10 µm sections were rehydrated in 1X PBS and then subjected to blocking of antibody cross-reactivity using blocking buffer containing 1% BSA (Sigma-Aldrich; St. Louis, MO, USA), 10% goat serum (Sigma-Aldrich; St. Louis, MO, USA), and 0.1% Tween 20 in 1X PBS. Subsequently, the sections were stained with the primary antibody diluted to the desired concentration (see Appendix IA). Primary antibodies were incubated

overnight at 4˚C with gentle agitation. Sections were then washed in 1X PBS, stained with Alexa Fluor–conjugated secondary antibody at room temperature for 1 hour, washed in 1X PBS, counterstained with 10 μg/mL of DAPI, and coverslipped using FluoroGel mounting medium (Electron Microscopy Sciences; Hatfield, PA, USA). Controls lacking primary antibodies were conducted on adjacent sections simultaneously and did not show fluorescent staining. Sections were analyzed using a Leica Thunder imaging platform at the UCONN Advanced Light Microscopy COR^{2}E.

3.3.7 Hematoxylin and eosin Y (H&E) staining

Sections were brought to room temperature, rehydrated in nanopure water, and placed in Mayer's hematoxylin (Sigma-Aldrich; St. Louis, MO, USA) for 8 minutes. After hematoxylin staining, sections were placed in a 2% ammonium bluing solution and dehydrated using a series of progressively concentrated ethanol solutions. Samples were stained with eosin Y (Sigma-Aldrich; St. Louis, MO, USA) for 5 seconds. Excess eosin Y was washed away with 95% ethanol washes, and sections were fully dehydrated using 100% ethanol and xylene. Samples were mounted using Permount mounting medium (Thermo Fisher; Waltham, MA, USA) and imaged using the Leica Thunder imaging platform the following day.

3.3.8 Whole nerve transplantation surgeries

SCID host GAs received a 100 μl of 10 mM cardiotoxin to induce an injury environment. The next day, 4- to 6-week-old *Acvr1*$^{tnR206H/+}$;Pdgfra-Cre mice were sacrificed via cervical dislocation. A small incision was made to separate the thigh and

hamstring. The hamstring was gently pulled back, exposing the sciatic nerve. As much surrounding muscle and connective tissue was removed as possible. The sciatic nerve was sterilely removed from the upper hindlimb and placed in sterile 1X PBS on ice. Next, the preinjured SCID hosts were subjected to continuous 2.5% isoflurane sedation, and Meloxicam analgesic (5 mg/kg) was administered subcutaneously immediately after sedation. The surgical site was prepared using standard aseptic techniques; the GA was washed 3X, alternating with betadine and 70% ethanol. A small incision was made in both the injured GAs of the SCID host, one being the recipient of the sciatic nerve and the other being a sham control. The sciatic nerve was gently placed in the SCID hosts' GA with fine forceps. The sham control incision and the transplanted nerve site were closed with wound glue. All mice were singly housed for the remainder of the study. HO formed from the transplanted nerve was quantified, as mentioned in Section 3.3.3, 14 days post-transplantation.

3.4 Results

3.4.1 Validation of PNC Osteogenic Capabilities

We previously identified a population of cells termed PNCs that exhibit cell-autonomous osteogenic capability when transplanted into a SCID host (Sections 2.4.5 and 2.4.7), suggesting the PNC population contains an additional causal cell of HO. A critical distinction between the PNC population and FAPs lies in the presence or absence of the surface receptor PDGFRα. The original detection method of determining FAPs and PNCs from the skeletal muscle environment utilized a monoclonal antibody that recognizes the PDGFRα receptor (Section 2.4.2). However, this antibody does not

provide optimal separation of current PDGFRα-expressing cells from non-expressing cells. Although utilizing the anti-PDGFRα monoclonal antibody to distinguish FAPs from other cells is a common isolation method in the FAP field, it may lead to FAP contamination in the PNC population. P*dgfra*$^{H2B\text{-}GFP}$ is a knockin GFP fluorescent reporter that labels cells expressing *Pdgfra* (Hamilton et al., 2003). We have previously validated the P*dgfra*$^{H2B\text{-}GFP}$ reporter as a reliable readout of *Pdgfra* expression based on scRNA-seq (Figure 2.6C). Transplantations of PNC and FAP populations were repeated using the *Pdgfra*$^{H2B\text{-}GFP}$ reporter as an isolation method. *Acvr1*$^{tnR206H/+}$;*Pdgfra*$^{H2B\text{-}GFP/+}$;Pdgfra-Cre mice 4- to 6-weeks-of-age were sacrificed and the *Acvr1*^{R206H}-expressing PNCs (R206H-PNC; tdTomato-;GFP- cells; Figure 3.1B) and FAPs (R206H-FAP - tdTomato-; GFP+ cells; Figure 3.1C) populations were collected, cultured for 14 days, and transplanted into the GA muscle of each hindlimb of a SCID host (Figure 3.1D). SCID hosts were used to avoid an immune rejection of the transplanted cells. R206H-PNC- and R206H-FAP-derived HO was observed 10 days post-transplantation, confirming that the R206H-PNC population exhibits a cell-autonomous osteogenic response (Figure 3.1C)

Figure 3.1

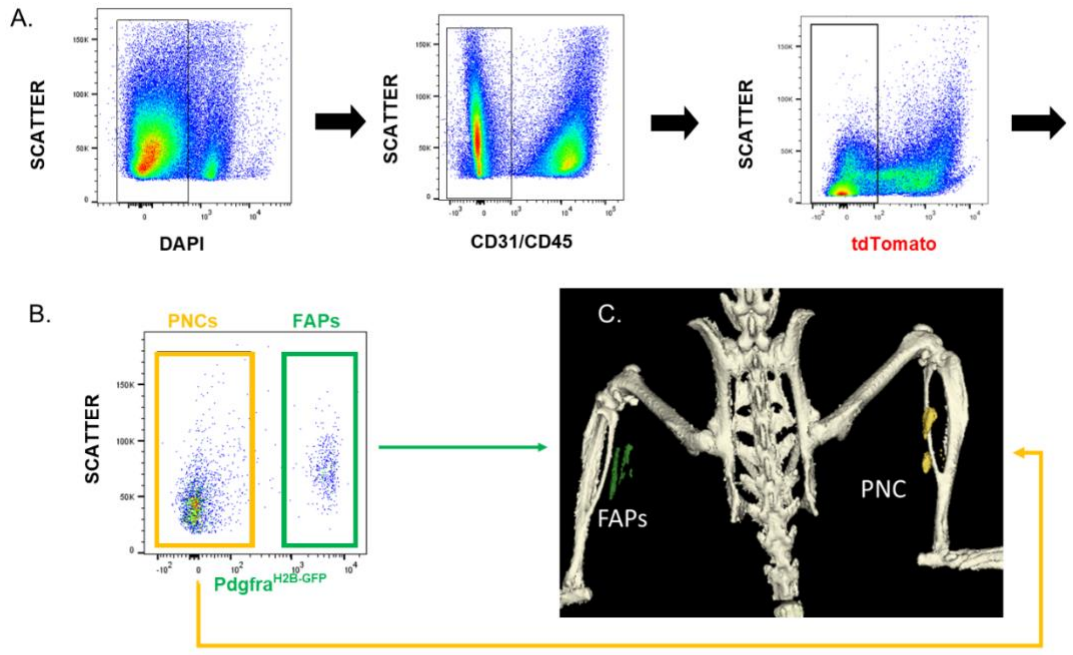

Figure 3.1 Validation of the osteogenic capabilities of the PNC population

A. PNC and FAP populations were isolated from 4- to 6-weeks-of-age *Pdgfra*$^{H2B\text{-}GFP/+}$;*R26*$^{mCherry/+}$;Pdgfra-Cre mice. FACS gating strategy used to remove DAPI+, CD31+, CD45+, and tdTomato- cells. **B.** PNC (yellow boxes) and FAP (green boxes) populations were collected from *Acvr1*$^{tnR206H/+}$;*Pdgfra*$^{H2B\text{-}GFP/+}$;Pdgfra-Cre mice and cultured for 14 days. **C.** PNCs and FAP populations were transplanted into opposing GAs of a SCID host. R206H-PNC-derived HO (pseudo-colored yellow) and R206H-FAP-derived HO (pseudo-colored green) were observed 10 days post-transplantation (N=4).

3.4.2 Pericytes, smooth muscle, and satellite cells do not contribute to HO

Transplantation of the PNC populations necessitates a culturing step prior to transplantation to attain the critical cell numbers required to induce an osteogenic response. We sought to determine if the percentages of cell types comprising the heterogeneous PNC population change with culturing. R206H-PNCs were isolated from *Acvr1*$^{tnR206H/+}$;*Pdgfra*$^{H2B\text{-}GFP/+}$;Pdgfra-Cre mice via FACS and placed in culture. Cells were cultured for approximately 14 days, mimicking the culturing step for PNC transplantations. The presence of Schwann cells, pericytes/smooth muscle, and satellite cells was determined via flow cytometry using surface receptor markers identified from scRNA-seq (Figure 3.2A – red arrows). Endothelial cell adhesion molecule (ESAM) was previously used to identify pericytes in lymph nodes and lungs (Sitnik et al., 2016; Kosyakova et al., 2020). scRNA-seq of the PNC population suggests that ESAM would also label skeletal muscle-derived pericytes and smooth muscle cells (Figure 3.2A – red arrows). CD59a is a surface marker previously shown to label Schwann cells in mice (Wiltbank et al., 2022) and was used here to label Schwann cells of the PNC population (Figure 3.2A – red arrows). It is important to note that neither ESAM nor CD59a are specific to the cell types they are intended to isolate within the PNC population. ESAM is expressed by vascular endothelial cells and hematopoietic cells, while CD59a is found to be expressed by endothelial cells of the PNS and by cells comprising the immune system (Vedeler et al. 1994; Li et al., 2022; Inoue et al., 2010). To combat the nonspecific expression of ESAM and CD59a, endothelial (CD31+) and hematopoietic cells (CD45+) were removed to avoid contamination (Figure 3.2B). Satellite cells were identified by VCAM expression (Figure 3.2A – red arrows) (Fukada et al., 2007). Due to the absence of cell-specific surface

markers identified within the tenocyte population, we could not confidently assess the contribution of tenocytes to the total PNC population after culturing. Schwann cells, pericytes and smooth muscle, and satellite cells were isolated from freshly dissociated skeletal muscle of *Acvr1*$^{tnR206H/+}$;*Pdgfra*$^{H2B\text{-}GFP/+}$;Pdgfra-Cre mice 6 weeks-of-age. The relative percentage of Schwann cells, satellite cells, and pericytes/smooth muscle cells were 15%, 14%, and 45% out of the total PNC population, respectively (Figure 3.2C). The PNC population was then isolated from *Acvr1*$^{tnR206H/+}$;*Pdgfra*$^{H2B\text{-}GFP/+}$;Pdgfra-Cre mice and cultured for 14 days. Flow cytometry revealed that the relative percentages of Schwann cells, satellite cells, and pericyte and smooth muscle cells post-culturing were 35%, 22%, and 10%, respectively, of the total PNC population (Figure 3.2B and Figure 3.2C). Culturing influences the proportion of the cell types present within the PNC population (Figure 3.2C).

Dey et al. investigated the contribution of pericyte and smooth muscle to HO using the syntenic *ACVR1*$^{Q207D\text{-}Tg/Q207D\text{-}Tg}$ mouse model of FOP (Dey et al., 2016). *ACVR1*$^{Q207D\text{-}Tg/Q207D\text{-}Tg}$ incorporates a man-made mutation not observed in the patient population and demonstrates a more robust HO response (Yu et al., 2008). Multiple Cre-drivers were tested to accommodate the inherent heterogeneity of the pericyte population. No HO was observed when the recombination of the *ACVR1*$^{Q207D\text{-}Tg/Q207D\text{-}Tg}$ allele was targeted to the pericyte and smooth muscle lineage, as outlined in Table 3.1.

Additionally, satellite cells have been examined for their osteogenic potential in both the *ACVR1*$^{Q207D\text{-}Tg/Q207D\text{-}Tg}$ and *Acvr1*^{tnR206H} mouse models of FOP (Dey et al., 2016; Lees-Shepard, 2018b). However, neither injury-induced nor spontaneous HO was observed in either mouse model of FOP (see Table 3.1). Given the flow cytometry results

and the lack of direct contribution to HO by the pericyte/smooth muscle and satellite cell lineages in a mouse model of FOP, we decided to exclude these populations from further analysis of the PNC cell type(s).

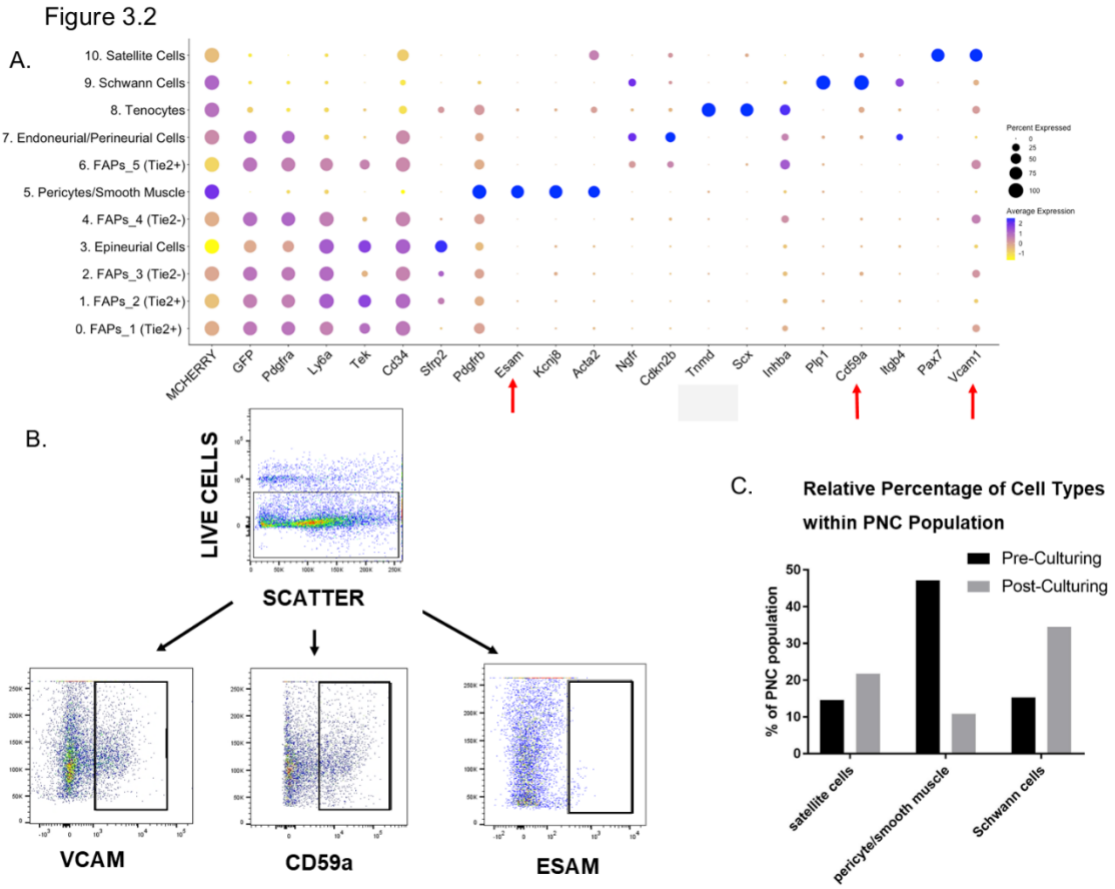

Figure 3.2 Relative percentages of PNC populations post-culturing

A. Dotplot of all cell types that historically express *Pdgfra* (scRNA-seq characterized in Section 4.7) identifying surface markers (red arrows) for Satellite cells, pericyte/smooth muscle, and Schwann cells. **B.** The PNC was isolated from *Acvr1*$^{tnR206H/+}$;*Pdgfra*$^{H2B\text{-}GFP/+}$;Pdgfra-Cre mice and cultured for 2 weeks. Cultured PNCs were separated into satellite cells, Schwann cells, and pericytes/smooth muscle. VCAM was used to identify satellite cells. CD59*a* was used to identify Schwann cells. ESAM was used to identify the pericyte/smooth muscle population. **C.** Quantification of pericytes/smooth muscle, Schwann cells, and satellite cells pre- and post-culturing.

Cre-Driver	Cell Types Targeted in Skeletal Muscle	Forms Traumatic HO Or Genetic HO	Causal Cell Identified * Identified in this study	Sources
Tie2-Cre (Kisanuki et al., 2001)	Hematopoietic, endothelial, subset of FAPs	Both	Tie2+ FAPs	(Woscznya et al., 2012), (Lees-Shepard et al., 2018)
Pdgfra-Cre (Roesch et al., 2008)	FAPs, neurogenic fibroblasts, Schwann cells*, satellite cells*, pericytes/smooth muscle*, TLCs	Both	FAPs, tenocytes, Schwann Cells*, TLC*	(Lees-Shepard, 2018), (Unpublished)
Pax7-Cre (Nishijo et al., 2009)	Satellite cell, myoblast, myofiber	NO	NO	(Dey et al., 2016)
Pax7-Cre^{ER} (Nishijo et al., 2009)	Satellite cell	NO	NO	(Dey et al., 2016)
MyoD^{iCre} (Kanisiack et al., 2009)	Satellite cells, myoblasts, muscle fibers	NO	NO	(Lees-Shepard et al., 2018)
VE-Cadeherin-Cre (Alva et al., 2006)	Endothelium, hematopoietic progenitors	NO	NO	(Lees-Shepard et al., 2018)
Scx-Cre (Pryce et al., 2007)	Tenocytes, tendon progenitors, TLCs	Both	Tenocytes, tendon progenitors (TLCs not tested)	(Dey et al., 2016), (Agarwal et al., 2017)
Scx^{CreERT2} (Howell et al., 2017)	Tenocytes, TLCs *	Both	Tenocytes, TLC*	(Agarwal et al., 2017), (*Unpublished)
Tppp3-Cre^{ER} (Harvey et al.,	Tendon Stem Cells	Traumatic HO (Not tested in Genetic HO)	*Tppp3*+, *Pdgfra*+ TDSC	(Yea et al., 2023)
Glast-Cre^{ER} (Goritz et al., 2011)	*Pdgfra*+ cells, Lymphocytes, adipocytes, connective tissue, macrophage	Traumatic HO	Mesenchymal populations (presumably FAPs)	(Kan et al., 2012)
SM22a-Cre (Lepore et al., 2005)	Pericytes, vascular smooth muscle, periosteal cells, *Pdgfra*+ cells	Traumatic HO	*Pdgfra*+ cells (presumably FAPs)	(Dey et al., 2016)
Wnt1-Cre (Lewis et al., 2013)	Schwann cells, neuronal fibroblasts, neurons	Both (*perinatal lethality in this study)	*Pdgfra*+ cells (did not test Schwann cell contribution)	(Zhao et al., 2023)
P0-Cre (Feltri et al., 1999)	Schwann cells, neuronal fibroblasts, neurons	Both	*Pdgfra*+ cells (did not test Schwann cell contribution)	(Zhao et al., 2023)
Cspg4-Cre^{ER} (Zhu et al., 2011)	NG2+ pericytes	NO	NO	(Dey et al., 2016)

Mx1-Cre (Adbel-Wahab et al., 2013)	Bone marrow, spleen, thymus, liver, mesenchymal cells	Genetic HO	*Pdgfra*+ cells (presumably FAPs)	(Dey et al., 2016)
Vav1-Cre (de Boer et al., 2003)	Bone Marrow hematopoietic and endothelial	NO	NO	(Dey et al., 2016)
FoxD1-Cre (Humphreys et al., 2010)	Pericytes, endogenous skeleton,	NO	NO	(Kan et al., 2012)
αSMA-Cre^{ERT2} (Grcevic et al., 2012)	Satellite cells, perivascular cells, *Pdgfra*+ cells	Traumatic HO	Perivascular (also express *Pdgfra*)	(Matthews et al., 2016)

Table 3.1: Cellular lineages tested for osteogenic capabilities in acquired and genetic HO

3.4.3 The Schwann cell lineage displays cell-autonomous osteogenic capabilities

Next, we wanted to identify whether cells within the peripheral nerves could contribute to the HO formed in *Acvr1*$^{tnR206H/+}$;Pdgfra-Cre mice. We developed a whole nerve transplantation assay where the sciatic nerve was aseptically removed from *Acvr1*$^{tnR206H/+}$;Pdgfra-Cre mice and transplanted into a preinjured GA of a SCID host (Figure 3.3A). GAs of the SCID hosts were injured one day before the transplantation via cardiotoxin injury. It is known that cardiotoxin does not induce an HO response in SCID hosts; thus, any observed bone formation would be attributed to the transplanted sciatic nerve. HO was observed 14 days post-transplantation of the sciatic nerve (Figure 3.3C – white arrows) and was not observed in the sham controls. The osteogenic response of the transplanted sciatic nerve shows that at least one cell type comprising the peripheral nerve can contribute to osteogenesis. Many *Pdgfra*-expressing cells are found within peripheral nerves (Figure 3.3B – GFP expression). Given the scRNA-seq analysis from Chapter 2, it is plausible that the *Pdgfra*-expressing cells of the nerves could be neuronal

connective tissue (Section 2.4.7). However, it is unclear if the neuronal connective tissue can directly contribute to HO.

Given that the sciatic nerve of *Acvr1*$^{tnR206H/+}$;Pdgfra-Cre mice display an osteogenic response when transplanted into a SCID host, we were interested in determining what cells within the sciatic nerve contribute to the formation of HO. We specifically tested whether Schwann cells can directly contribute to HO formation, as Schwann cells are a cell type that comprises the PNC population. We attempted to target the recombination of the *Acvr1*^{tnR206H} allele to the neural crest lineage using a Wnt1-Cre (Lewis et al., 2013). The Wnt1-Cre driver targets neural crest cells prior to migration from the neural tube. Therefore, many neural crest-derived cell types will be recombined; however, in the adult skeletal muscle environment, only peripheral neuronal structures are recombined by this model (Paylor et al., 2014). Recombination of the *Acvr1*^{tnR206H} allele in the *Wnt* lineage resulted in perinatal lethality. Perinatal lethality occurs when the *Acvr1*^{tnR206H} allele is recombined globally (Yamamoto et al., 2022) but typically is not observed when specific cell types are targeted (Lees-Shepard et al., 2018b; Lees-Shepard et al., 2018a; Lees-Shepard et al., 2018c).

As an alternative approach to testing whether R206H-Schwann cells contribute to HO formation, we FACS isolated R206H-Schwann cells (tdTomato-;GFP-;CD59a+) from *Acvr1*$^{tnR206H/+}$;*Pdgfra*$^{H2B\text{-}GFP/+}$;Pdgfra-Cre mice 6-weeks-of-age (Figure 3.4A). Schwann cells were cultured for 14 days, and the cells were transplanted into the TA of a SCID host. Testing the osteogenic capabilities of R206H-Schwann cells through a transplantation model of HO avoids the perinatal lethality complication. Using the *Pdgfra*$^{H2B\text{-}GFP}$ allele is essential to FACS isolate a pure Schwann cell population, as a

minor number of *Pdgfra*-expressing cells also express *Cd59a* (Figure 2.6A). The Schwann cell identity of the collected population was confirmed through SOX10 staining (Figure 3.4B) (Liu et al., 2015). The isolated Schwann cells were grown in culture, and 2.70 x 10^5 cells per 50 µL were transplanted into the TA of a SCID host. HO was observed 14 days post-transplantation (Figure 3.4C).

Schwann cells have the unique ability to dedifferentiate and redifferentiate when injured or cultured (Fawcett et al., 1990; Chen et al., 2007). To confirm that the osteogenic ability observed when R206H-Schwann cells are transplanted into a SCID host is not due to culturing of the cells, we pooled FACS-isolated Schwann cells from 5 *Acvr1*$^{tnR206H/+}$;*Pdgfra*$^{H2B\text{-}GFP/+}$;Pdgfra-Cre mice and directly transplanted the cells into the TA of a SCID host (Figure 3.4D). HO was observed 14 days post-transplantation. R206H-Schwann cells display a cell-autonomous osteogenic ability and are potentially an additional causal cell of HO in *Acvr1*$^{tnR206H/+}$;Pdgfra-Cre mice.

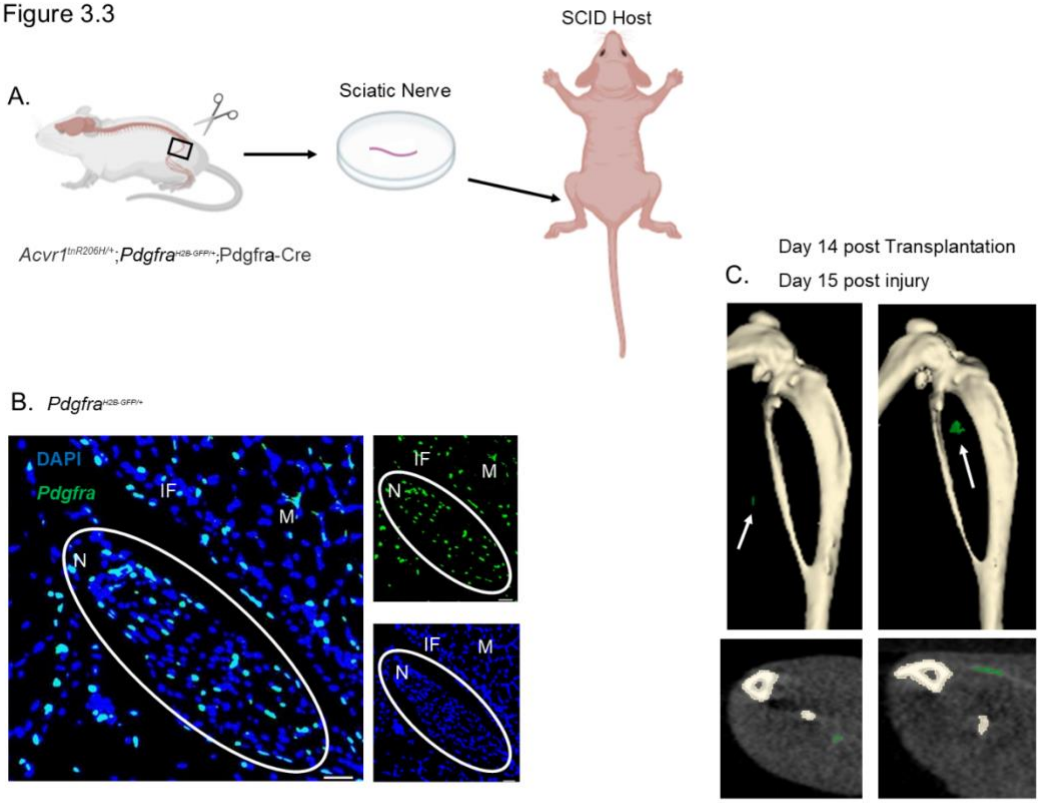

Figure 3.3: Whole nerve sciatic transplantation contributes to HO

A. Schematic representation of the sciatic whole nerve transplantation. Sciatic nerves were isolated from *Acvr1*$^{tnR206H/+}$;*R26*$^{NG/+}$;Pdgfra-Cre mice and transplanted into the preinjured GA of a SCID host (N=5). **B.** Peripheral nerves (white circle) of the hindlimb house *Pdgfra*-expressing cells. *Pdgfra* expression was determined via the *Pdgfra*$^{H2B-GFP}$ reporter. Nuclei were counterstained with DAPI. **C.** Representative images of the vast array of HO observed 14 days post-transplantation. Cross sections of the lesion are below the respective distal hindlimbs. N- nerve, IF- intermuscular fascial region, M- muscle

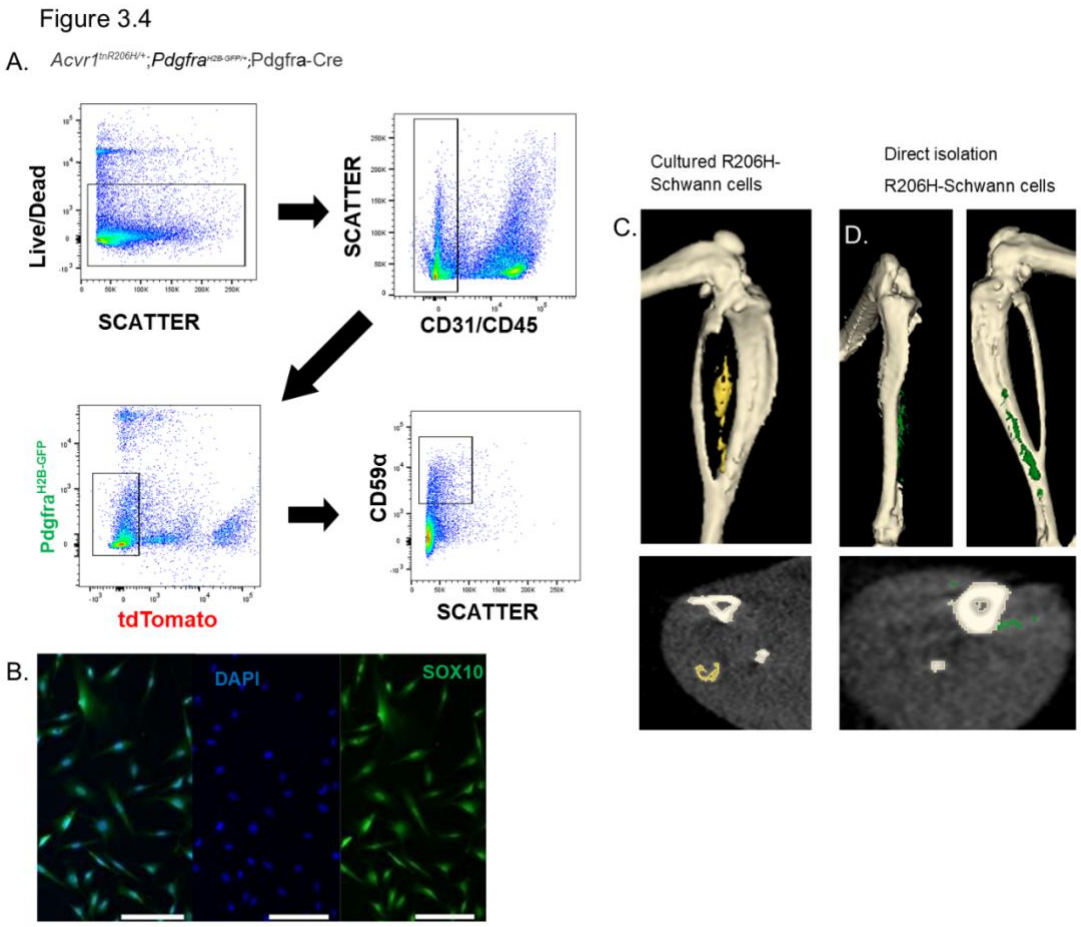

Figure 3.4: R206H-Schwann cells display a cell-autonomous osteogenic capability

A. Flow cytometry gating strategy used to isolate Schwann cells from *Acvr1*$^{tnR206H/+}$;*Pdgfra*$^{H2B-GFP}$;Pdgfra-Cre mice. Schwann cells were collected based on DAPI-;CD31-;CD45-;*Pdgfra*$^{H2B-GFP}$-;tdTomato-;CD59a+ expression. **B.** In vitro SOX10 staining of DAPI-;CD31-;CD45-;*Pdgfra*$^{H2B-GFP}$-;tdTomato-;CD59a+ cells confirming Schwann cell identity. **C.** Representative μCT images of R206H-Schwann cell transplantation into the TA of a SCID host, 14 days post-transplantation (N=3). Cross section of lesional tissue is shown below representative image. **D.** HO derived from directly isolated R206H-Schwann cells 14 days post-transplantation (N=2). Cross section of lesional tissue is shown below the representative image

3.4.4 TLCs localize to the intermuscular fascial regions

We previously determined that the hindlimb intermuscular fascial regions of the posterior compartment house a PNC cell type (Figure 2.9E), which was hypothesized to be the TLC population (Section 2.5). Scx$^{GFP/+}$;*R26*$^{mCherry/+}$;Pdgfra-Cre mice were used to fluorescently label TLCs via the dual expression of *Scx* and historical expression of *Pdgfra.* Current *Scx* expression was determined using the knockin fluorescent reporter, Scx^{GFP}, in which the GFP open read frame was targeted to exon 1 of the *Scx* locus (Pryce et al., 2007). Therefore, the presence of GFP serves as a direct readout of *Scx*-expressing cells. Historical *Pdgfra expression* was determined through the recombination of the *R26*$^{mCherry/+}$ allele (Peron et al., 2015) via Pdgfra-Cre (see Section 2.4.6). *Pdgfra*$^{H2B\text{-}GFP/+}$;*R26*$^{mCherry/+}$;Tie2-Cre mice were used to label Tie2+ and Tie2- FAPs (see Section 2.4.8). Current *Pdgfra* expression was determined using the knockin fluorescent reporter, *Pdgfra*$^{H2B\text{-}GFP}$, in which an H2B-eGFP fusion gene was knocked into the native *Pdgfra* locus (Hamilton et al., 2003). Thus, Cells that are currently expressing *Pdgfra* are labeled by GFP fluorescence. We directly compared the intermuscular fascial regions of 6-week-old Scx$^{GFP/+}$;*R26*$^{mCherry/+}$;Pdgfra-Cre and *Pdgfra*$^{H2B\text{-}GFP/+}$;*R26*$^{mCherry/+}$;Tie2-Cre mice. TLCs were found to be localized to the intrafascial regions of the intermuscular fascia (Figure 3.5B). Tie2+ and Tie2- FAPs were found localized to the outer perimeter of the intermuscular fascial regions (Figure 3.5C). Importantly, the *Pdgfra*-expressing cells on the perimeter of the intermuscular fascial regions were not expressing *Scx* (compare Figure 3.5B to Figure 3.5C) and would not be targeted from recombination through the *Scx*^{CreERT2} Cre-driver.

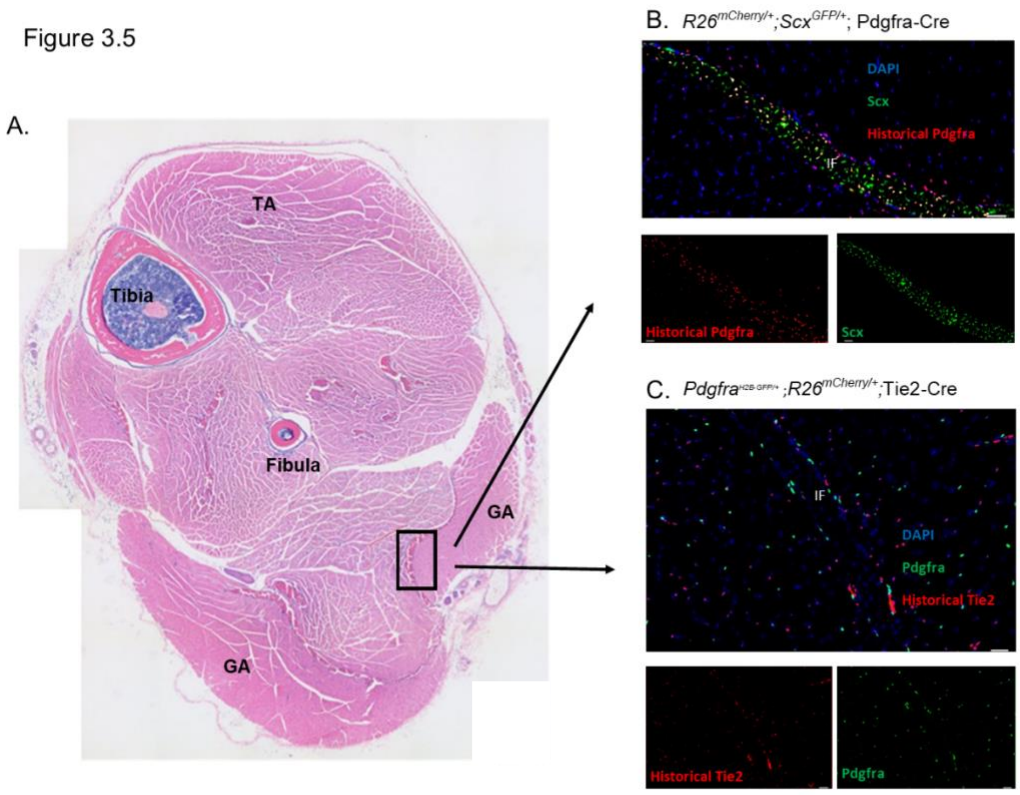

Figure 3.5: TLCs localize to the intermuscular fascial region

A. H&E staining of a whole limb cross-section. The intermuscular fascial region is boxed in black. **B.** Representative image of intermuscular fascial regions of *Scx*$^{GFP/+}$*;R26*$^{mCherry/+}$;Pdgfra-Cre mice. Cells currently expressing *Scx* are labeled via Scx^{GFP}. Cells of the *Pdgfra lineage* are labeled by *R26*^{mCherry} fluorescence. TLCs dual express GFP and mCherry. **C.** Representative images of the intermuscular fascial region of *Pdgfra*$^{H2B\text{-}GFP/+}$*;R26*$^{mCherry/+}$;Tie2-Cre mice. *Pdgfra*-expressing cells are labeled via *Pdgfra*$^{H2B\text{-}GFP}$. Cells of the *Tie2 lineage* are labeled by *R26*^{mCherry} fluorescence. Tie2+ FAPs are dual expressing GFP and mCherry, while Tie- FAPs only express GFP. GA- gastrocnemius, TA- tibialis anterior, IF- intermuscular fascial region

Figure 3.4.5 R206H-TLCs contribute to intramuscular injury-induced HO

Next, we sought to test whether the R206H-TLC population can contribute to injury-induced or spontaneous HO. Recombination of the *Acvr1*^{tnR206H} allele in the TLC population was accomplished using the temporally controlled Cre-driver, *Scx*^{CreERT2} (Figure 3.2A). R206H-FAPs have been shown to upregulate *Scx* as early as 3 days post-injury but do not express *Scx* in uninjured skeletal muscle tissue (unpublished data- RNA-sequencing of R206H-FAPs). Therefore, the inducible property of the *Scx*^{CreERT2} Cre-driver is critical in targeting the recombination of the *Acvr1*^{tnR206H} allele to TLCs and not FAPs. We deployed a specific dosing strategy that entailed tamoxifen treatment before injury to avoid recombination of the *Acvr1*^{tnR206H} allele to FAPs. *Acvr1*$^{tnR206H/+}$;*Scx*$^{CreERT2/+}$ mice 6- to 8-weeks-of-age were administered tamoxifen (150 mg/kg for 3 consecutive days), and the TA and GA muscles were injured through cardiotoxin injection after a 5- to 7-day washout period. Surprisingly, R206H-TLC-derived HO was first detected 4 days post-injury (Figure 3.6B- white arrow) and peaked around 7 days post-injury (Figure 3.6C). The majority of HO formed by day 7 was then resorbed (Figure 3.6D – Figure 3.5H). Interestingly, the HO present is not fused with the endogenous skeleton but forms at the intermuscular fascial regions of the hindlimb (compare Figure 3.6A – orange lines to cross-sections of μCT scans to HO cross sections in 3.6B- 3.6G). In conclusion, TLCs contribute to injury-induced HO and are an additional causal cell of HO in a mouse model of FOP.

Scx-expressing tenocytes of the Achilles tendon have been found to contribute to traumatic HO (Agarwal et al., 2017; Harvey et al., 2019). We were curious whether TLCs require the expression of the R206H mutation for HO formation. *Scx*$^{CreERT2/+}$ mice were

injected with cardiotoxin. HO was not observed at any time point post-injury (Figure 3.7A). (Menezes.)*Acvr1*$^{tnR206H/+}$;*Scx*$^{CreERT2/+}$ mice is due to the presence of the recombined *Acvr1*^{tnR206H} allele.

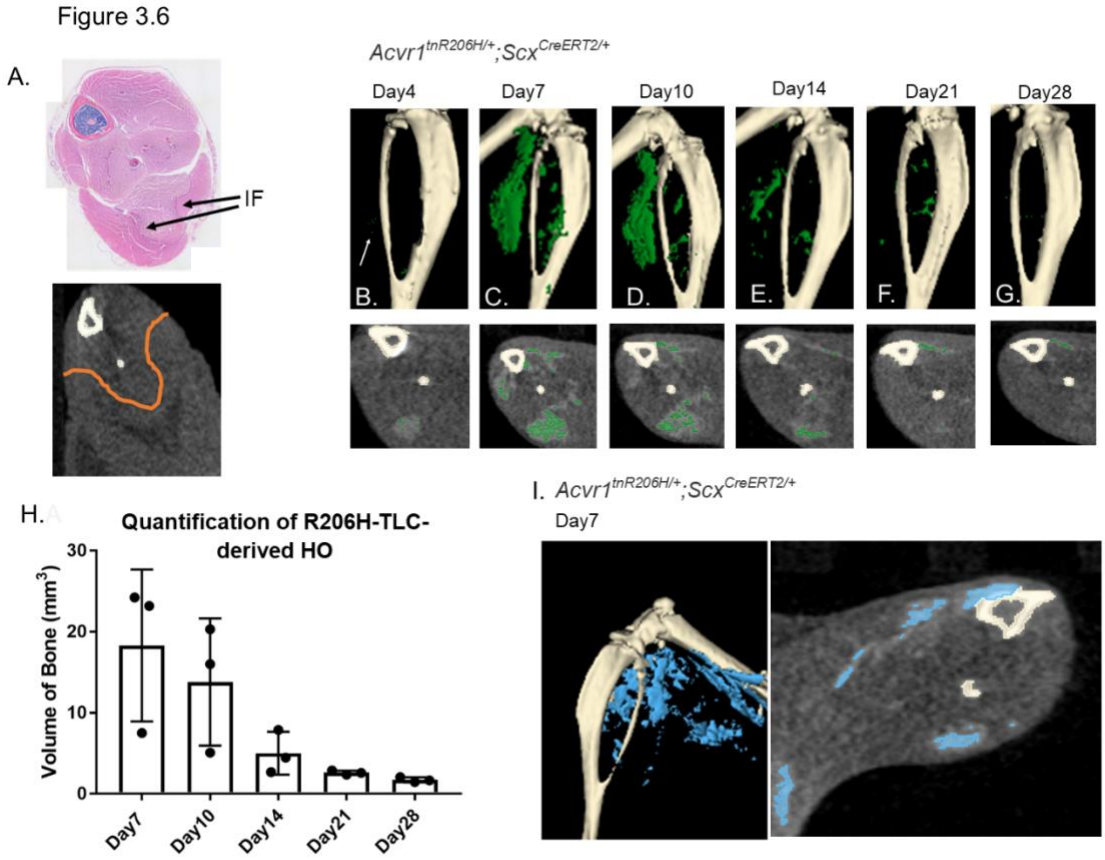

Figure 3.6: *Acvr1*$^{tnR206H/+}$;*Scx*$^{CreER/+}$ mice display an early onset and unstable HO response

A. H&E stained representative hindlimb cross-section. Intermuscular fascial regions are identified by black arrows (IF). µCT cross-section approximating where the IF region is located (orange line). **B-G.** Representative images of µCT scans post-cardiotoxin injury to the TA of *Acvr1*$^{tnR206H/+}$;*Scx*^{CreERT2} mice 6-weeks-of-age (N=3) mice. HO is pseudo-colored green. The endogenous skeleton is pseudo-colored white. Cross sections of peak lesional tissue are shown below the representative hindlimb µCT scan. **B.** Bone was detected 4 days post-injury. **C.** Peak HO formation observed 7 days post-injury. **D-G**. µCT scans showing HO resorption. **H.** Quantification of the volume of HO. **I.** Representative µCT scans and cross-section of R206H-TLC-derived HO 7 days post-cardiotoxin injury to the GA. IF- intermuscular fascial region

Figure 3.7

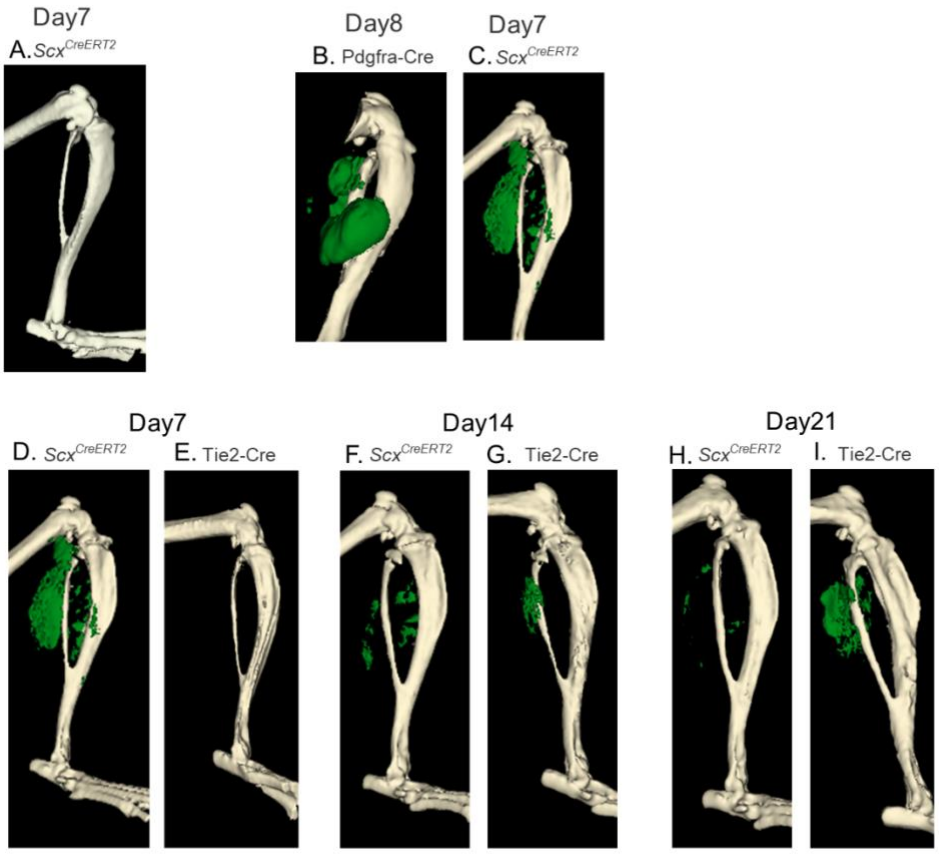

Figure 3.7: Qualitative comparison of R206H-TLC and R206H-FAP-derived injury-induced HO

A. Representative μCT scans of *Scx*$^{CreER/+}$ mice 7 days post-cardiotoxin injury to the TA. HO was not observed. **B-C.** Qualitative comparison of the HO response of *Acvr1*$^{tnR206H/+}$;Pdgfra-Cre (8 days post-cardiotoxin injury to the TA, **B**) and Acvr*1*$^{tnR206H/+}$;S*cx*$^{CreER/+}$ (7 days post-cardiotoxin injury to the TA, **C**) mice. **D-I.** Comparison of HO responses of *Acvr1*$^{tnR206H/+}$;S*cx*$^{CreER/+}$ and *Acvr1*$^{tnR206H/+}$;Tie2Cre mice post-cardiotoxin injury to the TA. 7 **(D, E)**, 14 **(F, G)**, and 21 **(H, I)** days post-injury were analyzed.

3.4.6 Qualitative comparative analysis of injury-induced HO responses of R206H-TLCs and R206H-FAPs

Given the novel R206H-TLCs-dervied HO response in *Acvr1*$^{tnR206H/+}$;*Scx*$^{CreERT2/+}$ mice, we sought to compare R206H-TLC- and R206H-FAP-derived HO (previously collected by the Goldhamer lab). *Acvr1*$^{tnR206H/+}$;Tie2-Cre mice were utilized to test the contributions of R206H-FAPs and *Acvr1*$^{tnR206H/+}$;Pdgfra-Cre mice were used to test the combination of R206H-FAPs- and R206H-TLCs-derived HO. Cardiotoxin was administered to the TA of *Acvr1*$^{tnR206H/+}$; *Scx*$^{CreERT2/+}$, *Acvr1*$^{tnR206H/+}$;Pdgfra-Cre, and *Acvr1*$^{tnR206H/+}$;Tie2-Cre mice. The peak bone formation of *Acvr1*$^{tnR206H/+}$;*Scx*$^{CreERT2/+}$ mice was observed around 7 days post-injury (Figure 3.7C and Figure 3.7D). *Acvr1*$^{tnR206H/+}$;Pdgfra-Cre mice showed injury-induced HO at 8 days post-injury (day 7 was not tested- Figure 3.7B), while HO derived from R206H-Tie2+ FAPs was not observed until 10 days post-injury (Figure 3.7E and Figure 3.7G). In *Acvr1*$^{tnR206H/+}$;*Scx*$^{CreERT2/+,}$ and *Acvr1*$^{tnR206H/+}$;Pdgfra-Cre mice, HO appears earlier than in *Acvr1*$^{tnR206H/+}$;Tie2-Cre mice. The accelerated appearance of HO in *Acvr1*$^{tnR206H/+}$;Pdgfra-Cre mice could result from R206H-TLC-derived HO.

Next, we compared the progression of HO formation between R206H-TLCs and R206H-FAPs. R206H-FAP-derived HO peaked between 14 to 21 days post-injury, contrasting with the progression of R206H-TLC-derived HO (Figures 3.7D – Figures 3.7I). The R206H-TLC-derived HO was less stable than the R206H-FAP-derived HO, as resorption of the mineralized bone occurred between 7 and 21 days post-injury, while R206H-FAP-derived HO remained stable once formed (Compare Figures 3.7D- 3.7I);

therefore, R206H-TLC-derived HO displays a different HO response than R206H-FAP-derived HO.

3.4.7 Investigation of early lesion formation of R206H-TLC-derived HO

It is known that R206H-FAP-derived HO is formed through the endochondral ossification pathway (Lees-Shepard et al., 2018b). Considering that TLCs are a novel causal cell of HO, we were curious whether TLCs also differentiate along the endochondral ossification pathway. The first appearance of mineralized material observed through μCT imaging in *Acvr1*$^{tnR206H/+}$;*Scx*$^{CreERT2/+}$ mice was at 4 days post-injury. To test the pathway of osteogenesis of R206H-TLC-derived HO, we harvested *Acvr1*$^{tnR206H/+}$;*Scx*$^{CreERT2/+}$ mice directly before the first appearance of HO (3 days post-cardiotoxin injury to the TA; Figure 3.8A) and when HO was at a maximum volume (7 days post-injury; Figure 3.8B). Bone was not observed 3 days post-injury by μCT detection; however, the cross-sectional area showed localized areas of inflammation around the intermuscular fascial regions (Figure 3.8A – white arrows). H&E staining showed an infiltration of cells in the injured tissue (Figure 3.8C). No histologically identifiable cartilage was observed 3 days post-injury (Figure 3.8C), although a lesion of potentially immature bone and hypertrophic cartilage was observed at the site where mineralized material was identified by μCT imaging 7 days post-injury (Figure 3.8E).

To further evaluate if R206H-TLCs differentiate along the endochondral ossification pathway of osteogenesis, we investigated whether recombined cells expressed cartilage or bone markers at 3 and 7 days post-cardiotoxin injury in *Acvr1*$^{tnR206H/+}$;*Scx*$^{CreERT2/+}$ mice. Chondrocytes were determined by SOX9 expression, and osteoprogenitors were determined by the OSX expression. Day 3 post-injury revealed an influx of tdTomato-

;SOX9+ cells in the early lesion, confirming that R206H-expressing cells undergo chondrogenesis prior to bone formation (Figure 3.8D). Day 7 post-injury revealed the presence of tdTomato-;OSX+ cells in the lesional environment (Figure 3.8F). Very few SOX9+ cells were present within the lesional tissue 7 days post-injury. The confirmation of OSX+ cells, lack of SOX9+ cells, and pattern of H&E staining suggest that the lesional tissue at 7 days post-injury could be composed of a mix of hypertrophic chondrocytes and immature osteoprogenitor cells. This data indicates that the R206H-TLC-derived HO forms along an accelerated endochondral ossification pathway.

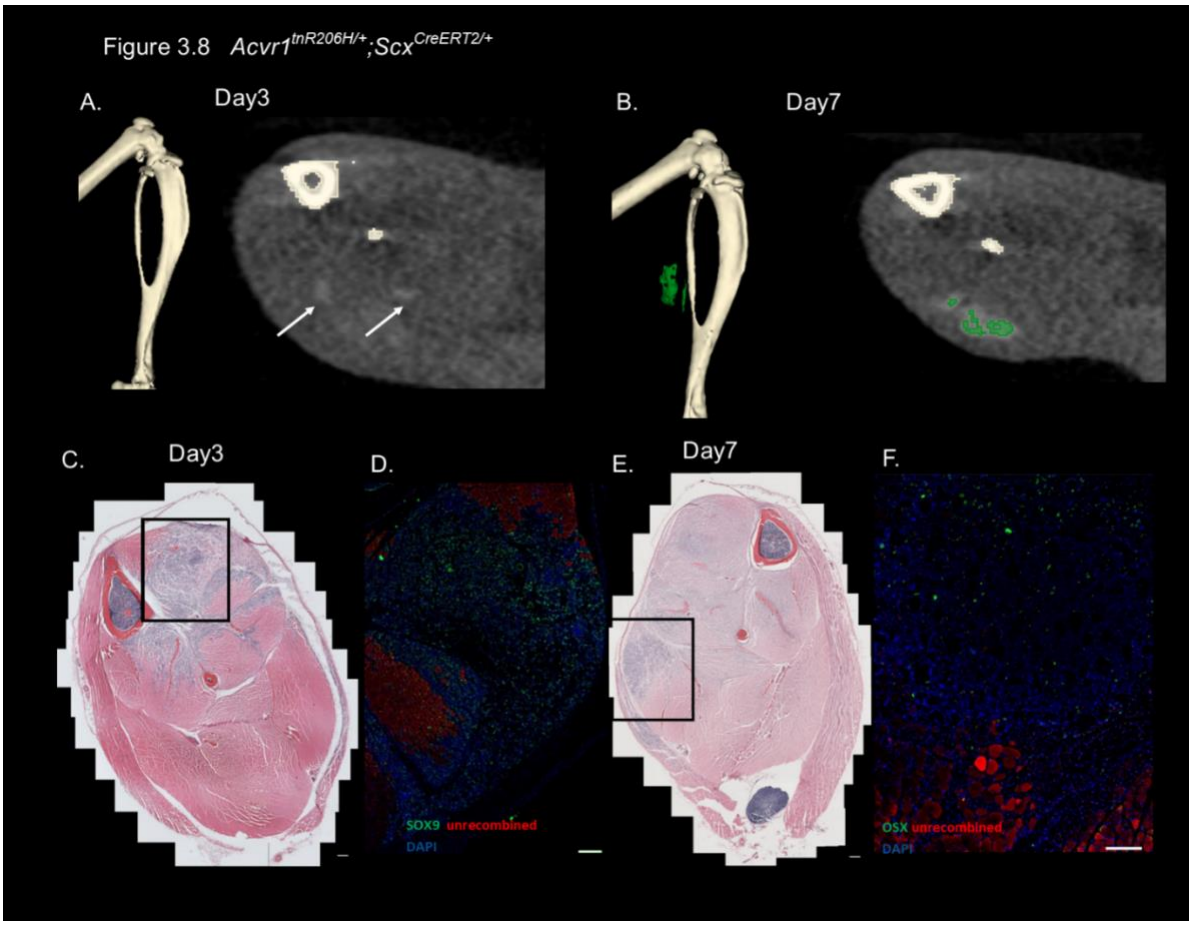

Figure 3.8: R206H-TLC-derived HO differentiates along the endochondral ossification pathway

A. μCT images of *Acvr1*$^{tnR206H/+}$;*Scx*$^{CreERT2/+}$ mice 3 days post-cardiotoxin injury to the TA. Cross section of HO formation is to the right of the distal hindlimb. **B.** μCT images of *Acvr1*$^{tnR206H/+}$;*Scx*$^{CreERT2/+}$ mice 7 days post-injury. Cross section of HO formation is to the right of the distal hindlimb. HO is pseudo-colored in green. The endogenous skeleton is pseudo-colored white. **C.** H&E staining of *Acvr1*$^{tnR206H/+}$;*Scx*$^{CreERT2/+}$ mice 3 days post-injury. The black box outlines the lesional area shown in D. **D.** Immunofluorescence of SOX9 expression 3 days post-cardiotoxin injury. **E.** H&E staining of *Acvr1*$^{tnR206H/+}$;*Scx*$^{CreERT2/+}$ mice 7 days post-injury. The black box outlines the lesional area shown in F. **F.** Immunofluorescence of OSX expression 7 days post-cardiotoxin injury. (N=2)

3.4.8 R206H-TLC-derived HO is unstable in an exacerbated model of HO

Given the accelerated HO response and instability of bone growth observed in *Acvr1*$^{tnR206H/+}$*;Scx*$^{CreERT2/+}$ mice that were injured with cardiotoxin, we were curious whether R206H-TLC-derived HO would exhibit the same HO response in an exacerbated model of HO. Anti-ACVR1 monoclonal antibodies were developed as a potential therapeutic of HO and intended to inhibit ligand binding to the ACVR1 receptor; however, anti-ACVR1 antibodies were found to be agonists of ACVR1, activating downstream osteogenic signaling and leading to an exacerbated HO response in *Acvr1*$^{tnR206H/+}$*;*Tie2-Cre mice (Lees-Shepard et al., 2022; Burdick et al., 2024). We used JAB0505, an anti-ACVR1 monoclonal antibody (Aykul et al., 2022), in attempt to exacerbate the formation of R206H-TLC-derived HO. *Acvr1*$^{tnR206H/+}$*;Scx*$^{CreERT2/+}$ mice were injured via cardiotoxin injection into the TA or GA muscles immediately after administering 10 mg/kg of JAB0505. R206H-TLCs displayed a greater and more robust HO response in the presence of JAB0505 (compare Figure 3.9E to 3.5H). JAB0505 administration causes a delayed response of peak HO formation in R206H-FAP-derived HO, with HO peaking around 21 to 28 post-injury in *Acvr1*$^{tnR206H/+}$*;*Tie2-Cre mice (Lees-Shepard et al., 2022; Burdick et al., 2024). The peak of HO formation of R206H-TLC-derived HO in the presence of JAB0505 occurred around 7 days post-injury (Figure 3.9A and Figure 3.9E). Additionally, most HO formed 7 days post-injury was resorbed by 14 days-post injury (Figure 3.9B and Figure 3.9E). This result suggests that the accelerated HO formation and HO resorption observed in R206H-TLC-derived HO is not specific to the mode of injury.

Figure 3.9 *Acvr1*$^{tnR206H/+}$;*Scx*$^{CreERT2/+}$

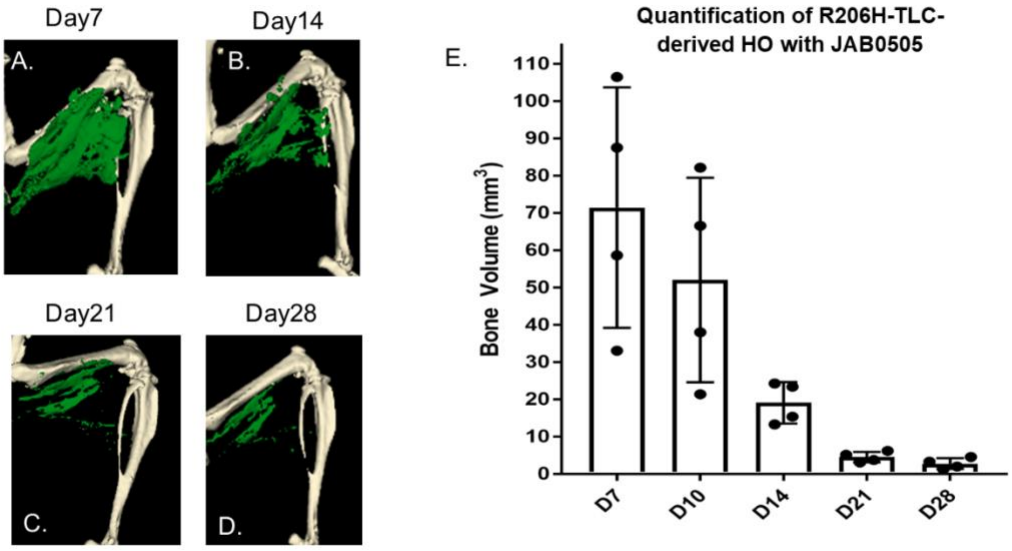

Figure 3.9: R206H-TLC-derived HO is resorbed in an exacerbated HO model

A-D. Representative images of HO formation of *Acvr1*$^{tnR206H/+}$;*Scx*$^{CreERT2/+}$ mice that were administered JAB0505 (10 mg/kg) immediately before cardiotoxin injection into the TA. HO is pseudo-colored green. The endogenous skeleton is pseudo-colored white. 7 **(A),** 14 **(B),** 21 **(C),** and 28 days post post-injury and JAB0505 injection. **E.** Quantification of HO volume (mm^3).

3.4.9 TLCs differentiate through the endochondral ossification pathway in a BMP-induced model of traumatic HO

The *Scx* lineage can contribute to traumatic HO. (Agarwal et al., 2017; Harvey et al., 2019). BMP6 is a bone morphogenetic protein (BMP) that predominantly signals through ACVR1 and is used to induce an acquired HO response (Burdick et al., 2024; Nickel et al., 2019). To test if TLCs can contribute to acquired HO, 2.5µg of rhBMP6 in 1% alum adjuvant carrier was injected into the GA muscle of *R26*$^{mCherry/+}$;*Scx*$^{CreERT2/+}$ mice. *R26*$^{mCherry/+}$;*Scx*$^{CreERT2/+}$ mice were used to fluorescently label cells of the TLC lineage.

Interestingly, no bone growth was observed 7 days post-injection (Figure 2.10B). H&E staining and μCT imaging revealed the formation of HO 10 days post-injection (Figure 2.10A and Figure 2.10C). Lesional tissue displayed SOX9+ cartilage (Figure 2.10D) and OSX+ bone cells at 10 days post-injection (Figure 2.10E). Within the lesional environment, we identified two distinct cell populations; mCherry- cells, likely FAPs, given their documented contribution to BMP-induced HO (Woscznya et al., 2012) and mCherry+ TLCs of the mCherry+ cells present in the lesional tissue 2% of cells stained positive for SOX9 and 11% stained positive for OSX expression, confirming the TLC contribution to acquired HO that was formed via the endochondral ossification pathway.

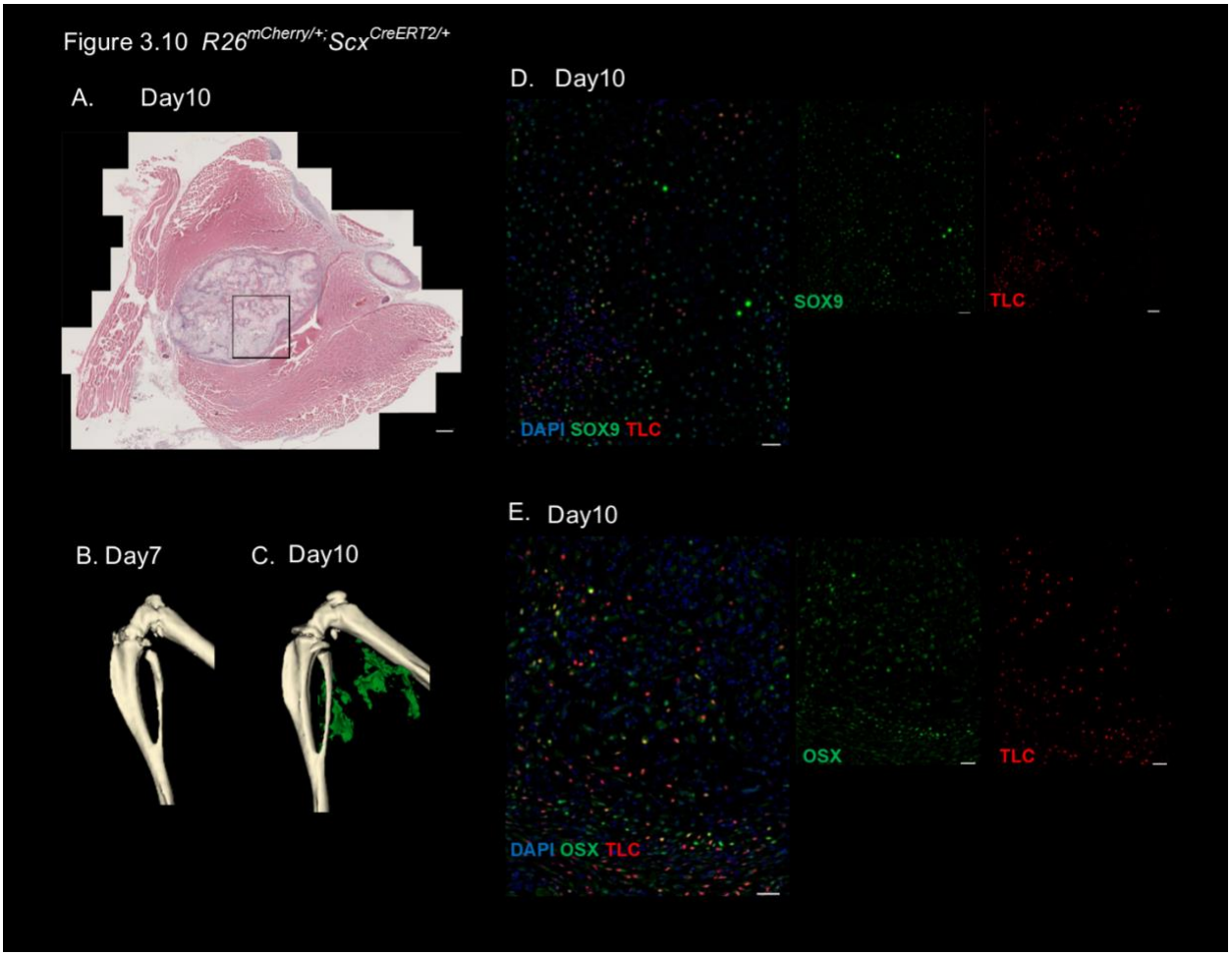

Figures 3.10: TLCs contribute to acquired HO through the endochondral ossification pathway

A. H&E staining cross-section of HO formed 10 days post-injection of BMP6. The black box outlines the area shown in D and E**. B-C.** Representative μCT images of BMP6 induced HO in *R26*$^{mCherry/+}$*;Scx*$^{CreERT2/+}$ mice 7 days (**B**) and 10 days (**C**) post-injection. HO is pseudo-colored green. The endogenous skeleton is pseudo-colored white. **D.** SOX9 staining of the lesional area 10 days post-injection. TLCs were labeled via *R26*^{mCherry}. **E.** OSX staining of lesional area 10 days post-injection. TLCs were labeled via *R26*^{mCherry}.

3.5.1 Discussion

This chapter aimed to identify the osteocompetent cell types within the PNC population. R206H-Schwann cells and R206H-TLCs both display the ability to contribute to HO directly. The remaining two cell types, comprising the PNC population, pericytes/smooth muscle, and satellite cells, were not tested for osteogenic potential. Lees-Shepard et al. showed that *Acvr1*^{R206H}-expressing satellite cells do not display an osteogenic response in our Cre-dependent mouse model of FOP (Table 3.1) (Lees-Shepard et al., 2018b). Dey et al. used an additional Cre-dependent mouse model of FOP (*ACVR1*$^{Q207D\text{-}Tg/Q207D\text{-}Tg}$), which incorporates a man-made mutation not observed in the patient population and demonstrates a more robust HO response, to test the osteogenic capacity of pericytes and smooth muscle (Dey et al., 2016). SM22a-Cre (Lepore et al., 2005), which targets vascular smooth muscle and a subset of pericytes, and Cspg4-CreER^{T2} (Zhu et al., 2011), which targets NG2 expressing pericytes, did not result in the formation of HO (Dey et al., 2016) (see Table 3.1).

We first identified that the neurogenic lineage contributes to HO through a sciatic nerve transplantation assay (Figure 3.3). The neural crest lineage was targeted using an additional mouse model of FOP (*P0-Cre*;*Rosa26-LSL-rtTA3*;*Col1a1-tetO-FOP-ACVR1*) (Zhoa et al. 2023). Doxycycline treatment through drinking water induced the recombination of the *Col1a1-tetO-FOP-ACVR1* allele in the Myelin protein zero (*P0*) lineage (Zhoa et al., 2023). Injury-induced HO was observed 14 days post-cardiotoxin injection (Zhoa et al., 2023). Zhoa et al. claimed that the PDGFRα+ cells of the *P0* lineage were the causal cells of HO; however, they did not test the osteocompetent ability of any PDGFRα- cells (Zhoa et al., 2023), potentially missing the Schwann cell contribution to

HO that we observed (Figure 3.4). Targeting the recombination of the *Acvr1*^{tnR206H} allele to the *Wnt* lineage resulted in perinatal lethality, which has been observed when recombination of the *Acvr1*^{tnR206H} allele was globally targeted (Yamamoto et al., 2022). To our knowledge, this is the first evidence of a cell lineage-specific Cre-driver resulting in a similar response, potentially suggesting that a cell of the *Wnt1* lineage could be responsible for the observed perinatal lethality.

Dey et al. revealed that cells of the *Scx* lineage that express *Pdgfra* contribute solely to spontaneous HO in a mouse model of FOP (Dey et al., 2016). The contribution to injury-induced HO of the *Scx* lineage was tested 21 days post-injury cardiotoxin injury to the GA. TLCs are part of the *Scx* lineage; however, they are distinct from the previously established *Scx* causal cells due to the absence of *Pdgfra* expression. In contradiction to Dey et al. we concluded that R206H-TLCs can directly contribute to injury-induced HO. Dey et al. did not test early time points post-injury, potentially missing any TLC-derived HO in their mouse model of FOP. Dey et al. utilized the constitutive Cre-driver, Scx-Cre; therefore, many cell types could potentially be transcribing the R206H mutation (Dey et al., 2016). One of those cell types includes chondrocytes derived from *Scx+;Sox9+* precursor cells (Sugimoto et al., 2013; Chen et al., 2007). *Scx+;Sox9+* precursor cells were found to be present in the articular cartilage of the joints (Sugimoto et al., 2013), where the spontaneous HO was identified (Dey et al., 2016). We did not observe spontaneous HO in *Avcr1*$^{tnR206H/+}$;*Scx*^{CreERT2} mice. It is possible that the *Scx+;Sox9+* precursor cells downregulate *Scx+* expression in adult mice and would not be targeted by the inducible *Scx*^{CreERT2} when tamoxifen is administrated at 6-weeks-of-age.

A histological analysis of the early HO lesional environment determined that R206H-TLC-derived HO is formed through the endochondral ossification pathway (Figure 3.8). *Acvr1*$^{tnR206H/+}$;*Scx*$^{CreERT2/+}$ mice collected 3 days post-cardiotoxin injury revealed SOX9-expressing TLCs (Figure 3.7), a necessary transcription factor of cartilage differentiation (Akiyama et al., 2002). 7 days post-injury revealed OSX-expressing TLCs in the lesional environment (Figure 3.7). Endochondral ossification is a pathway of bone development where cells differentiate into a cartilage intermediate that is then replaced by osteoprogenitors. Recent studies have shown that chondrocytes can directly differentiate into osteocytes at the growth plate and the articular subchondral bone regions (Jing et al., 2017). It is possible that the R206H-TLCs are differentiating to SOX9+ chondrocytes and then directly differentiating into bone; however, further experimentation is required.

The instability of injury-induced HO observed by *Acvr1*$^{tnR206H/+}$;*Scx*$^{CreERT2/+}$ mice is not observed in *Acvr1*$^{tnR206H/+}$;Pdgfra-Cre or *Acvr1*$^{tnR206H/+}$;Tie2-Cre mice (Figure 3.7). Interestingly, the instability of R206H-TLC-derived HO is still observed in an exacerbated model of HO (Figure 3.9). The instability of HO is potentially due to the lack of R206H-FAPs contributing to the HO lesion, as FAPs are not recombined in *Acvr1*$^{tnR206H/+}$;*Scx*$^{CreERT2/+}$ mice. RNA-sequencing of R206H-FAPs revealed an upregulation of activin A transcripts, the known osteogenic ligand of HO in FOP (Hatsell et al., 2015; Hino et al., 2015), compared to wild-type counterparts (unpublished data). The localized level of activin A in the lesional environment of *Acvr1*$^{tnR206H/+}$;*Scx*$^{CreERT2/+}$ mice may not be sufficient to sustain the formation of HO, as R206H-FAPs are not providing additional activin A to the injury environment. Non-osteocompetent cells could

potentially be a source of activin A. One cell type that is not thought to be recombined by *Scx*^{CreERT2} is osteoclasts. Osteoclasts are derived from the myeloid/monocyte lineage and are cells that degrade bone to initiate normal bone remodeling (Boyce et al., 2010). In the wild-type context, osteoclast function is inhibited by activin A (Fowler et al., 2015). It is possible that the localized levels of activin A present at the lesional site in *Acvr1*$^{tnR206H/+}$*;Scx*$^{CreERT2/+}$ mice may not be sufficient to inhibit osteoclast function; however, further experimentation is required (Section 5.1.2).

In conclusion, this chapter confirms the osteogenic potential of the PNC population by identifying two additional causal cells of HO: Schwann cells and TLCs. Moreover, it characterizes the novel osteogenic response of the R206H-TLC population not seen by other causal cells of HO or cells of the *Scx* lineage, suggesting that TLCs are a potentially novel cell type. A transcriptomic analysis comparing TLCs, tenocytes of the Achilles tendon, and FAPs is described in Chapter 4.

Chapter 4: A Comparative Analysis of the Gene Expression Profiles of TLC, FAPs, and Tenocytes

4.1: Abstract

We have previously identified Tendon-Like Cells (TLCs) as causal cells of HO in a mouse model of FOP. TLC-derived HO exhibited an earlier onset of HO and differences in HO stability and growth modality compared to other HO causal cells. The novel bone-forming pattern observed by TLCs suggests their genetic divergence from previously characterized causal cells. A transcriptomic analysis comparing TLCs, Tie2+ FAPs, tenocytes comprising the Achilles tendon (referred to as tenocytes), and muscle stem cells (MuSC) revealed that the TLC transcriptome was found to be most like FAPs; however, they lack the expression of conventional FAP markers. TLCs expressed a combination of markers characteristic of tenocytes and hindlimb fibroblasts. TLCs also naturally expressed markers of the endochondral ossification pathway. RNA-sequencing of cultured tenocytes and TLCs revealed that both cell types undergo transcriptomic changes towards a more tendon stem cell-like fate post-culturing. The data outlined throughout this chapter ultimately suggests that TLCs are a novel connective tissue cell type.

4.2: Introduction

Connective tissue is one of the four tissues that comprise the human body (Kamrani et al., 2023). Every organized tissue of the body has connective tissue associated with it that assists in the organization and structure of the tissue. For example, the organization of skeletal muscle tissue begins with individual myofibers. The endomysium is the layer of connective tissue at the basement membrane encasing the individual myofibers (Mukund et al., 2020). Myofibers are grouped into fascicles (Frontera and Ochala., 2014) surrounded by perimysial connective tissue (Contreras et al., 2021). Multiple fascicles are grouped to form a fully functional muscle (Dave et al., 2023). The epimysium surrounds each muscle and links muscles to tendons at the myotendinous junctions (Contreras et al., 2021; Mukund et al., 2020). The three layers of skeletal muscle connective tissue interconnect but can be distinguished by their distinct location and arrangement of collagen bundles (Gillies et al., 2013). The perimysium is mainly composed of Collagen I, while the epimysium and endomysium are equal parts Collagen I and Collagen III. Other collagens found in the connective tissue layers are Collagens VI, XV, XII, and IV (Gillies et al., 2011).

The connective tissue layers of skeletal muscle are mainly comprised of fibroblasts, FAPs, and tenocytes. Fibroblasts are responsible for synthesizing and secreting the majority of components forming the extracellular matrix (ECM) (Contreras et al., 2021; Chapman et al., 2016). Defining a fibroblast can be challenging due to ambiguity in distinguishing fibroblasts from other supportive cells within the hindlimb environment. A general definition of a fibroblast is a collagen-producing, spindle-shaped cell residing within the skeletal muscle space between muscle fibers and fascicles

(Chapman et al., 2016). Fibroblasts typically express Vimentin (*Vim*), Transcription factor 4 (*Tcf4*), and Fibroblast associated protein (*Fap*) and lack cell-specific gene markers of other connective tissue cell types (Chapman et al., 2016; Mathew et al., 2010). FAPs can differentiate into fibroblasts, establishing a relationship between the two cell types (Joe et al., 2010; Uzemi et al., 2011). Despite their relatedness, FAPs and fibroblasts exhibit differences in their gene expression profiles and differentiation potential. FAPs express Platelet-derived growth factor receptor a (*Pdgfra*), Stem cell antigen 1 (*Sca1*), and *Cd34* and can differentiate into adipogenic and fibrotic lineages. FAPs play a critical role in the maintenance and homeostasis of skeletal muscles (Woscznya et al., 2019; Contreras et al., 2021). Using the $Pdgfra^{H2B\text{-}GFP}$ reporter (Hamilton et al., 2003), FAPs were found in all muscle connective tissue layers but are thought to be more abundant in the epimysium and perimysium (Contreras et al., 2021). Tenocytes, which are a distinct cell type from FAPs and fibroblasts, are the primary cellular component of tendons, a dense connective tissue structure that connects muscle to bones. (Li et al., 2021). At the molecular level, tenocytes are characterized by the expression of Scleraxis (*Scx*), Tenomodulin (*Tnmd*), and Mohawk (*Mkx*) (see Section 1.2.2 for more information) (Schweitzer et al., 2001; Li et al., 2021). Tenocytes are responsible for secreting the components comprising Collagen 1 bundles, the most basic organizational structure of the tendon (He et al., 2022). Many Collagen I bundles are organized into fibrils, and many fibrils comprise a single collagen fiber (He et al., 2022). Collagen fibers form a fascicle, and bundles of fascicles form a fully functional tendon (He et al., 2022). Tendons are then wrapped in an epitenon connective tissue. In some tendons, such as the Achilles tendon, the epitenon

is encased in a sheath-like paratenon, which together makes the outermost structure of the tendon, the peritenon (Huang et al., 2021).

FAPs and tendon progenitors were found to directly contribute to HO in a mouse model of FOP (Lees-Shepard et al., 2018b; Dey et al., 2016). We have previously shown that TLCs are an additional causal cell of HO (Chapter 3). TLC-derived HO exhibited an earlier onset of HO and differences in HO stability and growth modality when compared to tenocyte- (Dey et al., 2016) or FAP-derived HO (Lees-Shepard et al., 2018b; Chapter 3). This chapter will characterize TLCs based on their location and gene expression profile. While the TLC transcriptome as a whole was found to be most similar to FAPs, they lacked the expression of conventional FAP markers and expressed a combination of tenocyte and hindlimb fibroblast genes. Additionally, we explore how culturing TLCs and tenocytes influences the transcriptomes of both cell types towards a more tendon stem cell-like gene expression (TDSC) profile. We will ultimately conclude that TLCs are a potential novel connective tissue cell comprising the intermuscular fascial regions.

4.3: Materials and Methods

4.3.1: Genetic mouse models and mouse crosses

R26$^{mCherry/+}$;*Scx*$^{GFP/+}$;Pdgfra-Cre and *Pdgfra*$^{H2B\text{-}GFP/+}$ mice used for the histological analysis were generated as previously described (Section 3.3.1). *Scx*$^{GFP/+}$ mice were kindly provided by Dr. Ronen Schweitzer (Shriners Hospital for Children; Portland, OR) (Pryce et al., 2007). *Scx*$^{GFP/+}$ mice express GFP under the endogenous *Scx* locus. The GFP open reading frame was inserted into exon 1, beginning at the initiator ATG of the *Scx* gene and replacing most of the first exon (Pryce et al., 2007). Mice were genotyped

by PCR and, when applicable, by the presence or absence of fluorescent reporters (see Appendix 1B). Mice were used 6- to 8-weeks-of-age and were maintained in a climate-controlled vivarium at the University of Connecticut. Males and females were used equally. All procedures were approved by the University of Connecticut Animal Care Committee in accordance with IACUC.

4.3.2: Histological analysis of *Scx* expression

R26$^{mCherry/+}$;*Scx*$^{GFP/+}$;Pdgfra-Cre and *Pdgfra*$^{H2B\text{-}GFP/+}$ mice were sacrificed via cervical dislocation, limbs were collected at desired time points, fixed in 4% paraformaldehyde (PFA) in 1X DPBS, and rocked at 4°C for 3 days. Samples were washed with 1X DPBS, and a decalcification step was performed to remove the calcium ions from the endogenous skeleton. Decalcification was obtained by incubating samples in decal solution, 12.5% ethylenediaminetetraacetic acid (EDTA) with 1% sodium hydroxide in 1X DPBS, for 1 month. The decal solution was replaced every other day. Once decalcification was completed, samples were washed with 1X PBS and placed in a cytoprotectant containing 30% sucrose in 1X PBS overnight. Samples were flash frozen in Tissue-Tek O.C.T. compound (O.C.T.; Thermo Fisher, Waltham, MA, USA) using a dry-ice and 70% ethanol slurry. Samples were stored at -80°C and sectioned using a Leica cryostat (CM3050S) at a 10 µm thickness. Samples were counterstained with DAPI and coverslipped using FluoroGel mounting medium (Electron Microscopy Sciences; Hatfield, PA, USA). Slides were imaged on a Leica Thunder imaging platform housed at the UCONN Advanced Light Microscopy COR^{2}E.

4.3.3: Hematoxylin and eosin (H&E) staining

Sections were brought to room temperature, rehydrated in nanopure water, and placed in Mayer's hematoxylin (Sigma-Aldrich; St. Louis, MO, USA) for 8 minutes. After hematoxylin staining, sections were placed in a 2% ammonium bluing solution and dehydrated using progressively concentrated ethanol solutions. Samples were placed in eosin Y (Sigma-Aldrich; St. Louis, MO, USA) for 5 seconds. Excess eosin Y was washed away with 95% ethanol washes, and sections were fully dehydrated using 100% ethanol and xylene. Samples were mounted using Permount mounting medium (Thermo Fisher; Waltham, MA, USA) and imaged the following day using the Leica Thunder imaging platform housed at the UCONN Advanced Light Microscopy COR^{2}E.

4.3.4: Isolation of the posterior intermuscular fascial regions of the hindlimb

Scx$^{GFP/+}$ mice were sacrificed via cervical dislocation. Fur and skin surrounding the hindlimbs were removed, exposing the distal hindlimb muscles. A slit in the fascia between the posterior and lateral hindlimb compartments was made, separating the posterior compartment muscles from the rest of the hindlimb. The posterior compartment was severed from the limb and secured in a dissection tray using dissection pins. The soleus and plantaris muscles were removed, leaving the gastrocnemius (GA) behind. Tendons and tendon insertion points were dissected away while preserving the intermuscular fascial regions of the GA and associated muscles. See Appendix IC for more information.

4.3.5 FACS isolation of the TLCs

Scx$^{GFP/+}$ mice were pooled, and the intermuscular fascial regions of the posterior compartment were isolated as previously described (Section 4.3.5 and Appendix IC). The intermuscular fascial regions and associated skeletal muscles were minced for 7 minutes and placed in digestion media containing Dulbecco's Modified Eagle Medium (DMEM; Thermo Fisher; Waltham, MA, USA), 5 mg/ml Collagenase Type II (Worthington Biochemical; Lakewood, NJ, USA), and .5 U/mL Dispase (Thermo Fisher; Waltham, MA, USA). Samples were placed at 37°C for 1 hour with constant agitation. Digestion was then quenched with quench media (DMEM containing 10% HyClone characterized fetal bovine serum (FBS; GEHealthcare, Lot #A00168; Chicago, IL, USA) and filtered through 70 μM mesh strainers (Corning Life Sciences; Tewksbury, MA, USA). Single-cell suspensions were spun down at 500g for 5 minutes at 4°C. Pellets were washed in 1X DPBS, spun down, and resuspended in FACS Buffer (DPBS supplemented with 2% FBS). Samples were filtered through FACS tubes with 35 μM cell strainer (Corning Life Sciences; Tewksbury, MA, USA) and brought to the University of Connecticut Flow Cytometry Facility where target populations were collected directly into TRIzol (Invitrogen; Waltham, MA, USA) using a BD FACSAria II Cell Sorter equipped with 5 lasers (355nm, 405nm, 488nm, 561nm, and 640nm).

4.3.6 Low-input RNA cDNA library preparation and RNA-sequencing

Samples were brought to the UCONN Center for Genomics Institute (CGI), where the Takara Bio Pico Input V3 kit generated cDNA libraries. Total RNA was collected and converted to cDNA. Illumina adapters were ligated to the cDNA, and ribosomal cDNA was

depleted. The remaining cDNA fragments were further amplified and purified to form a cDNA library. The libraries were then sequenced with roughly 30 million paired-end reads on the Novaseq 600 Illumina platform (Illumina; San Diego, CA, USA).

4.3.7 Culturing of TLCs and tenocyte samples

In each biological replicate, both of the Achilles tendons and posterior intermuscular fascial regions of an individual *Scx*$^{GFP/+}$ mouse were collected and processed separately. Each cultured tenocyte sample comprised both Achilles tendons, 2 per mouse. Each cultured TLC sample comprised both posterior intermuscular fascial regions, 2 per mouse, and were isolated as described in Section 4.3.3 (see Appendix IC). Achilles tendons were dissected out, and visible muscles were removed. The tendon samples were digested in tendon-specific digest media (DMEM supplemented with 5 mg/ml Collagenase Type II and 4 U/mL Dispase). All samples were placed at 37°C for 1 hour with constant agitation. The digestion of samples was quenched with quench media (DMEM containing 10% FBS). Samples were grown in growth media comprising 20% FBS in DMEM supplemented with 50 U/mL penicillin and 50 µg/mL streptomycin (Pen/Strep; Gibco, Grand Island, NY, USA), and 2.5 ng/mL recombinant Human Fibroblastic Growth Factor (bFGF; Gibco; Grand Island, NY, USA). The plates were coated with rat tail collagen I (Invitrogen; Waltham, MA, USA) before seeding and then incubated at 37°C with 5% CO2. Samples were cultured for 5 days, detached from the tissue culture dishes, washed in 1X DPBS, and resuspended in FACS buffer (DPBS containing 2% FBS). GFP-expressing cells were FACS isolated directly into TRIzol (Invitrogen; Carlsbad, California, USA) using a BD FACSAria II Cell Sorter equipped with

5 lasers (355nm, 405nm, 488nm, 561nm, and 640nm) and brought to the UCONN CGI for library prep and sequencing.

4.3.8 RNA-sequencing reads processing

MuSC (GEO: GSE126872) (Collins et al., 2019) and tenocyte (GEO: GSE213033) (Korcari et al., 2022) raw sequence reads were downloaded using the SRA toolkit and analyzed simultaneously with the Tie2+ FAP and TLC raw sequencing reads. The computational workflow consisted of read quality control using FastQC (Andrews, 2010) and FASTp (Chen et al., 2018) and read quality filtering using Fastx-toolkit. Filtered reads were aligned to the Mus_musculus.GRCm39.105 reference genome using Hisat2 (Kim et al., 2019). The read alignment quality control was performed using Qualimap (Okonechnikov et al., 2015). Lastly, a count matrix was generated using Htseq-count (Anders et al., 2015).

Count matrices were analyzed in R using the DESeq2 (Love et al., 2014). DESeq2 will eliminate genes with zero counts to allow for the focus to be placed on genes that are expressed above background levels. Next, size factor normalization is performed. This normalization process includes calculating a size factor or scaling factor, which is used to adjust for library size and sequencing depth differences between samples. Next, DESeq2 will estimate a gene-wise dispersion parameter, which is critical for accurately modeling the variance in the count data. This accounts for the relationship between the mean expression level and the variance of genes within biological replicates. Count plots display the normalized DESeq2 gene counts.

As standard in the field, the normalized DESeq2 gene counts are then transformed and utilized in heatmaps, PCA, and correlation plots. Transformations were done on the DESeq2 normalized read counts through variance stabilizing transformation (VST) or regularized logarithm transformation (Rlog). Both transformation methods stabilize the variances across the normalized samples, which helps to minimize bias from low gene counts. The analysis shown throughout this chapter utilized the VST normalization method; however, the Rlog method corroborates the findings.

All heatmaps, PCA, and count plots were created in R. Specifically, R software packages used in graph making included DESeq2, pheatmap (Kolde, 2012), and ggplot2 (Wickham, 2016).

4.4: Results

4.4.1: TLCs, FAPs, and tenocytes have distinct anatomical locations

Given that TLCs, FAPs, and tenocytes are all cells that comprise the hindlimb connective tissue, we were curious about where these cells localize within the hindlimb. We harvested hindlimbs from 6-week-old $R26^{mCherry/+}$;$Scx^{GFP/+}$; Pdgfra-Cre mice and directly compared the historical *Pdgfra,* current *Scx,* and current *Pdgfra* expression between TLCs, FAPs, and tenocytes. The *Pdgfra* lineage was determined through the recombination of the Cre-dependent $R26^{mCherry/+}$ allele (Peron et al., 2015) via Pdgfra-Cre; therefore, TLCs, tenocytes, and FAPs will be labeled by mCherry fluorescence. *Scx+* expression will be used to identify tenocytes and TLCs. Current *Scx* expression was determined using the knockin fluorescent reporter, Scx^{GFP}, in which the GFP open read frame was targeted to exon 1 of the *Scx* locus (Pryce et al., 2007). Therefore, the

presence of GFP serves as a direct readout of *Scx*-expressing cells. Intramuscular fascial regions of the hindlimb were identified by H&E staining (Figure 4.1A – blue box). *Scx*+;mCherry+ TLCs were found to be localized to the intermuscular fascial regions of the posterior compartments (Figure 4.1C, Figure 4.1D, and Figure 4.1E). We identified tenocytes based on the anatomical location and recognizable pattern of H&E staining (Figure 4.1F - blue box). Expectedly, tenocytes of the Achilles tendon express *Scx* and historical *Pdgfra* expression (Figure 4.1H, Figure 4.1I, and Figure 4.1J).

Given that FAPs and some subpopulations of the Achilles tendon have been documented to express the surface receptor *Pdgfra* (Harvey et al., 2019*;* De Micheli et al., 2020)*,* we were curious where the *Pdgfra*-expressing cell localize. We employed the knockin *Pdgfra* reporter, *Pdgfra*$^{H2B\text{-}GFP}$ (see Section 2.4.6 and Figure 2.5), which was created by knocking in an H2B-eGFP fusion gene into the native *Pdgfra* locus (Hamilton et al., 2003). Thus, cells currently expressing *Pdgfra* are labeled by GFP fluorescence. As expected, The TLC population showed no current *Pdgfra* expression (Figure 4.1B). The *Pdgfra*-expressing cells, presumed FAPs, were localized to the periphery of the intermuscular fascial regions and did not express *Scx* (compare Figure 4.1B to Figure 4.1C and Figure 4.1E). In contrast to TLCs, the tendon samples expressed *Pdgfra* sporadically (Figure 4.1G). The TLCs' lack of *Pdgfra* and the presence of *Scx* expression

within the intermuscular fascial regions of the posterior hindlimb confirm that the TLCs are distinct from tenocytes and FAPs at the histological level.

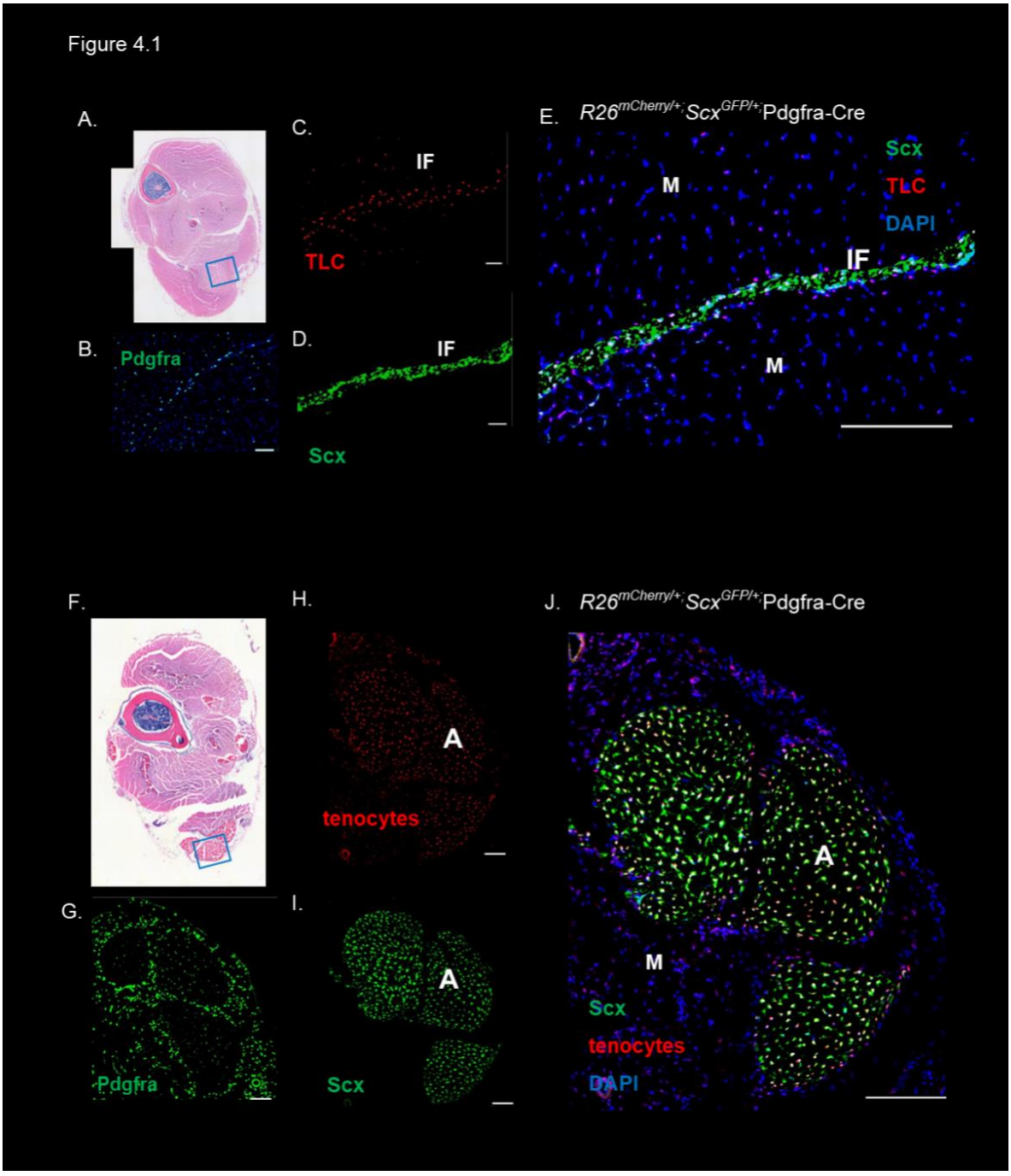

Figure 4.1: Comparison of the location of FAPs, TLCs, and tenocytes within the distal hindlimb

A. H&E stained cross-section of the midpoint of the distal hindlimb. The intermuscular fascial region, shown in **B-E,** is outlined in the blue box **B.** *Pdgfra* expression of FAPs, identified by $Pdgfra^{H2B\text{-}GFP}$ fluorescence, localized to the periphery of the intermuscular fascial regions. **C-E.** The intermuscular fascial region of the posterior compartment of the hindlimb. **C.** Historical *Pdgfra* expression of the intermuscular fascial region identified by $R26^{mCherry}$ fluorescence. **D.** *Scx* expression of the intermuscular fascial region identified by Scx^{GFP} fluorescence. **E.** TLCs localize to the intermuscular fascial region. **F.** H&E stained cross-section of the distal regions of the hindlimb. The blue box outlines the location of the Achilles tendon. **G.** *Pdgfra* expression, identified by $Pdgfra^{H2B\text{-}GFP}$ fluorescence, of the Achilles tendon. **H-J.** $R26^{mCherry/+}$;$Scx^{GFP/+}$;Pdgfra-Cre Achilles tendon of the distal hindlimb. **H.** Historical *Pdgfra* expression of the Achilles tendon determined by $R26^{mCherry}$ fluorescence. **I.** The current *Scx* expression of the Achilles tendon is determined by Scx^{GFP} fluorescence. **E.** Tenocytes of the Achilles tendon express Scx. N = 3**.** A- Achilles tendon, IF- intermuscular fascial region, M- muscle

4.4.2: The TLC transcriptome is related to FAPs

Given the differences between TLCs, FAPs, and tenocytes observed through histology (Figure 4.1), we were interested in whether the TLC transcriptome was similar to the tenocyte or FAP transcriptome. An overview of the experimental approach is outlined in Figure 4.2C. We developed a specialized dissection protocol (see Appendix IC), which resulted in the isolation of just the intermuscular fascial region of the posterior compartment and associated muscle. We harvested the intermuscular fascial regions from $Scx^{GFP/+}$ mice 6- to 8-weeks-of-age (Figure 4.2A, blue box). Live *Scx*-expressing cells were isolated via FACS (Figure 4.2B), and the transcriptome was obtained through bulk RNA-sequencing. The intermuscular fascial regions from 8 mice were pooled to comprise a single biological replicate of the TLC sample and 2 biological replicates were analyzed in total. Notably, the TLC population makes up a very low percentage of the total

skeletal muscle environment. We eliminated much of the posterior hindlimb compartment to avoid contamination from tendon insertion sites, which minimized the total sample, eliminating some of the TLC population.

The TLC transcriptome was compared to the transcriptomes of Tie2+ FAPs (generated by the Goldhamer lab - unpublished data), tenocytes comprising the Achilles tendon, referred to as tenocytes (GEO: GSE213033) (Korcari et al., 2022), and muscle stem cells (MuSCs) (GEO: GSE126872) (Collins et al., 2019). FAPs, TLCs, and tenocytes comprise the connective tissue of the hindlimb and are causal cells of HO in a mouse model of FOP. Tenocytes and TLCs express the common tenocyte marker, *Scx,* suggesting a potential similarity between the two populations. Additionally, when scRNA-seq of the *Pdgfra* lineage (described in Chapter 2- Figure 2.6) was compared to scRNA-seq data obtained from total cells of the hindlimb (both generated by the Goldhamer lab - unpublished), the TLCs clustered closer to FAPs than tenocytes, suggesting a potential overlap of the FAP and TLC transcriptomes. MuSCs were chosen as a negative control comparison to the TLC population. We anticipate fewer transcriptional similarities between TLCs and MuSC than between TLCs and tenocytes or FAPs.

scRNA-seq of the Achilles tendon revealed that it is a heterogeneous tissue comprised of 2 to 3 tenocyte subpopulations (De Micheli et al., 2020). To not limit or bias the comparison between TLCs and tenocytes, we chose to compare the TLC sample, whose heterogeneity is unknown, to a tenocyte sample that included all subpopulations of tenocytes. All tenocyte subpopulations comprising the Achilles tendon exhibit a classic gene expression profile typical of tenocytes; however, they demonstrate variations in the expression levels of these genes (De Micheli et al., 2020).

The raw reads of all samples were run through a standard RNA-seq pipeline, where they were quality-controlled, adaptors were ligated, reads were aligned to a reference genome, and counted to create a gene-by-count matrix. The matrix was then analyzed in RStudio using the standard DESeq2 pathway. Samples were normalized, filtered for low-quality reads, and transformed to account for variances hindering the biological differences between samples.

Principle Component Analysis (PCA) was used to assess the similarity of Tie2+ FAP, TLC, MuSC, and tenocyte transcriptomes. The PCA analysis revealed that TLCs are more similar to FAPs than tenocytes or MuSCs (Figure 4.3A). To confirm the PCA analysis and to determine how correlated the Tie2+ FAPs, MuSC, tenocyte, and TLC replicates were, we created a correlation matrix. Correlation coefficients were calculated for each replicate to determine the strength of the linear relationship between samples (Figure 4.3B). As expected, the replicates of each cell type were highly correlated, represented by a 1 or .99 correlation coefficient (Figure 4.3B). FAP and TLC populations were moderately correlated with each other, observed by a 0.55 to 0.69 correlation coefficient (Figure 4.3B). A heatmap, with unsupervised clustering between samples, was generated using the top 50 most variable genes between all samples, revealing that the transcriptomes of FAPs and TLCs are most related (Figure 4.3C). The PCA plot, correlation plot, and heatmap all agree that the TLC transcriptome is most similar to the Tie2+ FAP transcriptome.

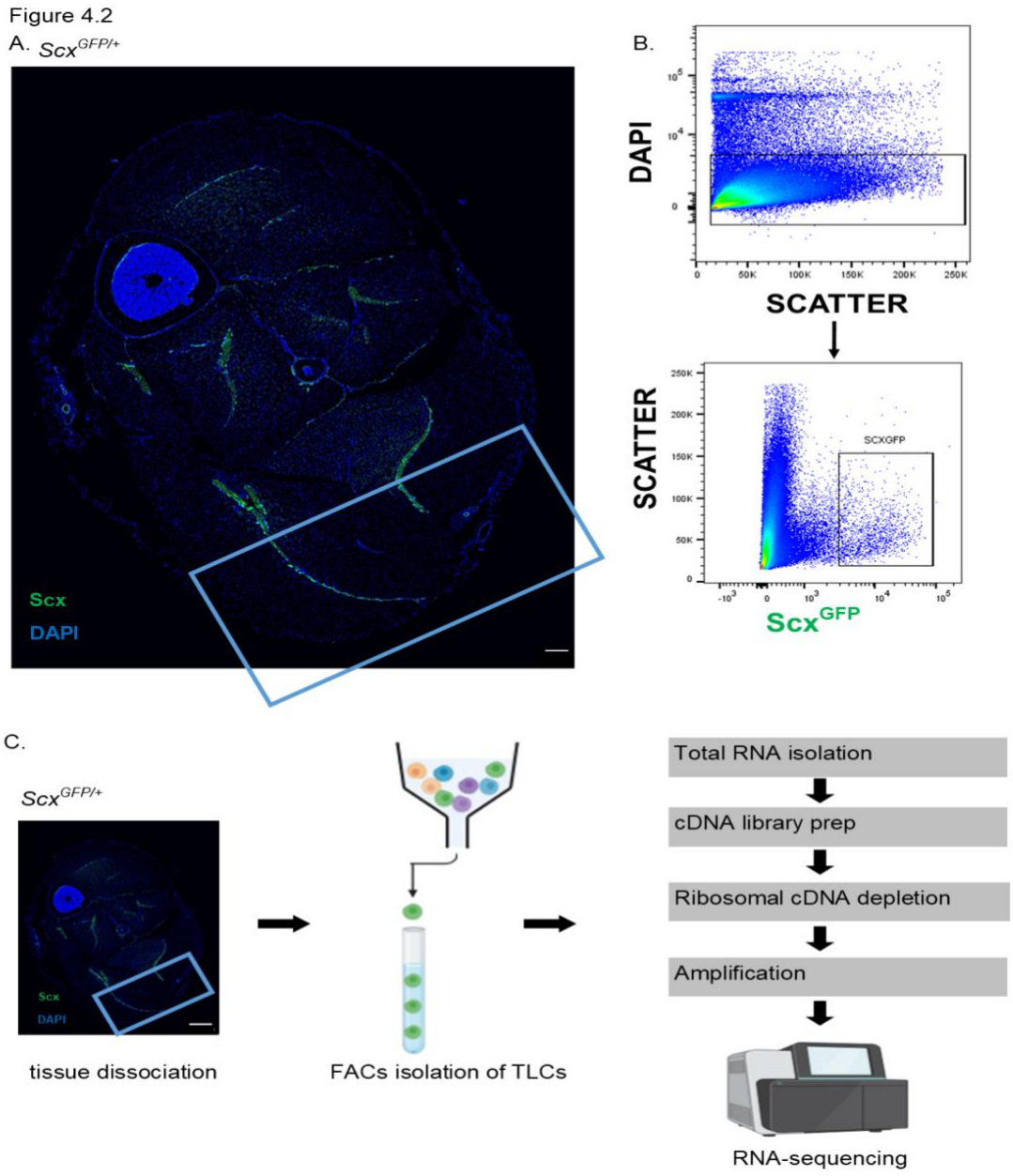

Figure 4.2: Overview of bulk RNA-sequencing of the TLC population

A. Cross-section of *Scx*$^{GFP/+}$ mouse hindlimb identifying the anatomical location harvested for sequencing (blue box). Nuclei were counterstained with DAPI. **B.** Flow cytometry scheme displaying the isolation of the TLC population for sequencing. **C.** Overview of the sequencing process. The TLCs and surrounding muscles of *Scx*$^{GFP/+}$ mice were digested into a single-cell suspension. TLCs were FACS isolated directly into TRIzol, based on DAPI-, GFP+ fluorescence. Total RNA was isolated and converted to cDNA, library prep was performed, the ribosomal cDNA was depleted, and the library was amplified. Sequencing was performed on the Novaseq600 sequencing platform, where roughly 30 million paired-end, 75 base pair reads were sequenced per sample (N = 2).

Figure 4.3

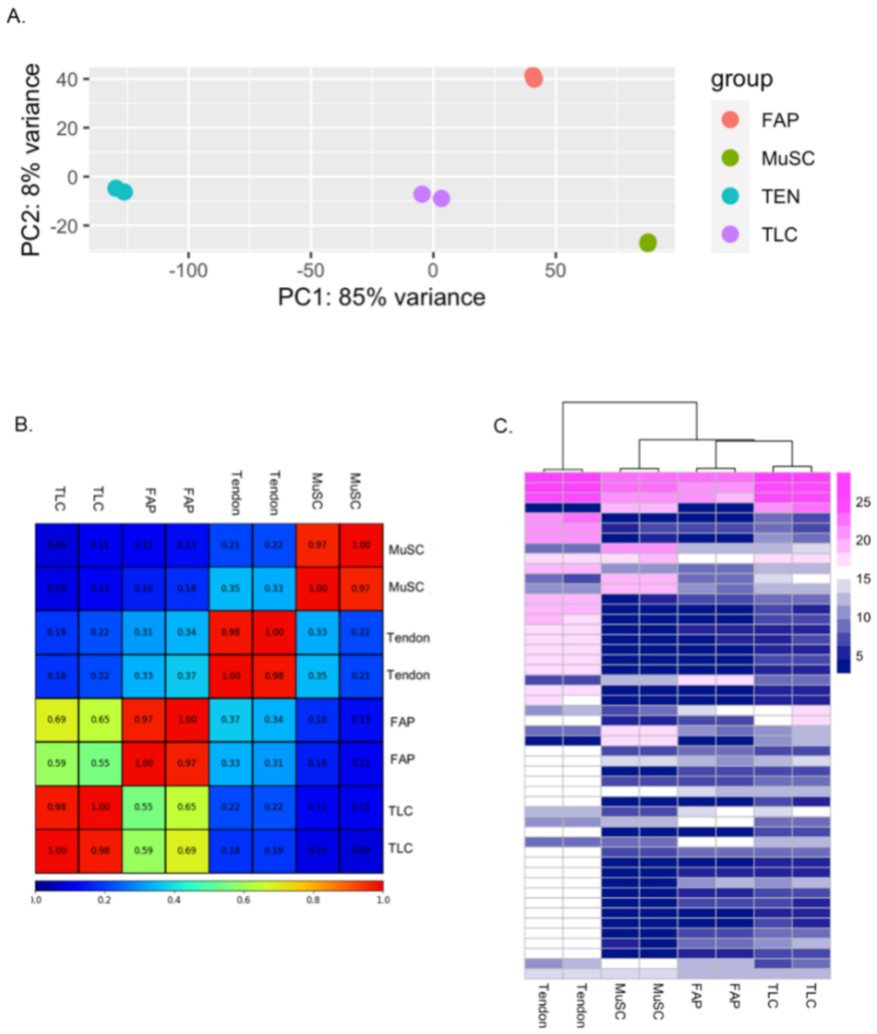

Figure 4.3: The TLC transcriptome is most similar to Tie2+ FAPs

A. Principal Component Analysis (PCA) displaying the general relatedness between Tie2+ FAPs, TLCs, MuSC, and tenocytes. **B.** Correlation plot with heatmap showing the relatedness of biological replicates and cell-type specific samples**. C.** Heatmap displaying the relative expression levels with unsupervised clustering of the top 50 most variable genes between samples. The heatmap color scale indicates log2 values representing the difference with respect to the mean log2-transformed counts. The TLCs transcriptome is most similar to that of a Tie2+ FAPs.

4.4.3: The TLC gene expression profile expresses conventional tenocyte and fibroblast markers

Next, we were curious whether the TLC population expresses any cell-type-specific markers of the skeletal muscle environment. A heatmap of the relative gene expression level of markers, the log2 values repressing the difference with respect to the mean log2-transformed counts, for MuSCs (Figure 4.4A - maroon box), cells comprising the myotendinous junctions (Figure 4.4 A - yellow box), Tie2+ FAPs (Figure 4.4A - blue box), and tenocytes (Figure 4.4A - green box) is shown in Figure 4.4A.

The MuSC sample highly and specifically expressed Paired box 7 (*Pax7),* Myoblast determination protein (*MyoD*), and Myogenic Factor 5 (*Myf5)* (Figure 4.4A - maroon box) (Wang et al., 2014). Cells comprising myotendinous junctions have been previously established to express *Scx* (Yan et al., 2022). They were initially identified based on their anatomical location and expression of tenocyte and muscle lineage genes, including *Scx,* Actin alpha cardiac muscle 1 (*Actc1*), Collagen XXII (*Col22*), and *MyoD* (Yan et al., 2022; Yaseen et al., 2021). TLCs did not express most genes associated with cells comprising the myotendinous junctions (Figure 4.4A - yellow box). Tie2+ FAPs expressed the classic FAP gene expression profile: *Pdgfr*a, *Sca1,* and *Cd34* (Figure 4.4A - blue box). TLCs lacked the expression of the classic FAP markers (Figure 4.4A- blue box). Tenocytes are characterized by their location and the expression of Mohawk (*Mkx*), *Scx,* Tenomodulin (*Tnmd*), and Fibromodulin (*Fmod*) (De Micheli et al., 2020; Korcari et al., 2022; Collins et al., 2019). TLCs and tenocytes shared the expression of tenocyte-associated genes (Figure 4.4A – green box).

Given that FAPs serve as precursors to fibroblasts and that the general transcriptome of the TLC sample aligns closest with FAPs, we were curious whether the

TLC population expressed markers of hindlimb fibroblasts. Fibroblast adhesion protein (*Fap*), Transcription factor 4 (*Tcf4*), Thrombospondin 4 (*Thbs4*), Glutamate aspartate transporter (*Glast*), *and* Collagen I (*Col1*) are markers that are highly expressed in TLCs (Figure 4.4B) and have been used to identify skeletal muscle fibroblast populations (Muhl et al., 2022; Mathew et al., 2010; Muhl et al., 2020).

Figure 4.4

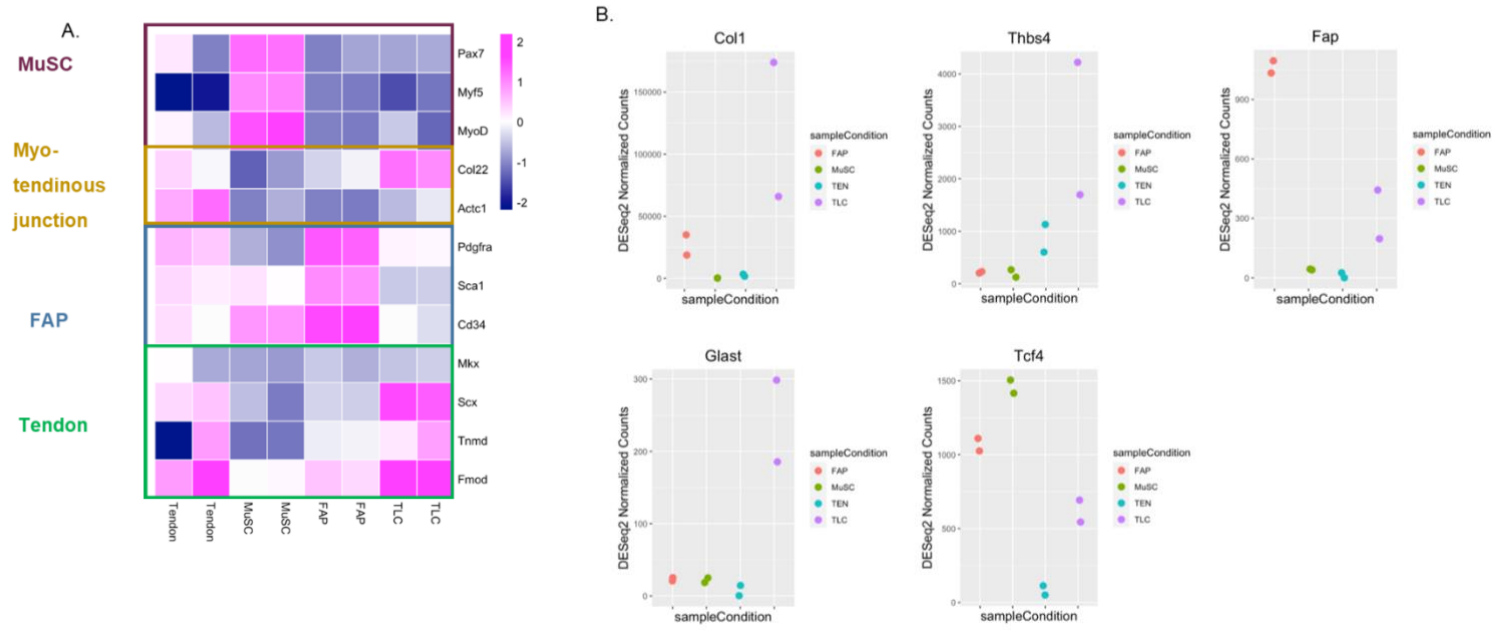

Figure 4.4: TLC transcriptome expresses fibroblastic and tenocyte markers

A. Heatmap comparing the relative expression) of classic gene markers of MuSC, FAPs, cells comprising myotendinous junctions, and tenocytes across samples. The heatmap color scale indicates log2 values representing the difference with respect to the mean log2-transformed counts. **B.** Count plots displaying the normalized read counts of fibrotic genes, *Col1, Glast, Thbs4, Tcf4,* and *Fap*. TLCs express hindlimb fibroblast and tenocyte markers.

4.4.4 The ECM composition of TLCs is distinct from other connective tissue cells

Given that the transcriptome of TLCs exhibits similarities to fibroblasts and that fibroblasts are responsible for ECM secretion, we were interested in comparing the expression of specific collagen genes among TLCs, FAPs, MuSC, and tenocytes. A heatmap comparing the relative expression levels of collagens associated with tendons, intramuscular cells, and cartilage between TLCs, FAPs, MuSCs, and tenocytes is presented in Figure 4.5A. The heatmap color scale indicates log2 values representing the difference with respect to the mean log2-transformed counts (Figure 4.5A). Collagen XXIV (*Col24*) and Collagen XIII (*Col13*) are tendon-specific collagens (Tresoldi et al., 2013) that were expressed by both TLCs and tenocytes but not FAPs or MuSCs (Figure 4.5A - maroon box and Figure 4.5B). Collagen III (*Col3*) and Collagen VI (*Col6*) are collagens associated with the skeletal muscle architecture and are expressed by cells located intramuscularly (Bielajew et al., 2020). FAPs and MuSC expressed *Col6* and *Col3* (Figure 4.5A - blue box and Figure 4.5B). The absence of the expression of *Col3* and *Col6* in the TLC population further differentiates TLCs from FAPs (Figure 4.5A – blue box and Figure 4.5B). The TLC population also expressed Collagen X (*Col10*), Collagen II (*Col2*), Collagen I (*Col1*), and Collagen XXV (*Col25*) to a greater extent. *Col2* and *Col10* were previously found to be associated with the ECM of chondrocytes (Suzuki et al., 2015). TLCs also highly express *Col25* (Figure 4.5B), which promotes myoblast fusion during myogenic differentiation and muscle formation (Goncalves et al., 2019).

Figure 4.5

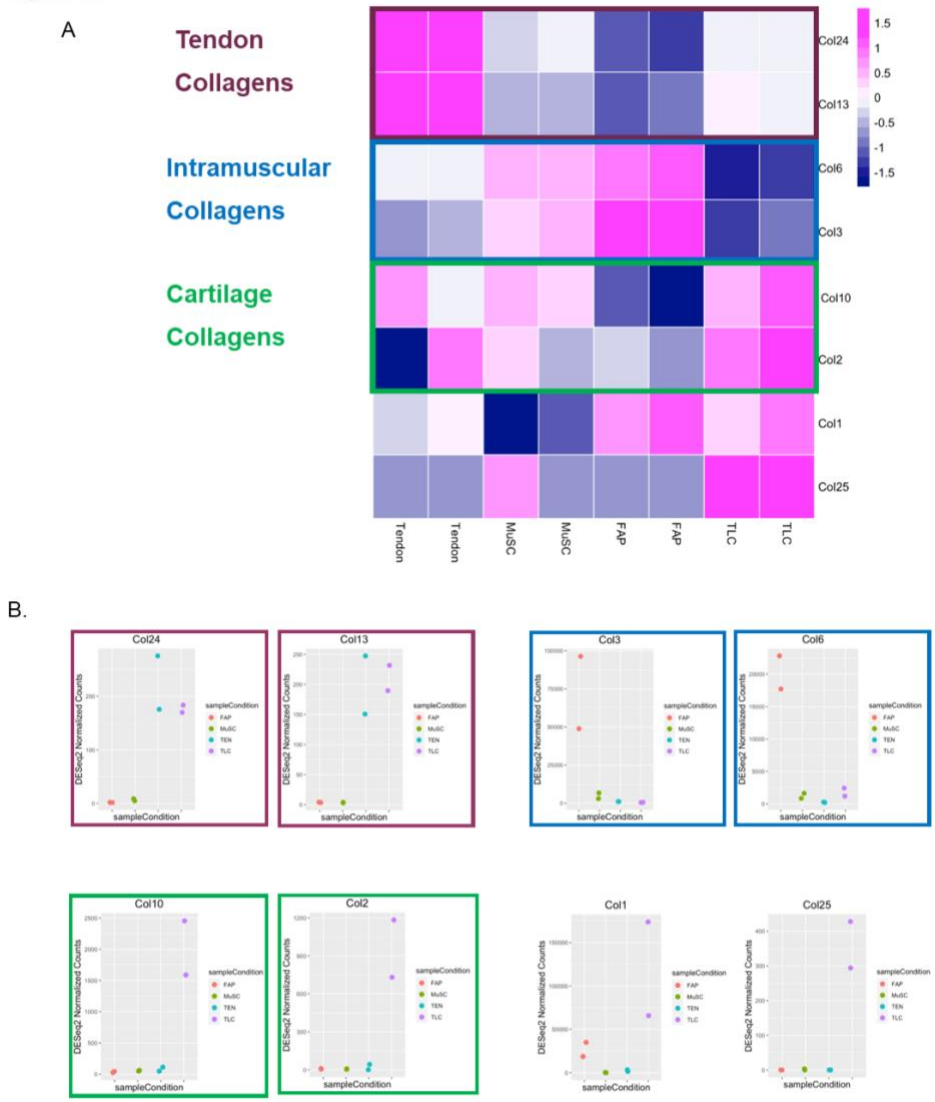

Figure 4.5: TLCs express distinct ECM collagens

A. Heatmap comparing the relative expression level of specific collagen genes across samples. The heatmap color scale indicates log2 values representing the difference with respect to the mean log2-transformed counts. **B.** Count plots displaying normalized gene counts of collagen ECM markers. *Col2 and Col10* have been associated with the ECM of chondrocytes. *Col24* and *Col13* are collagens expressed by tenocytes. *Col3* and *Col6* are collagens expressed by intramuscular cells of the hindlimb. TLC express *Col24, Col13, Col10, Col2, Col1, and Col25.*

4.4.5 TLCs express genes involved in the endochondral ossification pathway

Acvr1^{R206H}-expressing TLCs were previously shown to differentiate along an accelerated endochondral ossification pathway (Section 3.4.7). We were interested in whether wild-type TLCs expressed chondrogenic or osteogenic markers. The endochondral ossification pathway begins with the differentiation of progenitor cells into cartilage, marked by the expression of Aggrecan (*Acan*), Alkaline phosphatase (*Alpl*), SRY-box transcription factor 9 (*Sox9*), and *Col2 (*Akiyama et al., 2002; Ortega et al., 2006; Galea et al., 2020). *Alpl* and *Sox9* are not specific to cartilage differentiation and are expressed by FAPs, MuSC, vascular smooth muscle, and fibroblasts of non-skeletal tissue, including the liver, kidney, and heart (Sato et al., 2021; Jo et al., 2014; Zhang et al. 2021b). A heatmap comparing the relative expression level of the endochondral ossification genes across all samples is displayed in Figure 4.6A. The heatmap color scale indicates log2 values representing the difference with respect to the mean log2-transformed counts (Figure 4.6A). Count plots revealed that the TLC population expressed higher levels of *Acan* and *Col2* and lower levels of *Sox9* and *Alpl* (Figure 4.6A and Figure 4.6B). Additionally, we confirmed that TLCs express markers associated with early osteogenesis, specifically Osterix (*Sp7*) and *Col1,* which mark osteoprogenitor cells (Figure 4.6A – blue box) (Galea et al., 2020). The TLC population's expression of cartilage and osteogenic markers in a wild-type environment suggests they could be primed for osteogenesis.

Figure 4.6

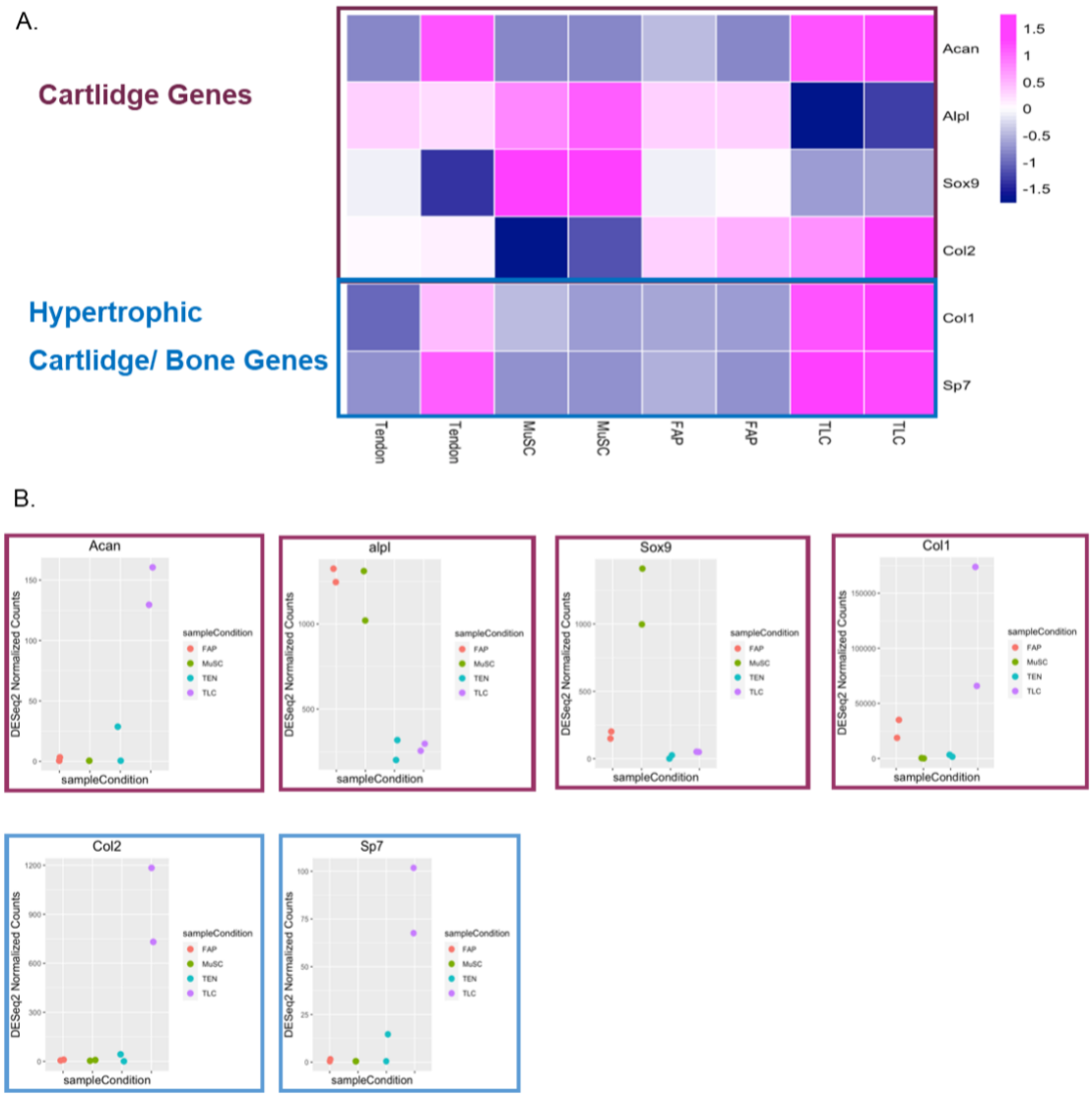

Figure 4.6: TLCs upregulate genes of the endochondral ossification pathway

A. Heatmap comparing the relative expression of endochondral ossification genes across samples. **B.** Count plot showing the normalized gene counts of cartilage (*Acan, Alpl, Sox9, and Col2)* and bone markers *(Col1 and Sp7)* of the endochondral ossification pathway. TLCs express chondrogenic and osteogenic markers.

4.4.6 The cultured TLC and tenocyte transcriptomes display a TDSC-like gene expression profile

The low abundance of TLCs in the hindlimb creates challenges for sample accessibility and mRNA quantity. To address this limitation, we attempted to culture TLCs and tenocytes to increase the cell count and the available mRNA. The intermuscular fascial regions and Achilles tendon from *Scx*$^{GFP/+}$ mice were treated separately and cultured for 5 days (Section 4.3.7 and Section 4.3.4). The *Scx*-expressing cells were FACS isolated and brought to the UCONN CGI for RNA-sequencing. The transcriptomes of cultured TLCs and tenocytes were compared to uncultured TLCs, FAPs, MuSCs, and tenocytes. Samples were filtered for low-quality reads, normalized, and transformed as done previously (Section 4.3.8). The relative relationship between samples was observed through a PCA analysis, which displayed that the cultured samples' transcriptomes closely resemble each other and are more like the transcriptomes of FAPs and MuSCs than the uncultured tenocytes and TLCs (Figure 4.7A). We created a correlation matrix to confirm the PCA analysis and determine the correlation of biological replicates (Figure 4.7B). Correlation coefficients were calculated for each replicate to assess the strength of the linear relationship between samples (Figure 4.7B). As expected, the replicates of each cell type were highly correlated, represented by a .97 to 1.00 correlation coefficient (Figure 4.7B). Unexpectedly, the cultured samples were highly correlated with each other, .99-1.00 correlation coefficient, and moderately correlated with the MuSC and FAP populations, observed by a 0.54 to .85 correlation coefficient (Figure 4.7B). A heatmap generated using the top 50 most variable genes across all samples, along with unsupervised clustering analysis, supported the findings from the PCA analysis (Figure

4.7C). The PCA, correlation plot, and heatmap analyses suggest that culturing samples resulted in a gene expression profile that deviates from the original sample identity, and the transcriptomes of the cultured samples are very similar.

Given the broad transcriptomic analysis results, we were curious whether the cultured samples' transcriptomes expressed markers associated with the transcriptomes of their uncultured identities. The cultured tenocyte and TLC transcriptomes expressed some classic tenocyte markers, such as *Mkx* and *Scx* (Figure 4.8C); however, they lacked the expression of other tenocyte markers, such as *Tnmd* or *Fmod* (Figure 4.8C). The downregulation of classic tenocyte markers in the cultured cells compared to the native samples suggests that culturing is influencing the gene expression profile and potentially modifying the cultured samples' identity. The cultured samples did not express the classic markers of MuSCs (*Pax7, MyoD, Myf5* - Figure 4.8A) or FAPs (*Cd34*, *Pdgfr*a, *or Sca1* - Figure 4.8B).

We hypothesized that culturing the TLC and tenocyte samples could shift their transcriptome from their original identity to a more tendon stem cell (TDSC)-like gene expression profile. TDSCs upregulate *Scx* compared to other tenocyte populations comprising the Achilles tendon and are a heterogeneous population of cells that is comprised of at least 4 subpopulations (Huang et al., 2021). Initially, TDSCs were identified by their gene expression profile, location, self-renewal and proliferative properties, and ability to differentiate into multiple lineages (Huang et al., 2021). The cultured tenocytes and TLC samples expressed the defining genes of the *Scx+;*Nestin+ (*Nes*) TDSC subpopulation (Figure 4.8C and Figure 4.8D – red boxes). This subpopulation of TDSCs is found in the perivascular niche of tendons (Huang et al., 2021)

and shares the expression of some of the common markers of perivascular pericytes (Splunder et al., 2024). The cultured TLCs and tenocytes exhibited the expression of Chondroitin sulfate proteoglycan 4 (*Cspg4*), Platelet-derived growth factor receptor b (*Pdgfrβ),* and Fibronectin 1 (*Fn1)* (Figure 4.8D - blue boxes), which are common pericyte markers (Splunder et al., 2024). Additionally, cultured TLCs and tenocytes expressed TDSC markers, including *Nes, Scx, and Cd146* (Figure 4.8D - red boxes). The cultured samples lacked the expression of recently identified pericyte markers such as Potassium voltage-gated channel subfamily j member 8 (*Kcnj8*) and Vitronectin (*Vtn*) (Splunder et al., 2024) (Figure 4.8D). Given the expression of tenocyte markers, *Scx* and *Mkx,* common pericyte markers, *Cspg4* and *Pdgfrb*, and perivascular TDSC stem cell genes, *Nes*, *Cd146*, and *Scx*, we hypothesize that culturing of TLCs and tenocytes resulted in a gene expression shift towards that of the perivascular *Scx+;Nes+* TDSC phenotype.

Figure 4.7

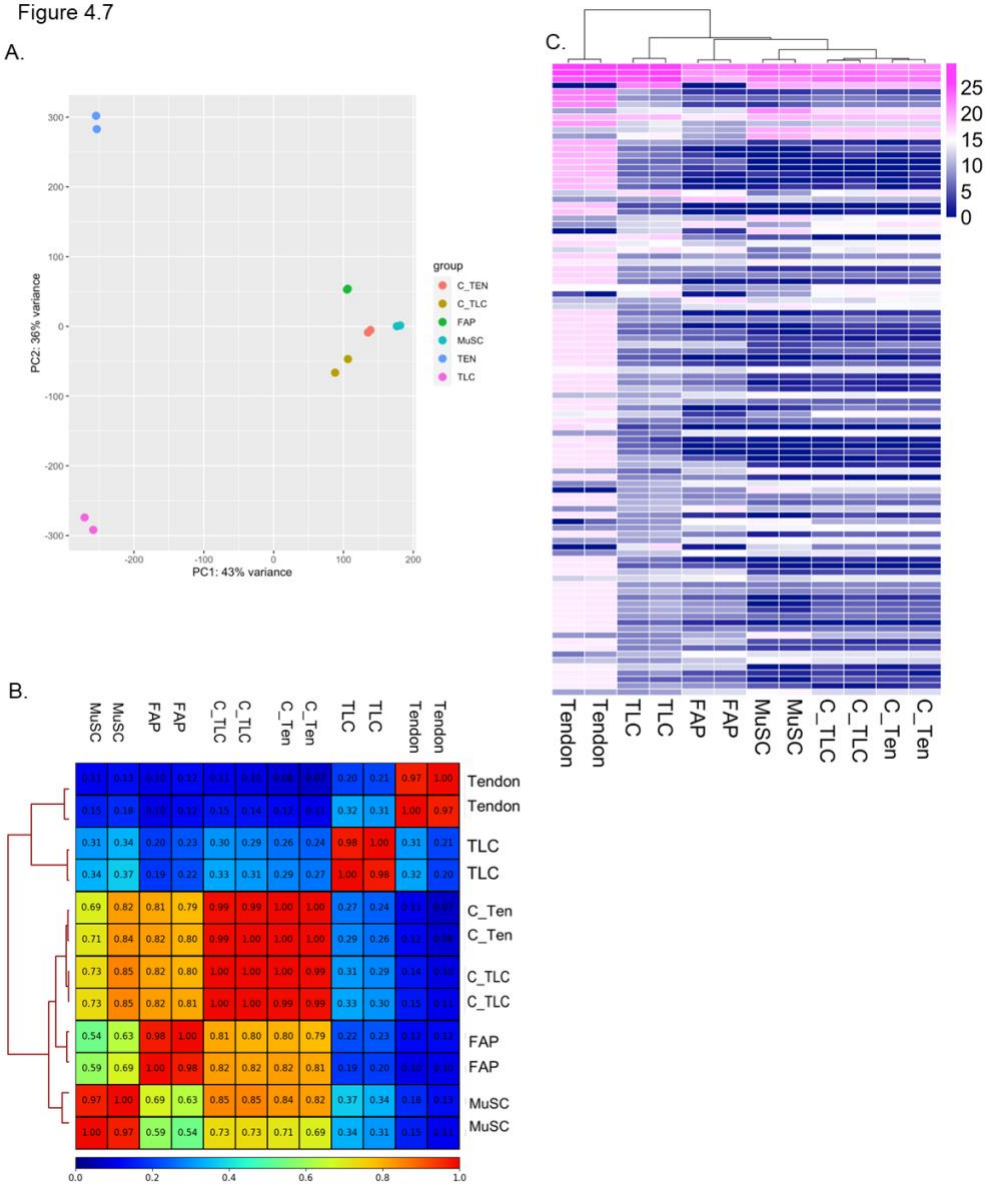

Figure 4.7: Culturing of TLCs and tenocytes altered the transcriptome from their original identity

A. PCA analysis of displaying the general relationships between the cultured and primary samples collected. **B.** Correlation plot displaying the linear relationship between replicates and samples**. C.** Heatmap of top 50 most variable genes between the cultured and primary samples. The heatmap color scale indicates log2 values representing the difference with respect to the mean log2-transformed counts. Unsupervised clustering showed that the cultured samples did not cluster with their original sample identities. Cultured samples are more like FAPs and MuSC than their original identities. C_TLC- cultured TLC; C_TEN- cultured tenocyte

Figure 4.8

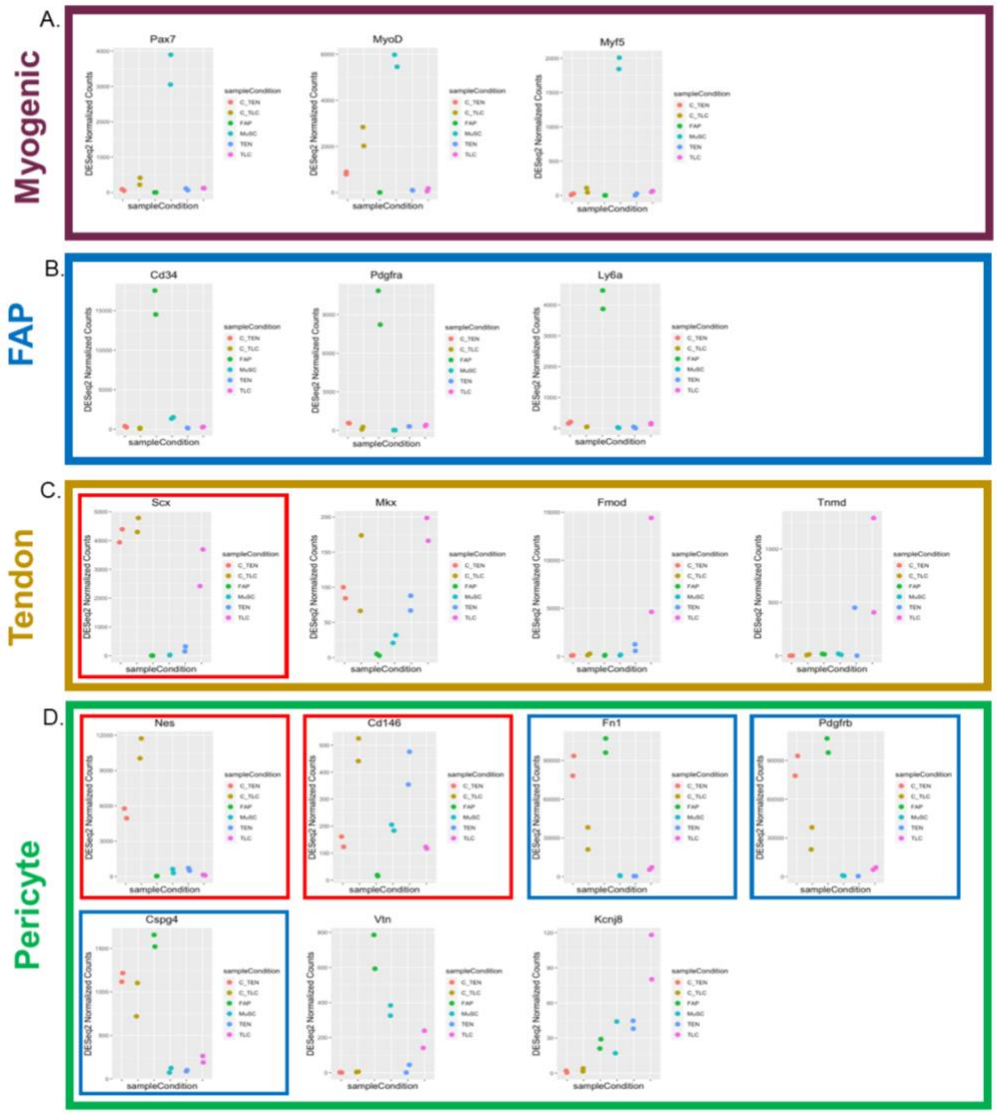

Figure 4.8: Cultured TLCs and tenocytes display a TDSC gene expression profile

A-D. Count plots displaying normalized read counts of classical cell-type specific genes. Genes corresponding to MuSC (**A**, maroon box)**,** FAPs (**B,** blue box), tenocytes (**C,** yellow box), and pericytes (**D,** green box) were analyzed. Count plots in the blue boxes identify pericyte genes also expressed in TDSCs. Count plots in red boxes identify genes expressed by TDSCs. Cultured tenocytes and TLCs express markers of *Scx+;Nes+* TDSCs.

4.5 Discussion

The overall goal of this chapter was to further define a TLC based on anatomical location and molecular characterization of the transcriptome. We compared the transcriptome of TLCs to other connective tissue cells of the hindlimb. To our knowledge, this is the first transcriptome of TLCs to be obtained. We also identified that culturing could influence the gene expression profile of tenocytes and TLCs. A study by Gumucio et al. obtained the transcriptome of cultured tenocytes from the Plantaris tendon and found a similar gene expression profile to our findings of cultured tenocytes (Gumucio et al., 2020).

We showed that TLCs are found in the intermuscular fascial regions of the posterior hindlimb (Figure 4.1E). In contrast, tenocytes and FAPs are not found within the intermuscular fascial areas of the posterior compartment. Giordani et al. revealed *Scx*-expressing cells that localize intramuscularly within the tibialis anterior (TA) muscle (Giordani et al., 2019). A full characterization of the intramuscular *Scx*-expressing cells was never completed. We have also observed *Scx*-expressing cells within the TA of the hindlimb; however, these cells are generally found in fascial planes and not intramuscularly (Figure 4.2A). It is possible that the *Scx*-expressing cells of the TA share similar characteristics with TLCs; however, TLCs are defined in part by their location within the intermuscular fascial regions of the posterior hindlimb. Therefore, *Scx*-expressing cells of the TA are distinct from TLCs. When the TA muscle of *Acvr1*$^{tnR206H/+}$;S*cx*$^{CreERT2/+}$ mice is injured through cardiotoxin injection, HO is observed at the intermuscular fascial regions of the posterior compartment (Figure 3.6). The *Scx*-expressing cells of the TA are sufficiently injured with the cardiotoxin injection; however,

HO is formed where TLC localizes in the hindlimb, supporting that TLCs are potentially distinct from the *Scx*-expressing cells of the TA. Further experimentation directly comparing the cells of the two distinct anatomical compartments is warranted.

The TLCs transcriptome was compared to the transcriptomes of Tie2+ FAPs, MuSC, and tenocytes. We were surprised to find that the transcriptome of the TLCs showed a closer relationship to Tie2+ FAPs rather than tenocytes (Figure 4.3A), despite TLCs expressing the typical tenocyte markers (Figure 4.4A). This further supports the finding that *Scx* expression is not specific to tenocytes and should be used cautiously when evaluating tenocyte identity, morphology, physiology, and function. TLCs appear distinct from tenocytes based on their location and gene expression profile of fibrotic and tendon-related genes. The absence of the classic FAP markers in TLCs, coupled with the lack of *Pdgfra* expression in the intermuscular fascial region, indicates their distinction from FAPs. FAPs and TLCs share the expression of common fibroblastic genes such as *Thbs4, Tcf4,* and *Fap*, an expected result as FAPs are direct precursor cells of fibroblasts within the skeletal muscle tissue (Joe et al., 2010; Uzemi et al., 2011). Fibroblasts are responsible for the synthesis and secretion of most of the ECM components and are characterized by their gene expression profile and general location between myofibers and fascicles (Chapman et al., 2016). The TLC population is distinct from fibroblasts due to their location and the expression of the classic tenocyte gene profile. Collectively, TLCs do not align directly with FAPs, tenocytes, or fibroblasts, suggesting that TLCs represent a novel connective tissue within the hindlimb environment.

scRNA-seq revealed that the Achilles and Plantar tendons of mice contain 2 to 3 fibroblastic populations of cells (Steffen et al., 2023; De Micheli et al., 2020). To not bias

our comparison, we chose a tenocyte transcriptome containing all tenocyte subpopulations to compare to the TLC transcriptome (Korcari et al., 2022). Choosing a tendon sample containing all tenocyte subpopulations may dilute the presence of each subpopulation; however, all express classic tenocyte markers, *Tnmd, Scx, Fmod,* and *Mkx* (Steffen et al., 2023; De Micheli et al., 2020). The goal of comparing the TLC and tenocyte transcriptomes was to broadly determine the similarity of the cell types. A different experimental approach would be required to assess how similar TLCs are to individual tenocyte subpopulations. The heterogeneity of the TLC population is unknown. A caveat of the sequencing approach employed is that any heterogeneity within the TLC population will be lost as the RNA from all cells is pooled into one sample. scRNA-seq could enable the detection of heterogeneity within the TLC population and warrants further exploration.

Notably, the tenocyte transcriptome was obtained from mice that were 12 weeks-of-age. Tenocytes have been documented to downregulate specific tendon markers as they age, potentially explaining the low expression level of *Pdgfra* and *Scx* observed by the count plots (Mendias et al., 2011; Sakabe et al., 2018). Given the functional and locational differences between TLC and tenocytes, we believe the TLCs are distinct from tenocytes comprising the Achilles tendon. However, a direct age-matched comparison may be warranted to potentially reveal further differences between TLCs and tenocytes.

The TLCs were found to be expressing distinct collagen genes when compared to FAPs, MuSC, and tenocyte populations (Figure 4.5). One of the critical components of the ECM in the hindlimb is collagen, which provides scaffolding for the attachment of proteoglycans and other ECM proteins (Csapo et al., 2020). The cell's functionality

directly impacts the composition of a cell type's ECM. TLCs highly upregulate *Col25,* which promotes myoblast fusion during myogenic differentiation and muscle formation (Goncalves et al., 2019). Based on the anatomical location and the collagen composition of the ECM, we speculate that one of the primary functions of the TLC within the skeletal muscle tissue is to create an ECM environment necessary for skeletal muscle renewal, formation, and function.

Interestingly, the TLC population expressed markers of endochondral ossification (Figure 4.6). In a mouse model of FOP, there is evidence of TLC-derived HO as early as 4 days post-injury, indicating an early onset of HO (Figure 3.5B). The upregulation of chondrogenic and osteogenic genes in TLCs from a wild-type signaling environment could suggest that TLCs are naturally primed for osteogenesis. Comparing the R206H-TLC and TLC transcriptomes in the presence and absence of injury could uncover additional molecular cues of the early osteogenic response of TLCs.

TLCs and tenocytes require their surrounding environmental cues to obtain their cellular identities; therefore, culturing can influence the gene expression profile and cell behavior. Two examples of culturing influencing the gene expression profiles of cells are Schwann cells, which can dedifferentiate and redifferentiate due to culturing conditions (Monje, 2020; Kim et al., 2014), and mouse ESCs, which can differentiate into *Scx*-expressing cells (Gaut et al., 2020). We showed that culturing TLCs and tenocytes altered their gene expression profile to that of a *Nes+;Scx+* TDSC (Figure 4.8C and Figure 4.8D). TDSCs were initially identified based on their multipotent and self-renewal capabilities, gene expression profiles, and anatomical location. To determine if the cultured TLCs and

tenocytes are TDSCs, the cultured cells' multipotent and self-renewal capabilities need to be addressed.

It should be noted that the TLCs were compared to Tie2+ FAPs and not all FAP subpopulations. Tie2+ FAPs were chosen based on the availability and accessibility of data, as the Goldhamer lab already generated a Tie2+ FAP transcriptome. The TLCs may be more similar or dissimilar to the Tie2- FAP subpopulations. However, given the lack of expression of conventional FAP markers in the TLC population (Figure 4.4A), which are expressed in all FAP subpopulations, this is an unlikely result.

Due to limitations in sample availability, only two biological replicates of the TLC populations were obtained. To gain a complete understanding of the TLC transcriptome, further sample collection and comprehensive differential gene expression analysis compared to all connective tissue cell types of the hindlimb should be conducted. Such analysis could reveal statistically significant differences between TLCs and additional cell types within the hindlimb environment, potentially uncovering additional TLC-specific differences.

The goal of this chapter was to molecularly characterize the TLC population. The current definition of TLCs is as follows: TLCs are cells that comprise the intermuscular fascial regions of the posterior compartment (Figure 4.1) and display the dual expression of tenocyte and fibroblastic markers (Figure 4.4). In a mouse model of FOP, TLCs display an early onset and unstable HO response (Figure 3.6). To our knowledge, this is the first cell type known with dual expression of skeletal muscle fibroblast markers and tenocyte markers that displays the unique osteogenic behavior in the presence of the FOP

mutation (see Section 5.1.2). We conclude that the TLC population may be a novel connective tissue cell type of the skeletal muscle hindlimb environment.

Chapter 5: Chapter Summaries and Future Directions

5.1: Chapter Summaries

The second chapter of this thesis outlines the discovery and characterization of the PNC population, a heterogeneous group of cells distinct from FAPs based on the lack of PDGFRα (Platelet-Derived Growth Factor Receptor a) expression that houses a new causal cell of HO in a mouse model of FOP. *Acvr1*^{R206H}-expressing PNCs (R206H-PNCs) exhibit a cell-autonomous capability to differentiate toward an osteogenic lineage when transplanted into a SCID host. PNCs were found to be comprised of Schwann cells, tenocytes (later shown to be TLCs), pericyte/smooth muscle cells, and satellite cells. The spatial organization of the PNC population was determined through a histological analysis. A PNC population was found to be localized to the intrafascial regions within the intermuscular fascia of the posterior hindlimb, while FAPs were isolated to the periphery.

The third chapter of this thesis determines what cell type(s) within the PNC population displays osteogenic potential in a mouse model of FOP. *Acvr1*^{R206H}-expressing Schwann cells and TLCs (R206H-Schwann cells and R206H-TLCs) displayed osteogenic potential. When transplanted into a SCID host, R206H-Schwann cells exhibited a cell-autonomous ability to differentiate into bone. In a mouse model of FOP, R206H-TLCs directly contribute to injury-induced HO that localized to the intermuscular fascial regions of the posterior hindlimb. This HO was unstable, as most of the formed HO resorbed 28 days post-injury, a phenomenon not previously observed in a mouse model of FOP. Additionally, bone formation was first detected 4 days post-injury, a remarkably rapid

response compared to other known causal cells. The presence of SOX9-expressing cells at 3 days and OSX-expressing cells at 7 days post-injury supports that R206H-TLCs-derived HO forms through the endochondral ossification pathway.

In the fourth chapter, we began to molecularly characterize the TLC population. We compared the TLC transcriptome to MuSCs, tenocytes of the Achilles tendon, and Tie2+ FAPs. PCA and correlation plots revealed that the TLC transcriptome aligns more towards a FAP transcriptome, suggesting similarities between TLC and FAPs. TLCs express markers of tenocytes and hindlimb fibroblasts but lack classic MuSC and FAP markers. The TLC population expressed ECM genes that are distinct from FAPs and tenocytes, indicating that TLCs may require different ECM components. An upregulation of endochondral ossification markers was observed in the TLC population compared to other cell types within the skeletal muscle environment, potentially suggesting that TLCs are primed for osteogenesis. Lastly, the transcriptome of tenocytes and TLCs post-culturing shifted toward a Nestin *(Nes)+;* Scleraxis (*Scx)*+ tendon stem cell fate (TDSC), potentially changing the original identity of the cells.

5.1.2: Future Directions and Leading Questions

The research presented in this thesis has revealed two additional causal cells of HO in a mouse model of FOP, including TLCs, a likely novel connective tissue cell type. These findings raise numerous intriguing questions and suggest several avenues for future studies.

One of this work's most interesting findings is the accelerated timeline of osteogenesis in R206H-TLC-derived HO. Injury assays of *Acvr1*$^{tnR206H/+;}$*Scx*$^{CreERT2/+}$ mice

(Figure 3.6), histological analysis of the early lesion (Figure 3.8), and the transcriptomic analysis of TLCs (Figure 4.6) all support that the TLC population is primed for osteogenesis and differentiates along an accelerated endochondral ossification pathway. In contrast to R206H-TLC-derived HO, where the exogenous bone is observed 4 days post-injury, the earliest appearance of R206H-FAP-derived HO is 10 days post-injury (Figure 3.7). We know through bulk RNA-sequencing if Tie2+ R206H-FAPs that *Scx* is upregulated 3 days post-injury (unpublished data), and *Scx* is the best-known marker for identifying the TLC population in the uninjured skeletal muscle environment (Figure 3.5). This strikes the fascinating question: Are FAPs differentiating towards a TLC-like fate before the initial onset of HO? It would be interesting to compare the uninjured and injured transcriptomes of R206H-TLCs and R206H-FAPs at early time points of lesion formation. A dual sequencing approach combining bulk RNA-seq and ATAC-seq will gain insights into the R206H-TLC- and R206H-FAP-derived HO mechanisms. Differential gene expression and clustering analyses of R206H-TLCs and R206H-FAPs post-injury can elucidate the potential relationship between R206H-TLCs and R206H-FAPs. ATAC-seq of the R206H-TLC and R206H-FAP populations could identify accessible chromatin structures. Specifically, assessing the chromatin accessibility of players within the endochondral ossification pathway could provide additional insights into the potential mechanistic differences of R206H-TLC and R206H-FAP differentiation.

The instability of the R206H-TLC-derived HO is another exciting avenue for further investigation. To our knowledge, this is the first instance of significant bone resorption observed in a mouse model of FOP (Figure 3.5). This raises several potential research questions: Why is the R206H-TLC-derived HO unstable? What is the potential resorption

mechanism? How do the injury environments and population dynamics differ when the *Acvr1*^{tnR206H} allele is recombined solely in FAPs, TLCs, and in both causal cells? A scRNA-seq analysis of the injury environment where R206H-TLCs are the sole osteocompetent cell type (*Acvr1*$^{tnR206H/+;}$*Scx*$^{CreERT2/+}$) compared with an injury environment where R206H-FAPs (*Acvr1*$^{tnR206H/+;}$Tie2-Cre), and both R206H-FAPs and R206H-TLCs (*Acvr1*$^{tnR206H/+;}$ Pdgfra-Cre) are the osteocompetent cell types could offer valuable insights into the differences in population dynamics and signaling environments. By comparing the injury environments of R206H-TLCs, R206H-FAPs, and both R206H-TLCs and R206H-FAPs, we can better understand how these cellular populations and cells within the lesional environment interact and contribute to the disease phenotype. One potential mechanism explaining the novel bone resorption of R206H-TLC-derived HO involves activin A, the osteogenic ligand of HO formation in FOP. We, and others, have previously identified that activin A is required for HO formation in a mouse model of FOP (Lees-Shepard et al., 2018b; Hatsell et al., 2015; Hino et al., 2015). When activin A is removed from the signaling environment of *Acvr1*$^{tnR206H/+;}$ Tie2-Cre mice, at 0 and 3 days post-injury, no HO is observed (Lees-Shepard et al., 2018b). RNA-seq of Tie2+ R206H-FAPs revealed that FAPs serve as a source of activin A (unpublished data) and continuously provide activin A to the mutated signaling environment during early lesion formation. Insufficient activin A levels could potentially explain the bone resorption of R206H-TLC-derived HO in *Acvr1*$^{tnR206H/+;}$*Scx*$^{CreERT2/+}$ mice. The immune system is a significant source of activin A (Sideras et al., 2013). Cells of the immune system infiltrate into the skeletal muscle injury environment as early as 0.5 days post-injury and will remain in the injured environment until 5 days post-injury (Oprescu et al., 2020), which coincides

with when R206H-TLC-derived HO is first observed (Figure 3.5). The immune system may provide the initial activin A levels required for R206H-TLC-derived HO; however, the localized activin A levels are insufficient to sustain the HO formation. Additionally, the bone-resorbing function of osteoclasts is inhibited in the presence of activin A (Fowler et al., 2015). The potential lack of activin A presence in the R206H-TLC injury environment could result in osteoclasts resorbing the newly formed HO. In conjunction with the proposed sequencing, performing injury assays in the presence or absence of activin A between *Acvr1*$^{tnR206H/+;}$*Scx*$^{CreERT2/+}$, *Acvr1*$^{tnR206H/+;}$ Pdgfra-Cre, and *Acvr1*$^{tnR206H/+;}$Tie2-Cre mice could investigate the potential of activin A contribution to HO stability. It would be interesting to observe R206H-FAP-derived HO stability in the absence of activin A by administering an activin A monoclonal antibody when immature bone and hypertrophic cartilage comprise the HO lesion.

In chapter 4 of this thesis, a limited analysis comparing the TLC transcriptome to the transcriptomes of tenocytes, FAPs, and MuSCs revealed that TLCs are transcriptionally similar to FAPs but lack the classic FAP gene expression markers (Figure 4.3 and Figure 4.4). This leads to an interesting question: How does the TLC transcriptome align with the transcriptome of other skeletal muscle resident cell types? A more in-depth study comparing the TLC transcriptome to all other known connective tissue cell types of the limb, including but not limited to FAPs, tenocytes, pericytes, hindlimb fibroblasts, adipocytes, and neuronal fibroblasts, would allow for further characterization of the TLC transcriptome and a greater understanding of the TLC population.

In Chapter 4, we show that culturing can alter the transcriptome of a cell. We cultured TLCs and tenocytes and compared their transcriptomes to uncultured TLCs, tenocytes, MuSCs, and Tie2+ FAPs (Figure 4.7). Cultured TLC and tenocyte transcriptomes displayed a gene expression profile of *Nes+;Scx+* TDSC (Figure 4.8). The change in the gene expression profile of the cultured TLCs and tenocytes suggests that the TLCs and tendons require environmental cues to retain their native cell-type transcriptomes. It was clear that culturing changes the transcriptomic signature of TLCs and tenocytes and decreases the differences between the populations (Figure 4.8). This uncovers the greater question of how culturing influences the gene expression and differentiation potential of a cell type? Additionally, when FAPs are cultured and transplanted into a SCID host, the timeline of HO formation is accelerated. Bone first appears 7 days post-transplantation (Lees-Shepard et al., 2018b). Is culturing FAPs influencing their osteogenic response? In vitro cell culturing differentiation assays and bulk RNA-sequencing of cultured wild-type FAP and R206H-FAPs could potentially explore how culturing is influencing the FAP transcriptome. This thesis focuses on culturing TLCs and tenocytes, but the themes can apply to many other cell types, as cell culturing is a widely used technique throughout the life science fields.

The contribution of TLCs to skeletal muscle disease phenotypes may not be specific to FOP. TLCs may contribute to various skeletal muscle-associated diseases, including muscular dystrophies, characterized by the progressive wasting of skeletal muscles. Duchenne muscular dystrophy (DMD), the most prevalent form of muscle dystrophy, results from mutations in the dystrophin gene, causing abnormalities in muscle fiber membranes (Duan et al., 2021). This condition is marked by the infiltration of adipose

and fibrotic tissue in affected muscles (Lovering et al., 2005). FAPs have been a candidate cell type that could be contributing to the increased adipogenic and fibrotic tissue (Lemos et al., 2015; Wang et al., 2024). It is possible that TLCs, whose transcriptome expresses fibrotic genes (Figure 4.4), could be contributing to the muscle-wasting phenotype of DMD. Lineage tracing experiments in a DMD mouse model could help address the potential involvement of TLCs in this skeletal muscle disease.

The nature of the work addressed in this thesis ultimately leads to the question of what defines a new cell type? A cell type has a multifactorial definition, as one specific characteristic does not define a cell type. The gene expression profile, location, function, and cellular behavior all play a role in cell type identity. TLCs localize to a specific connective tissue structure within the distal hindlimb, the intermuscular fascial regions of the posterior compartment (Figure 3.6 and Figure 4.1). The gene expression profile of TLCs exhibits a combination of characteristics from both tenocytes and hindlimb fibroblasts (Figure 4.3). The TLC transcriptome shares similarity with the FAP transcriptome but lacks the classic FAP gene expression profile (Figure 4.3 and Figure 4.4). Together the transcriptomic profiling of TLC suggests that TLC are not FAPs nor tenocytes. The unique behavior of R206H-TLC-derived HO further distinguishes TLCs from other known causal cells of HO in a mouse model of FOP (Dey et al., 2016; Agrawal et al., 2017; Lees-Shepard et al., 2018b; unpublished data – Figure 3.5). The combination of the tenocyte and hindlimb fibroblastic gene expression profile, location within the intermuscular fascial region, and the novel HO response suggest that TLCs are a previously unrecognized connective tissue cell type. One could argue that TLCs are potentially a subpopulation of tenocytes, given that TLCs express all conventional tendon-

specific markers. However, gene expression profiles are not the sole defining factor of a cell type. A set of core characteristics defines a cell type, while subpopulations follow those core characteristics with minor modifications. The core characteristics of TLCs are the expression of tenocyte and fibroblastic genes, localization to the intermuscular fascial regions of the posterior compartment of the hindlimb, and the accelerated and unstable HO response in the presence of the recombined *Acvr1*^{tnR206H} allele. The core characteristics of tenocytes are the expression of tenocyte genes, known anatomical locations connecting muscle to bone, dense irregular connective tissues with a hierarchical *Col1* structure, and a predictable and stable pattern of HO formation. Given the significant core differences between tenocytes and TLCs, we hypothesize that the TLCs are an additional connective tissue cell and not a subpopulation of tenocytes.

The primary objective of this thesis was to identify cells contributing to HO in a mouse model of FOP. Our research discovered that Schwann cells and TLCs are two additional causal cells of HO, a significant advancement in the FOP field. Characterizing the TLC population has a broader implication beyond the FOP field and provides a deeper understanding of the complex skeletal muscle connective tissue system, ultimately enhancing the knowledge in the broader field of connective tissue biology.

Chapter 6: References

Abdel-Wahab, O., Gao, J., Adli, M., Dey, A., Trimarchi, T., Chung, Y. R., Kuscu, C., Hricik, T., Ndiaye-Lobry, D., LaFave, L. M., et al. (2013). Deletion of Asxl1 results in myelodysplasia and severe developmental defects in vivo. *J. Exp. Med.* **210**, 2641–2659.

Abzhanov, A., Rodda, S. J., McMahon, A. P. and Tabin, C. J. (2007). Regulation of skeletogenic differentiation in cranial dermal bone. *Development* **134**, 3133–3144.

Achilleos, A. and Trainor, P. A. (2012). Neural crest stem cells: discovery, properties and potential for therapy. *Cell Res.* **22**, 288–304.

Agarwal, S., Loder, S. J., Cholok, D., Peterson, J., Li, J., Breuler, C., Brownley, R. C., Sung, H. H., Chung, M. T., Kamiya, N., et al. (2017). Scleraxis-Lineage Cells Contribute to Ectopic Bone Formation in Muscle and Tendon. *STEM CELLS* **35**, 705–710.

Agnew, C., Ayaz, P., Kashima, R., Loving, H. S., Ghatpande, P., Kung, J. E., Underbakke, E. S., Shan, Y., Shaw, D. E., Hata, A., et al. (2021). Structural basis for ALK2/BMPR2 receptor complex signaling through kinase domain oligomerization. *Nat. Commun.* **12**, 4950.

Akiyama, H., Chaboissier, M.-C., Martin, J. F., Schedl, A. and Crombrugghe, B. de (2002). The transcription factor Sox9 has essential roles in successive steps of the chondrocyte differentiation pathway and is required for expression of Sox5 and Sox6. *Genes Dev.* **16**, 2813–2828.

Alexander, K. A., Tseng, H.-W., Kulina, I., Fleming, W., Vaquette, C., Genêt, F., Ruitenberg, M. J. and Lévesque, J.-P. (2022). Lymphocytes Are Not Required for Neurogenic Heterotopic Ossification Development after Spinal Cord Injury. *Neurotrauma Rep.* **3**, 87–96.

Alva, J. A., Zovein, A. C., Monvoisin, A., Murphy, T., Salazar, A., Harvey, N. L., Carmeliet, P. and Iruela-Arispe, M. L. (2006). VE-Cadherin-Cre-recombinase transgenic mouse: A tool for lineage analysis and gene deletion in endothelial cells. *Dev. Dyn.* **235**, 759–767.

Anders, S., Pyl, P. T. and Huber, W. (2015). HTSeq—a Python framework to work with high-throughput sequencing data. *Bioinformatics* **31**, 166–169.

Andrews, S. (2010). FastQC: A Quality Control Tool for High Throughput Sequence Data [Online]. Available online at: http://www.bioinformatics.babraham.ac.uk/projects/fastqc/.

Aykul, S., Huang, L., Wang, L., Das, N. M., Reisman, S., Ray, Y., Zhang, Q., Rothman, N. J., Nannuru, K. C., Kamat, V., et al. (2022). ACVR1 antibodies exacerbate heterotopic ossification in fibrodysplasia ossificans progressiva (FOP) by activating FOP-mutant ACVR1. *J. Clin. Investig.* **132**, e153792.

Bagchi, R. A., Roche, P., Aroutiounova, N., Espira, L., Abrenica, B., Schweitzer, R. and Czubryt, M. P. (2016). The transcription factor scleraxis is a critical regulator of cardiac fibroblast phenotype. *BMC Biol.* **14**, 21.

Bagheri-Fam, S., Barrionuevo, F., Dohrmann, U., Günther, T., Schüle, R., Kemler, R., Mallo, M., Kanzler, B. and Scherer, G. (2006). Long-range upstream and downstream enhancers control distinct subsets of the complex spatiotemporal Sox9 expression pattern. *Dev. Biol.* **291**, 382–397.

Balakrishnan, A., Belfiore, L., Chu, T.-H., Fleming, T., Midha, R., Biernaskie, J. and Schuurmans, C. (2021). Insights Into the Role and Potential of Schwann Cells for Peripheral Nerve Repair From Studies of Development and Injury. *Front. Mol. Neurosci.* **13**, 608442.

Bhatheja, K. and Field, J. (2006). Schwann cells: Origins and role in axonal maintenance and regeneration. *Int. J. Biochem. Cell Biol.* **38**, 1995–1999.

Bielajew, B. J., Hu, J. C. and Athanasiou, K. A. (2020). Collagen: quantification, biomechanics and role of minor subtypes in cartilage. *Nat. Rev. Mater.* **5**, 730–747.

Biswas, A. A. and Goldhamer, D. J. (2016). FACS fractionation and differentiation of skeletal-muscle resident multipotent Tie2+ progenitors. In *Methods in Molecular Biology*, pp. 255–267. Humana Press Inc.

Boer, J. de, Williams, A., Skavdis, G., Harker, N., Coles, M., Tolaini, M., Norton, T., Williams, K., Roderick, K., Potocnik, A. J., et al. (2003). Transgenic mice with hematopoietic and lymphoid specific expression of Cre. *Eur. J. Immunol.* **33**, 314–325.

Bossche, L. V. and Vanderstraeten, G. (2005). Heterotopic ossification: A review. *Journal of Rehabilitation Medicine* **37**, 129–136.

Botman, E., Raijmakers, P. G. H. M., Yaqub, M., Teunissen, B., Netelenbos, C., Lubbers, W., Schwarte, L. A., Micha, D., Bravenboer, N., Schoenmaker, T., et al.

(2019). Evolution of heterotopic bone in fibrodysplasia ossificans progressiva: An [18F]NaF PET/CT study. *Bone* **124**, 1–6.

Boyce, B., Yao, Z. and Xing, L. (2009). Osteoclasts Have Multiple Roles in Bone in Addition to Bone Resorption. *Crit. Rev. Eukaryot. Gene Expr.* **19**, 171–180.

Brady, R. D., Shultz, S. R., McDonald, S. J. and O'Brien, T. J. (2018). Neurological heterotopic ossification: Current understanding and future directions. *Bone* **109**, 35–42.

Butler, S. J. and Bronner, M. E. (2015). From classical to current: Analyzing peripheral nervous system and spinal cord lineage and fate. *Dev. Biol.* **398**, 135–146.

Carr, M. J., Toma, J. S., Johnston, A. P. W., Steadman, P. E., Yuzwa, S. A., Mahmud, N., Frankland, P. W., Kaplan, D. R. and Miller, F. D. (2019). Mesenchymal Precursor Cells in Adult Nerves Contribute to Mammalian Tissue Repair and Regeneration. *Cell Stem Cell* **24**, 240-256.e9.

Chakkalakal, S. A., Zhang, D., Culbert, A. L., Convente, M. R., Caron, R. J., Wright, A. C., Maidment, A. D., Kaplan, F. S. and Shore, E. M. (2012). An Acvr1 R206H knock-in mouse has fibrodysplasia ossificans progressiva. *J. Bone Miner. Res.* **27**, 1746–1756.

Chakkalakal, S. A., Uchibe, K., Convente, M. R., Zhang, D., Economides, A. N., Kaplan, F. S., Pacifici, M., Iwamoto, M. and Shore, E. M. (2016). Palovarotene Inhibits Heterotopic Ossification and Maintains Limb Mobility and Growth in Mice With the Human ACVR1R206H Fibrodysplasia Ossificans Progressiva (FOP) Mutation. *J. Bone Miner. Res.* **31**, 1666–1675.

Chapman, M. A., Meza, R. and Lieber, R. L. (2016). Skeletal muscle fibroblasts in health and disease. *Differentiation* **92**, 108–115.

Chapman, M. A., Mukund, K., Subramaniam, S., Brenner, D. and Lieber, R. L. (2017). Three distinct cell populations express extracellular matrix proteins and increase in number during skeletal muscle fibrosis. *Am. J. Physiol.-Cell Physiol.* **312**, C131–C143.

Chartier, C., ElHawary, H., Baradaran, A., Vorstenbosch, J., Xu, L. and Efanov, J. (2021). Tendon: Principles of Healing and Repair. *Semin. Plast. Surg.* **35**, 211–215.

Chen, H.-C., Yang, J.-Y., Chuang, S.-S., Huang, C.-Y. and Yang, S.-Y. (2009). Heterotopic ossification in burns: Our experience and literature reviews. *Burns* **35**, 857–862.

Chen, S., Zhou, Y., Chen, Y. and Gu, J. (2018). fastp: an ultra-fast all-in-one FASTQ preprocessor. *Bioinformatics* **34**, i884–i890.

Chen, G., Luo, X., Wang, W., Wang, Y., Zhu, F. and Wang, W. (2019). Interleukin-1β Promotes Schwann Cells De-Differentiation in Wallerian Degeneration via the c-JUN/AP-1 Pathway. *Front. Cell. Neurosci.* **13**, 304.

Cipriano, C. A., Pill, S. G. and Keenan, M. A. (2009). Heterotopic Ossification Following Traumatic Brain Injury and Spinal Cord Injury. *J. Am. Acad. Orthop. Surg.* **17**, 689–697.

Collins, B. C., Arpke, R. W., Larson, A. A., Baumann, C. W., Xie, N., Cabelka, C. A., Nash, N. L., Juppi, H.-K., Laakkonen, E. K., Sipilä, S., et al. (2019). Estrogen Regulates the Satellite Cell Compartment in Females. *Cell Rep.* **28**, 368-381.e6.

Connor, J. M. and Evans, D. A. P. (1982). Fibrodysplasia ossificans progressiva. The clinical features and natural history of 34 patients. *Journal of Bone and Joint Surgery - Series B* **64**, 76–83.

Contreras, O., Rossi, F. M. V. and Theret, M. (2021). Origins, potency, and heterogeneity of skeletal muscle fibro-adipogenic progenitors—time for new definitions. *Skelet. Muscle* **11**, 16.

Csapo, R., Gumpenberger, M. and Wessner, B. (2020). Skeletal Muscle Extracellular Matrix – What Do We Know About Its Composition, Regulation, and Physiological Roles? A Narrative Review. *Front. Physiol.* **11**, 253.

Culbert, A. L., Chakkalakal, S. A., Theosmy, E. G., Brennan, T. A., Kaplan, F. S. and Shore, E. M. (2014). Alk2 Regulates Early Chondrogenic Fate in Fibrodysplasia Ossificans Progressiva Heterotopic Endochondral Ossification. *STEM CELLS* **32**, 1289–1300.

Dey, D., Bagarova, J., Hatsell, S. J., Armstrong, K. A., Huang, L., Ermann, J., Vonner, A. J., Shen, Y., Mohedas, A. H., Lee, A., et al. (2016). Two tissue-resident progenitor lineages drive distinct phenotypes of heterotopic ossification. *Science Translational Medicine* **8**, 366ra163-366ra163.

Dey, D., Wheatley, B. M., Cholok, D., Agarwal, S., Yu, P. B., Levi, B. and Davis, T. A. (2017). The traumatic bone: trauma-induced heterotopic ossification. *Translational Research* **186**,.

Duan, D., Goemans, N., Takeda, S., Mercuri, E. and Aartsma-Rus, A. (2021). Duchenne muscular dystrophy. *Nat. Rev. Dis. Prim.* **7**, 13.

Eames, B. F., Sharpe, P. T. and Helms, J. A. (2004). Hierarchy revealed in the specification of three skeletal fates by Sox9 and Runx2. *Dev. Biol.* **274**, 188–200.

Eisner, C., Cummings, M., Johnston, G., Tung, L. W., Groppa, E., Chang, C. and Rossi, F. M. V. (2020). Murine Tissue-Resident PDGFRα+ Fibro-Adipogenic

Progenitors Spontaneously Acquire Osteogenic Phenotype in an Altered Inflammatory Environment. *Journal of Bone and Mineral Research* **35**, 1525–1534.

ELLIOTT, D. H. (1965). STRUCTURE AND FUNCTION OF MAMMALIAN TENDON. *Biol. Rev.* **40**, 392–421.

Faweett, J. W. and Keynes, R. J. (1990). Peripheral Nerve Regeneration. *Annu. Rev. Neurosci.* **13**, 43–60.

Feltri, M. L., D'Antonio, M., Previtali, S., Fasolini, M., Messing, A. and Wrabetz, L. (1999). P0-Cre transgenic mice for inactivation of adhesion molecules in Schwann cells. *Ann. N. York Acad. Sci.* **883**, 116–23.

Feltri, M. L., Poitelon, Y. and Previtali, S. C. (2016). How Schwann Cells Sort Axons. *Neurosci.* **22**, 252–265.

Ferretti, E. and Hadjantonakis, A.-K. (2019). Mesoderm specification and diversification: from single cells to emergent tissues. *Curr. Opin. Cell Biol.* **61**, 110–116.

Florencio-Silva, R., Sasso, G. R. da S., Sasso-Cerri, E., Simões, M. J. and Cerri, P. S. (2015). Biology of Bone Tissue: Structure, Function, and Factors That Influence Bone Cells. *BioMed Res. Int.* **2015**, 421746.

Fowler, T. W., Kamalakar, A., Akel, N. S., Kurten, R. C., Suva, L. J. and Gaddy, D. (2015). Activin A inhibits RANKL-mediated osteoclast formation, movement and function in murine bone marrow macrophage cultures. *J. Cell Sci.* **128**, 683–694.

Freytag, S., Tian, L., Lönnstedt, I., Ng, M. and Bahlo, M. (2018). Comparison of clustering tools in R for medium-sized 10x Genomics single-cell RNA-sequencing data. *F1000Research* **7**, 1297.

Frontera, W. R. and Ochala, J. (2015). Skeletal Muscle: A Brief Review of Structure and Function. *Calcif. Tissue Int.* **96**, 183–195.

Fujimoto, M., Ohte, S., Osawa, K., Miyamoto, A., Tsukamoto, S., Mizuta, T., Kokabu, S., Suda, N. and Katagiri, T. (2015). Mutant Activin-Like Kinase 2 in Fibrodysplasia Ossificans Progressiva are Activated via T203 by BMP Type II Receptors. *Mol. Endocrinol.* **29**, 140–152.

Fukada, S., Uezumi, A., Ikemoto, M., Masuda, S., Segawa, M., Tanimura, N., Yamamoto, H., Miyagoe-Suzuki, Y. and Takeda, S. (2007). Molecular Signature of Quiescent Satellite Cells in Adult Skeletal Muscle. *STEM CELLS* **25**, 2448–2459.

Fukuda, T., Kohda, M., Kanomata, K., Nojima, J., Nakamura, A., Kamizono, J., Noguchi, Y., Iwakiri, K., Kondo, T., Kurose, J., et al. (2009). Constitutively

activated ALK2 and increased SMAD1/5 cooperatively induce bone morphogenetic protein signaling in fibrodysplasia ossificans progressiva. *Journal of Biological Chemistry* **284**, 7149–7156.

Galea, G. L., Zein, M. R., Allen, S. and Francis-West, P. (2021). Making and shaping endochondral and intramembranous bones. *Dev. Dyn.* **250**, 414–449.

Garcia, S. M., Lau, J., Diaz, A., Chi, H., Lizarraga, M., Wague, A., Montenegro, C., Davies, M. R., Liu, X. and Feeley, B. T. (2024). Distinct human stem cell subpopulations drive adipogenesis and fibrosis in musculoskeletal injury. *bioRxiv* 2023.07.28.551038.

Gaudet, A. D., Popovich, P. G. and Ramer, M. S. (2011). Wallerian degeneration: gaining perspective on inflammatory events after peripheral nerve injury. *J. Neuroinflammation* **8**, 110.

Gaut, L. and Duprez, D. (2016). Tendon development and diseases. *Wiley Interdiscip. Rev.: Dev. Biol.* **5**, 5–23.

Gaut, L., Bonnin, M.-A., Blavet, C., Cacciapuoti, I., Orpel, M., Mericskay, M. and Duprez, D. (2020). Mechanical and molecular parameters that influence the tendon differentiation potential of C3H10T1/2 cells in 2D- and 3D-culture systems. *Biol. Open* **9**, bio047928.

Genêt, F., Kulina, I., Vaquette, C., Torossian, F., Millard, S., Pettit, A. R., Sims, N. A., Anginot, A., Guerton, B., Winkler, I. G., et al. (2015). Neurological heterotopic ossification following spinal cord injury is triggered by macrophage-mediated inflammation in muscle. *J. Pathol.* **236**, 229–240.

Gerber, D., Pereira, J. A., Gerber, J., Tan, G., Dimitrieva, S., Yángüez, E. and Suter, U. (2021). Transcriptional profiling of mouse peripheral nerves to the single-cell level to build a sciatic nerve atlas (Snat). *eLife* **10**,.

Gillies, A. R. and Lieber, R. L. (2011). Structure and function of the skeletal muscle extracellular matrix. *Muscle Nerve* **44**, 318–331.

Giordani, L., He, G. J., Negroni, E., Sakai, H., Law, J. Y. C., Siu, M. M., Wan, R., Corneau, A., Tajbakhsh, S., Cheung, T. H., et al. (2019). High-Dimensional Single-Cell Cartography Reveals Novel Skeletal Muscle-Resident Cell Populations. *Molecular Cell* **74**, 609-621.e6.

GitHub - CBC-UCONN/RNA-seq-with-reference-genome-and-annotation.

Glenn, T. D. and Talbot, W. S. (2013). Signals regulating myelination in peripheral nerves and the Schwann cell response to injury. *Curr. Opin. Neurobiol.* **23**, 1041–1048.

Gonçalves, T. J. M., Boutillon, F., Lefebvre, S., Goffin, V., Iwatsubo, T., Wakabayashi, T., Oury, F. and Armand, A.-S. (2019). Collagen XXV promotes myoblast fusion during myogenic differentiation and muscle formation. *Sci. Rep.* **9**, 5878.

Göritz, C., Dias, D. O., Tomilin, N., Barbacid, M., Shupliakov, O. and Frisén, J. (2011). A Pericyte Origin of Spinal Cord Scar Tissue. *Science* **333**, 238–242.

Grcevic, D., Pejda, S., Matthews, B. G., Repic, D., Wang, L., Li, H., Kronenberg, M. S., Jiang, X., Maye, P., Adams, D. J., et al. (2012). In Vivo Fate Mapping Identifies Mesenchymal Progenitor Cells. *STEM CELLS* **30**, 187–196.

Griffin, J. W. and Thompson, W. J. (2008). Biology and pathology of nonmyelinating Schwann cells. *Glia* **56**, 1518–1531.

Gumucio, J. P., Schonk, M. M., Kharaz, Y. A., Comerford, E. and Mendias, C. L. (2020). Scleraxis is required for the growth of adult tendons in response to mechanical loading. *JCI Insight* **5**,.

Hamilton, D. L. and Abremski, K. (1984). Site-specific recombination by the bacteriophage P1 lox-Cre system Cre-mediated synapsis of two lox sites. *J. Mol. Biol.* **178**, 481–486.

Hamilton, T. G., Klinghoffer, R. A., Corrin, P. D. and Soriano, P. (2003). Evolutionary Divergence of Platelet-Derived Growth Factor Alpha Receptor Signaling Mechanisms. *Molecular and Cellular Biology* **23**, 4013–4025.

Hao, Y., Hao, S., Andersen-Nissen, E., Mauck, W. M., Zheng, S., Butler, A., Lee, M. J., Wilk, A. J., Darby, C., Zager, M., et al. (2021). Integrated analysis of multimodal single-cell data. *Cell* **184**, 3573-3587.e29.

Hardy, D., Besnard, A., Latil, M., Jouvion, G., Briand, D., Thépenier, C., Pascal, Q., Guguin, A., Gayraud-Morel, B., Cavaillon, J. M., et al. (2016). Comparative study of injury models for studying muscle regeneration in mice. *PLoS ONE* **11**,.

Harty, B. L. and Monk, K. R. (2017). Unwrapping the unappreciated: recent progress in Remak Schwann cell biology. *Curr. Opin. Neurobiol.* **47**, 131–137.

Harvey, A. L. (1985). Cardiotoxins from Cobra Venoms: Possible Mechanisms of Action. *J. Toxicol.: Toxin Rev.* **4**, 41–69.

Harvey, T., Flamenco, S. and Fan, C.-M. (2019). A Tppp3+Pdgfra+ tendon stem cell population contributes to regeneration and reveals a shared role for PDGF signalling in regeneration and fibrosis. *Nat. Cell Biol.* **21**, 1490–1503.

Hatsell, S. J., Idone, V., Wolken, D. M. A., Huang, L., Kim, H. J., Wang, L., Wen, X., Nannuru, K. C., Jimenez, J., Xie, L., et al. (2015). ACVR1R206H receptor mutation causes fibrodysplasia ossificans progressiva by imparting responsiveness to activin A. *Science Translational Medicine* **7**, 303ra137.

He, P., Ruan, D., Huang, Z., Wang, C., Xu, Y., Cai, H., Liu, H., Fei, Y., Heng, B. C., Chen, W., et al. (2022). Comparison of Tendon Development Versus Tendon Healing and Regeneration. *Front. Cell Dev. Biol.* **10**, 821667.

Hino, K., Ikeya, M., Horigome, K., Matsumoto, Y., Ebise, H., Nishio, M., Sekiguchi, K., Shibata, M., Nagata, S., Matsuda, S., et al. (2015). Neofunction of ACVR1 in fibrodysplasia ossificans progressiva. *Proceedings of the National Academy of Sciences of the United States of America* **112**, 15438–15443.

Hirasawa, T. and Kuratani, S. (2015). Evolution of the vertebrate skeleton: morphology, embryology, and development. *Zoöl. Lett.* **1**, 2.

Hope, M. and Saxby, T. S. (2007). Tendon Healing. *Foot Ankle Clin.* **12**, 553–567.

Hörner, S. J., Couturier, N., Gueiber, D. C., Hafner, M. and Rudolf, R. (2022). Development and In Vitro Differentiation of Schwann Cells. *Cells* **11**, 3753.

Hosoyama, T., Dyke, J. V. and Suzuki, M. (2012). Applications of skeletal muscle progenitor cells for neuromuscular diseases. *Am. J. stem cells* **1**, 253–63.

Howell, K., Chien, C., Bell, R., Laudier, D., Tufa, S. F., Keene, D. R., Andarawis-Puri, N. and Huang, A. H. (2017). Novel Model of Tendon Regeneration Reveals Distinct Cell Mechanisms Underlying Regenerative and Fibrotic Tendon Healing. *Sci. Rep.* **7**, 45238.

Hu, D. P., Ferro, F., Yang, F., Taylor, A. J., Chang, W., Miclau, T., Marcucio, R. S. and Bahney, C. S. (2017). Cartilage to bone transformation during fracture healing is coordinated by the invading vasculature and induction of the core pluripotency genes. *Development* **144**, 221–234.

Huang, L., Fukai, N., Selby, P. B., Olsen, B. R. and Mundlos, S. (1997). Mouse clavicular development: Analysis of wild-type and cleidocranial dysplasia mutant mice. *Dev. Dyn.* **210**, 33–40.

Humphreys, B. D., Lin, S.-L., Kobayashi, A., Hudson, T. E., Nowlin, B. T., Bonventre, J. V., Valerius, M. T., McMahon, A. P. and Duffield, J. S. (2010). Fate Tracing Reveals the Pericyte and Not Epithelial Origin of Myofibroblasts in Kidney Fibrosis. *Am. J. Pathol.* **176**, 85–97.

Huse, M., Muir, T. W., Xu, L., Chen, Y.-G., Kuriyan, J. and Massagué, J. (2001). The TGFβ Receptor Activation Process An Inhibitor- to Substrate-Binding Switch. *Mol. Cell* **8**, 671–682.

Inoue, M., Ishida, T., Yasuda, T., Toh, R., Hara, T., Cangara, H. M., Rikitake, Y., Taira, K., Sun, L., Kundu, R. K., et al. (2010). Endothelial cell-selective adhesion molecule modulates atherosclerosis through plaque angiogenesis and monocyte–endothelial interaction. *Microvasc. Res.* **80**, 179–187.

Jan., P. K. G. M. T. C. A. A. *Anatomy, Connective Tissue*. (ed. Publishing, T. I. (FL): S.).

Jessen, K. R., Mirsky, R. and Lloyd, A. C. (2015). Schwann Cells: Development and Role in Nerve Repair. *Cold Spring Harb. Perspect. Biol.* **7**, a020487.

Jing, Y., Jing, J., Ye, L., Liu, X., Harris, S. E., Hinton, R. J. and Feng, J. Q. (2017). Chondrogenesis and osteogenesis are one continuous developmental and lineage defined biological process. *Sci. Rep.* **7**, 10020.

Jo, A., Denduluri, S., Zhang, B., Wang, Z., Yin, L., Yan, Z., Kang, R., Shi, L. L., Mok, J., Lee, M. J., et al. (2014). The versatile functions of Sox9 in development, stem cells, and human diseases. *Genes Dis.* **1**, 149–161.

Jo, C. H., Lim, H.-J. and Yoon, K. S. (2019). Characterization of Tendon-Specific Markers in Various Human Tissues, Tenocytes and Mesenchymal Stem Cells. *Tissue Eng. Regen. Med.* **16**, 151–159.

Joe, A. W. B., Yi, L., Natarajan, A., Grand, F. L., So, L., Wang, J., Rudnicki, M. A. and Rossi, F. M. V. (2010). Muscle injury activates resident fibro/adipogenic progenitors that facilitate myogenesis. *Nature Cell Biology* **12**, 153–163.

Kaji, D. A., Montero, A. M., Patel, R. and Huang, A. H. (2021). Transcriptional profiling of mESC-derived tendon and fibrocartilage cell fate switch. *Nat. Commun.* **12**, 4208.

Kan, L., Peng, C.-Y., McGuire, T. L. and Kessler, J. A. (2013). Glast-expressing progenitor cells contribute to heterotopic ossification. *Bone* **53**, 194–203.

Kang, S. H., Fukaya, M., Yang, J. K., Rothstein, J. D. and Bergles, D. E. (2010). NG2+ CNS Glial Progenitors Remain Committed to the Oligodendrocyte Lineage in Postnatal Life and following Neurodegeneration. *Neuron* **68**, 668–681.

Kanisicak, O., Mendez, J. J., Yamamoto, S., Yamamoto, M. and Goldhamer, D. J. (2009). Progenitors of skeletal muscle satellite cells express the muscle determination gene, MyoD. *Dev. Biol.* **332**, 131–141.

Kaplan, F. S. and Shore, E. M. (2000). Progressive Osseous Heteroplasia. *J. Bone Miner. Res.* **15**, 2084–2094.

Kaplan, F. S., Merrer, M. L., Glaser, D. L., Pignolo, R. J., Goldsby, R. E., Kitterman, J. A., Groppe, J. and Shore, E. M. (2008). Fibrodysplasia ossificans progressiva. *Best Pr. Res. Clin. Rheumatol.* **22**, 191–205.

Kaplan, MDHahn, F. S., MDZasloff, G. V. and PhD, M. A. M. Heterotopic Ossification: Two Rare Forms and What They Can Teach Us. *Journal of the American Academy of Orthopaedic Surgeons* 288 – 296.

Katagiri, T. and Watabe, T. (2016). Bone Morphogenetic Proteins. *Cold Spring Harb. Perspect. Biol.* **8**, a021899.

Kim, J. K., Lee, H. J. and Park, H. T. (2014). Two faces of Schwann cell dedifferentiation in peripheral neurodegenerative diseases: pro-demyelinating and axon-preservative functions. *Neural Regen. Res.* **9**, 1952–1954.

Kim, H., Kim, M., Im, S.-K. and Fang, S. (2018). Mouse Cre-LoxP system: general principles to determine tissue-specific roles of target genes. *Lab. Anim. Res.* **34**, 147–159.

Kim, D., Paggi, J. M., Park, C., Bennett, C. and Salzberg, S. L. (2019). Graph-based genome alignment and genotyping with HISAT2 and HISAT-genotype. *Nat. Biotechnol.* **37**, 907–915.

Kisanuki, Y. Y., Hammer, R. E., Miyazaki, J. ichi, Williams, S. C., Richardson, J. A. and Yanagisawa, M. (2001). Tie2-Cre transgenic mice: A new model for endothelial cell-lineage analysis in vivo. *Developmental Biology* **230**, 230–242.

Kolde, R. (2018). Package 'pheatmap.

Korcari, A., Muscat, S., McGinn, E., Buckley, M. R. and Loiselle, A. E. (2022). Depletion of Scleraxis-lineage cells during tendon healing transiently impairs multi-scale restoration of tendon structure during early healing. *PLoS ONE* **17**, e0274227.

Kosyakova, N., Kao, D. D., Figetakis, M., López-Giráldez, F., Spindler, S., Graham, M., James, K. J., Shin, J. W., Liu, X., Tietjen, G. T., et al. (2020). Differential functional roles of fibroblasts and pericytes in the formation of tissue-engineered microvascular networks in vitro. *npj Regen. Med.* **5**, 1.

Leadbetter, W. B. (1992). Cell-matrix response in tendon injury. *Clin. sports Med.* **11**, 533–78.

Lees-Shepard, J. B. and Goldhamer, D. J. (2018). Stem cells and heterotopic ossification: Lessons from animal models. *Bone* **109**, 178–186.

Lees-Shepard, J. B., Nicholas, S. A. E., Stoessel, S. J., Devarakonda, P. M., Schneider, M. J., Yamamoto, M. and Goldhamer, D. J. (2018a). Palovarotene reduces heterotopic ossification in juvenile fop mice but exhibits pronounced skeletal toxicity. *eLife* **7**,.

Lees-Shepard, J. B., Yamamoto, M., Biswas, A. A., Stoessel, S. J., Nicholas, S. A. E., Cogswell, C. A., Devarakonda, P. M., Schneider, M. J., Cummins, S. M., Legendre, N. P., et al. (2018b). Activin-dependent signaling in fibro/adipogenic progenitors causes fibrodysplasia ossificans progressiva. *Nature Communications* **9**, 1–14.

Lees-Shepard, J. B., Stoessel, S. J., Chandler, J. T., Bouchard, K., Bento, P., Apuzzo, L. N., Devarakonda, P. M., Hunter, J. W. and Goldhamer, D. J. (2022). An anti-ACVR1 antibody exacerbates heterotopic ossification by fibro-adipogenic progenitors in fibrodysplasia ossificans progressiva mice. *J. Clin. Investig.* **132**, e153795.

Lendahl, U., Muhl, L. and Betsholtz, C. (2022). Identification, discrimination and heterogeneity of fibroblasts. *Nat. Commun.* **13**, 3409.

Lepore, J. J., Cheng, L., Lu, M. M., Mericko, P. A., Morrisey, E. E. and Parmacek, M. S. (2005). High-efficiency somatic mutagenesis in smooth muscle cells and cardiac myocytes in SM22α-Cre transgenic mice. *genesis* **41**, 179–184.

Levay, A. K., Peacock, J. D., Lu, Y., Koch, M., Jr, R. B. H., Kadler, K. E. and Lincoln, J. (2008). Scleraxis Is Required for Cell Lineage Differentiation and Extracellular Matrix Remodeling During Murine Heart Valve Formation In Vivo. *Circ. Res.* **103**, 948–956.

Lewis, A. E., Vasudevan, H. N., O'Neill, A. K., Soriano, P. and Bush, J. O. (2013). The widely used Wnt1-Cre transgene causes developmental phenotypes by ectopic activation of Wnt signaling. *Dev. Biol.* **379**, 229–234.

Li, L. and Tuan, R. S. (2020). Mechanism of traumatic heterotopic ossification: In search of injury-induced osteogenic factors. *J. Cell. Mol. Med.* **24**, 11046–11055.

Li, L., Ding, P., Lv, X., Xie, S., Li, L., Chen, J., Zhou, D., Wang, X., Wang, Q., Zhang, W., et al. (2022). CD59-Regulated Ras Compartmentalization Orchestrates Antitumor T-Cell Immunity. *Cancer Immunol. Res.* **10**, 1475–1489.

Lin, J., Yang, Y., Zhou, W., Dai, C., Chen, X., Xie, Y., Han, S., Liu, H., Hu, Y., Tang, C., et al. (2022). Single cell analysis reveals inhibition of angiogenesis attenuates the progression of heterotopic ossification in Mkx−/− mice. *Bone Res.* **10**, 4.

Logan, M., Martin, J. F., Nagy, A., Lobe, C., Olson, E. N. and Tabin, C. J. (2002). Expression of Cre recombinase in the developing mouse limb bud driven by a Prxl enhancer. *genesis* **33**, 77–80.

Love, M. I., Huber, W. and Anders, S. (2014). Moderated estimation of fold change and dispersion for RNA-seq data with DESeq2. *Genome Biol.* **15**, 550.

Lovering, R. M., Porter, N. C. and Bloch, R. J. (2005). The muscular dystrophies: from genes to therapies. *Phys. Ther.* **85**, 1372–88.

Lui, P. P. Y. and Wong, C. M. (2020). Biology of Tendon Stem Cells and Tendon in Aging. *Front. Genet.* **10**, 1338.

Mackie, E. J., Ahmed, Y. A., Tatarczuch, L., Chen, K.-S. and Mirams, M. (2008). Endochondral ossification: How cartilage is converted into bone in the developing skeleton. *Int. J. Biochem. Cell Biol.* **40**, 46–62.

Malecova, B., Gatto, S., Etxaniz, U., Passafaro, M., Cortez, A., Nicoletti, C., Giordani, L., Torcinaro, A., Bardi, M. D., Bicciato, S., et al. (2018). Dynamics of cellular states of fibro-adipogenic progenitors during myogenesis and muscular dystrophy. *Nature Communications 2018 9:1* **9**, 1–12.

Marco, F., Alessandra, T., Marilisa, Q., Ester, O. and Victoria, O. (2007). Collagen Structure of Tendon Relates to Function. *Sci. World J.* **7**, 404–420.

Massagué, J. (2012). TGFβ signalling in context. *Nat. Rev. Mol. Cell Biol.* **13**, 616–630.

Mathew, S. J., Hansen, J. M., Merrell, A. J., Murphy, M. M., Lawson, J. A., Hutcheson, D. A., Hansen, M. S., Angus-Hill, M. and Kardon, G. (2010). Connective tissue fibroblasts and Tcf4 regulate myogenesis. *Development* **138**, 371–384.

Matthews, B. G., Torreggiani, E., Roeder, E., Matic, I., Grcevic, D. and Kalajzic, I. (2016). Osteogenic potential of alpha smooth muscle actin expressing muscle resident progenitor cells. *Bone* **84**, 69–77.

McCarthy, E. F. and Sundaram, M. (2005). Heterotopic ossification: a review. *Skelet. Radiol.* **34**, 609–619.

McKellar, D. W., Walter, L. D., Song, L. T., Mantri, M., Wang, M. F. Z., Vlaminck, I. D. and Cosgrove, B. D. (2021). Large-scale integration of single-cell transcriptomic data captures transitional progenitor states in mouse skeletal muscle regeneration. *Commun. Biol.* **4**, 1280.

Mendias, C. L., Gumucio, J. P., Bakhurin, K. I., Lynch, E. B. and Brooks, S. V. (2012). Physiological loading of tendons induces scleraxis expression in epitenon fibroblasts. *J. Orthop. Res.* **30**, 606–612.

Menezes., G. B. M. A. S. R. G. *Embryology, Bone Ossification*.

Meyers, C., Lisiecki, J., Miller, S., Levin, A., Fayad, L., Ding, C., Sono, T., McCarthy, E., Levi, B. and James, A. W. (2019). Heterotopic Ossification: A Comprehensive Review. *JBMR Plus* **3**, n/a-n/a.

Micheli, A. J. D., Laurilliard, E. J., Heinke, C. L., Ravichandran, H., Fraczek, P., Soueid-Baumgarten, S., Vlaminck, I. D., Elemento, O. and Cosgrove, B. D. (2020). Single-Cell Analysis of the Muscle Stem Cell Hierarchy Identifies Heterotypic Communication Signals Involved in Skeletal Muscle Regeneration. *Cell Rep.* **30**, 3583-3595.e5.

Monje, P. V. (2020). Schwann Cell Cultures: Biology, Technology and Therapeutics. *Cells* **9**, 1848.

Morrison, S. J., White, P. M., Zock, C. and Anderson, D. J. (1999). Prospective Identification, Isolation by Flow Cytometry, and In Vivo Self-Renewal of Multipotent Mammalian Neural Crest Stem Cells. *Cell* **96**, 737–749.

Muhl, L., Genové, G., Leptidis, S., Liu, J., He, L., Mocci, G., Sun, Y., Gustafsson, S., Buyandelger, B., Chivukula, I. V., et al. (2020). Single-cell analysis uncovers fibroblast heterogeneity and criteria for fibroblast and mural cell identification and discrimination. *Nature Communications* **11**,.

Mukund, K. and Subramaniam, S. (2020). Skeletal muscle: A review of molecular structure and function, in health and disease. *Wiley Interdiscip. Rev.: Syst. Biol. Med.* **12**, e1462.

Murchison, N. D., Price, B. A., Conner, D. A., Keene, D. R., Olson, E. N., Tabin, C. J. and Schweitzer, R. (2007). Regulation of tendon differentiation by scleraxis distinguishes force-transmitting tendons from muscle-anchoring tendons. *Development* **134**, 2697–2708.

Nagy, A. (2000). Cre recombinase: The universal reagent for genome tailoring. *genesis* **26**, 99–109.

Nah, H., Pacifici, M., Gerstenfeld, L. C., Adams, S. L. and Kirsch, T. (2000). Transient Chondrogenic Phase in the Intramembranous Pathway During Normal Skeletal Development. *J. Bone Miner. Res.* **15**, 522–533.

Nickel, J. and Mueller, T. D. (2019). Specification of BMP Signaling. *Cells* **8**, 1579.

Nishijo, K., Hosoyama, T., Bjornson, C. R. R., Schaffer, B. S., Prajapati, S. I., Bahadur, A. N., Hansen, M. S., Blandford, M. C., McCleish, A. T., Rubin, B. P., et al. (2009). Biomarker system for studying muscle, stem cells, and cancer in vivo. *FASEB J.* **23**, 2681–2690.

Okonechnikov, K., Conesa, A., García-Alcalde, &, Bioinformatics, F. (2015). "Qualimap 2: advanced multi-sample quality control for high-throughput sequencing data." and btv566 Qualimap 2: advanced multi-sample quality control for high-throughput sequencing data.

Oprescu, S. N., Yue, F., Qiu, J., Brito, L. F. and Kuang, S. (2020). Temporal dynamics and heterogeneity of cell populations during skeletal muscle regeneration. *iScience*.

Orr-Urtreger, A. and Lonai, P. (1992). Platelet-derived growth factor-A and its receptor are expressed in separate, but adjacent cell layers of the mouse embryo. *Development* **115**, 1045–1058.

Ortega, N., Behonick, D. J. and Werb, Z. (2004). Matrix remodeling during endochondral ossification. *Trends Cell Biol.* **14**, 86–93.

Owecki, M. K. (2021). Theodor Schwann (1810–1882). *J. Neurol.* **268**, 4921–4922.

Parrinello, S., Napoli, I., Ribeiro, S., Digby, P. W., Fedorova, M., Parkinson, D. B., Doddrell, R. D. S., Nakayama, M., Adams, R. H. and Lloyd, A. C. (2010). EphB Signaling Directs Peripheral Nerve Regeneration through Sox2-Dependent Schwann Cell Sorting. *Cell* **143**, 145–155.

Paylor, B., Joe, A. W., Rossi, F. M. V. and Lemos, D. R. (2014). In vivo characterization of neural crest-derived fibro/adipogenic progenitor cells as a likely cellular substrate for craniofacial fibrofatty infiltrating disorders. *Biochem. Biophys. Res. Commun.* **451**, 148–151.

Peron, S. P., Freeman, J., Iyer, V., Guo, C. and Svoboda, K. (2015). A Cellular Resolution Map of Barrel Cortex Activity during Tactile Behavior. *Neuron* **86**, 783–799.

Peterson, J. R., Agarwal, S., Brownley, R. C., Loder, S. J., Ranganathan, K., Cederna, P. S., Mishina, Y., Wang, S. C. and Levi, B. (2015). Direct Mouse Trauma/Burn Model of Heterotopic Ossification. *J. Vis. Exp.* e52880.

Pignolo, R. J., Bedford-Gay, C., Liljesthröm, M., Durbin-Johnson, B. P., Shore, E. M., Rocke, D. M. and Kaplan, F. S. (2016). The Natural History of Flare-Ups in Fibrodysplasia Ossificans Progressiva (FOP): A Comprehensive Global Assessment. *J. Bone Miner. Res.* **31**, 650–656.

Pizza, F. X. and Buckley, K. H. (2023). Regenerating Myofibers after an Acute Muscle Injury: What Do We Really Know about Them? *Int. J. Mol. Sci.* **24**, 12545.

Potter, B. K., Burns, T. C., Lacap, A. P., Granville, R. R. and Gajewski, D. A. (2007). Heterotopic Ossification Following Traumatic and Combat-Related Amputations. *J. Bone Jt. Surg.* **89**, 476–486.

Prummel, K. D., Nieuwenhuize, S. and Mosimann, C. (2020). The lateral plate mesoderm. *Development* **147**, dev175059.

Qi, J., Dmochowski, J. M., Banes, A. N., Tsuzaki, M., Bynum, D., Patterson, M., Creighton, A., Gomez, S., Tech, K., Cederlund, A., et al. (2012). Differential expression and cellular localization of novel isoforms of the tendon biomarker tenomodulin. *J. Appl. Physiol.* **113**, 861–871.

Ranganathan, K., Loder, S., Agarwal, S., Wong, V. W., Wong, V. C., Forsberg, J., Davis, T. A., Wang, S., James, A. W. and Levi, B. (2015). Heterotopic Ossification. *J. Bone Jt. Surg.* **97**, 1101–1111.

Roberts, A. B., Anzano, M. A., Lamb, L. C., Smith, J. M. and Sporn, M. B. (1981). New class of transforming growth factors potentiated by epidermal growth factor: isolation from non-neoplastic tissues. *Proc. Natl. Acad. Sci.* **78**, 5339–5343.

Robinson, M. D., McCarthy, D. J. and Smyth, G. K. (2010). edgeR: a Bioconductor package for differential expression analysis of digital gene expression data. *Bioinformatics* **26**, 139–140.

Roesch, K., Jadhav, A. P., Trimarchi, J. M., Stadler, M. B., Roska, B., Sun, B. B. and Cepko, C. L. (2008). The transcriptome of retinal Müller glial cells. *J. Comp. Neurol.* **509**, 225–238.

Salzer, J. L. (2012). Axonal regulation of Schwann cell ensheathment and myelination. *J. Peripher. Nerv. Syst.* **17**, 14–19.

Sato, M., Saitoh, I., Kiyokawa, Y., Iwase, Y., Kubota, N., Ibano, N., Noguchi, H., Yamasaki, Y. and Inada, E. (2021). Tissue-Nonspecific Alkaline Phosphatase, a Possible Mediator of Cell Maturation: Towards a New Paradigm. *Cells* **10**, 3338.

Sauer, B. and Henderson, N. (1988). Site-specific DNA recombination in mammalian cells by the Cre recombinase of bacteriophage P1. *Proc. Natl. Acad. Sci.* **85**, 5166–5170.

Schatteman, G. C., Morrison-Graham, K., Koppen, A. V., Weston, J. A. and Bowen-Pope, D. F. (1992). Regulation and role of PDGF receptor a-subunit expression during embryogenesis. *Development* **115**, 123–131.

Schmierer, B. and Hill, C. S. (2007). TGFβ–SMAD signal transduction: molecular specificity and functional flexibility. *Nat. Rev. Mol. Cell Biol.* **8**, 970–982.

Schulze-Tanzil, G. G., Cáceres, M. D., Stange, R., Wildemann, B. and Docheva, D. (2022). Tendon healing: a concise review on cellular and molecular mechanisms with a particular focus on the Achilles tendon. *Bone Jt. Res.* **11**, 561–574.

Schweitzer, R., Chyung, J. H., Murtaugh, L. C., Brent, A. E., Rosen, V., Olson, E. N., Lassar, A. and Tabin, C. J. (2001). Analysis of the tendon cell fate using Scleraxis, a specific marker for tendons and ligaments. *Development* **128**, 3855–3866.

Shore, E. M. (2012). Fibrodysplasia ossificans progressiva: A human genetic disorder of extraskeletal bone formation, or-how does one tissue become another? *Wiley Interdisciplinary Reviews: Developmental Biology* **1**, 153–165.

Shore, E. M., Xu, M., Feldman, G. J., Fenstermacher, D. A., Brown, M. A. and Kaplan, F. S. (2006). A recurrent mutation in the BMP type I receptor ACVR1 causes inherited and sporadic fibrodysplasia ossificans progressiva. *Nature Genetics* **38**, 525–527.

Sideras, P., Apostolou, E., Stavropoulos, A., Sountoulidis, A., Gavriil, A., Apostolidou, A. and Andreakos, E. (2013). Activin, neutrophils, and inflammation: just coincidence? *Semin. Immunopathol.* **35**, 481–499.

Smith, C. L. and Tallquist, M. D. (2010). PDGF function in diverse neural crest cell populations. *Cell Adhes. Migr.* **4**, 561–566.

Soeda, T., Deng, J. M., Crombrugghe, B. de, Behringer, R. R., Nakamura, T. and Akiyama, H. (2010). Sox9-expressing precursors are the cellular origin of the cruciate ligament of the knee joint and the limb tendons. *genesis* **48**, 635–644.

Solovieva, T. and Bronner, M. (2021). Schwann cell precursors: Where they come from and where they go. *Cells Dev.* **166**, 203686.

Song, H. and Park, K.-H. (2020). Regulation and function of SOX9 during cartilage development and regeneration. *Semin. Cancer Biol.* **67**, 12–23.

Splunder, H. van, Villacampa, P., Martínez-Romero, A. and Graupera, M. (2024). Pericytes in the disease spotlight. *Trends Cell Biol.* **34**, 58–71.

Stanley, A., Tichy, E. D., Kocan, J., Roberts, D. W., Shore, E. M. and Mourkioti, F. (2022). Dynamics of skeletal muscle-resident stem cells during myogenesis in fibrodysplasia ossificans progressiva. *npj Regen. Med.* **7**, 5.

Stolinski, C. (1995). Structure and composition of the outer connective tissue sheaths of peripheral nerve. *J. Anat.* **186 (Pt 1)**, 123–30.

Sugimoto, Y., Takimoto, A., Hiraki, Y. and Shukunami, C. (2013a). Generation and characterization of ScxCre transgenic mice. *genesis* **51**, 275–283.

Sugimoto, Y., Takimoto, A., Akiyama, H., Kist, R., Scherer, G., Nakamura, T., Hiraki, Y. and Shukunami, C. (2013b). Scx+/Sox9+ progenitors contribute to the establishment of the junction between cartilage and tendon/ligament. *Development* **140**, 2280–2288.

Sullivan, M. P., Torres, S. J., Mehta, S. and Ahn, J. (2013). Heterotopic ossification after central nervous system trauma. *Bone Jt. Res.* **2**, 51–57.

Suzuki, W., Yamada, A., Aizawa, R., Suzuki, D., Kassai, H., Harada, T., Nakayama, M., Nagahama, R., Maki, K., Takeda, S., et al. (2015). Cdc42 Is Critical for Cartilage Development During Endochondral Ossification. *Endocrinology* **156**, 314–322.

Takarada, T., Nakazato, R., Tsuchikane, A., Fujikawa, K., Iezaki, T., Yoneda, Y. and Hinoi, E. (2015). Genetic analysis of Runx2 function during intramembranous ossification. *Development* **143**, 211–218.

Tani, S., Chung, U., Ohba, S. and Hojo, H. (2020). Understanding paraxial mesoderm development and sclerotome specification for skeletal repair. *Exp. Mol. Med.* **52**, 1166–1177.

Tekari, A., Luginbuehl, R., Hofstetter, W. and Egli, R. J. (2014). Chondrocytes expressing intracellular collagen type II enter the cell cycle and co-express collagen type I in monolayer culture. *J. Orthop. Res.* **32**, 1503–1511.

Thomopoulos, S., Parks, W. C., Rifkin, D. B. and Derwin, K. A. (2015). Mechanisms of tendon injury and repair. *J. Orthop. Res.* **33**, 832–839.

Tresoldi, I., Oliva, F., Benvenuto, M., Fantini, M., Masuelli, L., Bei, R. and Modesti, A. (2013). Tendon&#xfffd;s ultrastructure. *Muscles, Ligaments Tendons J.* **3**, 2–6.

Tseng, H.-W., Girard, D., Alexander, K. A., Millard, S. M., Torossian, F., Anginot, A., Fleming, W., Gueguen, J., Goriot, M.-E., Clay, D., et al. (2022). Spinal cord injury reprograms muscle fibroadipogenic progenitors to form heterotopic bones within muscles. *Bone Res.* **10**, 22.

Uezumi, A., Fukada, S. I., Yamamoto, N., Takeda, S. and Tsuchida, K. (2010). Mesenchymal progenitors distinct from satellite cells contribute to ectopic fat cell formation in skeletal muscle. *Nature Cell Biology* **12**, 143–152.

Uezumi, A., Ikemoto-Uezumi, M. and Tsuchida, K. (2014). Roles of nonmyogenic mesenchymal progenitors in pathogenesis and regeneration of skeletal muscle. *Front. Physiol.* **5**, 68.

Upadhyay, J., Xie, L., Huang, L., Das, N., Stewart, R. C., Lyon, M. C., Palmer, K., Rajamani, S., Graul, C., Lobo, M., et al. (2017). The Expansion of Heterotopic Bone in Fibrodysplasia Ossificans Progressiva Is Activin A-Dependent. *J. Bone Miner. Res.* **32**, 2489–2499.

Urist, M. R. and Strates, B. S. (1971). Bone Morphogenetic Protein. *J. Dent. Res.* **50**, 1392–1406.

Valer, J. A., Sánchez-de-Diego, C., Pimenta-Lopes, C., Rosa, J. L. and Ventura, F. (2019). ACVR1 Function in Health and Disease. *Cells* **8**, 1366.

Vedeler, C., Ulvestad, E., Bjørge, L., Conti, G., Williams, K., Mørk, S. and Matre, R. (1994). The expression of CD59 in normal human nervous tissue. *Immunology* **82**, 542–7.

Walia, B. and Huang, A. H. (2019). Tendon stem progenitor cells: Understanding the biology to inform therapeutic strategies for tendon repair. *J. Orthop. Res.* **37**, 1270–1280.

Wang, Y. X., Dumont, N. A. and Rudnicki, M. A. (2014). Muscle stem cells at a glance. *J. Cell Sci.* **127**, 4543–4548.

Wang, L., Valencak, T. G. and Shan, T. (2024). Fat infiltration in skeletal muscle: Influential triggers and regulatory mechanism. *iScience* **27**, 109221.

Wickham, H. (2016). ggplot2: Elegant Graphics for Data Analysis.

Wiltbank, A. T., Steinson, E. R., Criswell, S. J., Piller, M. and Kucenas, S. (2022). Cd59 and inflammation regulate Schwann cell development. *Elife* **11**, e76640.

Wolbert, J., Li, X., Heming, M., Mausberg, A. K., Akkermann, D., Frydrychowicz, C., Fledrich, R., Groeneweg, L., Schulz, C., Stettner, M., et al. (2020). Redefining the heterogeneity of peripheral nerve cells in health and autoimmunity. *Proc. Natl. Acad. Sci.* **117**, 9466–9476.

Wong, K. R., Mychasiuk, R., O'Brien, T. J., Shultz, S. R., McDonald, S. J. and Brady, R. D. (2020). Neurological heterotopic ossification: novel mechanisms, prognostic biomarkers and prophylactic therapies. *Bone Res.* **8**, 42.

Wosczyna, M. N., Biswas, A. A., Cogswell, C. A. and Goldhamer, D. J. (2012). Multipotent progenitors resident in the skeletal muscle interstitium exhibit robust

BMP-dependent osteogenic activity and mediate heterotopic ossification. *J. Bone Miner. Res.* **27**, 1004–1017.

Wosczyna, M. N., Konishi, C. T., Carbajal, E. E. P., Wang, T. T., Walsh, R. A., Gan, Q., Wagner, M. W. and Rando, T. A. (2019). Mesenchymal Stromal Cells Are Required for Regeneration and Homeostatic Maintenance of Skeletal Muscle. *Cell Rep.* **27**, 2029-2035.e5.

Wozney, J. M. and Rosen, V. (1998). Bone Morphogenetic Protein and Bone Morphogenetic Protein Gene Family in Bone Formation and Repair. *Clin. Orthop. Relat. Res.* **346**, 26–37.

Wrana, J. L. (2013). Signaling by the TGFβ Superfamily. *Cold Spring Harb. Perspect. Biol.* **5**, a011197.

Xu, R., Hu, J., Zhou, X. and Yang, Y. (2018). Heterotopic ossification: Mechanistic insights and clinical challenges. *Bone* **109**, 134–142.

Xu, Y., Huang, M., He, W., He, C., Chen, K., Hou, J., Huang, M., Jiao, Y., Liu, R., Zou, N., et al. (2022a). Heterotopic Ossification: Clinical Features, Basic Researches, and Mechanical Stimulations. *Front. Cell Dev. Biol.* **10**, 770931.

Xu, J., Wang, Y., Li, Z., Tian, Y., Li, Z., Lu, A., Hsu, C.-Y., Negri, S., Tang, C., Tower, R. J., et al. (2022b). PDGFRα reporter activity identifies periosteal progenitor cells critical for bone formation and fracture repair. *Bone Res.* **10**, 7.

Yamamoto, M., Shook, N. A., Kanisicak, O., Yamamoto, S., Wosczyna, M. N., Camp, J. R. and Goldhamer, D. J. (2009). A multifunctional reporter mouse line for Cre- and FLP-dependent lineage analysis. *genesis* **47**, 107–114.

Yamamoto, M., Legendre, N. P., Biswas, A. A., Lawton, A., Yamamoto, S., Tajbakhsh, S., Kardon, G. and Goldhamer, D. J. (2018). Loss of MyoD and Myf5 in Skeletal Muscle Stem Cells Results in Altered Myogenic Programming and Failed Regeneration. *Stem Cell Rep.* **10**, 956–969.

Yamamoto, M., Stoessel, S. J., Yamamoto, S. and Goldhamer, D. J. (2022). Overexpression of Wild-Type ACVR1 in Fibrodysplasia Ossificans Progressiva Mice Rescues Perinatal Lethality and Inhibits Heterotopic Ossification. *J. Bone Miner. Res.* **37**, 2077–2093.

Yamazaki, T. and Mukouyama, Y. (2018). Tissue Specific Origin, Development, and Pathological Perspectives of Pericytes. *Front. Cardiovasc. Med.* **5**, 78.

Yan, R., Zhang, H., Ma, Y., Lin, R., Zhou, B., Zhang, T., Fan, C., Zhang, Y., Wang, Z., Fang, T., et al. (2022). Discovery of Muscle-Tendon Progenitor Subpopulation in Human Myotendinous Junction at Single-Cell Resolution. *Research* **2022**, 1–16.

Yaseen, W., Kraft-Sheleg, O., Zaffryar-Eilot, S., Melamed, S., Sun, C., Millay, D. P. and Hasson, P. (2021). Fibroblast fusion to the muscle fiber regulates myotendinous junction formation. *Nat. Commun.* **12**, 3852.

Yea, J.-H., Gomez-Salazar, M., Onggo, S., Li, Z., Thottappillil, N., Cherief, M., Negri, S., Xing, X., Qin, Q., Tower, R. J., et al. (2023). Tppp3+ synovial/tendon sheath progenitor cells contribute to heterotopic bone after trauma. *Bone Res.* **11**, 39.

Yin, H., Price, F. and Rudnicki, M. A. (2013). Satellite Cells and the Muscle Stem Cell Niche. *Physiol. Rev.* **93**, 23–67.

Yoshimoto, Y., Takimoto, A., Watanabe, H., Hiraki, Y., Kondoh, G. and Shukunami, C. (2017). Scleraxis is required for maturation of tissue domains for proper integration of the musculoskeletal system. *Sci. Rep.* **7**, 45010.

Yu, P. B., Deng, D. Y., Lai, C. S., Hong, C. C., Cuny, G. D., Bouxsein, M. L., Hong, D. W., McManus, P. M., Katagiri, T., Sachidanandan, C., et al. (2008). BMP type I receptor inhibition reduces heterotopic ossification. *Nature Medicine* **14**, 1363–1369.

Yu, Q., Liu, J.-X., Zheng, X., Yan, X., Zhao, P., Yin, C., Li, W. and Song, Z. (2022). Sox9 mediates autophagy-dependent vascular smooth muscle cell phenotypic modulation and transplant arteriosclerosis. *iScience* **25**, 105161.

Zhang, Z., Nam, H. K., Crouch, S. and Hatch, N. E. (2021). Tissue Nonspecific Alkaline Phosphatase Function in Bone and Muscle Progenitor Cells: Control of Mitochondrial Respiration and ATP Production. *Int. J. Mol. Sci.* **22**, 1140.

Zhao, C., Inada, Y., Sekiguchi, K., Hino, K., Nishio, M., Yamada, Y., Matsuda, S., Toguchida, J. and Ikeya, M. (2023). Myelin protein zero (P0)- and Wnt1-Cre marked muscle resident neural crest-derived mesenchymal progenitor cells give rise to heterotopic ossification in mouse models. *Genes Dis.* **10**, 731–734.

Zheng, G. X. Y., Terry, J. M., Belgrader, P., Ryvkin, P., Bent, Z. W., Wilson, R., Ziraldo, S. B., Wheeler, T. D., McDermott, G. P., Zhu, J., et al. (2017). Massively parallel digital transcriptional profiling of single cells. *Nature Communications* **8**,.

Zhou, G., Zheng, Q., Engin, F., Munivez, E., Chen, Y., Sebald, E., Krakow, D. and Lee, B. (2006). Dominance of SOX9 function over RUNX2 during skeletogenesis. *Proc. Natl. Acad. Sci.* **103**, 19004–19009.

Zhu, X., Hill, R. A., Dietrich, D., Komitova, M., Suzuki, R. and Nishiyama, A. (2011). Age-dependent fate and lineage restriction of single NG2 cells. *Development* **138**, 745–753.

Appendix I: Reagents and Protocols

Appendix IA: Antibodies used in Flow Cytometry and Immunofluorescent assays

Antibody	Concentration	Company	Experiment
CD31 Rat anti-Mouse, Brilliant Violet 711, Clone: 390 BD Optibuild	1:800	BD Biosciences	Flow Cytometry
CD45 Rat anti-Mouse, Brilliant Violet 711, Clone: 30-F11, BD	1:500	BD Biosciences	Flow Cytometry
Anti-Mouse CD140a (PDGF Receptor a) APC 50 ug	1:100	eBiosciences	Flow Cytometry
Anti-Mouse, Ly-6A/E, BV450, Clone D7	1:400	BD Biosciences	Flow Cytometry
APC anti-mouse ESAM Antibody	1:100	Biolegend	Flow Cytometry
PE anti-mouse CD59a antibody	1:100	Biolegend	Flow Cytometry
Cd106 (VCAM 1) Rat anti Mouse, Biotin, Clone: 429	1:00	eBiosciences	Flow Cytometry
Brilliant Violet 421™ Streptavidin l	1:100	Fisher Scientific	Flow Cytometry
Rabbit Anti Mouse-Sox9 Antibody, AB5535	1:100	Sigma-Aldrich	Immunofluorescence
Anti-Sp7 / Osterix Antibody (ab22552)	1:200	Abcam	Immunofluorescence
Rabbit anti-SOX10 antibody	1:100	Abcam	Immunofluorescence
Goat anti-Rabbit IgG (H+L) Highly Cross-Adsorbed Secondary Antibody, Alexa Fluor 488	1:250	Thermofisher	Immunofluorescence

Appendix: IB PCR primer sequences used in genotyping

Allele	Fluorescence	Forward 5'-3'	Reverse 5'-3'
Cre-recombinase	N/A	GCGGTCTGGCAGTAAAAACTATC	GTTCGAACGCTAGAGCCTGTTT
Scx-Cre^{ERT2}	N/A	GCAGAACCTGAAGATGTTCGC	ACACCAGAGACGGAAATCCATC
Scx^{GFP}	GFP	CCTGCTGGAGTTCGTGACCGC	GAGGGGTAGTGGCACATCAGC
Acvr1^{tnR206H}	TdTomato	CAACAGGGTTATCTG ATGG	TCACATGTCCAGAGTTGCT
R26^{NG}	N/A	GATCAGCAGCCTCTGTTCCACA	CGCTGAACTTGTGGCCGTTTAC
Pdgfra$^{H2B-GFP}$	GFP	CCCTTGTGGTCATGCCAAAC	ACGAAGTTATTAGGTCCCTCGAC
R26^{mCherry}	N/A	TTATGTAACGCGGAACTCCA	AAAGTCGCTCTGAGTTGTTAT

Appendix IC: Dissection and FACS isolation of TLCs

This protocol is intended for the isolation of TLCs from the intermuscular fascial region of the posterior hindlimb compartment.

Recipes:

Digestion media: 2 mg/mL collagenase II; 0.5 mg/mL dispase; in DMEM
Quench media: 20% FBS in DMEM
FACS Buffer: 2% FBS in DMEM

Procedure:

1. *Scx*$^{GFP/+}$ mice were amnestied through isoflurane exposure and sacrificed by cervical dislocation.
2. Skin is removed and the hindlimb muscles were exposed (Fig A). Remove leg from mouse ad secure in a dissection tray using dissection pins.

   Fig A.

   

   * a fluorescent dissecting scope was used for the following steps
3. Sever the fascia between the lateral compartment and the posterior compartment
4. Slide forceps under in the slit in the fascia, separating out the posterior compartment form the hindlimb (Fig B)

   Fig B.

   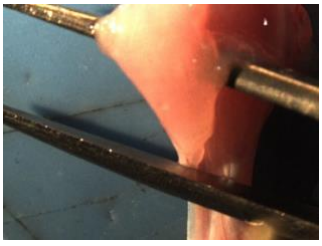

5. Use a scapple to sever the anterior portion of the posterior compartment from the back of the knee, keeping the Achilles tendon attached to the hindlimb
   a. If done correctly the entire posterior compartment (composed of three muscles) will be removed (Fig C)

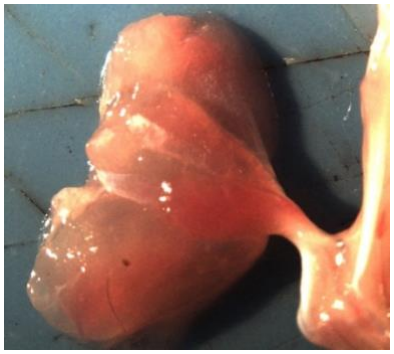

Fig C.

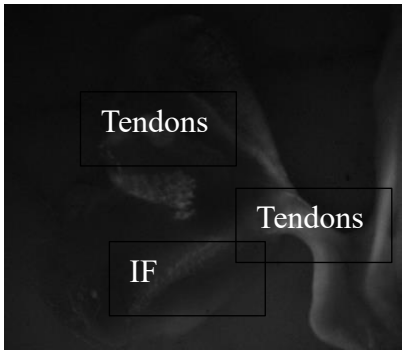

Fig D. fluorescence of Scx-expressing cells

6. Peel back the soleus and plantaris muscles leaving both the lateral and medial GA heads (Fig E)

Fig E.

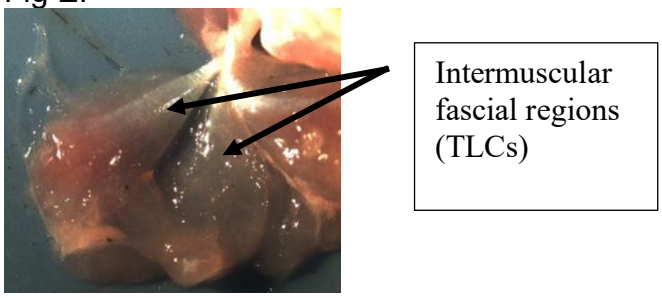

   a. Associated tendons will be attached to the soleus and plantaris muscles and will be removed with the muscles
7. Sever the Achilles tendon connection removing the two gastrocnemius heads from the hindlimb (red line- Fig F)

Fig F.

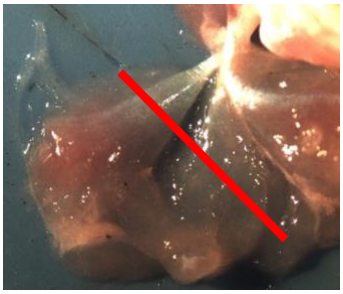

8. Check the GFP fluorescence of the GA heads to ensure the intermuscular fascial regions are present and the tendons and tendon insertions are removed
   a. Tendons will have a strong GFP fluorescence with bundles of collagen 1
   b. Intermuscular fascial regions will have diffuse GFP staining and lack the ladder like collagen 1 bundles

    c. Tendon insertion sites have bright GFP fluorescence
9. Once all tendon insertion sites and tendons are removed place the intermuscular fascial connective tissue and associated muscle in a 35 mM cell culture dish with 100 µL digestion media and mince with scissors for 8 minutes
10. Place the minced sample into a 5 mL conical tube with 5 mL of digestion media and incubated at 37°C for 1 hour with constant agitation
11. After digestion, quench with 5 mL of quench media and filter samples through a 70 µM cell strainer
12. Wash the strainer with an addition 5mL of quench media
13. Spin samples at 500G for 4 minutes at 4°C
14. Aspirate supernatant and resuspend in 5mL of DPBS
15. Spin samples at 500G for 4 minutes at 4°C
16. Resuspend samples in 500 µL to 1 mL of FACS buffer at bring to the Flow Cytometry Facility
17. Add .02µg of DAPI and incubate for 10 minutes in low light conditions
18. Collect the DAPI-;GFP+ cells and then smile

Appendix II: Publications and Addition Projects

Appendix IIA: Citations of Publications

Burdick LN, DelVichio AH, Hanson LR, Griffith BB, Bouchard KR, Hunter JW, Goldhamer DJ. Sex as a Critical Variable in Basic and Pre-Clinical Studies of Fibrodysplasia Ossificans Progressiva. Biomolecules. 2024 Feb 1;14(2):177. doi: 10.3390/biom14020177. PMID: 38397414; PMCID: PMC10886767.

Appendix IIB: Fibrodysplasia ossificans Progressiva on the tongue

The following section outlines work conducted by an undergraduate researcher, Amy Backal, under my direct supervision. Experiments were performed collaboratively by Ms. Backal and me. The written document was drafted by Ms. Backal.

Abstract:

FOP is a rare genetic disorder in which skeletal muscle and associated connective tissue progressively turn to bone through a process called heterotopic ossification (HO). The extra skeletal bone growth is cumulative, eventually trapping patients in a second skeleton that eventually leads to death by asphyxiation. The FOP mutation is autosomal dominant that can be inherited or acquired sporadically. Unfortunately, FOP is currently incurable with no therapeutic options to inhibit bone growth or reduce existing bone nodules. My project intends to further our understanding of the cellular mechanisms of the disease within the tongue muscle. A population of cells known to be an origin of HO resides in the skeletal muscle of the tongue, but patients

have clinically never been afflicted with HO in th tongue. The goal of this research is to consider the cellular environment of the tongue and the population of cells that reside there as possible inhibiting factors for bone growth. Using an FOP accurate mouse model, experiments priming the tissue for HO found that chemical injury in the presence of a specific cell population induced HO in the tongue. Cross transplantation experiments confirmed this finding. Further analysis into the heterogenous population of causal cells in the tongue is necessary.

Introduction

Fibrodysplasia Ossificans Progressiva (FOP) is a rare genetic disorder in which skeletal muscle and associated connective tissue progressively turn to bone through a process called heterotopic ossification (HO)[5,7,10,13,14]. HO can be provoked by soft tissue injury or spontaneously, with no known cause. The extraskeletal bone growth causes chronic pain for patients and progresses throughout their life. HO fuses with endogenous bone, locking afflicted tissue into place, eventually trapping patients into positions in which they are wheelchair bound and reliant on a feeding tube[10,13]. Progressive HO often leads to death due to asphyxiation. Since the disease is so rare, affecting one in every million individuals, physicians often misdiagnosed FOP due to lack of awareness and education. The only sign of FOP at birth is malformation of the big toes, which is found in all afflicted individuals, but not unique to FOP. This, paired with early swelling of soft tissue and HO presentation can lead to a proper diagnosis[10,13]. Once diagnosed, medical intervention is limited. There are currently no approved therapeutics that block bone growth or diminish pre-existing lesions. Surgical removal of bone lesions is not an option, because it acts as

a form of injury, eliciting a painful, larger HO to form in its place. Rather, medicines are often prescribed to alleviate symptoms as they present[5,10,13,14].

The FOP mutation is an autosomal dominant mutation that can be inherited or acquired sporadically[5,7,10,13]. In most patients, there is a point mutation in the gene encoding the bone morphogenetic protein (BMP) type 1 signaling receptor, Activin A Receptor Type 1 (ACVR1). This mutation leads to an amino acid switch of an arginine to histidine at position 206 in the ACVR1 receptor (*ACVR1*^{R206H})[5,7,10,13]. Only one mutated allele is required to induce a malfunctioning ACVR1 receptor. This amino acid switch alters the receptor's ligand binding activity, creating a hyperactive BMP receptor that has a newfound responsiveness to the ligand activin A, a member of the transforming growth factor-ß family[5,7,14,17]. ACVR1 without the R206H mutation activates SMAD 2/3 phosphorylation and inhibits BMP activity when activin A is bound. In the presence of the mutation, signaling is altered, so upon activin A binding, SMAD 1/5/8 phosphorylation is activated, leading to an osteogenic response in competent cells. Activin A is secreted in response to injury or illness, which explains why HO is often found following soft tissue injury[5,7,14].

An FOP mouse model which accurately mimics clinical FOP was created to further research the disease. This is a conditional knockin mouse model of FOP in which the expression of the FOP mutation at *Acvr1* gene is present in exon 5 (**Figure 1a)**[7]. Expression of this mutation is controlled by activity of a site-specific recombinase, Cre, which establishes temporal and cell specific activation[7,18]. Cre is controlled by *Tie2* or *Pdgfra* promoters[7]. Upstream of the *Acvr1*^{R206H} mutation, in intron 4, is a stop cassette with a tdTomato reporter and a CAG promoter, flanked by two LoxP sites[7,18]. The CAG promoter is a constitutively active promoter that allows the expression of the tdTomato, which provides a red fluorescent label to indicate that the cell contains the *Acvr1*^{R206H} mutation and Cre is not active. The stop cassette inhibits the read out of the downstream *Acvr1*^{R206H}. When Cre is active, the tdTomato reporter stop cassette will be cleaved at the LoxP sites, the cell will lose its red fluorescence, and the mutated *Acvr1* gene will be transcribed (**Figure 1a)**[7]. This cleavage only occurs once, and then the gene will be indefinitely turned on. Additionally, a Cre dependent enhanced green fluorescent protein (eGFP) reporter is knocked in at the *Rosa26* locus, providing a lineage tracer to

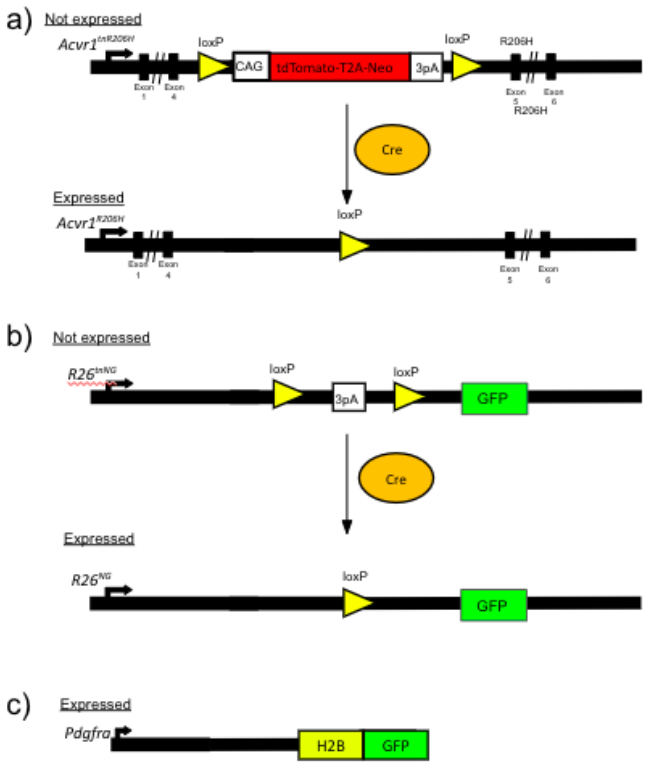

Figure 1: FOP accurate Mouse model. a) Knockin of Cre-dependent FOP mutation at the ACVR1 loci with a red fluorescently labelled stop cassette. When Cre is not active, red fluorescence is present and *Acvr1*^{R206H} is not expressed. When Cre is active, the tdTomato and Stop cassette (3pA) are cut at the loxP sites, and the *Acvr1*^{R206H} mutation is expressed. b) Knockin of Cre-dependent eGFP at the Rosa26 loci. When Cre is not active, no fluorescence is present. When Cre is active, the Stop cassette is cut at the loxP sites, and the GFP fluoresence is expressed. c) A knock-in fusion gene targeted to the *Pdgfra* gene. GFP expression reflects current *Pdgfra* expression. The GFP will be nuclear localized in the cell due to the H2B tag.

confirm Cre activity[7] (**Figure 1b**). In other words, when a cell loses its red fluorescence and gains green fluorescence, it is understood that is Cre is active and the cell is recombined. The *Rosa26* locus is transcriptionally active throughout development and adulthood, as well as uniformly and ubiquitously expressed. Additionally, mice with knockin mutations at the *Rosa26* loci are still viable and develop normally, making it an efficient, safe loci to use for lineage labeling. In a different mouse model, green fluorescence is controlled by current *Pdgfra* expression. An H2B-eGFP fusion gene is knocked in downstream of the the *Pdgfra* promoter, so GFP fluorescence indicates current *Pdgfra* expression (*Pdgfra*$^{H2B\text{-}GFP/+}$)(**Figure 1c**).

Using this accurate mouse model of FOP, the Goldhamer lab identified fibro/adipogenic progenitors (FAPs) as a major causal cell of injury induced and spontaneous HO[7]. To decipher which cell type was responsible for HO, many different Cre drivers were tested for all cell types implicated in HO. *MyoD*^{iCre} and VE-Cadherin-Cre were used to recombine muscle stem cells and endothelial cells, respectively. When these cells expressed the *Acvr1*^{R206H} mutation they did not form HO[7]. Tie2-Cre was used to recombine FAP cells. The *Tie2* gene, also known as *Tek*, codes for a tyrosine kinase receptor found on endothelial, hematopoietic and FAP cells[8]. When these cells expressed the *Acvr1*^{R206H} mutation, HO occurred. To confirm FAP origin rather than endothelial or hematopoietic, *Pdgfra* (platelet-derived growth factor receptor alpha) expression was used to drive Cre. PDGFRa is a membrane receptor specific to FAP cells found in adult muscle tissue[1,7,9]. In a separate experiment, FAPs expressing the *Acvr1*^{R206H} mutation and the TIE2+ receptor were isolated and transplanted into SCID mice. Results from both experiments proved that recombined FAPs are sufficient to produce HO[7,9,].

Specific cell surface receptors and lack of myogenic capacity distinguish FAPs from other cell types. They are found within the skeletal muscle interstitium but are distinct from endothelial and hematopoietic cells due to their cell surface receptors[1,7,8,9]. FAPs display the membrane markers platelet-derived growth factor receptor alpha (PDGFRa) and stem cell antigen 1 (SCA1). FAPs also exhibit multipotency, capable of forming fibrotic or adipogenic tissue in a non-diseased state[1,7,8,9]. When FAPs actively express the *Acvr1*^{R206H} mutation, they respond to activin A binding by initiating osteogenic signaling[5,7,9]. FAPs are a heterogenous population with multiple subtypes[7,8,9]. In uninjured muscle, these subtypes upregulate specific genes for different biological processes. The TIE2 receptor labels a subtype of FAPs implicated in BMP signaling, while the PDGFRa receptor is found on all FAPs[7,8,9].

In a healthy individual FAPs are imperative for skeletal muscle homeostasis and regeneration[1,8]. Muscle has an impressive regenerative capacity because of the muscle stem cells present. Muscle stem cells efficiently enter the cell cycle to increase the myogenic cells present for repair of tissue[12,13]. To do this, muscle stem cells rely on signaling from non-myogenic cells in the environment, and FAPs are a major contributor in this process[1,8,13]. Similar to muscle stem cells, FAPs enter the cell cycle following injury or illness, but FAPs have a quicker response than the muscle stem cells[1,9,13]. FAP cell count peaks around three days post injury to promote neutrophil and monocyte recruitment. FAPs work to regulate the activity of these immune cells from their pro-inflammatory to anti-inflammatory phenotypes[1,9]. Simutaneously, these immune cells work to regulate FAP density and activity in injured tissue. FAPs also interact with myogenic cells, stimulating differentiation and aiding with muscle maturation[1,8,9]. In non-

diseased cells, FAPs return to a similar state to non-injured tissue around seven to ten days after injury[9]. In the presence of the *Acvr1*^{tnR206H} mutation, this precise balance of cell communication is disturbed. By day six post injury, there is a difference in FAP behavior in diseased tissue compared to non-disease tissue[8,9]. At this time point, non-diseased tissue exhibits regenerated fibers, while diseased tissue shows a high number of chondrocytes. By day 14 post injury, non-diseased tissue has completely regenerated, while cartilage in diseased tissue has turned to bone through endochondral ossification[7,9].

Flow cytometry is a technology that uses fluorescent markers that are analyzed and standardized to identify cell populations[10]. Using flow cytometry, a population of FAP cells was identified in the tongue, a skeletal muscle with dense myofibers surrounded by connective tissue[3,12,16]. In the presence of the active *Acvr1*^{R206H} mutation, the tongue presumably has optimal conditions for HO. For unknown reasons there have been no clinical or experimental HO findings in the tongue. The absence of HO in the tongue is an understudied topic. My project was intended to increase our understanding of inhibiting factors for HO in an FOP diseased tongue.

Many skeletal muscles contain densely packed myofibers which are aligned parallel, but the tongue is organized in a complex way[3,16]. There are separate bundles of myofibers in the tongue that run in different directions to accommodate the versatile movement required of the tongue. The tongue is unique in that there is no tendentious attachment of the muscle to a joint and it is not connected to bone at both ends[3,16]. The mid-belly of the tongue is most densly packed with myofibers and little connective tissue[16]. Connective tissue, adispose tissue, and interstitial space are found in greater quantity anterior, near the tip of the tongue. Most connective tissue resides between the bundles

of myofibers that run on different planes, in different directions[16]. Unfortunately, information on structural organization, regeneration, and cell types within the tongue is limited[3,12]. Interestingly, there have been five clinical cases of osteolipomas in the oral cavity unrelated to FOP, and at least one reported case specifically within the tongue[15]. Lipomas with osseous metaplasia are scarce, and rarely found in the oral cavity. These tumors often come from deep soft or subcutaneous tissues. This is significant because it indicates that the tongue has the capacity to ossify in the presence of other mutations[15].

To further elucidate why an FOP diseased tongue is not known to ossify, we considered the subpopulation of FAPs that reside in the tongue, and the extracellular environment of the tongue as possible inhibitory factors. FAPs are a heterogenous population, and the presence and behavior of the subpopulations of FAPs present in the tongue are unknown. The specific subpopulation of FAPs within the tongue may dictate the tissue's ability to ossify. Additionally, skeletal muscle regeneration and growth involves recruitment of surrounding cells to stimulate specific signals for muscle stem cells to correctly differentiate into myofibers; therefore, the extracellular environment can also influence a tissue's ability to ossify. We utilized injury assays to determine if the tongue forms bone following injury. It was found that Tie2-Cre; $R26^{NG/+}$; $Acvr1^{R206H}$ mice did not form bone following pinch injury, and cardiotoxin injury results were ambiguous. Pdgfra-Cre; $R26^{NG/+}$; $Acvr1^{R206H}$ mice did not form bone following pinch injury, but did form bone from cardiotoxin injury. This led us to consider a difference in osteogenic capacity of Tie2-Cre; $R26^{NG/+}$; $Acvr1^{tnR206H}$ and Pdgfra-Cre; $R26^{NG/+}$; $Acvr1^{tnR206H}$ FAPs. We performed histological analysis on injured and uninjured tissue to evaluate the structure, organization, and regenerative process in nondiseased tongues and diseased tongues.

Histology proved that HO, cartilage and/or lack of structural integrity were found following a sufficient injury to induce regeneration in an FOP diseased tongue. More research into the regenerative processes in the tongue could prove beneficial in understanding the range in results. We conducted cross transplantation assays to separately evaluate the osteogenic capacity of tongue FAPs and the extracellular environment of the tongue. We evaluated tongue FAP osteogenic competence by transplanting tongue FAPs in an environment known to be competent for HO. Similarly, we transplanted HO competent FAPs into the tongue to test osteogenic capacity of the tongue environment. We found that Tie2-Cre; *Acvr1*^{R206H} hindlimb FAPs transplanted into the tongue reproducibly formed HO, Tie2-Cre; *Acvr1*^{R206H} tongue FAPs did not form HO in the tongue or hindlimb, and Pdgfra-Cre, *Acvr1*^{R206H} tongue FAPs formed HO in the tongue. This further supported the results from the injury assays that there could be an osteogenic deficit in the TIE2+ FAP subpopulation. Further research on intrinsic differences in the subpopulation of FAPs within the tongue is necessary.

My intention was to help the FOP community further understand the cellular mechanisms of the disorder. The data stimulates the need for further research into the mechanisms responsible for the varying phenotypes in the different mouse models. This could be helpful in understanding HO origins, leading to a treatments that inhibit this process.

Methods

Genotyping

To conduct experiments on FOP accurate mice, new litters were genotyped to ensure that the experimental mice had the phenotypes necessary to see intended results. We ear punched the mice in a specific location that also acts to number them within their litter. This tissue was visualized under a Leica MZ FL III stereoscope for preliminary information on the gene expression. Then the tissue was transferred to a 100 µL of alkaline lysis buffer with 25 mM NaOH and 0.2 mM of disodium ethylenediamine tetra acetic acid (EDTA) in water (Fisher Scientific, BP1201). This was placed in a heat block and heated to ~96℃ and remained there for an hour. After an hour we added 100 µL of neutralizing buffer with 40 mM of Tris hydrochloride salt in water, was added to the DNA, and this solution was spun down. The DNA was amplified using traditional PCR methods and then run on a gel to identify which mice have the genes of interest. For this project, I was interested in the presence of expressed Tie2-Cre; Pdgfra-Cr;*, $Acvr1^{R206H}$; $R26^{NG/+}$;* and $Pdgfra^{H2B\text{-}GFP/+}$.

Pinch Injury

To initiate a regenerative response, and create an environment primed for HO, a pinch injury was used as a physical form of injury. Following IACUC protocols, the experimental mice were placed in a chamber to be anesthetized using a steady flow of O2 and isoflurane, from Animal Care services. Following this, the mice were placed on their back, and forceps were used to gently guide the tongue out of the mouth to expose the tissue. Once exposed, the serrated forceps were used to pinch down on the mid-belly of the tongue, a few micrometers from the tip of the tongue. As much force as possible was used for every tongue injury, in an effort to maintain consistent pressure between

injuries, and limit human error. The mice were then placed back in the chamber to anesthetize in the same way previously mentioned. Once anesthetized, the mice were placed on their back to expose their right hindlimb. Holding the foot of the hindlimb to be pinched, the serrated forceps were used to pinch injure the gastrocnemius muscle of the right hindlimb in the same manner as the tongue. At the spot of injury, observations were made to confirm that marks were made suitable to signify injury occurred. The injured mice were housed separately from non-injured mice and given wet food. The mice were weighed every other day to verify they were not losing too much weight, following IACUC protocol. 14 days post injury the mice were placed in a chamber with kimtech paper that had four drops of isoflurane to anesthetize the mice. While the mice were being anesthetized, a dissection station was made. The area was cleansed with ethanol and covered with a layer of aluminum foil and multiple kimtech wipes. The area was sprayed once more with ethanol. Once the mouse's breaths were spaced out a few seconds, they were sacrificed by cervical dislocation. A small incision with scissors was made in the skin to expose the musculoskeletal structures. The entire hindlimb was collected by cutting the limb with dissection scissors at the hip joint. The feet were also cut off. Harvested hindlimbs were placed directly into 4% Paraformaldehyde (PFA) for three days and then transferred to PBS. 4% PFA was made by diluting a stock solution of 16% Paraformaldehyde (Electron microscopy science, 15710) with PBS. To harvest the tongue the jaw bones were cut using dissection scissors. The lingual frenulum was cut at the base of the tongue, and the larynx was cut at the back of the tongue far enough to collect the tongue tissue and hyoid bone. Harvested tongues were placed directly into 4% PFA for 24 hours and then transferred to PBS. Once in PBS, the tissue was scanned in the In

Vivo Imaging System (IVIS), a μCT machine, which scans for bone growth. The IVIS was set on CT, photograph, and visual field C. The tongue tissue was scanned with the hindlimb to maintain a consistent threshold for endogenous bone. Any exogenous bone growth found was quantified using 3D Slicer. This is an online software created for image processing and three-dimensional visualization.

Cardiotoxin Injury

To initiate a regenerative response, and create an environment primed for HO, cardiotoxin injury was used as a chemical form of injury. Following IACUC protocols, the mice were cardiotoxin injured using 10 μM cardiotoxin (Latoxan, L8102-1MG). The experimental mice were placed in a chamber to anesthetize the mice for the injury using the same steps as pinch injury. During this time, 20 μL of cardiotoxin was measured using a lo-dose insulin syringe 50cc, (MedPlus services, EXEL 26028). From previous optimization experiments, we found that 20 μL of liquid was the threshold the mouse tongue could maintain without bursting. Following this, the mice were placed on their back and forceps were used to gently guide the tongue out of the mouth to expose it. Once exposed, the needle was inserted parallel to the tongue to minimize the chance of it poking out and ensure the cardiotoxin was injected into the mid-belly of the tongue (**Figure 2a)**. As the cardiotoxin was injected, the needle was slowly pulled out of the tongue, dispersing the liquid, to decrease the chance of bursting. The mice were then placed back in the chamber to anesthetize once more. Once anesthetized again, the mice were placed on their back to expose their hindlimb. Holding the foot of the hindlimb to be injured a needle with 50 μL of cardiotoxin was injected into the right hindlimb into the

gastrocnemius muscle (**Figure 2b)**. The injured mice were housed separately from non-injured mice and given wet food. The mice were weighed every other day to verify they were not losing too much weight, following IACUC protocol. 14 days post injury the mice were sacrificed and harvested using the same methods as pinch injury. Once in PBS, the tissue was ready to be scanned in the IVIS, to visualize for HO and then quantified.

Histology

To prepare harvested tissue for histological analysis, there is a month-long process to properly embed and section it. From dissection, a tongue went into 4% PFA for 24 hours, and a hindlimb for three days, to fix the tissue. Both tissues were then washed with PBS for three cycles and then placed in 12% EDTA in water. A harvested tongue requires two weeks for full decalcification, while a hindlimb takes 4 weeks to decalcify. The EDTA solution is changed every other day. Following their respective timelines, both tissues were then transferred to a 1% sucrose solution (Sigma-Aldrich, S5016-1KG) for at least

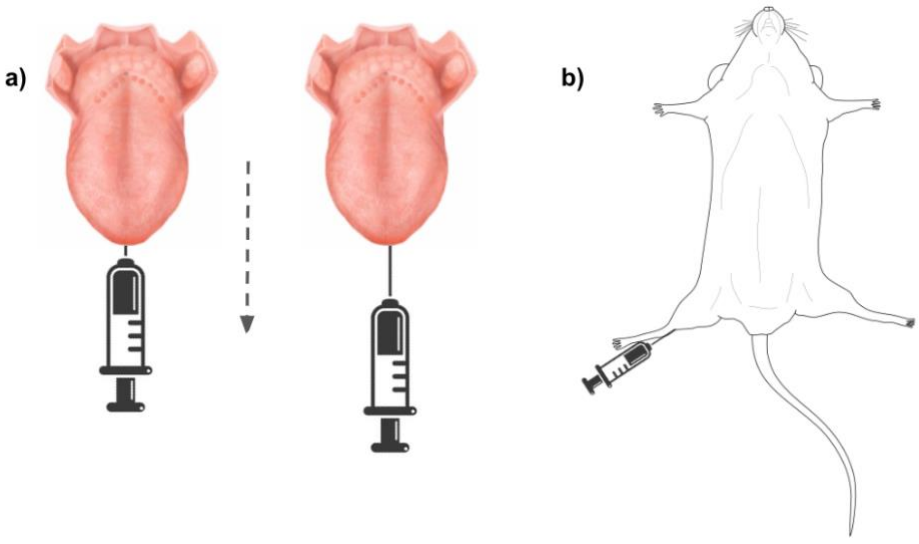

Figure 2: Cardiotoxin method for the tongue and hindlimb. a) The needle is inserted parallel to the tongue, far enough to get the tip in the center. Depth of the needle was estimated based on how much needle was showing. The needle was slowly pulled out, maintaining a parallel position, as the cardiotoxin was expelled. b) The needle was injected along the achilles tendon into the gastrocnemius muscle. The cardiotoxin was expelled when most of the needle was in the tissue, verifying it was deep in the mid-belly of the muscle.

24 hours. Once this process was complete, the tissue was flash frozen in OTC. Embedded tissue was kept in a -80℃ freezer until ready to be sectioned.

A cryostat, which maintains low cryogenic temperatures of samples, was used to slice the tissue into 10 µm sections. The cryostat was set to -25℃. The tissue was captured on histology slides. The slides were stained using 4′,6-diamidino-2-phenylindole (DAPI) (Sigma-Aldrich, 10236276001) or Hematoxylin and Eosin (H&E). A conventional DAPI stain procedure was used to fluorescently label nuclei as blue. For the H&E procedure, slides were washed in water twice, for three minutes and then sat in Mayer's hematoxylin (Sigma-Aldrich, MHS16-500ML) for ~8 minutes. The slides then went through three more water washes for 30 seconds each, followed by a minute bluing step, which is a 0.2% ammonia water solution (Sigma-Aldrich, 221228-500ML-A). The slides were transferred to two 70% ethanol bathes, a minute each, followed by three washes in 95% ethanol for 30 seconds each. Slides were dunked in an Eosin Y working solution (0.25%), (Sigma-Aldrich, E4382-25G) for 5-10 seconds. The slides went through two more 95% ethanol washes for a minute each, followed immediately by two washes in 100% ethanol for three minutes each. The staining process ends with two washes in xylene (Fisher Scientific, X3P-1GAL) for five minutes each, and then cover slipped using a thin line of paramount down the middle of the slide. This had to set overnight in the histology hood. An inverted confocal microscope with three excitation wavelengths and bright field was used to visualize histology. The microscope contained fluorescent channels to visualize green, red, and blue, as well as a bright field feature. Magnitudes of 100x, 200x and 400x were used to focus on certian areas of the sections.

Cross Transplantations

We conducted cross transplantations to test the osteogenic capacity of the tongue tissue and the FAPs within the tongue. Mice were genotyped for expression of Tie2-Cre or Pdgfra-Cre; *Acvr1*^{tnR206H}*; R26*$^{NG/+}$ or *Pdgfra*$^{H2B\text{-}GFP/+}$. Tongue tissue and hindlimb tissue from mice expressing these genes of interest were dissected in the same manner as the pinch injured tissue. The harvested tissue was minced in digestion media with 2 mg/mL of collagenase type 2, (Worthington Biochemical, LS004177) and 0.3 mg/mL of dispase (Invitrogen, 17105041) in DMEM for 8-10 minutes, until no large clumps were visible. Minced tissue was placed in 10 mL of the same digestion media and sat in a hot bath for an hour and vortexed every 10 minutes. The cells were plated at a seating density to promote growth with growth media containing 10% fetal bovine serum (FBS) (R&D systems, S11510) and 1% Penicillin-Streptomyocin, (Sigma-Aldrich, P4333-100ML) in DMEM. Growth media was changed every other day and cells were split if they were over 80% confluent. To split cells, growth media is aspirated up and the cells were washed with DPBS. After the wash, the DPBS was aspirated and replaced with trypsin (Thermo-Fisher Scientific, 15090046) and placed back in the incubator for 3-5 minutes. After confirming the cells had detached by visualizing under a Nikon Exlipse E600 compound microscope, the trypsin was neutralized with an equal volume of quench buffer made with 10% FBS in DMEM and transferred to a 15 mL conical. The cells were spun down at 4°C for five minutes at 1500 rpm. The supernatant was aspirated up and replaced with growth media. The cells were then split 1:2 or 1:3 depending on their confluency prior to splitting. 5-7 days after the cells were plated, they were prepared for the FACS (fluorescence activated cell sorting) machine to isolate the FAPs. Cells were stained with fluorescently

conjugated antibodies that bind surface receptors. APC, BV7/11, BV421, and 7AAD, stain for PDGFRa, CD31/45, SCA1, and live/dead marker, respectively. When an *Pdgfra*$^{H2B\text{-}GFP/+}$ mouse was used for transplantations, the APC was omitted, because PDGFRa was denoted by endogenous green fluorescence. Some samples contained only one antibody stain in each, while some samples had all stains but one, to calibrate the FACs machine. Experimental samples to be isolated were stained with all fluorescent markers. These stains and endogenous fluorescence allowed the FACS machine to calibrate which cells to keep and which to discard. The result of the FACS was an isolated population of recombined FAP cells from the tongue and the hindlimb. After isolation, the FAPs were plated in growth media for another 5-7 days to increase population size. Growth media was changed every other day and cells were split according to their confluency. Previous research has shown that transplanting 50 µL of 1 million FAP cells is sufficient to initiate HO in a pre-injured HL. 20 µL of 400k cells were transplanted into the tongue to maintain an equal density. The density of recombined FAPs transplanted into no color SCID mice remained constant for both mouse models, Tie2-Cre and Pdgfra-Cre. To have enough cells for the transplantation, the goal is to collect around 1.5 million cells per SCID mouse. When a sufficient population of cells was reached, they were collected from culture. Growth media was aspirated out and replaced with DPBS for a wash. DPBS was aspirated and replaced with trypsin, and the cells were moved back into the incubator for 3-5 minutes. To fully detach the cells from the plate, the trypsin was pipetted up and down a few times around the plate to add physical force. Trypsin was neutralized with an equal volume of quench buffer. The cells were spun down and counted using a hemocytometer. This number was used to calculate the volume of DPBS to resuspend the cells in to have

1 million cells in every 50 µL of volume. The SCID mice to be used were anesthetized in the same way previously mentioned. Cells isolated from the tongue were transplanted into an injured hindlimb and tongue, and those from the hindlimb into an injured hindlimb as a control. FAPs isolated from the hindlimb were transplanted into an injured tongue and an injured hindlimb as a control. These mice were housed separately and given wet food. 14 days post transplantation the mice were collected. Tongue and hindlimb tissue were dissected using the same methods previously mentioned. Prior to a 4% PFA wash, whole mounts images were observed of the tissue under a Leica MZ FL III stereoscope. Tongues and hindlimbs then went through the same process as injured tissue for IVIS scans, embedding and histological analysis.

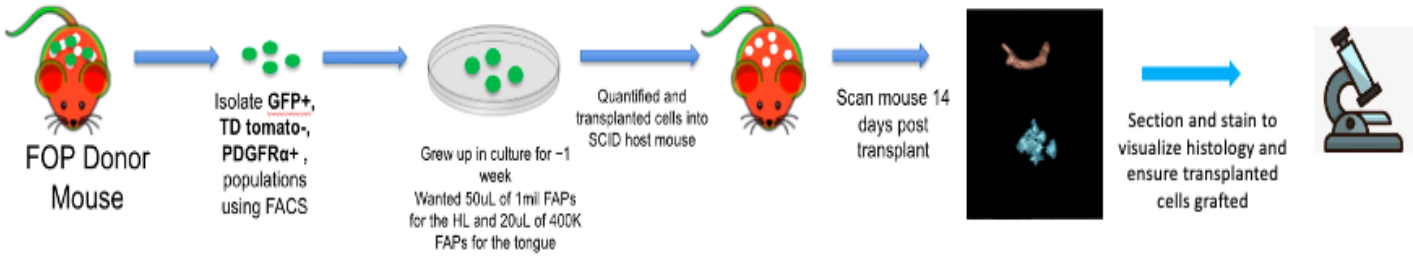

Figure 3: FAP isolation and Cross-transplantation procedure. Genotype mice for Tie2-Cre or Pdgfra-Cre, *Acvr1*^{R206H}, *R26*$^{NG/+}$ or *Pdgfra*$^{H2B\text{-}GFP/+}$. Collect tongue and hindlimb tissue to culture cells from host mice with the genes of interest. Isolate the FAP cells using FACS, gating for CD31/45-, SCA1+, PDGFRa+, GFP+ and tdTomato- cells. Grow up FAPs in culture for a week. Resuspend cells in DPBS to a calculated volume resulting in 1 million cells/50 µL and transplant cells into SCID mice. Isolated tongue FAPs were transplanted into the tongue and left hindlimb, using the same methods as cardiotoxin injection. Hindlimb FAPs were transplanted into the right hindlimb of these SCID mice as a control. Hindlimb FAPs were also transplanted into the tongue and right hindlimb of other experimental SCID mice. 14 days post injury tissue was collected and scanned for HO. Harvested tissue was then prepared for histological analysis.

Results

Testing HO Capacity of the Tongue through Injury Assays

Pinch injury does not induce HO in the tongue of a mouse with FOP. Pinch injury assays were conducted on the tongue to test whether the tongue is competent for HO. The right hindlimb was also injured as a positive control. Initially, five Tie2-Cre; *R26*$^{NG/+}$*; Acvr1*^{tnR206H} mice were pinch injured and one Tie2-Cre; *R26*$^{NG/+}$ mouse was pinch injured as a control. 14 days post injury, the mice were sacrificed and imaged. All six mice did not from HO (**Figure 4)**. Bone growth was seen in the hindlimbs of the experimental mice, confirming the mice were competent to form HO (data not shown). The tissue was then fixed and decalcified for two weeks to prepare it for the embedding process. Embedded tissue was sectioned assess regeneration with histological analysis. Two experimental tongues were sectioned and stained with DAPI to visualize centralized nuclei. Centralized nuclei were difficult to find in both tongues, because they were dispersed and in low concentration(**Figures 5a)**. The section stained is from the mid-belly of the tongue in a medial location that was pinch injured. A few myofibers show regeneration, but they are not in a centralized location. From histology, we speculate that not enough myofibers were injured by the force of the pinch to provoke injury-induced HO. The injured tongue maintains structural and organizational integrity compared to the uninjured tissue (**Figure5a, c**). Following these results, we pinch injured Pdgfra-Cre; *R26*$^{NG/+}$*; Acvr1*^{tnR206H} mice. From previous data we know that Pdgfra-Cre has a higher recombination efficiency and reproducibly results in a more robust HO response to injury[7]. Four Pdgfra-Cre; *R26*$^{NG/+}$*; Acvr1*^{tnR206H} mice were pinch injured at the midbelly of the tongue in a medial location. All four of the mice were negative for HO (**Figure 4)**. HO was found in all four injured hindlimbs, confirming that the mice were comptent to form HO (not shown). Two of the tongues were sectioned and stained using DAPI. Histology

showed that few myofibers contained centralized nuclei (**Figure 5b**). This section represents the midbelly of the tissue that was pinch injured. Myofibers presenting centralized nuclei were found in closer proximity to each other compared to the Tie2-Cre model. Injured tissue lacked structural integrity and organization found in unijured tissue. (**Figure 5b, d**).

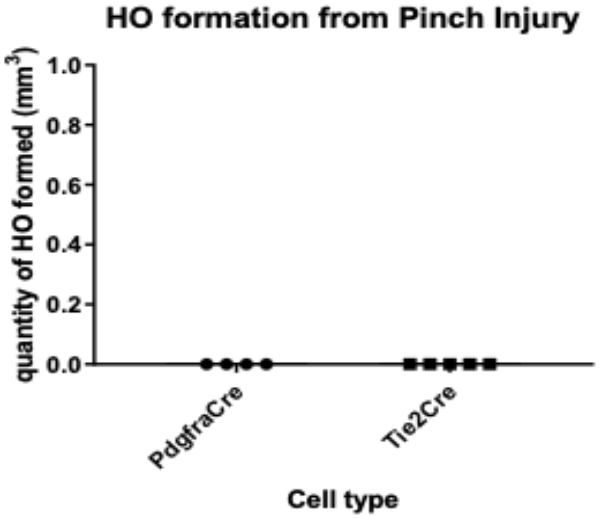

Figure 4: HO data from pinch injured mice. Four Pdgfra-Cre; *Acvr1*^{tnR206H}; *R26*$^{NG/+}$ (PdgfraCre) mice were pinch injured on their tongue. Two weeks post injury the tongues were harvested and scanned for bone growth. None of these mice formed HO in their tongue. Five Tie2-Cre; *Acvr1*^{tnR206H}; *R26*$^{NG/+}$ (Tie2Cre) mice were pinch injured on their tongue. Two weeks post injury the tongues were harvested and scanned for bone growth. None of these mice formed HO in their tongue. The right HL of each experimental mouse was also pinch injured as a positive control; these limbs did form HO (data not

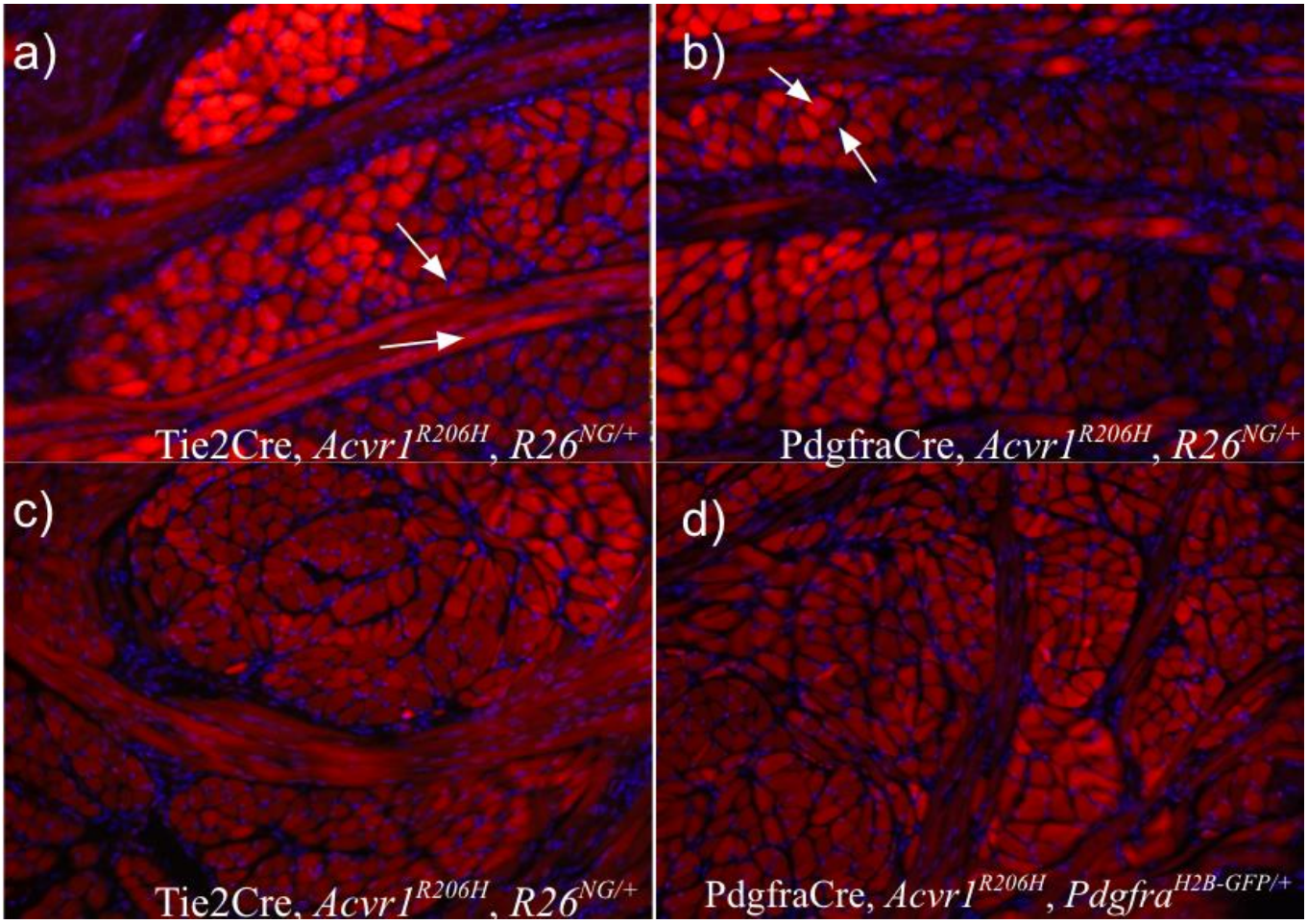

Figure 5: Pinch injured tongues in comparison to uninjured tongues of mice with the *Acvr1^{tnR206H}* mutation. a) A DAPI stained image of a Tie2-Cre; *Acvr1^{tnR206H}*; *R26$^{NG/+}$* pinch injured tongue at 200x magnification. This image shows the myofibers in the midbelly of the tongue at the location the injury was performed. White arrows point to DAPI stained nuclei that can be seen in a centralized location within the cell. Few centralized nuclei were seen. Organzation and structure of myofibers remain intact **b)** A DAPI stained image of a Pdgfra-Cre; *Acvr1^{tnR206H}*; *R26$^{NG/+}$* pinch injured tongue at 200x magnification. This image shows the myofibers in the midbelly of the tongue, where the injury was administered. White arrows point to DAPI stained nuclei that can be seen in a centralized location within the cell. This indicates regeneration. Additionally, the DAPI stain shows a lot of cellularization, also commonly seen in regenerating tissue. Organization and structure of myofibers remain intact **c)** A DAPI stained image of a Tie2-Cre; *Acvr1^{tnR206H}*; *R26$^{NG/+}$* uninjured tongue at 200x magnification. No centralized nuclei are seen here. Organization and structure of myofibers are highly complex **d)** A DAPI stained image of a Pdgfra-Cre; *Acvr1^{tnR206H}*; *Pdgfra$^{H2B-GFP/+}$* uninjured tongue at 200x magnification. No centralized nuclei are seen here. Organization and structure of myofibers are highly complex.

Cardiotoxin injury is sufficient to produce HO in a Pdgfra-Cre; *R26*$^{NG/+}$*; Acvr1*^{tnR206H} tongue, but not in a Tie2-Cre; *R26*$^{NG/+}$*; Acvr1*^{tnR206H} tongue. Cardiotoxin injury was used as a chemical form of injury to test if the tongue is competent to form HO. A consistent volume of toxin is injected, limiting human error, and injection can be directed to the center of the dense myofiber and connective tissue. After multiple trials, 3 of 15 Tie2-Cre mice presented HO following cardiotoxin injury on the IVIS machine. The volume of these bone nodules was determined using Slicer; quantification revealed nodules of 0.040 mm^3, 0.203 mm^3 and 0.126 mm^3 (**Figure 6**). All the hindlimbs injured did form HO (data not shown). Two tongues that formed HO and two tongues that did not form HO were sectioned. Bone morphology was not seen following DAPI or H&E staining of sections of the tongues that showed HO on the IVIS. Disorganization and degeneration of myofibers was evident in these sections (**Figure 7a, c**). Further analysis using stains for bone markers is necessary to confirm an absence of bone tissue. This section is from the mid-belly of the tongue where the cardiotoxin injection initiated. There are still intact myofibers present which have maintained some organization (**Figure 7a, c**). The injured tissue is highly cellularized and centralized nuclei can be seen near the site of disorganization (**Figure 7c**). We see centralized nuclei in the mid-belly of the tissue in more abundance from the cardiotoxin injury than the pinch injury (**Figure 5a, 7c**). Multiple trials were done on Pdgfra-Cre mice, and 6 of 7 injured mice formed HO (**Figure 6**). Quantification of the HO was 10.045mm^3, 0.578mm^3, 5.198mm^3, 4.141mm^3, 0.298mm^3, and 0.443mm^3 (**Figure 6**). All the hindlimbs injured did form HO (data not shown). Three tongues that formed HO were sectioned and analyzed. Consistently, there was a complete loss of structural integrity and organization of the myofibers in the midbelly of

the tongue (**Figure 7b, d, f)**. There was a large GFP presence, and minimal tdTomato presence. As expected, the bone nodule was surrounded by GFP+ cells. The loss of myofibers expands the width of the tongue, far greater than the size of the bone nodule (**Figure 7b**). H&E stain of the tissue surrounding the bone nodule shows a cartilage morphology (**Figure 7d**). If the injured tissue was collected at a later time point, this area of cartilage may have ossified, forming a larger bone nodule. The HO volume was consistently greater in the Pdgfra-Cre mice (>0.250mm^3) than the Tie2-Cre mice (<0.250mm^3) (**Figure 6**). Similarly, there was consistently greater structural damage to myofibers n the Pdgfra-Cre model (**Figure 7a, b**). This pattern suggests there could be a difference in osteogenic competence of both FAP populations or recombination efficiency can have a large effect on phenotype. There was no apparent sex difference in HO formed in the Pdgfra-Cre model.

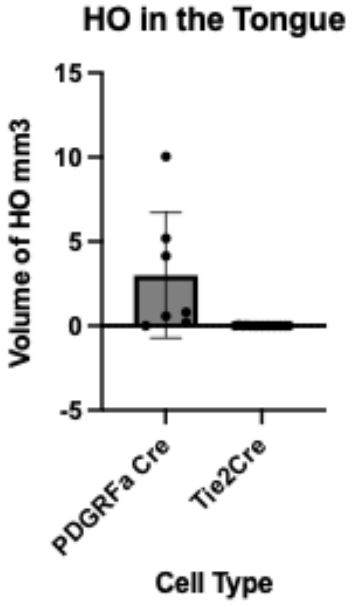

Figure 6: Cardiotoxin injury Assay results in Tie2-Cre mice and Pdgfra-Cre mice. Cardiotoxin was sufficient to constitently produce HO in the Pdgfra-Cre; *Acvr1*^{tnR206H}; *R26*$^{NG/+}$ (Pdgfra-Cre) model, but not consistently in the Tie2-Cre; *Acvr1*^{tnR206H}; *R26*$^{NG/+}$ (Tie2-Cre) model. Tongues were collected and scanned two weeks post cardiotoxin injection. There was bone growth in 6 of 7 Pdgfra-Cre models, with a variation in quantity. In contrast, only 3 of 14 Tie2-Cre tongues exhibited osteogenic capability, to a much lesser extent than the Pdgfra-Cre model. HO volume in Tie2-Cre model was consistently <0.250 mm^3, while Pdgfra-Cre consistently formed HO >0.250 mm^3. There was no discernible pattern in quantity of HO in Pdgfra-Cre mice.

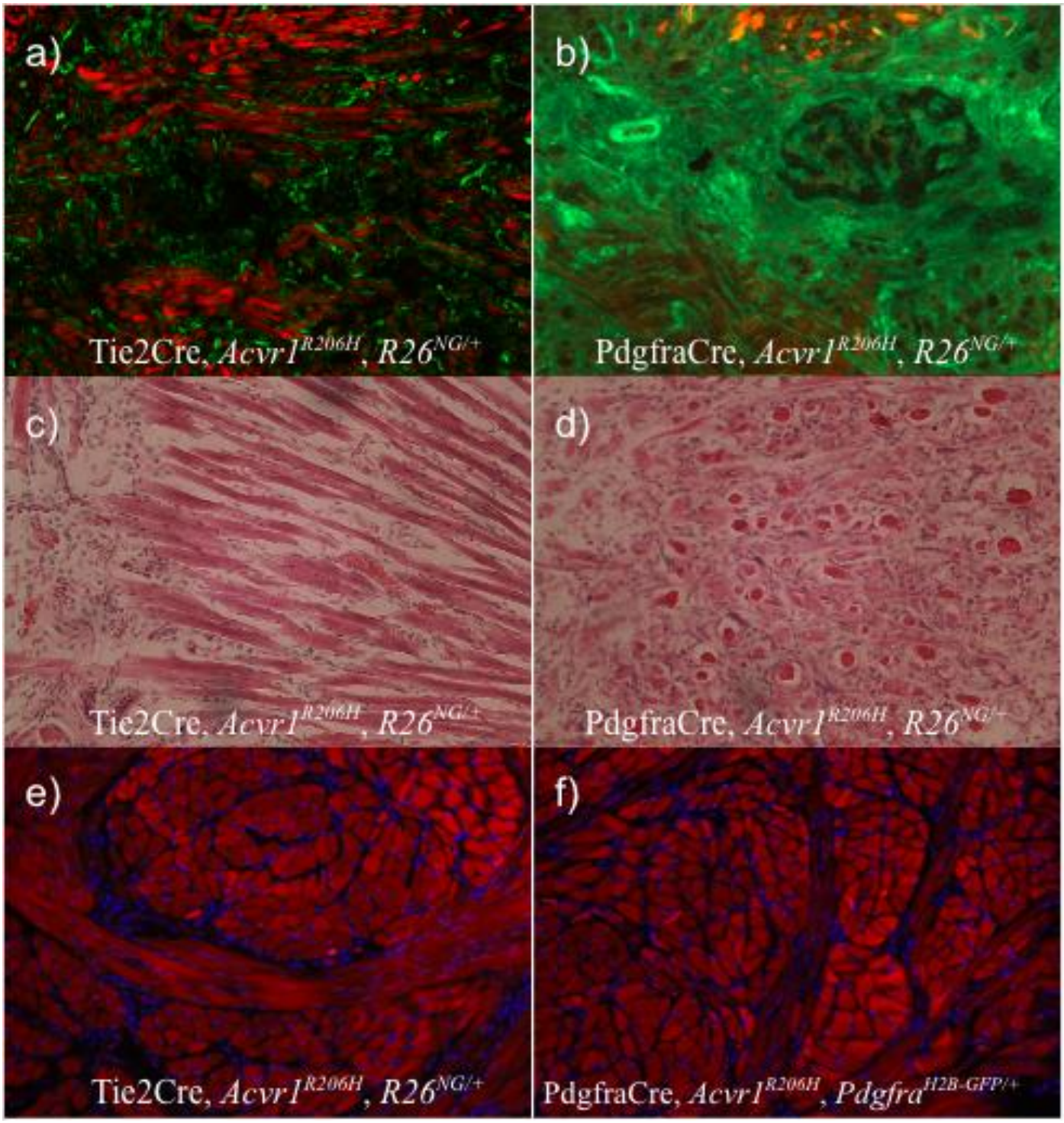
a)
Tie2Cre, Acvr1R206H, R26NG/+
b)
PdgfraCre, Acvr1R206H, R26NG/+
c)
Tie2Cre, Acvr1R206H, R26NG/+
d)
PdgfraCre, Acvr1R206H, R26NG/+
e)
Tie2Cre, Acvr1R206H, R26NG/+
f)
PdgfraCre, Acvr1R206H, PdgfraH2B-GFP/+

Figure 7: DAPI and H&E stained cardiotoxin injured *Acvr1^{tnR206H}* tongue in comparison to uninjured tongue. a)A 100x image of a cardiotoxin injured Tie2-Cre; *Acvr1^{tnR206H}; R26$^{NG/+}$* tongue. This image is of the tissue in the midbelly of the tongue, where the cardiotoxin was injected and the small bone nodule was seen in the CT scan. Green fluorescence is indicating recombined TIE2 labelled FAPs; red labels unrecombined cells with the *Acvr1^{R206H}* mutation. Disorganization and lack of myofibers is evident. No bone nodule morphology is observed. **b)** A 100x image of a cardiotoxin injured Pdgfra-Cre; *Acvr1^{tnR206H}; R26$^{NG/+}$* tongue. This image is of the tissue in the midbelly of the tongue, where the cardiotoxin was injected and the bone nodule was seen in the CT scan. Green fluorescence is indicating all recombined FAPs; red labels unrecombined cells with the *Acvr1^{R206H}* mutation. Disorganization and lack of myofibers is evident. A white arrow points to a bone nodule in the upper right corner of the image. There is no retention of myofibers surrounding the bone nodule, just complete disorganization. **c)** A 200x image of an H&E stain of a cardiotoxin injured Tie2Cre; *Acvr1^{tnR206H}; R26$^{NG/+}$* tongue. This image is shows part of the disorganization seen in **a**, and a view of the intact myofibers. There is a great amount of cellularization (marked by blue dye) normally seen in injured tissue at the sight of disorganization. Disorganization of myofibers is visible on the left side of the image, and myofibers can be seen on the right. **d)** A 200x image of an H&E stain of a cardiotoxin injured Pdgfra-Cre; *Acvr1^{tnR206H}; R26$^{NG/+}$* tongue. This image was taken of the area surrounding the bone nodule in **b**, reflecting the morphology of cartilage, indicating the disorganization seen in **b** is at least partially cartilage. There is no retention of myofibers surrounding the bone nodule. **e)** A DAPI stained image of a Tie2-Cre; *Acvr1^{tnR206H}; R26$^{NG/+}$* uninjured tongue at 200x magnification. Complexity and structure of myofibers is apparent, in contrast to the section in **a,** where myofibers are seen, but not in structured bundles. **f)** A DAPI stained image of a Pdgfra-Cre; *Acvr1^{tnR206H}; R26$^{NG/+}$* uninjured tongue at 200x magnification. Complexity and structure of myofibers is apparent, in contrast to the section in **b** and **d**, where no myofiber morphology is present.

Cross Transplantations

Cross transplantation of Tie2-Cre, *R26$^{NG/+}$, Acvr1^{R206H}* Hindlimb FAPs into a SCID tongue forms HO. In the first cross transplantation experiment, tongue and hindlimb cells from Tie2-Cre; *R26$^{NG/+}$; Acvr1^{tnR206H}* mice were collected and grown in culture for a week. During this week, the tongue cells were contaminated, making them inviable for the experiment. The hindlimb FAPs were FACS isolated and then spent another week in culture. After the week in culture, there were just under 6 million hindlimb FAPs, providing enough cells to transplant into four SCID mice (n=4). The tissue was pinch injured prior to transplantation to offer an environment primed for HO. 400k cells/20μL was transplanted into each tongue and 1 million cells/50μL was transplanted into the right hindlimb of each SCID mouse. The right hindlimb was a control in each mouse. 14 days after the injury and transplantation, the mice were collected and scanned

for HO using the IVIS machine. We found that all four SCID mice formed HO in the tongue and the hindlimb. Quantification of HO for each mouse was 0.494mm^3, 0.0961mm^3, 0.958mm^3, and 0.734mm^3. These tongues were prepared for histological analysis, but histology was not completed for this tissue. These results support findings that the tongue is competent to form HO.

Tie2-Cre; *R26$^{NG/+}$; Acvr1^{R206H}* tongue and hindlimb FAPs were transplanted into the hindlimb and tongue of SCID mice, respectively. From the prior experiment, we found that we needed to collecte more tongue cells to have a sufficient number for transplantations. In the second experiment, tongues from three Tie2-Cre; *R26$^{NG/+}$; Acvr1^{tnR206H}* mice were pooled together to increase the number of starting cells. The cells were grown in culture for a week, and then FAPs were FACS isolated, and grown in culture for one more week. Just under 3 million tongue FAPs were collected at the end of two weeks in culture, providing enough cells to transplant into an injured tongue and left hindlimb of two SCID mice. Hindlimb FAPs were transplanted into the right hindlimb of these SCID mice as a control. 14 days after injury and transplantation, the tissue was harvested and scanned using the IVIS. Tongue FAPs transplanted into the left hindlimb and tongue did not form HO in both experimental mice. The hindlimb FAPs did form HO in the right hindlimb of both mice. The tissue was fixed and decalcified following their respective protocols, and embedded for histological analysis. The two tongues were sectioned and stained. GFP+ cells were present in the tongue tissue that received tongue FAPs indicating that the transplanted cells engrafted, but did not form HO(**Figure 8**). Wholemount observations of the hindlimb's that received tongue FAPs showed GFP+

cells (data not shown). Histology was not completed on the hindlimbs that received tongue FAPs. Due to the lack of histology, we cannot confidently claim that transplanted tongue FAPs engrafted into the hindlimbs of the SCID mice. Additionally, cells from two hindlimbs of Tie2-Cre; $R26^{NG/+}$; $Acvr1^{tnR206H}$ mice were pooled together. After a week in culture, FAPs were FACS isolated from this population, and grown for another week. These hindlimb FAPs were used as controls for the two SCID mice that received tongue FAPs. Just under 3 million hindlimb FAPs were still available to also transplant hindlimb FAPs into the tongue and right hindlimb of two SCID mice. The tongues and hindlimbs that received hindlimb FAPs formed HO in both SCID mice after 14 days. Using Slicer, quantifications of these bone nodules in SCID tongues that received hindlimb cells were 1.077mm^3 and 1.499mm^3. This data further confirms injury assay data and the first cross transplantation experiment, showing a deficit in the Tie2-Cre tongue FAPs and osteogenic capacity of tongue tissue.

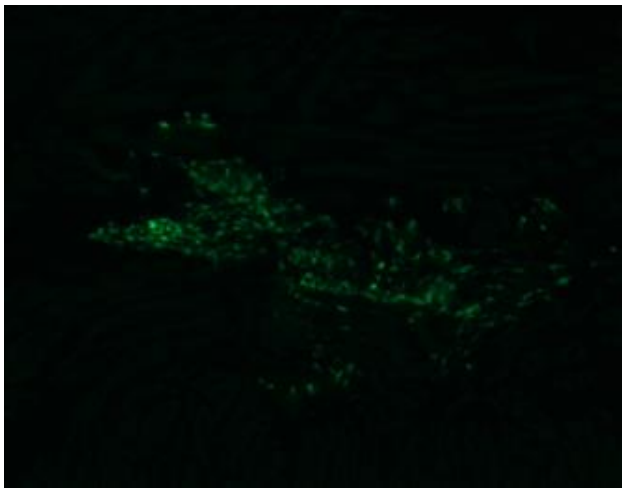

Figure 8: GFP Fluorescence of transplanted tongue FAP cells indicate successful engraftment. This image shows a section from the mid-belly of the tongue, where the transplanted FAPs were injected. Presence of GFP fluorescence indicates that FAPs from the host, Tie2-Cre; $Acvr1^{tnR206H}$; $R26^{NG/+}$, engrafted into the SCID tongue. The GFP+ cells are surrounded by no color WT myofibers of the SCID mouse. The results confirm that the transplantation was successful.

Tongue FAPs from a Tie2-Cre, *Pdfra*$^{H2B\text{-}GFP/+}$, *Acvr1*^{tnR206H} mice and Pdgfra-Cre, *Pdgfra*$^{H2B\text{-}GFP/+}$, *Acvr1*^{tnR206H} mice were transplanted into the tongues of SCID mice. In the third transplantation experiment, only two tongues of each mouse model were pooled together due to available mice. These cells were grown in culture for a week, then FAPs were FACS isolated, and grown in culture for another week. An equivalent amount of recombined FAPs were collected from FACS from each mouse type, which eliminates the difference in recombination efficiency between the two mouse models. Pdgfra-Cre FAP cells grew more quickly in culture than Tie2-Cre FAPs and had to be split two extra times. To keep an equal density of cells being transplanted and the same amount of experimental SCID mice for each model, Tie2-Cre FAPs were a limiting factor. Hindlimb cells were not transplanted in this experiment, as adequate data proved the hindlimb FAPs induce HO in the tongue. *Pdgfra*$^{H2B\text{-}GFP/+}$ mice were used in this experiment, because endogenous fluoresence offers a more accurate read out for PDGFRa expression than the antibody, providing a more precise isolation method. At the end of the two weeks in culture, there were 1 million Tie2-Cre FAPs, and more Pdgfra-Cre FAPs, so 400k cells/20μL were transplanted into two SCID mice tongues each. Not enough cells were collected to transplant the isolated tongue FAPs into the hindlimb of the SCID mice. 14 days after injury and transplantation, the tongues were harvested and scanned on the IVIS to verify HO formation. The two SCID mice that received Tie2-Cre; *Pdgfra*$^{H2B\text{-}GFP/+}$; *Acvr1*^{R206H} FAPs in the tongue did not form HO. These tongues were fixed, decalcified, embedded and sectioned for histological analysis. GFP+ cells were present in these tongues, suggesting engraftment of transplanted cells (**Figure 9a**). H&E stain does not show bone morphologies within the area of engrafted cells. Degradation

of myofibers, a common phenotype found in a tongue with the *Acvr1*^{tnR206H} mutation, is observed in the area of engrafted cells (**Figure 9a, b**). The two SCID mice that received Pdgfra-Cre; *Pdgfra*$^{H2B\text{-}GFP/+}$; *Acvr1*^{R206H} FAPs in the tongue did form HO. Bone nodules were quantified on Slicer and found to be 0.290mm^3 and 0.537mm^3. These are comparable volumes to bone nodules formed upon cardiotoxin injury in Pdgfra-Cre; *R26*$^{NG/+}$*; Acvr1*^{tnR206H} mice. GFP+ presence suggests that transplanted FAPs engrafted into the SCID host tissue (**Figure 9c**). H&E stain of this tissue shows a bone nodule and high cellularization to the area of engrafted cells (**Figure 9c,** d). Tissue surrounding the bone nodule looks like it maintained structural integrity, which is a different phenotype than cardiotoxin injury of Pdgfra-Cre; *R26*$^{NG/+}$*; Acvr1*^{tnR206H} mice. This data supports and enhances the findings from the previous cross transplantation experiments, and the injury assays.

A summarization of all the transplantation results from the three experiments can be found in **Table 1.**

Table 1: A summary of the cross-transplantation data from all three experiments.

Experiment	HO from Tie2Cre Tongue Cells into Tongue	HO from Tie2Cre HL cells into Tongue	HO from Tie2Cre Tongue cells into the HL	HO from PdfraCre Tongue cells into Tongue
1	N/A	4/4	N/A	N/A
2	0/2	2/2	0/2	N/A
3	0/2	N/A	N/A	2/2

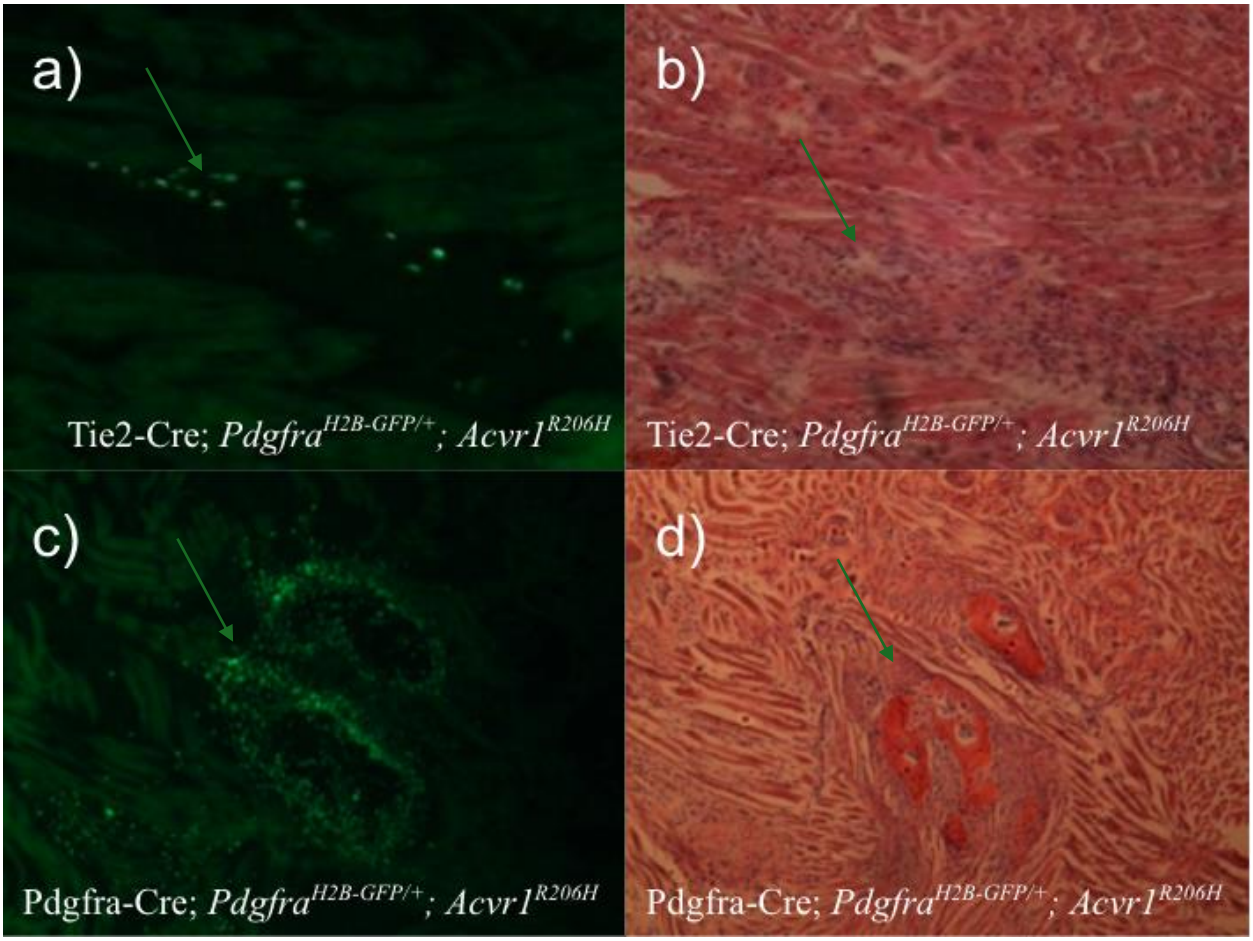
a)
Tie2-Cre; Pdgfra^H2B-GFP/+; Acvr1^R206H
b)
Tie2-Cre; Pdgfra^H2B-GFP/+; Acvr1^R206H
c)
Pdgfra-Cre; Pdgfra^H2B-GFP/+; Acvr1^R206H
d)
Pdgfra-Cre; Pdgfra^H2B-GFP/+; Acvr1^R206H

Figure 9: Histology of tissue from cross transplantations using Tie2-Cre; *Acvr1*^{tnR206H}; *Pdgfra*$^{H2B\text{-}GFP/+}$ and Pdgfra-Cre; *Acvr1*^{tnR206H}; *Pdgfra*$^{H2B\text{-}GFP/+}$ mice. Transplanted cells have endogenous GFP fluorescence when upregulating PDGFRa. H&E stains show exogenous bone growth and muscle tissue morphology. **a)**200x image of a section of a SCID tongue that received Tie2-Cre; *Acvr1*^{R206H}; *Pdgfra*$^{H2B\text{-}GFP/+}$ tongue FAP cells. This image shows the midbelly of the tongue where the host cells were transplanted. GFP presence supports engrafting of the transplanted cells. This is surrounded by a larger area where no myofibers are present. This could indicate that the cells engrafted into surrounding connective tissue, or degeneration of surrounding muscle tissue. **b)**200x image of an H&E stain of the same area, on the same section of the tongue tissue as **a**. Arrows point to very cellularized area and an absence of myofibers. GFP+ cells seen in **a** are at the same location of the disorganization and degeneration of myofibers seen in **b**. **c)**100x image of a section of a SCID tongue that received Pdgfra-Cre; *Acvr1*^{R206H}; *Pdgfra*$^{H2B\text{-}GFP/+}$ tongue FAP cells. GFP presence supports engrafting of the transplanted cells. The pattern of GFP+ cells is comparable to what is normally seen in FOP induced HO, in which it surrounds the bone nodules. **d)**100x image of an H&E stain of the same area, on the same section of tongue tissue as **c**. Arrows point to bone morphologies on this section. GFP+ cells seen in **c** are at the same location of the HO seen in **d**.

Discussion

Fibrodysplasia ossificans progressive is characterized by heterotopic ossification, the debilitating growth of exogenous bone in soft tissue[5,7,11,14]. Since the work of the Goldhamer lab identified a cell of origin for this bone growth, our understanding of the disease has changed substantially. FAPs are now a large focus for FOP research, as our knowledge of the behavior of mutated FAPs could lead to therapeutics. FAPs are a heterogenous population that play a role in growth and regeneration in response to environmental signals[1,7,8,9]. In diseased tissue, FAPs inappropriately signal for osteogenesis during muscle regeneration[5,7,10,14]. The tongue muscle contains a population of FAPs, but does not from HO clinically in an FOP diseased tongue. In this report we conducted research to evaluate the osteogenic capacity of the population of FAPs present within the tongue muscle.

We used mice with a knockin FOP mutation to test the effect of the disease on the tissue in the tongue[7,19]. Pinch injury did not form HO in Tie2-Cre; *R26*$^{NG/+}$*; Acvr1*^{tnR206H}

and Pdgfra-Cre; *R26*$^{NG/+}$*; Acvr1*^{tnR206H} mice. Histology showed that there were few centralized nuclei throughout the mid-belly of the tongue. Previous literature states that the anterior of the tongue has the lowest percent of muscle tissue, but the highest percent of connective tissue. In the medial tissue of the tongue there is more muscle tissue and less connective tissue[17]. The pinch injuries were more medial, where the myofibers are more densely packed and complex. Due to the nature of the myofiber organization and the minimal centralized nuclei, we speculate that the pinch injury did not have enough force to provoke injury and regeneration in the tongue. Clinically, the major forms of injury of the tongue tissue are burns, which would only affect the outer mucosal layers, and bites. As the pinch injury did not provide enough force to cause regeneration within the tongue to induce HO, we could speculate that biting the tongue would not either. These could serve as reasons we do not clinically see HO in the tongue, but we do in a lab setting.

The limitations of pinch injury assay were resolved by cardiotoxin injury. Cardiotoxin is a myonecrotic agent that spreads throughout the soft tissue[2,7]. We injected the cardiotoxin into the medial tongue area to affect the myofibers in the mid-belly of the tongue. This form of injury reproducibly induced HO in Pdgfra-Cre; *R26*$^{NG/+}$*; Acvr1*^{tnR206H} tongues. These findings indicate that the extracellular environment of the tongue is competent for HO in the presence of the *Acvr1*^{R206H} mutation. Interestingly, histology of this tissue showed complete disorganization of the myofibers in the mid-belly of the tongue that was far more expansive than the size of the bone nodule. This is an atypical phenotype of regenerative tissue with the *Acvr1*^{R206H} mutation [15]. Research on tongue muscle satellite cell biology is limited, hindering our understanding of the regenerative

process in the tongue[12]. Further research into the regenerative process and cellular composition of the tongue may explain this injury induced phenotype.

In contrast, HO formation in Tie2-Cre; *R26*$^{NG/+}$*; Acvr1*^{tnR206H} tongues following cardiotoxin injury had ambiguous results. This mouse model formed HO less consistently, and in smaller quantities. These tongues were fixed in 4% PFA before they were scanned using the IVIS CT machine; in recent conversations with members of my lab, it has been brought to my attention that fixing tissue prior to CT scans can have an effect on the readings from the IVIS machine. Previous scans with wild-type mice, which should not have any HO, showed positive results for HO only if they were fixed beforehand. Since the bone nodules seen in the Tie2-Cre model were notably small, this is worthy of consideration for the three Tie2-Cre mice that had HO. Additionally, histological analysis showed cellularization and disorganization of injured tissue, but no bone nodules were observed. While bone morphologies were not seen with an H&E stain, we cannot confidently state that osteocytes were not present until this tissue is stained for bone markers.

Our next goal was to understand why there were different findings in osteogenic ability, quantity of HO and myofiber retention between the two mouse models. We speculated that these results could be explained by recombination efficiency or an intrinsic difference in the two FAP populations. Previous research using flow cytometry, shows that Pdgfra-Cre has almost a three-fold greater recombination efficiency than that of Tie2-Cre[7]. Therefore, more FAPs are recombined to have the *Acvr1*^{R206H} mutation when controlled by the *Pdgfra* promoter, than the *Tie2* promoter. This could explain the deficit of HO observed in the Tie2-Cre; *R26*$^{NG/}$*; Acvr1*^{tnR206H} model in the injury assay.

Additionally, this difference could be due to the specific FAP population that is recombined in each model. Subpopulations of FAPs are present at different times throughout regeneration of muscle tissue[8,9]. A distribution profile of subpopulations of FAPs showed that TIE2+ FAPs peaked a day after acute injury, and slowly returned to baseline levels[8,9]. Interestingly, ossification occurs at later timepoints following injury, when different subpopulations of FAPs peak [8,9]. Therefore, there could be a population of osteo-competent FAPs that are recombined in the Pdgfra-Cre; *R26*$^{NG/+;}$ *Acvr1*^{tnR206H} mouse model that are not recombined in the Tie2-Cre; *R26*$^{NG/;}$ *Acvr1*^{tnR206H} mouse model.

The cross-transplantation experiments revealed that there may be an intrinsic cell difference between the Tie2-Cre FAPs and the Pdgfra-Cre FAPs. We collected an equal number of recombined tongue FAPs from both mouse models through FACS isolation and transplanted an equal density of isolated FAPs. This eliminated the recombination efficiency difference seen *in vivo* between Tie2-Cre; *Pdgfra*$^{H2B-GFP/+}$; *Acvr1*^{R206H} and Pdgfra-Cre; *Pdgfra*$^{H2B-GFP/+}$; *Acvr1*^{R206H} FAPs. With the same population of recombined FAPs, cells with a Pdgfra-Cre driver still showed a greater capacity for HO. Pdgfra-Cre; *Pdgfra*$^{H2B-GFP/+}$; *Acvr1*^{R206H} tongue FAPs formed HO when transplanted into the tongue, supporting findings from the injury assays. In contrast Tie2-Cre; *Pdgfra*$^{H2B-GFP/+}$; *Acvr1*^{R206H} and Tie2-Cre; *R26*$^{NG/+}$; *Acvr1*^{R206H} tongue FAPs did not form HO in the tongue or the hindlimb.

These results suggest that Tie2-Cre; *R26*$^{NG/+;}$ *Acvr1*^{R206H} tongue FAPs have an intrinsic inability to produce HO. More cross transplantation and cardiotoxin injury experiments must be done to increase the *n* to make a confident claim. Further, cardiotoxin injury of tongue tissue of Tie2-Cre; *R26*$^{NG/+;}$ *Acvr1*^{tnR206H} mice must be redone

without fixing the tissue prior to IVIS scans. This will eliminate the possibility that there are artifacts from fixing the tissue that register as ossified tissue. From the present data, we speculate that there is a subpopulation of FAPs that are imperative for tongue ossification that are not recombined when the *Tie2* promoter is the driver of Cre expression. This can be analyzed through FACS isolation and transplantation of PDGFRa+, TIE2- tongue FAPs. Testing osteogenic ability of this population will confirm if the osteogenic origin resides in a different subpopulation of FAPs.

Notably, Tie2-Cre; $R26^{NG/+}$; $Acvr1^{R206H}$ tongue FAPs did not form HO when transplanted into the hindlimb. In contrast, Tie2-Cre; $R26^{NG/+}$; $Acvr1^{R206H}$ hindlimb FAPs can form bone in the hindlimb. This would indicate that there is an intrinsic difference between Tie2-Cre tongues FAPs and hindlimb FAPs. FAPs are dynamic throughout the regenerative process, upregulating subpopulations at different time points depending on extracellular signals[8,9]. However, there is no literature on different subpopulations within the Tie2+ subpopulation of FAPs. One hypothesis is that environmental signals in the tongue shutoff certain genes in Tie2+ cells during development that are active in the hindlimb Tie2+ cells, or vice versa. Single-cell RNA-sequencing is a technology that can identify the expression of genes and distinguish cells at the molecular level[6]. This would be an advantageous next step to detect differences in cell surface markers or internal cellular components at play.

Conclusion

The findings in these experiments indicate that the extracellular environment of the tongue is competent for HO. While there have been no reported cases of clinical HO in an FOP diseased tongue, upon thorough injury HO can be provoked.

It is also important to acknowledge a possible intrinsic deficit in the Tie2+ FAP cells within the tongue. However, injury of Tie2-Cre; $R26^{NG/+}$; $Acvr1^{tnR206H}$ without fixing the tissue prior to IVIS scans and repeated cross transplantation experiments need to be conducted before we can confidently draw this conclusion. These results will dictate the need for further exploration of this population.

Ultimately, the tongue is a supportive environment for HO. More information on the unique behaviors of the subpopulations of FAPs that reside within the tongue can be very beneficial for our understanding of FOP.

Literature Cited:

1. Biferali, B., Proietti, D., Mozzetta, C., & Madaro, L. (2019). Fibro–Adipogenic Progenitors Cross-Talk in Skeletal Muscle: The Social Network. *Fronteirs in Physiology*, *10:1074*(10.3389). https://www.ncbi.nlm.nih.gov/pmc/articles/PMC6713247/
2. Dalle, S., Hiroux, C., Poffe, C., Ramaekers, M., Deldicque, L., & Koppo, K. (2020). Cardiotoxin-induced skeletal muscle injury elicits profound changes in anabolic and stress signaling, and muscle fiber type composition. *SpringerLink*,

41(10.1007), 375–387. https://link.springer.com/article/10.1007/s10974-020-09584-5

3. Dotiwala, A. K., & Samra, N. S. (2021). Anatomy, Head and Neck, Tongue. *StatPearls*, *NBK507782*. https://www.ncbi.nlm.nih.gov/books/NBK507782/
4. Giuliani, G., Rosina, M., & Reggio, A. (2021). Signaling pathways regulating the fate of fibro/adipogenic progenitors (FAPs) in skeletal muscle regeneration and disease. *Federation of European Biochemical Societies*, *10.1111*. https://febs.onlinelibrary.wiley.com/doi/pdf/10.1111/febs.16080
5. Hatsell, S. J., Idone, V., Alessi Wolken, D. M., Huang, L., Kim, H. J., Wang, L., Wen, X., Nannuru, K. C., Jimenez, J., Kie, L., Das, N., Makhoul, G., Chernomorsky, R., D'Ambrosio, D., Corpina, R. A., Schoenherr, C., Feeley, K., Yu, P. B., Yancopoulos, G. D., … Economides, A. N. (2015). ACVR1R206H receptor mutation causes fibrodysplasia ossificans progressiva by imparting responsiveness to activin A. *Science Translational Medicine*, *7*, 303–303. https://www.ncbi.nlm.nih.gov/pmc/articles/PMC6164166/
6. Hwang, B., Hyun Lee, J., & Bang, D. (2018). Single-cell RNA sequencing technologies and bioinformatics pipelines. *Experimnetal and Molecular Medicine*, *50*, 1–14. https://www.nature.com/articles/s12276-018-0071-8
7. Less-Shepard, J. B., Yamamoto, M., Biswas, A. A., Stoessel, S. J., Nicholas, S. E., Cogswell, C. A., Devarakonda, P. M., Schneider, M. J., Cummins, S. M., Legendre, N. P., Yamamoto, S., Kaartinen, V., Hunter, J. W., & Goldhamer, D. J. (2018). Activin-dependent signaling in fibro/adipogenic progenitors causes fibrodysplasia

ossificans progressiva. *Nature Communications*, *9*(471). https://www.nature.com/articles/s41467-018-02872-2

8. Malecova, B., Gatto, S., Etxaniz, U., Passafaro, M., Cortez, A., Nicoletti, C., Giordani, L., Torcinaro, A., de Bardi, M., Bicciato, S., de Santa, F., Madaro, L., & Lorenzo Puri, P. (2018). Dynamics of cellular states of fibro-adipogenic progenitors during myogenesis and muscular dystrophy. *Nature Communications*, *9*(3670). https://www.researchgate.net/publication/327559642_Dynamics_of_cellular_states_of_fibro-adipogenic_progenitors_during_myogenesis_and_muscular_dystrophy/fulltext/5b96a46e4585153a531d8bdf/Dynamics-of-cellular-states-of-fibro-adipogenic-progenitors-during-myogenesis-and-muscular-dystrophy.pdf
9. McKinnon, K. M. (2018). Flow Cytometry: An Overview. *U.S. National Library of Medicine*, *120*, 1–11. https://www.ncbi.nlm.nih.gov/pmc/articles/PMC5939936/
10. Molina, T., Fabre, P., & Dumont, N. A. (2021). Fibro-adipogenic progenitors in skeletal muscle homeostasis, regeneration and diseases. *The Royal Society*, *12*(210110). https://www.ncbi.nlm.nih.gov/pmc/articles/PMC8651418/
11. Pignolo, R. J., Shore, E. M., & Kaplan, F. S. (2011). Fibrodysplasia Ossificans Progressiva: Clinical and Genetic Aspects. *U.S. National Library of Medicine*, *1*(6), 80.
12. Randolph, M. E., & Pavlath, G. K. (2015). A muscle stem cell for every muscle: variability of satellite cell biology among different muscle groups. *Frontiers in Aging Neuroscience*, *7*(190). https://www.frontiersin.org/articles/10.3389/fnagi.2015.00190/full

13. Relaix, F., & Zammit, P. S. (2012). Satellite cells are essential for skeletal muscle regeneration: the cell on the edge returns centre stage. *The Company of Biologists*, *139*(16). https://journals.biologists.com/dev/article/139/16/2845/45218/Satellite-cells-are-essential-for-skeletal-muscle
14. Shore, E. M. (2012). Fibrodysplasia ossificans progressiva (FOP): A human genetic disorder of extra-skeletal bone formation, or - How does one tissue become another? *U.S. National Library of Medicine*, *1*(1), 153–165. https://www.ncbi.nlm.nih.gov/pmc/articles/PMC3297114/
15. Tasic, D., Pavlovic, M., Stankovic, D., Dimov, I., Stanojevic, G., & Dimov, D. (2012). Ossifying chondrolipoma of the tongue. *U.S. National Library of Medicina*, *69*(11), 1009–1012. https://scindeks.ceon.rs/
16. Miller, J. L., Watkin, K. L., & Chen, M. F. (2002). Muscle, Adipose, and Connective Tissue Variations in Intrinsic Musculature of the Adult Human Tongue. *EBSCO Host*, *45*, 51–65. https://web-s-ebscohost-com.ezproxy.lib.uconn.edu/ehost/pdfviewer/pdfviewer?vid=0&sid=3acc0b44-1451-410c-a848-be214c322769%40redis
17. Wosczyna, M. N., Biswas, A. A., Cogswell, C. A., & Goldhamer, D. J. (2012). Multipotent progenitors resident in the skeletal muscle interstitium exhibit robust BMP-dependent osteogenic activity and mediate heterotopic ossification. *Journal for Bone and Mineral Research*, *27*(5), 1004–1017. https://asbmr.onlinelibrary.wiley.com/doi/10.1002/jbmr.1562

18. Yamamoto, M., Shook, N. A., Kanisicak, O., Yamamoto, S., Wosczyna, M. N., Camp, J. R., & Goldhamer, D. J. (2009). A Multifunctional Reporter Mouse Line for Cre- and FLP-Dependent Lineage Analysis. *U.S. National Library of Medicina*, *47*(2), 107–114. https://www.ncbi.nlm.nih.gov/pmc/articles/PMC8207679/